SPECTROSCOPY AND REACTIVITY OF SILICON SURFACES

Glen Allen Ferguson

Submitted to the faculty of the University Graduate School
in partial fulfillment of the requirements
for the degree
Doctor of Philosophy
in the Department of Chemistry,
Indiana University
February 2010

Accepted by the Graduate Faculty, Indiana University, in partial fulfillment of the requirments for the degree of Doctor of Philosophy.

Doctoral Committee

_____

Professor Krishnan Raghavachari

_____

Professor Randall Bramley

_____

Professor Srinivasan Iyengar

_____

Professor Caroline Jarrold

15th February 2010

Acknowledgments

The author would like to thank those whose contributions were invaluable to the completion of this document. The patience, persistence and prudence of the author's advisor Dr. Krishnan Raghavachari are very much appreciated. His kindness and the careful manner in which he thinks about science were exemplary behaviors that the author has strived to emulate. He is a credit to himself, Indiana University and the scientific establishment. The assistance and support of the remaining graduate committee members including Dr. Randall Bramley, Dr. Caroline Jarrold and Dr. Srinivasan Iyengar were critical to the author's success. Most especially Dr. Iyengar who spent a considerable amount of time and energy directing the author's energies.

The author's is indebted to his collaborators Dr. Yves Chabal, Dr. David Michalak and Dr. Sandrine Rivillon for high quality experimental data as well as insightful conversation. Notable undergraduate collaborators were Christopher Than and Kevin Tiwari.

Others who contributed meaningfully to the author's success were Dr. Hrant Hratchian, Dr. Priya Parandekar, Dr. Parathasarthi Ramakrishnan and Dr. Aliaksandr Krukau. These postdoctoral fellows assistance and experience were essential to my success. Dr. Hratchian's mentorship was one of the most important of the author's time in graduate school.

The author's peers were a source of support and inspirations. Foremost among these are Dr. Ujjal Das and Nick Mayhall. Ujjal's mentorship and collaboration were deep and helped the author stay focused during difficult times in graduate school. Others

deserving thanks are Isaiah Sumner, Xiaohu Li, Ryan Fenno, Benjamin Gamoke and Raghunath Ramabhadran.

The support of the author's family is well appreciated. Gilbert and Gail Ferguson the author's parents have helped not only with graduate school but also with undergraduate and before. The author's wife Melissa-Ann Scotti was a constant source of love and support that helped in more ways than can be said.

Finally the author appreciates the help of the administrative and ITG staff of IU chemistry. The author would like to specifically thank Ms. Toni Lady for helping to navigate Byzantine administrative requirements, Mr. Steve Crepes for helping us understand the intricacies of Linux and Mr. Brian Crouch for outstanding computing support and advice.

Glen Allen Ferguson
Bloomington, IN
15st February 2010

This work is dedicated to both my loving wife and my mentors: Ignacio, Caesar, Big C, Ken, Ray, Johnny and Krishnan.

Sonnet to Science

Science! true daughter of Old Time thou art!
Who alterest all things with thy peering eyes.
Why preyest thou thus upon the poet's heart,
Vulture, whose wings are dull realities?
How should he love thee? or how deem thee wise?
Who wouldst not leave him in his wandering
To seek for treasure in the jewelled skies,
Albeit he soared with an undaunted wing?
Hast thou not dragged Diana from her car?
And driven the Hamadryad from the wood
To seek a shelter in some happier star?
Hast thou not torn the Naiad from her flood,
The Elfin from the green grass, and from me
The summer dream beneath the tamarind tree?

Edgar Alan Poe, 1829

SPECTROSCOPY AND REACTIVITY OF SILICON SURFACES

Glen Allen Ferguson

Functionalized silicon surfaces constitute an area of intense scientific interest. Our theoretical work in this exciting area can be broadly divided into two categories; the first is calculating the spectra of functionalized silicon surfaces to understand surface structure and the second is calculating the chemistry of funtionalization of the silicon surface with the surface as a reagent. Using electronic structure theory we have investigated the relationship between the molecular vibrations of cluster and periodic models for the functionalized Si(111) surface. From this work, we have developed a technique for calculating periodic vibrational frequencies using small cluster models. In addition, we have used the method to explain the coupling of near-surface phonon modes with adsorbate vibrational frequencies seen in experimental spectra. The method has been shown to be robust for uniform and mixed coverage (halide/hydrogen) surfaces. A careful study of the silicon hydrogen modes for many reconstructions at the same level of theory has been carried out to understand the spectra of hydrogen-passivated silicon surfaces. For the Si(100) surface we have examined the radical-initiated chain reactions of allylic mercaptan that have the unique property of growing exclusively across dimer rows on the Si(100) surface. We discuss the mechanisms of Lewis acids degrading on the silicon surface and the hydrogen induced insertion of oxygen or nitrogen into the silicon surface.

_____

_____

_____

_____

Table of Contents

List of Tables

List of Figures

Synopsis

The use of modeling to understand physical phenomenon has become increasingly important in recent years. While the techniques of classical mechanics have been long used to explain the macroscopic world it was not until the formulation of quantum mechanics in the 20th century that it became possible to consider subjecting the chemical world to serious mathematical investigation. As P.A.M. Dirac noted "The fundamental laws necessary for the mathematical treatment of the whole of chemistry are thus completely known, and the difficulty lies only in the fact that application of these laws leads to equations that are too complex to be solved." It was not until serious numerical techniques and advances in computing technology evolved much later that approximate solutions to many chemical problems have become practical. Today it is the case that the use of modeling to solve real chemical problems has become *de rigueur*. Even with this increased acceptance quantum chemistry is not as ubiquitous or routine as could be the case. The use of computations to provide scientific insight is necessary for the continued the acceptance of the field. It is frequently the case that many problems cannot be solved without significant advances in theoretical methods, numerical implementation and computing power. With current methods it is possible for a clever scientist to find novel insights into chemical problems that are relevant for the advancement of technology and society.

One of the most well formulated disciplines in chemical modeling is electronic structure theory. The field uses either exact solutions to approximate equations or approximate solutions to exact equations to find approximate solutions the insoluble Schrödinger equation. While many scientists contributed to advancements in the

discipline is was John Pople and Walter Kohn who won the 1998 Nobel Prize in chemistry for the development of these methods. Electronic structure theory has been used throughout this work to solve a number of problems related to the technology of semiconductors and silicon-based devices.

In the first chapter electronic structure theory has been used to model the vibrational spectroscopy of silicon surfaces. Determining surface structure at the molecular level is challenging. One of the most powerful techniques to solve surface structure is infrared vibrational spectroscopy. The interpretation of these IR surface spectra can be difficult and subjective. Using novel and established techniques we have modeled the surface spectra of several Si(111) and Si(100) surfaces to understand the surfaces after chemical modification. The goal of this chapter is to understand the vibrations of the surface and use these to assign experimental spectra. In addition to the practical aspect of understanding surface structure we have looked into several fundamental relationships, i.e., the correspondence between finite and infinite surface vibrations and the coupling of surface phonons to surface functional group vibrations.

In the second chapter the focus is on the reactivity of the silicon surface with various functional groups. The starting assumption is that patterning of silicon can be used to form molecular-scale devices. These devices could be used to manufacture new microelectronics devices. Two major challenges in this research area are the chemistry of various molecules interacting with the surface and the formation of nanopatterns on the surface. The ability to pattern the surface can lead to the chemical construction of devices and interconnects. In the first section the interaction of Lewis acids on the silicon and germanium surface is examined. In the following two sections the mechanism of an

important type of molecular line growth is studied and a new mechanism is proposed. The subsequent reactivity of surfaces containing existing lines was also studied. These results are useful in understanding the fundamentals of nanopatterning. The final section looks at the process of creating surface silicon-oxide and silicon-nitride layers using a chemical rather than thermal process.

The final chapter explores extensions to currently available techniques of chemical modeling. In particular the use of constrained density functional theory to find electronic states of interest was explored. A serious problem in computational chemistry is converging to particular electronic states. The numerical techniques that are commonly used to solve the equations used in electronic structure theory can result in solutions that are unstable. While it is sometimes desirable to find a *particular* electronic state that is unstable it is usually the case that a stable solution is desired. Using current implementations this goals can be challenging for some systems, e.g., transition metals. A possible solution is the use of constrained density functional theory to solve for the state of interest. In the final section we also examined modeling of core-level ionization spectroscopy. This experimental technique uses X-rays to ionize molecules. The electron binding energy gives information about the energy levels of the core electronic regions of an element. These energy levels are very specific to a bonding environment and can be used to identify the chemical bond types that are present in a material. In electronic structure theory the energy of the core-ionized state has a correspondence to the electronic binding energy. The currently available methods for determining the binding energy are benchmarked and compared to experimental data.

Chapter One

Vibrational Frequencies of Functionalized Silicon Surfaces

1.1 Introduction

The topic "is it possible to use mathematical calculations to understand chemistry" has long been are area of contention. Two quotes from the nineteenth century exemplify this controversy.

> *We are perhaps not so far removed from the time when we shall be able to submit the bulk of Chemical Phenomena to calculation.*
>
> Joseph Louis Gay-Lussac, Memoires de la Societe D'Arcueil, 1808

Every attempt to employ mathematical methods in the study of chemical questions must be considered profoundly irrational and contrary to the spirit of chemistry… If mathematical analysis should ever hold a prominent place in chemistry – an aberration which is almost impossible – it would occasion a rapid and widespread degeneration of that science.

Auguste Comte, Philosophie Positive, 1830

After two centuries the assertion of the chemist Gay-Lussac has finally come to pass and that of the philosopher Comte has simply become an incorrect prediction. Theoretical chemistry and computing have advanced to the point at which computations are considered a valuable addition to chemical knowledge. While we cannot yet submit the whole of chemistry to computation but recent advances have rapidly propelled computational chemistry to the point where it can calculate many if not the bulk of chemical phenomena. In favorable cases these calculations can yield results that are superior to what is experimentally measurable. In many cases calculations can probe phenomena that are beyond direct experimental scrutiny.

Quantum chemistry can be divided into two broad areas. The first area is made up of those who attempt to solve the time-dependent Schrödinger equation and the second those who approximately solve the time-independent Schrödinger equation.[1] The former is used to obtain dynamical properties and the latter is used to calculate chemical energies and static properties. The time-independent case is significantly better developed and will be discussed hereafter. Time-independent quantum chemistry starts from the Born-

Oppenheimer approximation involving the separation of the motions of the nuclei from that of the electrons. The entire discipline then consists of how to solve the electronic Schrödinger equation. This equation contains all of the information it is possible to know the electronic structure about a system. If the energy of a system can be solved it is possible to calculate the relevant molecular properties as derivatives of the energy expression. There are two approaches to solving these problems. One method, traditionally preferred by chemists, is based on the Hartree-Fock approximation.[1] In this method one uses a mean-field approximation where each electron moves in an average field of the other electrons. The remaining energy not included in this formalism is termed the electron correlation energy of a system. Several techniques such as perturbation theory, configuration interaction and the coupled-cluster ansatz have been used to systematically improve these results.[2] While coupled cluster theory yields results that are known to be reliable for many small molecules these calculations involve a significantly higher computational expense. At the limit of full configuration-interaction the energy expression becomes formally exact. Unfortunately, calculations of this type are intractable for all but the smallest systems. Quantum Monte Carlo techniques provide a different approach to solving the time-independent Schrödinger equation that is accurate for somewhat larger systems. The most widely used approach to solving the time-independent Schrödinger equation is density functional theory. This theory solves for the energy by solving directly for the electron density. The early formal developments of density functional theory were carried out the physics community. In this method the electronic energy is determined as a functional of the electronic density. If the exact functional were known the theory would be exact. Unfortunately, significant parts of the

exact functional are unknown and, more importantly, there is no systematic manner in which they can be derived or improved.[1] This has lead to a deluge of density functionals in recent year. Not all of these functionals are of equal utility. However, the accuracy of the theory has advanced sufficiently as to become much more widely used than its wavefunction-based counterpart. Indeed much of the work contained herein is based on density functional theory. Once the formalism of performing the energy calculation is realized it is then possible to perform calculations on a myriad of different systems. One important class of systems is surfaces and interfaces. These systems are more difficult than molecules because of their infinite nature. The formalism used to perform calculations on these systems is either via cluster models or via periodic boundary conditions. Cluster models perform calculations on an appropriate molecule that simulates the surface possibly subject to some constraints. Periodic boundary conditions use a set of repeating unit cells for each system and formally calculate an infinite system. Using these theories it is possible to submit semiconductor surfaces to mathematical calculations and realize, in part, Guy-Lussac's conjecture from over 200 years ago.

First identified by Antoine Lavoisier in 1787, silicon is the most common metalloid, the eighth most common element (by mass) in the universe and the second most common element in the Earth's crust. It is an important constituent of many important materials including ceramics, glasses and silicones (a polymer composed of silicon, oxygen, carbon and hydrogen).[3] Its most important contemporary use is as the material of choice for the semiconductor industry.[3] Some of the reasons for its widespread use are the native oxide layer that for many years was used as the dielectric layer of choice for semiconductor devices, the ability to prepare an ultrapure surface

without many defects, and the quality of retaining its semiconducting nature at higher temperatures.[4]

The industrial use of silicon in microelectronics has resulted in a plethora of scientific interest directed at silicon and its many derivatives. This interest has in generally been focused on two areas. The first is the practical application of silicon to produce better semiconductor devices. To this end silicon based materials and surfaces were characterized in precise detail. This wealth of knowledge along with its desirable electronic properties has led to the second area of interest, the use of silicon to study the basic chemistry and physics of semiconductor surfaces.[3] While silicon may not remain the preeminent material for semiconductor devices it is likely to remain important due to the abundance of high quality information in the scientific literature and the large infrastructure supporting silicon-based microelectronics devices.

The dominance of silicon in the microelectronics industry is also due to its relationship to the communications industry. Prior to the middle of the 1950's germanium was the material of choice for electronics devices. The largest player in early microelectronics research was Bell Telephone Laboratories. Their early research was directed at germanium-based devices. The invention of the silicon transistor in 1954 opened the possibility of changing from germanium-based devices to silicon-based devices but the cost and reliability of silicon was inferior to germanium. The most important advantage of silicon over germanium is that silicon has superior semiconducting properties at temperatures above 70° C and a larger band gap. It could be argued these advantages were outweighed by other advantages of germanium. The final advance that made silicon more attractive than germanium was the ease of forming a

silicon-oxide layer that protects the silicon from contamination and acted as the gate dielectric. This process dramatically reduced the cost of producing high-quality silicon-based transistors, giving silicon an edge over germanium and driving the research interest towards silicon-based devices. The research interest in silicon and the use of silicon as the material of choice for electronics devices has continued to this day. While devices based on other materials such as indium combined with a group 15 element (e.g. indium-phosphide), silicon-carbide and germanium-arsenide are used for specific applications, silicon-based devices are dominant.[4]

The three-dimensional crystal structure of pure single crystal silicon is easy to understand. As a tetravalent group 14 atom, silicon's valence electronic structure is the same as carbon. It therefore forms a crystal structure analogous to the diamond structure of carbon, i.e., a face-centered cubic Bravais lattice and an Fd3m space group, figure 1.1.1. The lattice spacing is longer for silicon, 5.43 Å than for carbon, 3.57 Å.[3] This structure results in a semiconductor, with an indirect band gap of 1.12 eV. Doping with elements such as boron, arsenic or phosphorous can be used to add or remove states from the band gap. By cutting the three-dimensional crystal it is possible to form very uniform surfaces crystal. In this work we will two surfaces in particular, Si(111) and Si(100).

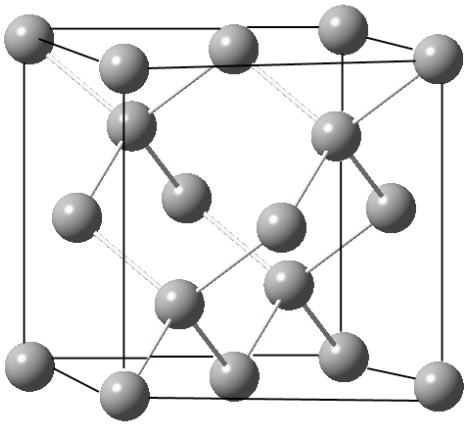

Figure 1.1.1. The unit cell of the diamond lattice of silicon.

Surfaces are defined using the Miller indices of the plane along which they were cut to form the surface. For a cubic unit-cell the Miller indices are the inverse of the points where the plane of interest intersects the lattice vectors. In the case of silicon a simplification can be made. The cubic Bravais lattice means the lattice vectors are orthogonal and equal; therefore interchanges of the indices are equivalent e.g., (001) is equal to (100). The Miller indices of the plane forming the surfaces of interest are shown in figure 1.1.2.

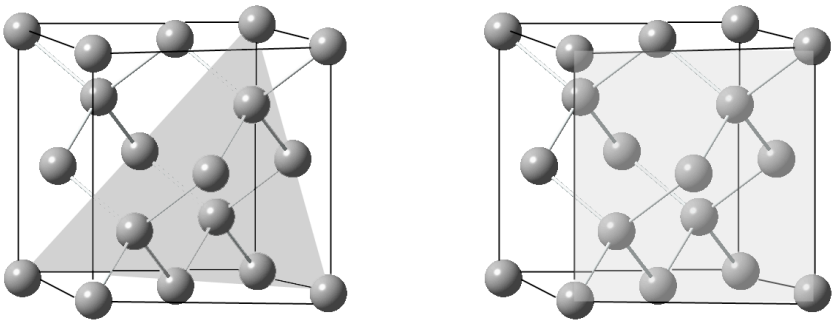

Figure 1.1.2. The (001), left, and (111), right, faces of the silicon diamond lattice, planes are shown as translucent grey.

The simpler of the two surfaces, Si(111), can be seen in figure 1.1.2 on the right while the slightly more complex surface, Si(100), is shown on the left. These surfaces form when the bulk is cut along the planes defined by the (111) or (100) Miller indices. Figure 1.1.3 shows how the surfaces are related to one another. The importance of the Si(100)-2×1 surface (*vide infra*) is its use as the surface of choice for the microelectronics industry making research into this material directly important to silicon-based devices. The Si(111) surface is currently less economically important but scientifically very interesting. After the surfaces are formed they are covered with dangling bonds formed from breaking the covalent bonds between silicon atoms.

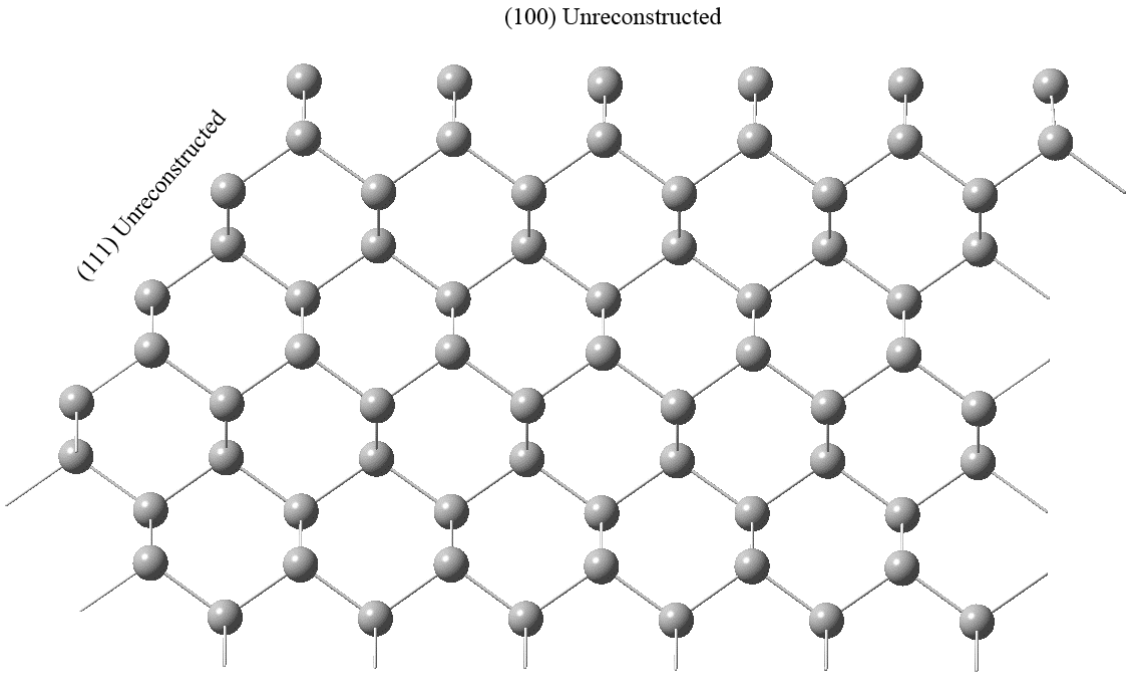

Figure 1.1.3. The relationship between the Si(100) and Si(111) surfaces.

For the Si(100) surface two silicon-silicon bonds are cut while for the Si(111) surface only a single bond is cut, figure 1.1.3. To minimize the strain of cutting these bonds the surfaces reconstruct to lower energy, i.e., more stable structures. For the Si(100) case pairs of uppermost silicon surface atoms join to form a surface dimer, figure 1.1.4. The notation to designate a reconstruction is $n \times m$, where m and n are the number of atoms in the unit cell along the orthogonal unit vectors. The Si(100) reconstruction is Si(100)-2×1. These dimers form in rows along the surface with troughs in between. In the Si(111) case there is a complex reconstruction 7×7 reconstruction involving 49 atoms in the unit cell. For our purposes it is unnecessary to explain this reconstruction. When the surface is etched using hydrofluoric acid or ammonium fluoride the reconstruction is eliminated and an unreconstructed surface with each dangling bond passivated by hydrogen is

formed. The two surfaces are shown in figure 1.1.4; the dimer rows of the Si(100) surface and the unreconstructed Si(111) surface.

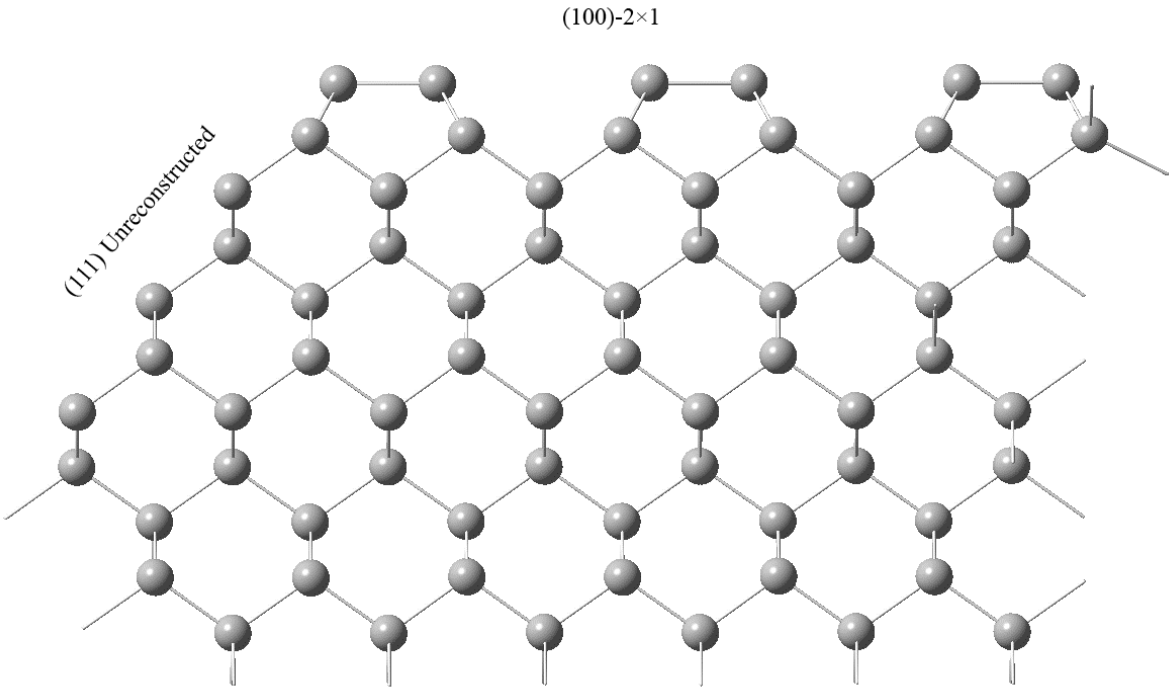

Figure 1.1.4. The reconstructed Si(100) surface and the unreconstructed Si(111) surface. The Si(111) surface is identical to the hydrogen passivated Si(111) surface.

An important difference between the surfaces is their electronic state. The Si(100)-2×1 surface is not electronically passivated like the hydrogen-terminated Si(111) surface. In the Si(100)-2×1 surface the reconstruction does not completely eliminate the surface dangling bonds as with the H-Si(100) surface. To understand the electronic state of the surface it is helpful to consider two adjacent silicon atoms. Collectively these atoms have four dangling bonds (four unpaired e^-). The formation of the dimer bond eliminates one electron per atom leaving two unpaired e^-. There are several possible electronic states:

the unpaired e^- join to form a weak double bond with a singlet spin multiplicity, the unpaired e^- do not join and the surface is a diradical with an open-shell singlet, a triplet spin multiplicity or possibly a multireference electronic state (linear combination of electronic configurations). The bare surface is believed to have a buckled surface involving an "up" atom and a "down" atom of the dimer. The recent work by the Gordon group at Iowa State University favors multireference description.[5] Due to the small energy difference between the multireference and singlet total energies it is possible to use the singlet surface as a good approximation for the total energy of a cluster.

While not as ideal as the Si(111) surface the Si(100) surface is relatively defect-free. It does contain domains in particular directions at step defects, figure 1.1.5. At a step defect the direction of the surface reconstruction changes, giving a surface with two perpendicular domains. A possible way to alleviate this issue is by miscutting the surface by 9° forming a slightly different reconstruction involving only a single domain (all of the dimers).

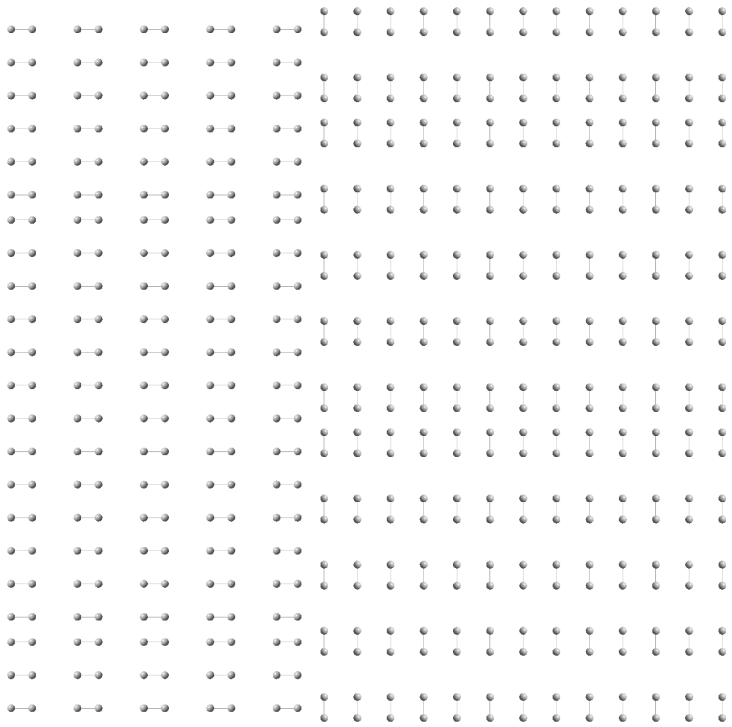

Figure 1.1.5. The domains caused by step defects on the Si(100)-2×1 surface. Only the top layer is shown, lower layers omitted for clarity.

Molecular vibrations are an important property that is related to the molecular structure, and are experimentally investigated via infrared and Raman spectroscopy. It is possible to calculate molecular vibrations as the Hessian of the energy expression where the partial derivatives are taken with respect to the nuclear displacements. The eigenvalues of the resulting mass-weighted force constant matrix yield the vibrational frequencies while the eigenvectors represent the corresponding molecular displacements of the normal modes of vibration. Procedures for calculating the molecular vibrations using analytical second derivatives for a variety of theoretical models are well developed and commonly used. This is not the case for the vibrations involving periodic systems, in

particular surfaces and their adsorbates. In general, while it is possible to employ a similar formalism involving the Hessian, analytic formulations have only been recently published and are not yet available in most quantum chemical packages. The surface vibrations are, however, very important for determining surface structure.[6]

In this work we have made several key advances relevant to the investigations of surface vibrations. We have explored new ways to calculate surface adsorbate vibrational spectra, we have characterized trends in adsorbate vibrational spectra that are useful for determining surface coverage, examined the interaction of a phonons with hydrogen & deuterium adsorbates and carefully benchmarked the hydrogen vibrations for several import silicon surfaces.

1.2 Methylated Si(111) Surface

The silicon (111) surface, when hydrogen terminated, forms a nearly ideal atomically flat surface,[7] and could potentially be used for preparing well-ordered organic and bioorganic derivatives on a silicon surface. Unfortunately, the hydrogen passivated surface oxidizes too rapidly when exposed to the atmosphere[8] to be of serious technological interest. The chlorinated surface is more stable than the hydrogen passivated surface[9, 10] but does not provide a convenient route for functionalization. Alkylation using the Grignard reagent, stabilizes the surface to atmospheric oxygen for long time periods (> 600 hours)[8] and is convenient for functionalization. These qualities of the alkylated silicon (111) surface immediately suggest the possibility of preparing semiconductor-based materials that offer molecular level control, potentially leading to novel applications in chemistry.[3, 11-26] Among the different possible alkylated surfaces, the methylated surface offers the most scope for controlled functionalization. The van der Waals radius of the methyl groups on the surface allows for complete monolayer coverage with every silicon atom bound to a single methyl group. Recent studies by Yang, Lewis and coworkers have shown these methyl groups can act as nanowires.[27] Though larger alkyl groups, e.g., ethyl have also been seen on Si(111), theoretical calculations[28, 29] suggest that full coverage is not possible for such surfaces due to steric considerations.

Lewis and coworkers have synthesized and characterized the alkylated surface using several techniques. It was observed that while many routes lead to alkylation, the two step chlorination/alkylation using the Grignard Reagent was preferable yielding stable products resistant to oxidation.[8] Characterization of the methylated surface using synchrotron x-ray photoelectron spectroscopy strongly implicated a carbon–silicon bond

indicating that the linkage of the alkyl groups through an intermediate such as oxygen is unlikely.[28-30] Low-temperature STM corroborated the direct bonding of methyl groups to the surface.[31] STM and LEED indicated a 1×1 layer on top of the silicon surface. Additionally, the orientation of the surface methyl groups (as defined by the dihedral angle, H–C–Si–Si) has been derived from STM measurements to be approximately 23º. This differs significantly from the corresponding theoretical values obtained from density functional calculations (*vide infra*). An explanation for this difference has been proposed by Solares et al.[29]

High resolution electron energy loss spectroscopy (HREELS) experiments were preformed by Yamada et al. to elucidate the vibrational modes of the methylated surface.[32] They also demonstrated the thermal stability of the methylated surface up to 600 K. The vibrational modes were also measured using IR spectroscopy by Rivillon et al.[9, 33] Relatively sharp features were observed to yield vibrational modes similar to those in the HREELS measurements. The methyl group symmetric deformation, i.e., umbrella mode, was clearly observed perpendicular to the surface, again supporting the idea that a methyl group is bound to the surface via a single carbon-silicon bond.

In the present report we present harmonic frequencies for the methylated Si(111) surface from quantum chemical calculations using both periodic boundary conditions and cluster models. In addition to offering a reasonable interpretation of the previously determined experimental spectra, we have sought to derive a general method for determining vibrational modes for extended surfaces (i.e., periodic systems) from cluster models. We also discuss an adsorbate vibrational mode that has a significant coupling to the near-surface phonon modes.

Cluster approach vs. two-dimensional periodic approach

Theoretical calculations investigating vibrational properties of semiconductor surfaces have frequently used the cluster approach. Within the cluster approach, an individual cluster molecule is used to represent an atomically resolved region of the surface along with its immediate environment. The main advantage of the cluster approach is that the power and accuracy of newly emerging quantum chemical methods can be immediately applied to surface chemical problems. In addition, the availability of analytical second derivative techniques using hybrid density functionals has contributed to their use in many successful investigations of the vibrational spectra of adsorbate species.

While relatively modest sized clusters have been successfully used to investigate localized species on surfaces, a fundamental problem arises when the method is applied to periodic systems, as considered in this study. In the limit of complete coverage, all the CH_3 groups on the Si(111) surface are equivalent. Hence the resulting vibrational modes are collective modes that are not easily described using small clusters. There is intrinsic asymmetry in the cluster calculations. Unlike the extended system, the different CH_3 groups in finite clusters do not have the same local environment and, hence, are not all equivalent. Thus the corresponding bond lengths and the associated intrinsic vibrational frequencies of the different methyl groups are different, resulting in broad vibrational features. In this work, we show that the emergence of collective vibrational modes can be successfully investigated using relatively small cluster models. In a recent combined experimental and theoretical study, we have used surface infrared spectroscopy in

conjunction with quantum chemical cluster calculations to investigate similar collective vibrational modes for Cl-terminated Si(111) surfaces.[10]

Cluster models also suffer from other limitations. The termination of the back bonds with hydrogen, while a well-established procedure, can lead to artifacts (e.g., spurious vibrational coupling). In many cases, the configurations adopted by the surface groups can be different compared to analogous free molecules due to the constraints from the mechanical force of the bulk atoms. In order to mimic this effect and to avoid unphysical relaxations, the lower layer atoms are frozen in many cluster models.[34] While this technique helps to describe the structures adopted by surface or adsorbed groups it may also be a significant approximation.

An alternative approach to materials modeling is via the slab approach using periodic boundary conditions (PBC). In this approach, a periodic unit cell is used to perform calculations on the extended system (solid or surface) with full periodicity, typically using density functional techniques. This procedure allows the groups to "feel" the effects of the entire extended surface allowing for a constraint-free description in many cases. If the PBC unit cell is well chosen (i.e., repeats correctly throughout the system while being of reasonable size), the PBC model is a better approximation to the extended surface than the cluster models, at a given model chemistry. For problems involving periodic systems, it would thus seem more appropriate to use PBC models rather than cluster models. However, modest sized cluster models have several benefits not available for PBC models. First, DFT methods that include exact exchange (e.g., B3-LYP)[35, 36] or post-Hartree-Fock methods can be inexpensively included in cluster models.

In most PBC implementations the introduction of exact exchange or post-Hartree-Fock methods is either not available or computationally prohibitive.

Another problem when using PBC calculations is that analytical second derivative techniques have not yet been implemented in most quantum chemical packages and second order properties (e.g., vibrational frequencies) must be calculated numerically. As the number of atoms increases, the cost of the many force evaluations rapidly become prohibitively expensive, thwarting the use of PBC models for harmonic frequencies. Thus cluster models are a reasonable choice when properties greater then first-order are required.

Computational Details

In this work, we have evaluated the vibrational frequencies using cluster models as well as PBC using *identical theoretical procedures*. Both cluster and PBC calculations used the Becke 88 exchange[35, 36] functional and the Lee-Yang-Parr electron correlation functional[37] with the 6-31G(d,p) basis set[38] as the model chemistry (BLYP/6-31G(d,p)). The use of the same functional and basis sets allows for a careful calibration of the performance of cluster models. As noted earlier, more sophisticated hybrid functionals can also be used in the cluster models. However, comparison of the results of BLYP/6-31G(d,p) and B3LYP/6-31G(d,p) calculations showed that, while the absolute frequencies are different by a few percent, the qualitative features are exactly analogous.

Periodic boundary condition calculations for atom-centered basis functions utilized the method of Scuseria and Kudin.[39-41] Starting geometries were generated from the bulk silicon structure. The simplicity of the terminated silicon (111) surface

containing only one unique atom per atomic layer makes it easy to construct appropriate structural models. Figure 1.2.1 shows the PBC models used for the present study. Four, six, and ten layer models for PBC calculations, denoted PBC-4, PBC-6 and PBC-10 were constructed with the valence on the lowest atom terminated with hydrogen and the surface atom terminated with a methyl group. The structures were optimized using fully two-dimensional periodic boundary conditions.

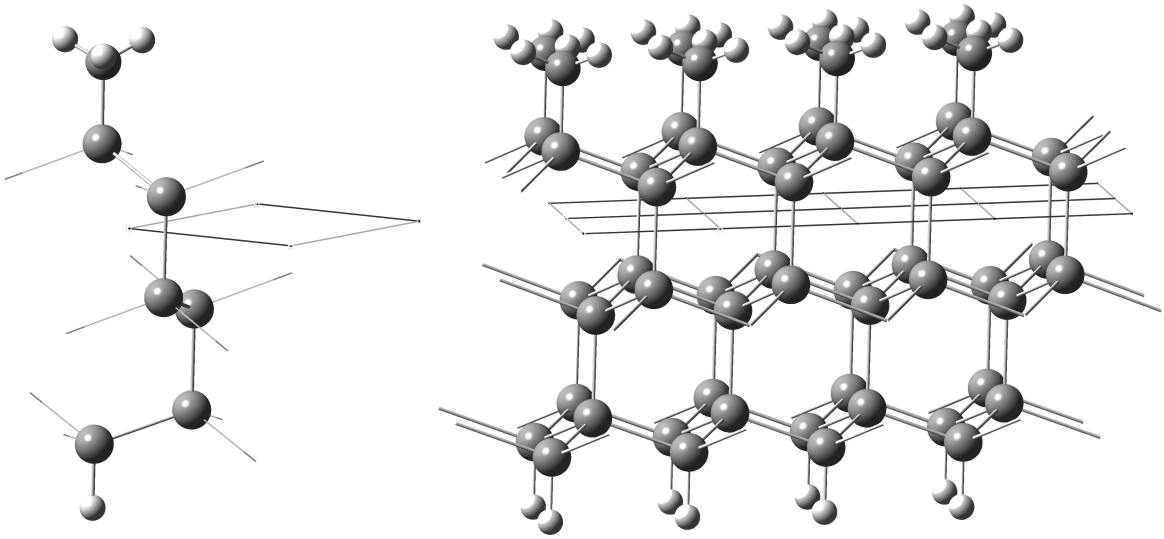

Figure 1.2.1. Side-view of the PBC model with a single unit cell (left) and an 8 unit cells (right), with light grey representing silicon, dark grey representing carbon, and white representing hydrogen.

As mentioned earlier, analytical force constant methods are not available for such PBC methods. We have used numerical finite difference techniques to determine the PBC vibrational frequencies. In our case, the forces are determined analytically and the numerical differentiation of the forces with respect to atomic displacements yields the second derivatives (force constant matrix). Using symmetric finite differences with a step

size of 0.001 Å, the harmonic force constants have been calculated using Cartesian coordinates and then mass-weighted and diagonalized to yield the normal vibrational modes. This calculation is equivalent to evaluating the Γ-point (k=0 or zone center) surface-phonon modes. Such a calculation assumes that the unit cell is appropriate and considers only concerted displacements of the atoms in all the unit cells. The associated phonon dispersions (dependence of the phonon frequencies on k) have not been evaluated but are not needed to make definitive vibrational assignments. The finite difference method has been used with the four and six layer models to evaluate the vibrational frequencies. These PBC frequencies can then be used to calibrate the performance of cluster models. All the calculations were performed with a modified version of the *Gaussian* program suite.[42]

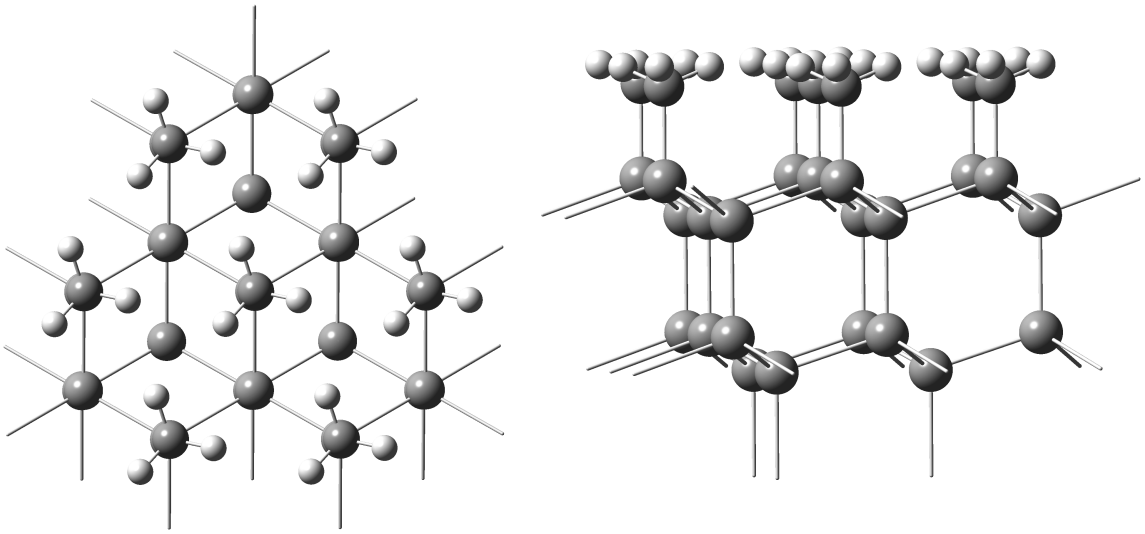

Figure 1.2.2. Side (left) and top-down (right) views of the $Si_{22}H_{21}(CH_3)_7$ cluster model.

Figure 1.2.2 is a ball and stick representation of the cluster model used in our study. Cluster models for the methyl-terminated silicon surface were built from the optimized PBC structures with only slight modifications to atomic positions to preserve the intrinsic C_3 symmetry of the system. The resulting cluster contains 22 silicon atoms and 21 terminating hydrogen atoms that represent the silicon surface and seven methyl groups giving it an overall stoichiometry of $Si_{22}H_{21}(CH_3)_7$. The sites, which result in dangling bonds on the silicon due to cluster truncation, are terminated with hydrogen atoms (H–Si = 1.47 Å) in accordance with well-established precedent.[34] While the distribution of the vibrational frequencies in such cluster models is likely to be somewhat broad, the emergence of the associated intensities should show the evolution of collective behavior. Our investigations show that the $Si_{22}H_{21}(CH_3)_7$ cluster is already sufficient to reach general conclusions about the performance of such cluster models.

Two different classes of cluster models have been used in this work. In the first class, the extracted cluster structure is optimized to a true minimum. The hydrogen atoms below the second layer are frozen in Cartesian space to simulate the constraints from the extended surface. Frequency calculations were then carried out on these optimized structures to determine the surface vibrational frequencies within the harmonic approximation. It should be mentioned that the geometry optimization and the frequency evaluation should employ the same constraints in a consistent manner. This can be achieved by projecting out their contributions from the force constant matrix or by using infinite masses for the frozen atoms.

An alternative strategy is to use the geometry determined from the periodic system (with hydrogen termination of the truncated bonds) to determine the vibrational

frequencies in the clusters. However, the frequencies are now determined at a non-equilibrium geometry for the cluster. As the cluster gets larger, the optimized cluster geometry will converge to the bulk geometry. Both optimized and bulk-like geometries have been used to explore the vibrational modes and their approach to collective behavior.

Results and Discussion

Geometrical Parameters

The optimized structure of the methyl-terminated silicon surface was first determined using a PBC-4 model with periodic boundary conditions. As mentioned previously, the bottom layer was terminated with hydrogen atoms while the surface layer was terminated with methyl groups. While there is only one methyl group in the unit cell making them all equivalent to each other, the orientation of the methyl groups with respect to each other is a key geometrical parameter. There are two competing factors that determine the orientation of the surface methyl groups. If the methyl groups do not interact with each other or if isolated methyl groups are present on the surface, we expect a staggered configuration with respect to the second layer atoms (H–C–Si–Si dihedral angle of 60°). However, such a staggered configuration places the methyl hydrogen atoms pointing toward each other on the surface. The distance between the nearest hydrogen atoms (1.9 Å) is smaller than the sum of their van der Waals radii (2.4 Å) suggesting that steric repulsions will be present. This causes a rotation of the methyl groups moving the hydrogen atoms away from each other (and from the staggered configuration with respect to the second layer atoms). Such steric repulsions are minimized at a dihedral angle of 30°. The optimized value of the dihedral angle

represents the balance between the two factors. Our optimized value at the BLYP/6-31G** level (41°) is close to the value obtained by Goddard and coworkers (38°) using the PBE functional and a plane wave basis set, and is different from the experimentally derived value of 23±3°. In addition, we used 6-layer and 10-layer models with periodic boundary conditions and obtained optimized values almost identical to that with the 4-layer model. In order to determine if the inclusion of exact exchange has an effect on the dihedral angle, we optimized the structure using the HSE[43-45] screened Coulomb hybrid functional and obtained a value of 38°. Thus it appears that the difference between the density functional values and the experimentally derived values is real and may be due to the effect of etch pits seen in the experimental work as suggested by Solares et al.[29] An additional factor that we have not considered is the effect of dispersion interactions on the methyl group dihedral angles. While we think that such effects are likely to be small, it may be necessary to perform MP2 calculations, which give a better representation of dispersion forces, to explore this possibility. However, the principal focus of our work is to determine the vibrational frequencies as seen in the surface infrared spectra, and we expect such differences in dihedral values to play a negligible role.

The performance of the cluster model for the geometry is disappointing. The inherent limitations of the model are clearly evident in the optimized structure. As pointed out earlier, the starting cluster model has a central methyl group and six surrounding methyl groups in an overall C_3 symmetry arrangement. While the local environment of the central methyl group is similar to that in the extended system, the six surrounding methyl groups do not have the same steric constraints on the outside. This manifests itself in two significant deficiencies in the resulting optimized structure. First,

the optimized dihedral angle (H–C–Si–Si) has a value of 60°, collapsing to C_{3v} symmetry as expected in small isolated clusters.[29] Second, the six surrounding methyl groups bend away from the central methyl group by about 10°. Thus the Si–C bonds are no longer parallel to each other, figure 1.2.3. Obviously, the two deficiencies are related to each other both providing mechanisms for steric relief. While the imposition of additional constraints may yield better results, we conclude that the optimized cluster model is clearly inappropriate. We have thus used the cluster structure obtained from the PBC geometry to perform the vibrational analysis in the following discussion.

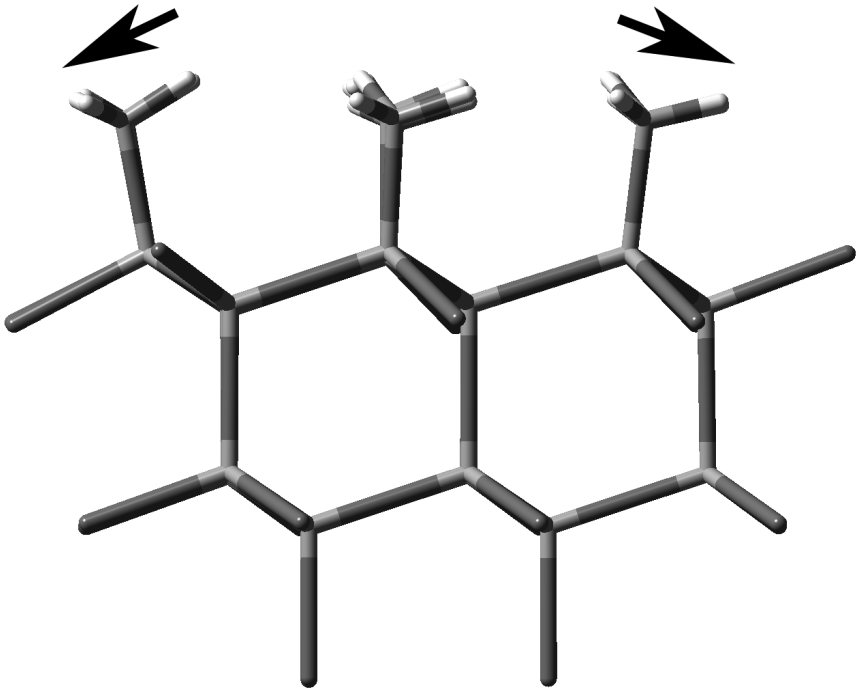

Figure 1.2.3. A side view of the relaxed cluster model, which shows the bending of the peripheral methyl groups away from the central methyl group.

Vibrational Frequencies

As mentioned above, we have optimized the structure using PBC and then excised the structure to obtain the cluster model used in the vibrational analysis. It should be noted that caution must be exercised in obtaining harmonic frequencies at non-equilibrium geometries. In particular, the three rotational degrees of freedom do not yield zero frequencies in such cases and can be coupled to low frequency vibrations (typically < 100 cm^{-1}). We have rigorously projected out the rotational modes from the force constant matrix to ensure that true vibrational modes are obtained. In addition, the modes of interest as seen experimentally (> 500 cm^{-1}) are relatively high-frequency modes, and are not likely to be influenced by such spurious couplings.

Assignment of the surface infrared spectroscopic features requires a careful analysis of the various vibrational frequencies present in the cluster model. In our study, the model contains seven methyl groups and has C_3 point group symmetry. Note that an analogous cluster for a H-terminated (or Cl-terminated) surface would have C_{3v} symmetry whereas the rotation of the methyl groups discussed earlier reduces it to C_3. Within C_3 symmetry, parallel unit vectors (along *x* and *y* directions) belong to the doubly degenerate "*e*" representation while a perpendicular unit vector (along the *z* direction) belongs to the non-degenerate "*a*" representation. The number of surface groups determines the number of vibrations seen in the cluster model. If there is only one methyl group, parallel modes of silicon and carbon as well as the asymmetric methyl vibration will be part of the *e* representation while the symmetric perpendicular modes will have the *a* representation. The presence of seven groups complicates the problem yielding seven sets of modes resulting from combinations of the vibrations of the individual

groups. In a larger cluster, there would be an even larger number of coupled vibrational modes. This is much more complicated than the real situation that has a relatively simple spectrum resulting from a single methyl group in a periodic unit cell. A possible solution is to focus on the modes that correspond to the most concerted motion of all the methyl groups involving the greatest coupling of the vibrations. Another possibility is to consider the vibrational frequencies of the central methyl group (whose environment is most like the true surface) as the relevant frequencies. However, there is no well-defined and unique procedure to isolate its frequencies. One of our main objectives is to develop a method for understanding which cluster frequencies evolve into collective modes of oscillation that correspond to the observed surface vibrations. We show that this can be seen clearly even for our modest-sized cluster.

Table 1.2.1. The frequencies (cm^{-1}) and intensities (km/mol) for the methyl umbrella and carbon-silicon stretch modes from the cluster model.

Mode	**Frequency, cm^{-1}**	**Intensity**	**Mode**	**Frequency, cm^{-1}**	**Intensity**
CH_3 Symmetric Deformation 1	1274	17.1	C–Si Stretch 1	637	81.0
CH_3 Symmetric Deformation 2	1264	0.1	C–Si Stretch 2	627	16.1
CH_3 Symmetric Deformation 3	1264	0.1	C–Si Stretch 3	627	16.1
CH_3 Symmetric Deformation 4	1255	0.2	C–Si Stretch 4	622	1.9
CH_3 Symmetric Deformation 5	1255	0.2	C–Si Stretch 5	620	1.7
CH_3 Symmetric Deformation 6	1251	0.0	C–Si Stretch 6	620	1.7
CH_3 Symmetric Deformation 7	1249	0.1	C–Si Stretch 7	616	0.1

A careful analysis of the infrared intensities provides an important clue in this context. We illustrate this concept by considering two sets of modes, *viz.* the Si–CH_3 stretching vibrations and the symmetric deformations of the methyl groups. Table 1.2.1 lists the frequencies as well as the corresponding intensities of the two sets of modes. The Si–CH_3 stretching modes have seven frequencies ranging from 616 to 637 cm^{-1}. Among them are two sets of degenerate *e* modes but we have listed them individually in this analysis. The calculated intensities of the modes show an interesting observation. The mode at 637 cm^{-1} has an intensity that is greater than that of all the other modes put together. The nature of this mode corresponds to the concerted stretching motion of all the Si–CH_3 groups in tandem. For comparison, the vibration that corresponds to the largest contribution from the central methyl group is at 622 cm^{-1} and is fairly weak. It is clear that as the cluster grows larger the concerted vibration of the methyl groups will pick up more intensity and emerge as the collective vibrational mode that will correspond to the observed vibration in the experimental spectrum. For the other modes, the antagonistic nature of the individual oscillators results in a canceling of the change in dipole moment reducing the vibrational intensity. If the cluster is extended to larger and larger sizes the infrared intensities of the other modes would drop off while the intensity of the concerted motion would rise resulting in the observed vibrational frequency.

In a similar manner, the seven modes corresponding to the symmetric deformation of the methyl groups are also shown in table 1.2.1. In this case, the collective mode corresponding to the symmetric oscillation of all the umbrella modes is the only one with significant intensity while all the other couplings of the umbrella modes have very small intensities.

The assignment of the parallel modes is analogous. For example, the collective methyl group asymmetric deformation mode occurs at 1443 cm^{-1} and is the only mode with significant intensity. From these examples the principles of how to determine which modes correspond to experimentally observed modes can be clearly understood. It is evident that a study of the nature of the modes along with their associated intensities allows us to assign the collective vibrational modes as the modes seen in the experimental spectrum. Our final assignments are illustrated in figure 1.2.4.

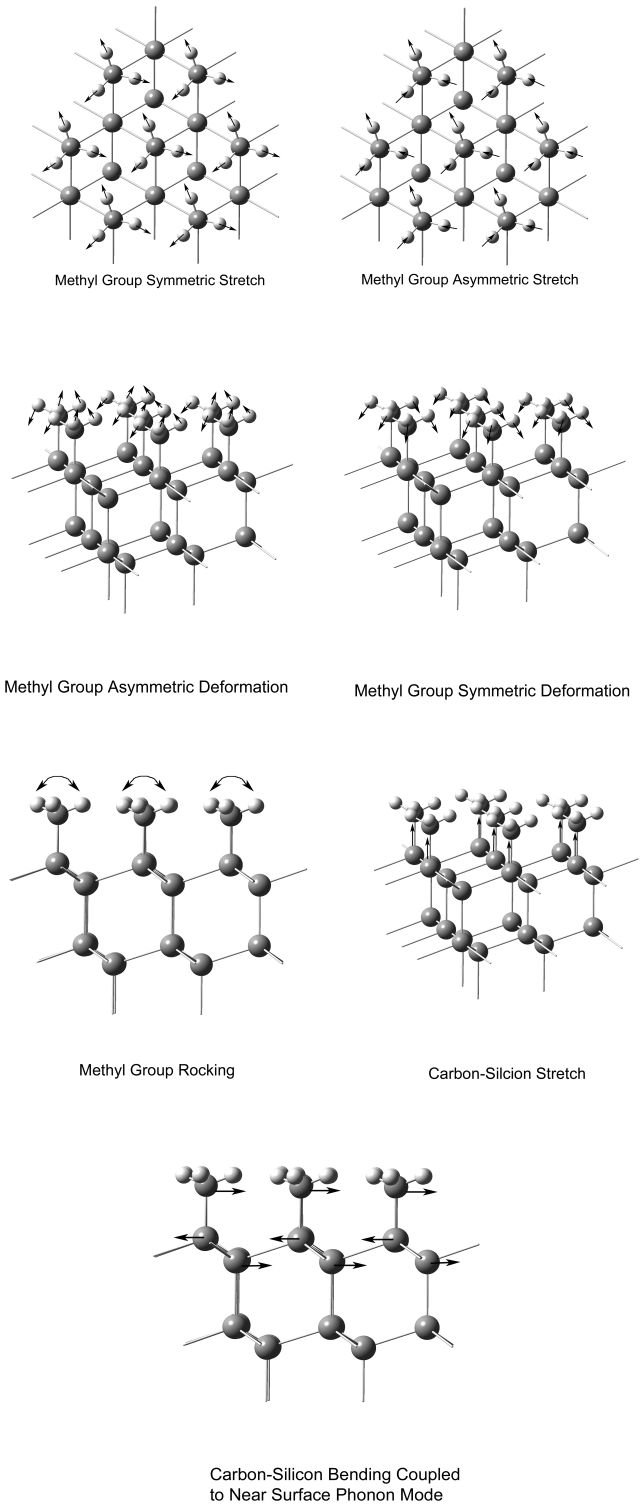

Figure 1.2.4. Pictorial representation of the collective vibrations of the cluster model used for the assignment of the experimentally observed modes.

Table 1.2.2. Comparison of the cluster model and the four- and six-layer PBC models. All frequencies are in wavenumbers, cm^{-1}.

Mode	Cluster	PBC–4	PBC–6
CH_3 Asymmetric Stretch	3063	3055	3060
CH_3 Symmetric Stretch	2991	2993	2992
CH_3 Asymmetric Deformation	1443	1462	1444
CH_3 Symmetric Deformation	1274	1296	1277
CH_3 Rock	782	778	763
C–Si Stretch	637	643	642
C–Si Bend	497	484	478

In order to determine is these models represent a reasonable approximation to the surface, the results of the cluster calculations are compared to PBC calculations with the same model chemistry. Table 1.2.2 summarizes the key collective modes from the cluster calculations along with the Γ-point surface phonons obtained with PBC models containing four and six layers. The results reveal an excellent agreement between the PBC and cluster model vibrations. The mean absolute deviation for 7 vibrational modes between the cluster model and an analogous PBC-4 model is only 10 cm^{-1} and the maximum deviation is 22 cm^{-1}. Such remarkable agreement indicates the frequencies for the small cluster models are well converged with respect to the PBC frequencies. In a similar manner, comparison of the PBC-4 and PBC-6 models shows a mean absolute deviation of about 10 cm^{-1}.

Table 1.2.3 shows a comparison between the frequencies of the unrelaxed cluster model (*vide supra*) and the corresponding optimized structure. If we focus on the collective modes, the differences are within ~27 cm^{-1}. While both methods yield

reasonable frequencies, the optimized structures are inherently asymmetric since the environment of the central methyl group is different than that of the peripheral methyl groups. More importantly, the asymmetry makes it more difficult to identify the emergence of collective modes with the associated intensities. While both models are reasonable in the limit of a large cluster, the truncated cluster model appears to be more appropriate in providing a good approximation of the properties of the extended surface.

Table 1.2.3. Comparison of frequencies (cm^{-1}) between the cluster model obtained from the PBC structure without further optimization (Stiff), and the corresponding cluster model including subsequent optimization (Relax).

Mode	**Stiff**	**Relax**
CH_3 Asymmetric Stretch	3063	3048
CH_3 Symmetric Stretch	2991	2975
CH_3 Asymmetric Deformation	1443	1447
CH_3 Symmetric Deformation	1274	1274
CH_3 Rock	782	792
C–Si Stretch	637	664
C–Si Bend	497	479

Comparison with Experiment

Table 1.2.4 shows the vibrational frequencies determined experimentally from HREELS[46] and Surface IR[33] along with the cluster and PBC calculations from the current study. Since IR typically has a higher resolution, the calculations will be compared to the IR study unless the frequencies are unresolved in the spectrum. The cluster and PBC calculations show the asymmetric stretch for the methyl groups at 3063 cm^{-1} and 3060

cm^{-1} respectively. The symmetric stretch is also in close agreement at 2991 cm^{-1} for the cluster model and 2992 cm^{-1} for the PBC model. These frequencies are overestimated with respect to experiment by a few percent due to the neglect of anharmonicity effects. In the case of the asymmetric deformation, the HREELS value of 1423 cm^{-1} and the surface IR value of 1410 cm^{-1} [17] are close to the PBC value of 1444 cm^{-1} and the cluster value of 1443 cm^{-1}. The symmetric deformation is at 1274 cm^{-1} and 1277 cm^{-1} for the cluster and PBC, respectably. The methyl rock is computed at 782 cm^{-1} and 763 cm^{-1} for the cluster and PBC, respectably. Both these modes are in excellent agreement with the results from the experiments (table 1.2.4).

Table 1.2.4. The frequencies (cm^{-1}) from the 6-layer PBC model, the cluster model, and the experimental HREELS and surface IR spectra.

Mode	**HREELS[a]**	**Surface IR[b]**	**Cluster**	**PBC–6**
CH_3 Asymmetric Stretch	2944	2967, 2960[c]	3063	3060
CH_3 Symmetric Stretch	2854	2910, 2900[c]	2991	2992
CH_3 Asymmetric Deformation	1423	1410[c]	1443	1444
CH_3 Symmetric Deformation	1268	1258, 1255[c]	1274	1277
CH_3 Rock	789	754	782	763
C–Si Stretch	683	678	637	642
C–Si Bend	507	-	497	478

[a] ref 232 [b] ref 8,93 [c] ref 17

The two lower frequencies are underestimated by a few percent. In the case of lower frequencies, the uncertainty in the computations is typically larger than the effect of anharmonicity making it possible for computed frequencies to be higher or lower than experiment. The carbon-silicon stretch at 639 cm^{-1} in the cluster model and 642 cm^{-1} in

the PBC model is a small underestimation of the HREELS (683 cm^{-1}) and IR (678 cm^{-1}) experimental assignments. Finally, a mode observed at 507 cm^{-1} was assigned to the carbon-silicon bend in the HREELS spectrum. While such a mode was not assigned in the IR spectrum, a small peak is clearly discernible ~ 522 cm^{-1}. This is close to the calculated value of a mode at 476 cm^{-1} for the cluster and 478 cm^{-1} for the PBC model. This mode results from the coupling of near surface phonon modes to the carbon-silicon bend and will be discussed in more detail (*vide infra*). The final two modes are exactly analogous to the corresponding modes seen in the case of Cl-terminated Si(111) surface. It is interesting to note that the model chemistry used in the current work underestimated these two frequencies for Cl/Si(111) by ~ 35 cm^{-1}, similar to the underestimation seen in the current work. Preliminary explorations with B3LYP/6-31G(d,p) yield higher frequencies, closer to the observed values. Overall there is excellent agreement between the cluster model and PBC model frequency assignments. The assignments of the modes give an accurate interpretation of the experimental spectra.

The low frequency mode at 522 cm^{-1} deserves further comment. The mode clearly shows mixed character, indicating a coupling between the parallel vibration of the carbon-silicon atoms and the surface phonon modes. In particular, it has a strong contribution from the motion of the silicon atoms in the first two layers. It is very similar to parallel mode seen on the chlorinated Si(111) surface at 527 cm^{-1} that was also dominated by the motion of the near surface silicon atoms.[10] Such phonon modes usually do not appear in difference spectra. The phonon vibrations should be very similar in the sample and reference spectra and would not be expected to have a measurable intensity. However, if they are coupled to the adsorbate vibrations and increase in intensity due to

this coupling, they can be seen in surface spectra. It will be interesting to see if this is a general feature of singly terminated silicon (111) surfaces for other functional groups.

There is also excellent qualitative agreement between the relative intensities of the cluster model and the IR spectrum. Table 1.2.5 shows the relative intensity agreement. The exception is the asymmetric deformation of the methyl group, which was not resolved in the experimental spectrum.

Table 1.2.5. The relative intensities of the vibrations in the cluster model calculations and the surface IR spectrum, in arbitrary units.

Mode	**Cluster**	**Surface IR**
CH_3 Asymmetric Stretch	medium	medium
CH_3 Symmetric Stretch	medium	medium
CH_3 Asymmetric Deformation	medium	weak
CH_3 Symmetric Deformation	medium	medium
CH_3 Rock	strong	strong
C–Si Stretch	medium	medium
C–Si Bend	medium	medium

Conclusions

We have clearly demonstrated that the complexity of the vibrational spectrum for the methyl-terminated silicon surface can be captured with cluster models. We demonstrate that relatively small cluster models already show the emergence of collective vibrational modes and provide a general method for the assignment of vibrational frequencies for extended surfaces from cluster models. The computed frequencies are in good agreement with those from PBC calculations and are used to explain the features observed in the experimental spectra. Finally, we discuss a vibrational mode that results from the coupling between near-surface phonons and the silicon-carbon bending modes.

1.3 Acetyl and Methylacetylated Si(111) Surfaces

Organic functionalization of semiconductor surfaces is an area of growing interest with a large body of literature.[3, 13, 14, 21, 22, 25, 26, 28, 47] Organic functionalization of silicon offers chemists the possibility of molecular-level control of semiconductor surface features and tailored electronic properties.[11, 12, 19, 24, 48-50] Hybrid organic-inorganic materials have great potential for improving silicon and silicon oxide based devices, and could potentially lead to important applications in areas such as biosensors.[20] Unfortunately, the bare silicon surface is far too reactive for use in industrial applications. Rapid oxidation occurs upon atmospheric exposure. Early methods to address this problem utilized hydrogen[7] or chloride[10] passivation, and thermal, ultraviolet or free radical activation.[16] A more promising possible route to passivation is alkylation of the surface. Much work has been accomplished in the alkylation of silicon surface.[51-58] Recently, organic functionalization involving a two-step chlorination/alkylation has been improved by Lewis and coworkers.[28-30, 59] Methyl passivation was found to be effective using a two-step chlorination/methylation with the Grignard reagent. The resulting surface has been characterized using several experimental methods by Fidelis et al.,[17] Yamada et al.[32, 46], and by Web et al.[33, 60] Methyl passivation stabilizes the silicon (111) surface to oxidation for long periods of atmospheric exposure (> 600 hours).[8] Stabilized surfaces are critically important for the manufacture of complex materials.

A significant factor in passivation of the surface by methylation is steric interactions. The distance between the nearest surface silicon atoms (3.8 Å) and the van der Waals radius of a methyl group (2.3 Å) are such that it is possible for the methyl groups to form a complete, albeit strained, monolayer on the silicon (111) surface.

Results for larger chain alkyls indicate complete coverage is not possible.[8, 29] As previously noted by Solares et al.[29] and in our previous work,[61] the dihedral angle adopted by the surface methyl groups results from a balance between the steric repulsion of the hydrogen atoms and the torsional strain of the methyl groups with respect to the underlying silicon surface. This balance of forces will be discussed in detail (*vide infra*).

While the two-step chlorination/methylation procedure stabilizes the surface, it does not readily facilitate further functionalization.[18] Attachment of organic groups to the surface is more readily achieved through unsaturated organic species. Advancement toward this end was recently achieved by Lewis and coworkers, who functionalized the silicon (111) surface with Si–C≡C–R moieties, with R = H, CH_3. With R = H, there are greater opportunities for functionalization. With R = CH_3, the steric strain of the methyl groups is removed while maintaining passivation. In addition, the R = CH_3 moiety allows for further exploration of the steric interactions between the methyl groups by spacing them away from the surface.

Currently, high-resolution vibrational spectra of these functionalized surfaces over a large frequency range are not available in the literature. Accurate vibrational spectra are a powerful tool in analyzing structural features of surface adsorbates as demonstrated in recent work.[7, 9-12, 33, 48, 62] Theoretical modeling of vibrational spectra can easily be carried out for reasonably sized molecular systems, greatly simplifying the interpretation. If treated as a fully periodic system the surface structure can be accurately modeled but analytical second derivative techniques to evaluate the force constants are computationally expensive. In a recent paper we have investigated the use of cluster models and periodic boundary conditions (PBC) numerical frequencies to model

vibrations of methylated Si(111) surfaces.[61] The procedure (*vide infra*) allows for the simple assignment of surface adsorbate vibrational frequencies making it possible to accurately predict vibrational frequencies from cluster models. In the present work we have used this method to predict the structure and vibrational frequencies of ideally passivated acetylenyl and methylacetylenyl functionalized Si(111) surfaces.

Computational Details:

Vibrational frequencies of acetylenyl and methylacetylenyl functionalized Si(111) surfaces were evaluated using a procedure that combines PBC optimization with harmonic frequency analysis using finite clusters. These calculations were then compared to PBC numerical frequencies. The PBC and cluster model calculations used the B88 exchange functional[35, 36] with the Lee-Yang-Parr electron correlation functional.[37] All calculations were performed with the 6-31G(d,p) basis set[38] (BLYP/6-31G(d,p) model chemistry). Hybrid functionals such as B3LYP that are usually prohibitively expensive for PBC calculations could be easily used with cluster models to improve the accuracy of the computed frequencies; however, for the systems under investigation in this study, the behavior of BLYP and B3LYP with the same basis set were similar. The largest difference is the Si–Si distance that is systematically longer by 0.04 Å in BLYP/6-31G(d,p) relative to B3LYP/6-31G(d,p). The PBC implementation of Kudin and Scuseria[39-41] using atom centered basis functions was used for PBC calculations.

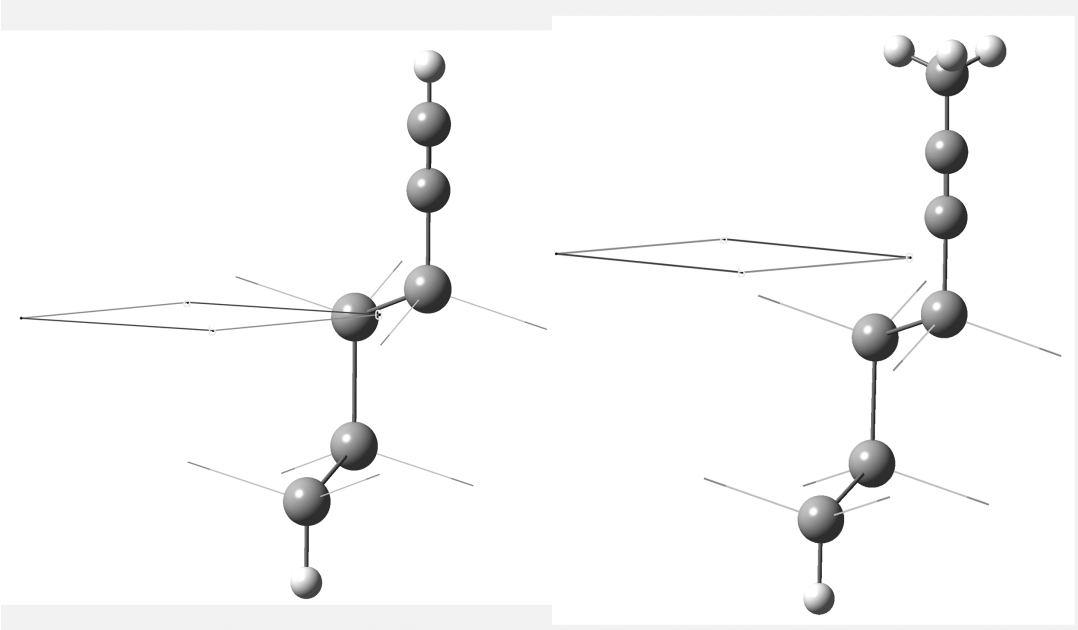

Figure 1.3.1. Side-view of the PBC models with a single unit cell for the acetylenyl (left) and methylacetylenyl (right), with light grey representing silicon, dark grey representing carbon, and white representing hydrogen.

The silicon surface was represented by both PBC and cluster models. Ball and stick representations of the PBC models used are shown in figure 1.3.1. Models used included four silicon layers, which have been shown to be sufficient for the relatively unstrained Si(111) surface.[61] Hydrogen termination was used on the lowest layer silicon atom to maintain the hybridization and to avoid dangling bonds.[34] All PBC calculations were preformed without adding constraints to the atoms. Cluster models were built from the optimized PBC structures with small modifications to maintain symmetry. More specifically, cluster models of increasing size containing seven and thirteen acetylenyl groups bound to the surface were built. This allows us to explore the convergence of the

computed vibrational frequencies with cluster size. Figure 1.3.2 shows cluster models containing seven acetylenyl and methylacetylenyl groups (and four silicon layers). The dangling bonds on the silicon atoms that were created in forming the cluster models were terminated with hydrogen (Si–H = 1.47 Å) to maintain the valence state of the silicon atoms found in the extended system.

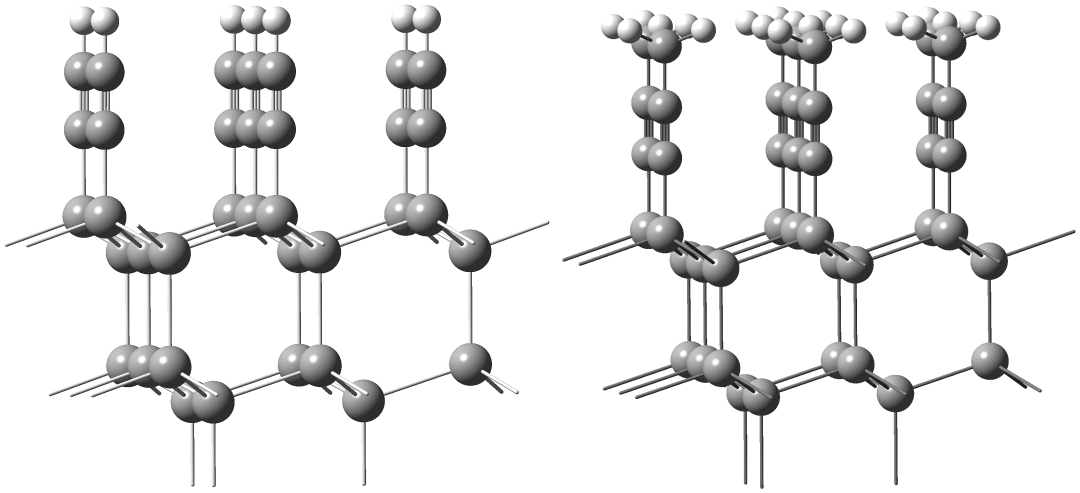

Figure 1.3.2. Acetylenyl (left) and methylacetylenyl (right) side views of the $Si_{22}H_{21}(R)_7$ cluster models. For simplicity, the methylacetylenyl structure is shown with linearized C≡C–CH_3 and Si–C≡C angles.

To our knowledge, analytic force constants for periodic systems have not been implemented in any widely available quantum chemical code and their implementation is beyond the scope of this work. In order to obtain frequencies for the PBC optimized structures the finite difference method was used. The analytically obtained forces were numerically differentiated using small perturbations to the Cartesian coordinates (0.001

Å). The resulting force constant matrix was then mass-weighted and diagonalized to yield the harmonic vibrational frequencies (eigenvalues) and normal modes (eigenvectors). There are several assumptions implicit in this calculation. The first is that the chosen unit cell faithfully replicates the extended surface. The other is that including only Γ-point surface-phonon modes is sufficient to interpret the observed infrared vibrational modes. The second assumption is supported by previous calculations on the methyl-terminated surface.[61] We therefore believe definitive assignment of the vibrational frequencies is possible for such surfaces even without including phonon-dispersions. Implementation of the finite difference method used a modified version of the *Gaussian* program suite.[42]

Results and Discussion

Geometric Parameters

The structure of the acetylenyl silicon (111) surface is much simpler than the methylacetylenyl silicon (111) surface. As previously observed, it is possible to form a complete acetylenyl monolayer on the silicon (111) surface. The linear adsorbate can satisfy the dangling bonds on all surface silicon atoms as illustrated in figure 1.3.2. Upon adsorption, the acetylenyl group stays linear and is oriented perpendicular to the surface. The distance between neighboring acetylenyl groups on the surface is ~ 3.9 Å, which provides no steric hindrance between groups, leading to complete monolayer coverage.

In the case of the methylacetylenyl surface, however, significant steric interactions are present between adjacent methyl groups. In previous work on the methylated silicon (111) surface, the key geometric parameter is the dihedral angle of the methyl groups relative to the surface. This parameter, defined by H–C–Si–Si, has the competing forces of torsional strain with respect to the underlying surface and steric

repulsion from the neighboring methyl groups on the surface. The optimized dihedral angle of the methyl groups to balance these forces has been calculated at around 40°.[29, 31, 61, 63] It is interesting to note that all calculated values differ from the experimentally measured value of 23°, and this difference has been explained by Goddard and coworkers to be the result of etch pits.[29, 31, 63] In the case of the methylacetylenyl functionalized silicon (111) surface, the torsional strain with the underlying surface is removed due to the intervening –C≡C– group. The only remaining factor is the steric repulsion from the neighboring methyl groups on the surface, leading to methyl group dihedral relaxation to minimize this repulsion. This occurs at a dihedral angle of 30°, and this relaxation increases the distance between neighboring hydrogen atoms from 2.32 Å in the methylated surface to 2.56 Å in the methylacetylenyl silicon (111) surface. In the absence or other structural defects (e.g. etch pits) the dihedral angle of the methyl group will thus be at the ideal value of 30°. Indeed, our optimized value at the BLYP/6-31G(d,p) level occurs at 29.5°, confirming this expectation.

When discussing the symmetry of a periodic arrangement of surface adsorbed species, the local point groups of the molecular analogs may no longer be sufficient. In the case of the ideal Si(111) surface, the local point group of a surface atom attached to a simple adsorbate, e.g., H or Cl, has C_{3v} symmetry. In the case of our acetylenyl species, the linear adsorbate maintains the same C_{3v} symmetry. If we consider the two-dimensional or wallpaper space group symmetry, the corresponding symmetry is P3m1 where the planes of reflection pass through the lower layer silicon atoms.

In the case of the methylacetylenyl surface, however, the recognition of the symmetry elements is more difficult. In particular, the methylacetylenyl surface contains

higher symmetry at rotations of the H–C–Si–Si dihedral angle of 60° (C_{3v} symmetry) and 30° (C_3 symmetry). While the symmetry of the 60° form is similar to that of the simple adsorbates mentioned above, the higher symmetry of the 30° conformation is not obvious. In order to see these symmetry elements it is instructive to examine the distances between the methyl hydrogen atoms. Figure 1.3.3 shows the distance between the methyl groups for the 60° form. The two hydrogen-hydrogen distances shown capture all of the necessary details to explain the surface symmetry. At the BLYP/6-31G(d,p) level, the distance of 2.17 Å is at a minimum in the rotation space while the distance of 3.42 Å is a maximum in the rotation space. As the angle changes from 60°, the shorter distance gradually increases while the longer distance gradually decreases. The angle of 30° is the point at which both distances become equal, 2.56 Å, as seen in Figure 1.3.3. This is the structure that minimizes the steric interactions between neighboring methyl groups and thus has higher apparent symmetry. The difficulty in describing the 30° structure with point groups is because some of the symmetry elements result from two-dimensional periodicity. If the lower layer atoms are ignored, it is possible to assign two-dimensional space groups to the surface adsorbates. All general dihedral angles less than 90° but not 30° or 60° belong to the P3 space group. The angles of 60° and 30° have the higher symmetry space groups of P3m1 and P31m, respectively. For 60° the mirror planes formed in the group are true mirror planes even when the underlying atoms are taken into account (full C_{3v} local symmetry). Similar symmetry elements are not present for the case of 30° where the symmetry is reduced to P3 (C_3 local symmetry) if the second layer and below are included.

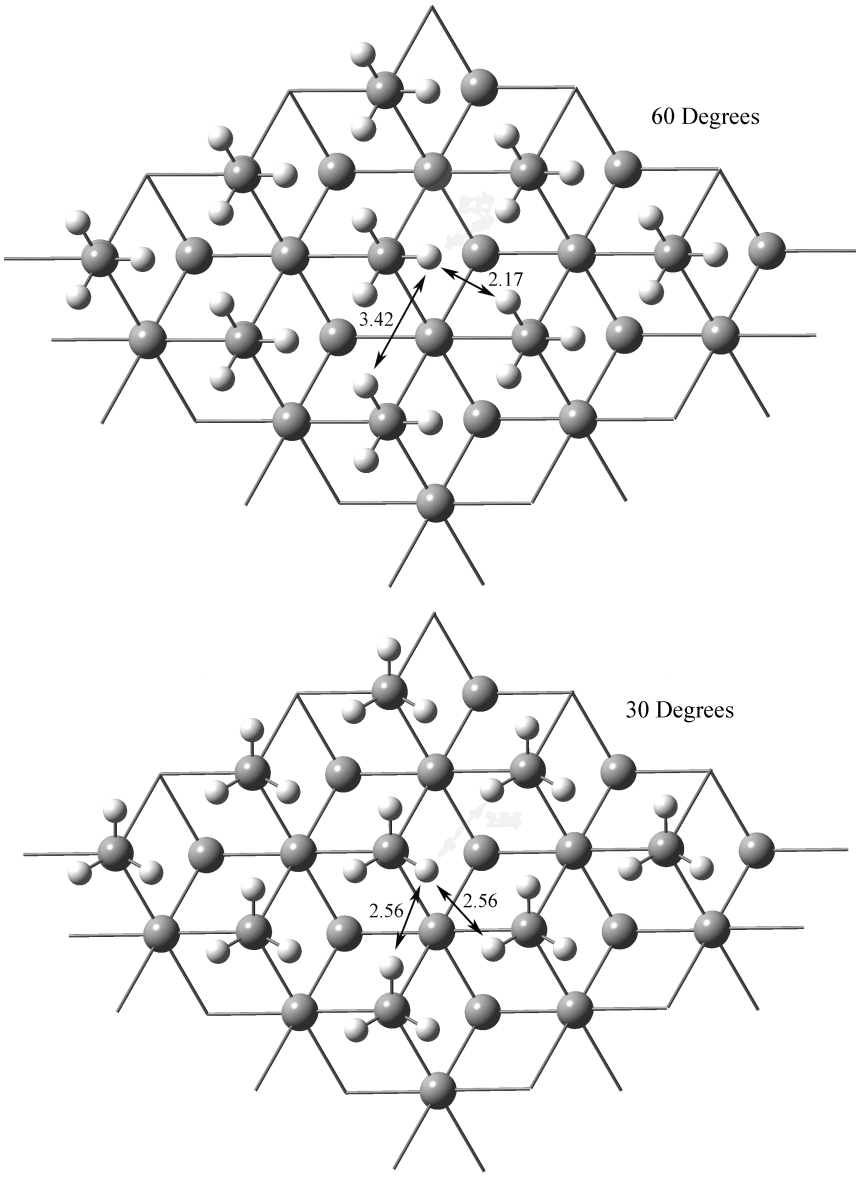

Figure 1.3.3. A top down view of the key hydrogen-hydrogen distances from rotation of the H-C-Si-Si dihedral angle 60° (top) and 30° (bottom). Distances are given in angstroms. For the angle of 60° (top) these distances indicate a minimum distance between one set of hydrogens at 2.17 Å while the other hydrogen-hydrogen distance is at a maximum of 3.42 Å. The angle of 30° (bottom) is the point at which these two distances become equal at 2.56 Å.

In the case of the methylacetylenyl surface, the Si–C≡C–CH_3 moiety in the optimized PBC structure was found to be bent slightly away from linearity. The optimized C≡C–CH_3 and Si–C≡C angles were found to be 177° and 172°, respectively. In order to determine if this is significant, we performed single point PBC calculations where these two angles were linearized, while the rest of the geometrical parameters were held at their optimized values. The energy difference between these structures is, however, very small, ~ 0.21 kcal/mol, and may be indicative of a slight residual strain relief. To test the effect of this non-linearity on the computed frequencies, we performed calculations on the cluster model with the structure extracted from the PBC optimization and with linearized C≡C–CH_3 and Si–C≡C bond angles. Both calculations give essentially the same values for all the frequencies of interest that are discussed in this work. We have therefore concluded that this feature, though somewhat interesting, is not important from the vibrational point of view, and may be examined in future studies.

Vibrations

The method for obtaining the vibrational frequencies of the cluster model is as follows. The structure is first obtained using a fully two-dimensional PBC optimization. The resulting structure is then used to construct a cluster model (*vide supra*). A frequency calculation is then performed on the cluster model *without optimization*. In our previous paper on the methylated surface, we showed that optimizing the structure without additional constraints results in unphysical relaxation of the adsorbates (such as methyl or methylacetylenyl groups) and destroys the intrinsic symmetry of the system.[61] While it is never a good idea to perform a frequency calculation on non-equilibrium geometries *without careful consideration*, in this case it is justified. As the cluster is made larger it

goes increasingly toward the PBC minimum. At the limit of a very large cluster it can be expected to be the true PBC minimum. Since the cluster minimum can have unphysical structural distortions due to the steric interactions, the PBC minimum is the true minimum of interest. While the resulting vibrations are not the true vibrations of the cluster (since the cluster is not at a minimum) they do correspond to the vibrations of the infinite system.

Table 1.3.1. The frequencies (cm^{-1}) for the seven and thirteen acetylenyl adsorbate clusters compared to the PBC values.

Mode	**7 Adsorbate Cluster**	**13 Adsorbate Cluster**	**PBC**
CH Stretch	3413	3412	3410
C≡C Stretch	2076	2070	2071
C-Si Stretch	646	641	645
CH Bend	589	584	568
Phonon-Bend Coupling	484	485	492

In order to determine how quickly the cluster frequencies converge to the PBC frequencies we have performed vibrational calculations with seven and thirteen surface acetylenyl groups. To find the correspondence between the cluster and the PBC vibrations we have previously developed a simple method.[61] The presence of seven (or thirteen) different groups on the surface will give seven (or thirteen) different vibrational frequencies for each mode perpendicular to the surface (the non-degenerate *a* representation), and seven (or thirteen) pairs of different frequencies for each mode parallel to the surface (the doubly degenerate *e* representation). Our previous study shows that the only a collective vibration (concerted motion of the groups in different unit cells) picks up significant vibrational intensity with increasing cluster size. The intensities of

non-concerted modes fall off as cluster size increases. Therefore we have been able to identify the vibrations corresponding to the periodic structure as corresponding to the collective vibrational modes from a relatively modest cluster calculation. As can be seen in table 1.3.1, the modes for both seven and thirteen surface acetylenyl adsorbates are very close to the PBC values, indicating relatively quick convergence with cluster size. The mean absolute deviation from the PBC frequencies is only 8 cm^{-1} for the smaller cluster (seven groups) and even smaller (6 cm^{-1}) for the larger cluster (thirteen groups). In fact, the only mode with a deviation greater than 10 cm^{-1} is the C–H bend, perhaps indicating a greater long-range effect to the force constant of this mode. Overall, it is clear that a small cluster containing only seven groups is adequate to make an accurate prediction of the vibrational frequencies of the fully periodic system.

Table 1.3.2. The frequencies (cm^{-1}) for the methylacetylenyl Si(111) surface from the PBC and cluster models containing seven adsorbates.

Mode	**Cluster**	**PBC**	**Difference**
CH_3 Asymmetric Stretch	3003	2999	4
CH_3 Symmetric Stretch	2957	2956	1
C≡C Stretch	2208	2205	3
CH_3 Asymmetric Deformation	1449	1448	1
CH_3 Symmetric Deformation	1392	1393	−1
C-C Stretch	1031	1029	2
CH_3 Rock	1018	1018	0
C-Si Stretch	580	558	22
Phonon-Bend Coupling	487	489	−2

Table 1.3.3. The frequencies (cm^{-1}) for the acetylenyl Si(111) silicon surface using PBC and cluster models containing seven adsorbates.

Mode	Cluster	PBC	Difference
CH Stretch	3413	3410	3
C≡C Stretch	2076	2071	5
C-Si Stretch	646	645	1
CH Bend	589	568	21
Phonon-Bend Coupling	484	492	−8

Using the above-mentioned technique, assignment of the surface and adsorbate frequencies is relatively straightforward. Modes for the acetylenyl and methylacetylenyl silicon (111) surface are shown in figures 1.3.4 & 1.3.5. Cluster (seven adsorbate groups) and PBC calculated frequencies give excellent agreement, tables 1.3.2 & 1.3.3. The mean absolute deviation (MAD) is ~ 8 cm^{-1} and 4 cm^{-1} for the acetylenyl and methylacetylenyl Si(111) surface, respectively. For the acetylenyl Si(111) surface, the largest difference between the PBC and cluster calculations is 21 cm^{-1}, which corresponds to the low-frequency carbon-hydrogen bending mode. The largest deviation between the PBC and cluster calculations of methylacetylenyl Si(111) surface is 22 cm^{-1} and corresponds to the carbon-silicon stretching mode. It is, therefore, reasonable to assume the cluster model is an accurate representation of the extended surface within the harmonic approximation.

The experimental spectrum of each surface absorbed species will have characteristic modes that can be used to assist in the interpretation of the spectrum. For a mode to be characteristic it must be out of the phonon region (i.e., > 500 cm^{-1} for silicon), in an area of the spectrum that is free from overtones, and in an area of the

spectrum with relatively few modes. The calculated acetylenyl Si(111) vibrational spectrum has two possible characteristic high-frequency modes, the C–H stretch occurring at 3413 cm^{-1} and the C≡C stretch at 2076 cm^{-1}. However, the C≡C stretch at 2076 cm^{-1} is too close to the Si−H stretch region to be very useful. The methylacetylenyl surface shows two characteristic modes, the umbrella mode (i.e., methyl symmetric deformation) at 1393 cm^{-1} and the C≡C stretch at 2205 cm^{-1}.

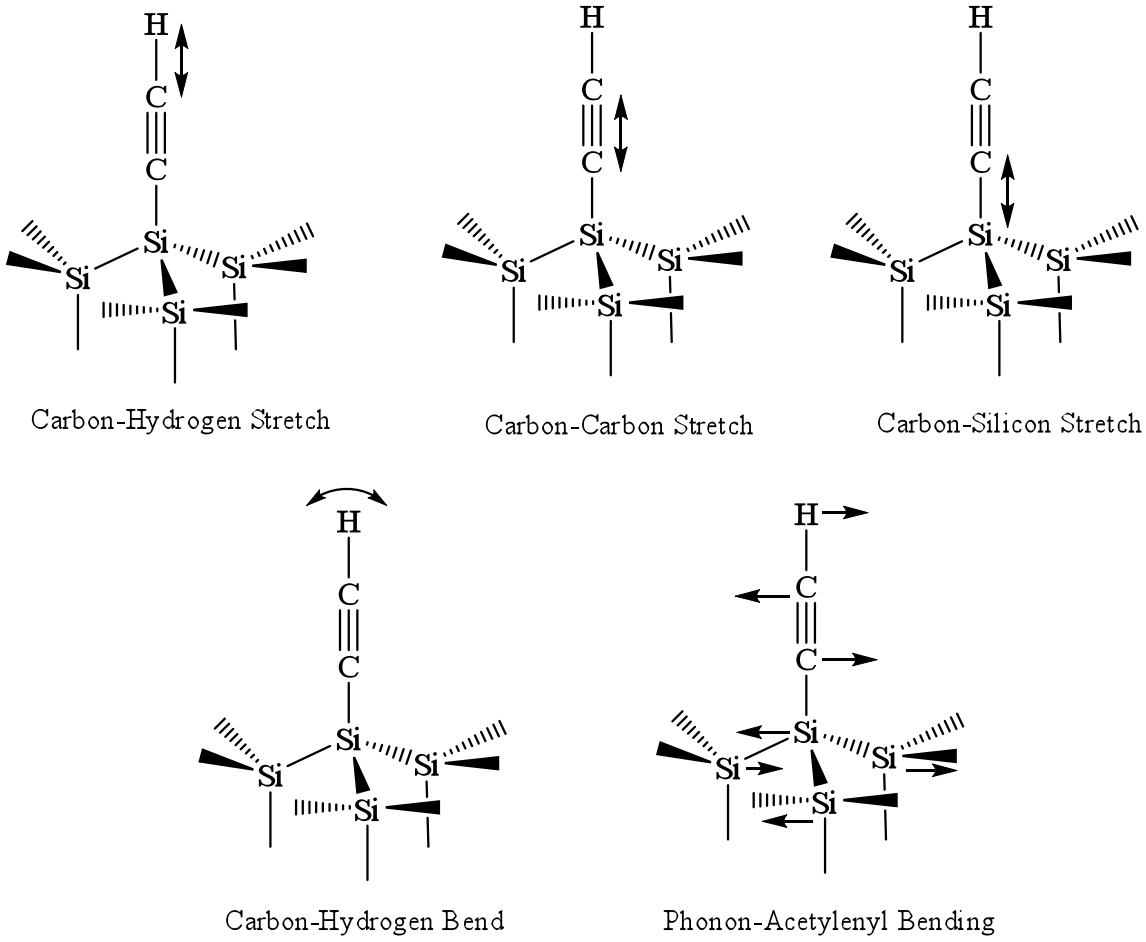

Figure 1.3.4. A schematic representing the vibrational modes of the acetylenyl Si(111) surface. Only normal modes corresponding to a surface vibration or the coupling of adsorbate-phonon modes are shown.

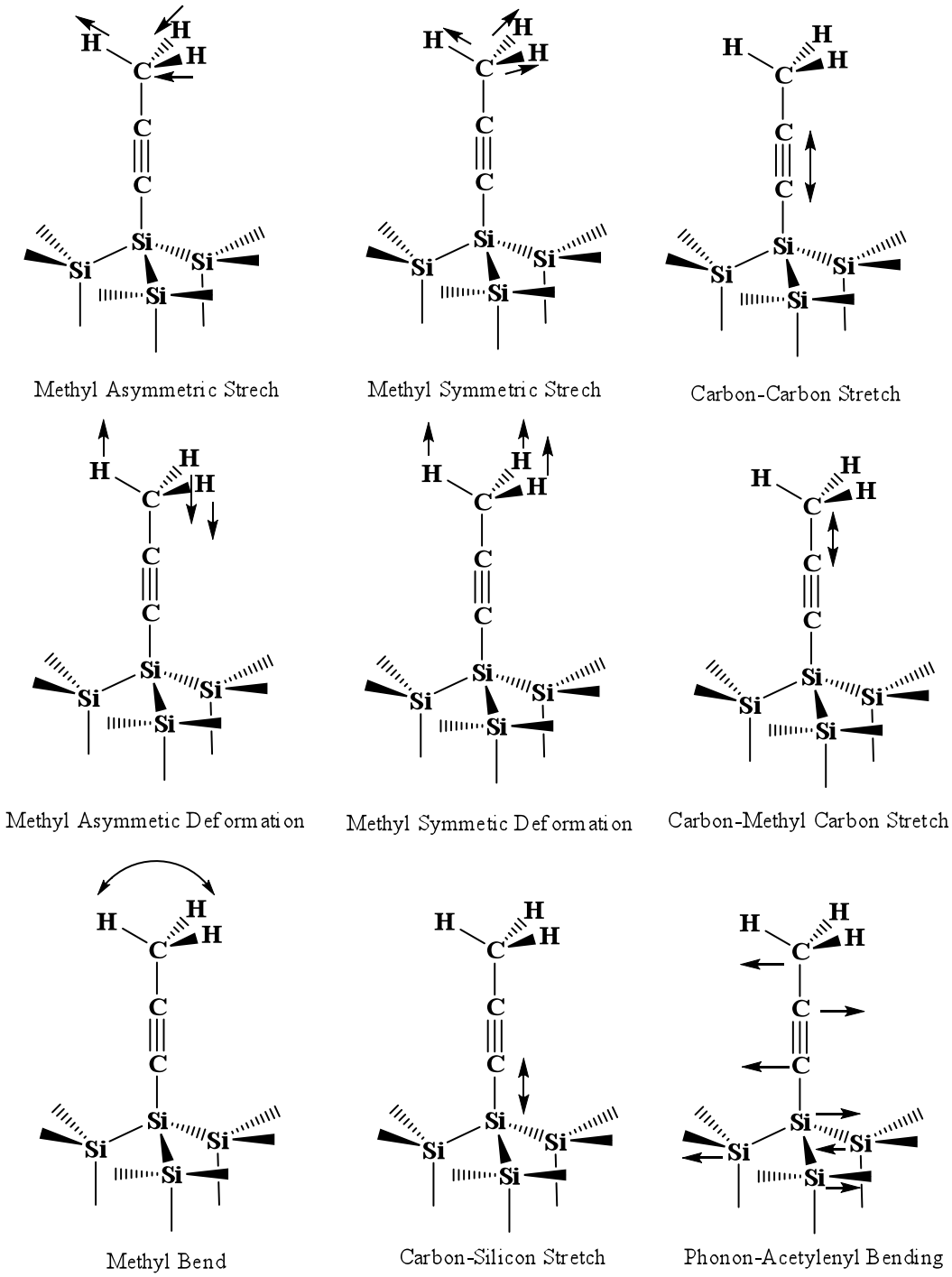

Figure 1.3.5. A schematic representing the vibrational modes of the methylacetylenyl Si(111) surface. The normal modes for the surface adsorbate and the coupling between the adsorbate and the surface phonons are shown.

As previously mentioned (*vide supra*) no high quality experimental results are available for systems of this type. However, in a recent paper, the C≡C stretch mode was reported in the acetylenyl spectrum published by Hurley et al.[18] at 2176 cm^{-1}. This is much higher than the corresponding computed value of 2076 cm^{-1} which is surprising since uncorrected theoretical harmonic frequencies for such high frequency modes tend to be higher than experiment. It is also interesting that the measured value is closer to the computed value for methylacetylenyl surface. Investigations with molecular analogs suggest that a dimerized form such as $H_3Si–C≡C–C≡C–H$ will have significantly higher C≡C frequencies than a monomeric form such as $H_3Si–C≡C–H$. A possible explanation for the difference between experiment and theory could be that the experimentally observed mode corresponds to a dimerized or derivatized acetylenyl surface instead of a clean monolayer as reported.

Table 1.3.4. Differences in methyl group frequencies (cm^{-1}) between methylated and methylacetylenyl Si(111) surfaces using cluster models containing seven adsorbates.

Mode	**Methyl**	**Methylacetylenyl**	**Difference**
CH_3 Asymm Stretch	3063	3003	60
CH_3 Symm Stretch	2991	2957	34
CH_3 Asymm Deformation	1443	1449	−7
CH_3 Symm Deformation	1274	1392	−118
CH_3 Rock	782	1018	−237
C-Si Stretch	637	580	57
Phonon-Bend Coupling	497	487	10

The differences between the methylacetylenyl and the methylated Si(111) surfaces allow us to probe the shifting of the methyl group frequencies due to differences in the environment. Several large differences can be seen in table 1.3.4. Most notable is the large shift of 237 cm^{-1} for the methyl rocking mode. While large, it is not unexpected

considering the change of bonding environment from a tetrahedral silicon in the methylated Si(111) surface to the linear –C≡C– group in the methylacetylenyl Si(111) surface and the removal of the strain with the underlying surface. The remaining large difference of 118 cm^{-1} for the umbrella mode is due to a change in the bond length of the nearest neighbor from 1.50 Å (C–C) in the methylacetylenyl surface to 1.94 Å (C–Si) in the methylated surface. The asymmetric deformation does not show a similar sensitivity to the local bond distance, shifting by only 7 cm^{-1}. A possible reason for this small change is the removal of the interaction with the first surface layer. The same trend was observed in calculated values for the small molecule analogs of the system. A similar argument accounts for the frequency shift of the carbon-silicon stretch and the phonon--bend coupling mode (*vide infra*). The C–Si bond distance changes from 1.94 Å for the methylated to 1.83 Å for the methylacetylenyl resulting in a shift of 57 cm^{-1} for the carbon-silicon stretch and a shift of 10 cm^{-1} for the phonon-bend coupling. The difference of 60 cm^{-1} in the methyl asymmetric stretch and 34 cm^{-1} in the methyl symmetric stretch can also be explained by small changes in the corresponding carbon-hydrogen bond lengths.

All of the vibrational modes thus far discussed are not unique to surface bound species. Each of the modes can be found in cleverly chosen molecular analogs and while the effect of the surface may shift the mode its quintessence remains the same. This is not true for the mode which occurs at 484 cm^{-1} in the acetylenyl Si(111) surface or the mode at 487 cm^{-1} in the methylacetylenyl Si(111) surface. These modes are the result of weak coupling between the surface adsorbate bending and near-surface phonon motion parallel to the surface. In most surface infrared spectroscopic measurements, a difference

spectrum between the sample spectrum and a reference spectrum is measured and phonon modes (relatively constant between the reference and the sample) are usually not observed. However, in the case of the coupled vibrations under discussion, it may be possible to observe such modes experimentally even in difference spectra due to a shift in the position or the intensity of the sample modes from the reference modes. Such a mode has been previously observed experimentally in the chlorinated[10, 33] case at 527 cm^{-1} and the methylated case at 522 cm^{-1}.[33] The mode appears quite general for unreconstructed Si(111) surfaces and we expect most functional groups that have modes parallel to the surface to include a phonon-coupled bending mode in this region of the spectrum.

Conclusions

In summary, we have predicated the structures and vibrational spectra of acetylenyl and methylacetylenyl Si(111) surfaces using a cluster model approach. We have also shown the collective vibrational frequencies of small cluster models are sufficient to make vibrational assignments. These frequencies will be useful in the interpretation of any future experimental spectra. In addition, we have identified characteristic vibrational modes that can be used to determine if these groups are adsorbed on the surface and explained the vibrational shifts between the previously characterized methylated and methylacetylenyl surface. Finally, we have observed a phonon-bend coupling mode we believe to be a general feature in spectra of this type.

1.4 Mixed H/Cl Si(111) Surfaces

The chemistry of functionalized silicon surfaces is an area of great scientific interest due to the ubiquitous use of silicon in microelectronics devices.[3] Functionalized silicon surfaces offer the possibility of extending the range of applications of semiconductor materials with tailored physical and chemical properties.[13, 14, 16, 18, 23, 26, 47, 50, 64-66] However, the determination of surface structure and properties after functionalization is a challenging task. A powerful approach to this problem is the use of surface infrared spectroscopy to characterization the surface.[6, 67] While experimental spectra may be analyzed to determine surface structures in favorable cases, the technique is most powerful when spectra are interpreted using accurate quantum chemical calculations.[34, 47, 68] Using this composite approach, previously ambiguous and difficult spectra can be definitively interpreted. In particular, the combination of theoretical calculations and experimental observations has been used successfully to understand semiconductor surface spectra for many adsorbates on the Si(100) surface. Relatively small cluster calculations treating a single dimer or a pair of adjacent dimers have been found to be adequate in most cases.[34, 61, 69] Interestingly, such cluster models are somewhat deficient for adsorbates such as methyl groups on the Si(111) surface, particularly at high coverage where they undergo unphysical deformations if optimized fully.[34, 61, 69] We have recently developed techniques to calculate the vibrations of these surfaces that combine periodic boundary conditions (PBC) optimization with efficient cluster vibrational calculations. Thus far the technique has only been applied to uniform monolayers of a single adsorbate (Cl, H, D, CH_3, etc.). In order to extend the range of applicability of such methods, we now investigate the Si(111)-H/Cl surface, and compare

the results to experimental data to gain a complete understanding of mixed coverage surface spectra.

Organic derivatives are some of the most promising functional groups currently being studied for modifying silicon surfaces. These molecules have many novel and interesting properties along with a vast body of literature making them attractive molecules for functionalizing surfaces. The most basic functionalization is the alkylation of the Si(111) surface.[9, 11, 12, 17, 25, 28, 29, 32, 34, 46, 54-56, 61, 62, 69] Alkylation can be accomplished by a three-step procedure starting with the bare Si(111) surface. The surface is hydrogen passivated which converts it from the complex 7×7 reconstruction to the nearly atomically flat unreconstructed 1×1 surface.[7, 70] The surface is then chlorinated using a reagent such as PCl_5[8, 9, 11, 31, 60, 71, 72] or molecular chlorine,[73] and finally alkylated using a Grignard type reagent.[9, 18, 46, 54, 56, 59, 72] Initial studies were carried out with methyl termination while subsequent studies have examined unsaturated groups such as acetylenyl and methylacetylenyl. Such functional groups can presumably be used for further functionalization to attach more complex organic molecules or biomolecules on silicon surfaces.

Whatever the subsequent functionalization, the initial chlorination process is critical to the chemistry of these surfaces. During the chlorination process the surface is partially covered by chlorine and hydrogen. The goal of chlorination is to replace the nearly ideal hydrogen monolayer with a nearly ideal chlorine monolayer. Knowledge of the percent surface coverage would allow a deeper understanding of the functionalization process and give us a tool for controlling the reaction and allowing for process optimization. An accurate determination of surface coverage is inherently difficult. While

it is possible to use intensity to measure coverage, if the frequencies shift with coverage with accompanying changes in intensities, it is difficult to make definitive determinations. Computationally, if the relationship between the IR frequency shift and the percentage of surface coverage is established, it is not necessary to determine coverage by inexact means. Coverage could be quantitatively determined from shifts in the surface IR spectrum.

In this paper we investigate the relationship between IR vibrational frequencies and coverage using the Si(111)-Cl/H surface as an example. The experimental observations (Courtesy of the Chabal Group UT at Dallas) provide evidence for coverage dependence of surface vibrations. PBC models with a range of partial coverage are used to derive the appropriate geometric and vibrational parameters. The relationship between the PBC vibrations and cluster model vibrations is discussed. The frequencies of the Si(111)-H/Cl surfaces observed in the experimental spectra are assigned. The origin and implications of coverage on the vibrational frequencies are discussed.

Computational Details

We model the Si(111)-H and Si(111)-Cl surfaces by creating PBC models of the surface. These models are made from the bulk crystal structures by choosing the smallest structures that repeat the slab properly in two dimensions at the desired slab thickness. At complete coverage, they have one unique atom per layer, thus requiring only small models. For convenience, the upper and lower surfaces of the slab models are mirror images of one another. The resulting model, figure 1.4.1, contains Si_n silicon atoms

where n is the number of layers (n=4 in figure 1.4.1) with two terminating chlorine or hydrogen atoms.

The heterogeneous Si(111)-H/Cl surfaces were modeled using PBC with some modifications. To ensure our calculations are tractable and to allow ease of interpretation, we have used four-site surface unit cells. This allows for variation of the surface coverage at 0, 25, 50, 75, and 100% and should be sufficient to understand the trends.[74] Since the strain resulting from surface adsorbates is fairly low, a small number of intermediate layers (typically four layers) are sufficient to yield reliable results. If we consider the coverage of the adsorbates on the upper as well as lower faces, several non-equivalent structures are possible that differ in their orientation relative to each other. When multiple arrangements exist, the structures used correspond to the lowest energy configuration.

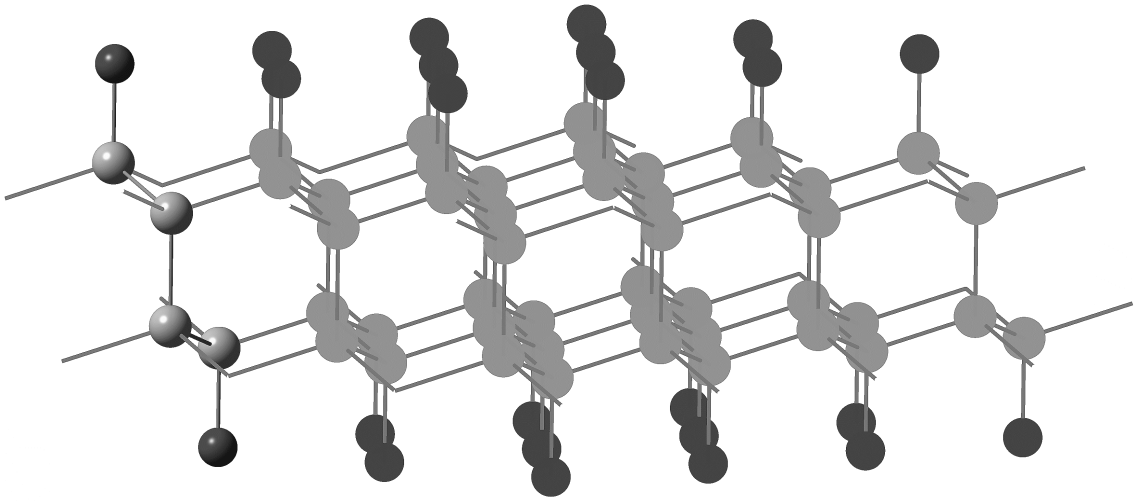

Figure 1.4.1. The Si(111)-Cl surface showing the unit cell as spheres on the far left with the cell repeated as circles over the supercell. The chlorine atoms are represented by dark spheres and the silicon atoms by grey spheres.

The cluster models were built from the optimized PBC models in all cases. The resulting dangling backbonds were terminated with hydrogen (Si–H=1.47 Å) in accordance with previously established procedure.[34] For all of the Si(111) surfaces, a seven surface site cluster containing four layers of atoms was used. These clusters have a stoichiometry of $Si_{22}H_{21}$ in addition to the seven surface atoms or groups.

For this study we use density functional theory with the BLYP functional (B88 exchange functional[35, 36, 75] in conjunction with the Lee-Yang-Parr correlation functional[37]). All calculations were performed with the 6-31G(d,p) basis set[38] to give the BLYP/6-31G(d,p) model chemistry. This model chemistry has been shown to give accurate vibrational frequencies in previous studies of similar systems. While hybrid functionals using Becke's three-parameter exchange functional such as B3LYP have been shown to improve the accuracy of many calculations, the behavior of the different

functionals is similar in our case. The largest difference is the Si–Si bond distance that is calculated to be systematically too long by 0.04 Å with the BLYP/6-31G(d,p) model chemistry.[10, 61, 69, 76] In order to ease comparisons of the models, calculations on the cluster and PBC used identical model chemistries. For the PBC calculations we have used the implementation of Kudin et al.[39-41]

Our technique for modeling surface vibrations for the uniform Si(111) surface has been detailed elsewhere[61, 69] and will only be presented in brief. PBC models are first generated and fully optimized. The corresponding vibrational frequencies are then determined numerically for the PBC calculations using the same unit cell. While analytical PBC frequencies are just beginning to be available, they are not yet implemented in most popular available program packages and their implementation is beyond the scope of this work. We have used the finite difference method to obtain the numerical frequencies for the PBC calculations at the Γ-point (wave vector k=0). The analytic forces were differentiated with respect to the Cartesian displacements (step size equal to 0.001 Å). The resulting force constant matrix is mass weighted, diagonalized and scaled (to cm^{-1}) giving the vibrational frequencies (scaled eigenvalues of the force constant matrix) and the normal modes (the corresponding eigenvectors). Our method has been shown to work well in our previous work on the Si(111) surface.[61, 69] When used with larger unit cells such calculations can be used to include some phonon dispersions (frequency spreading over the wave vector).

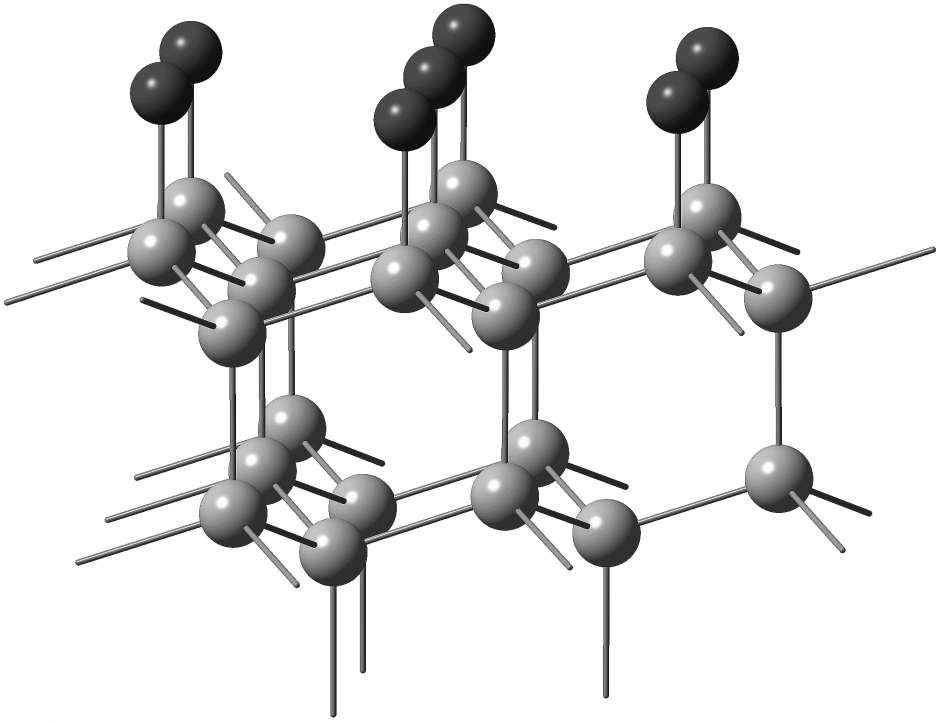

Figure 1.4.2. The seven site cluster model used throughout this work. The sites are varied to produce the various coverages used. The chlorine atoms are represented by dark spheres and the silicon atoms by grey spheres.

Cluster models are then constructed from the optimized periodic system as shown in figure 1.4.2 for the case of complete chlorine coverage. The cluster model is truncated using a standard procedure[34] and the cluster frequencies are computed using analytic force constants for the unoptimized cluster model. The full justification and pitfalls of the method are detailed elsewhere.[61, 69] In particular, it helps to avoid unphysical structural relaxations due to steric interactions in the case of larger surface groups. Since the cluster lacks the symmetry of the infinite system, there can be a spread in the calculated

vibrational modes since different surface atoms can have different environments. We have shown previously that the appropriate surface vibrations correspond to the collective vibrations of the cluster model. The resulting vibrational frequencies with this technique are comparable to the numerical differentiation of the full PBC frequencies using an appropriate unit cell. While using cluster models, spurious vibrational coupling with the terminating back bonds that can result in unphysical frequency shifts is eliminated using appropriate isotopic substitution. All calculations were done with a modified version of the Gaussian development suite of programs.[42] NBO (natural bond order) charges were calculated using NBO 3.0.[77]

Results and Discussion:

Results from transmission infrared absorption spectroscopy on the intermediates of the reaction of molecular chlorine with a hydrogen-passivated Si(111) surface, as summarized in figure 1.4.3 have been provided by the Chabal group at UT Dallas. Significant frequency shifts are apparent in all relevant vibrational features as the reaction proceeds, i.e., as H is replaced by Cl. For example, the Si–H stretch shifts from a starting value of 2084 cm^{-1} to 2097 cm^{-1} (3 min, ~50%H coverage) to 2102 cm^{-1} (5 min, ~35% H coverage) to 2109 cm^{-1} (10 min, 12% H coverage), as summarized in table 1.4.1. Interestingly, the Si–H bending mode, seen at 625 cm^{-1} (3 min), shifts only slightly during the reaction (< 2 cm^{-1}). A similar difference between the stretching and bending modes is also seen for chlorine. The Si–Cl stretch shifts significantly from 565 cm^{-1} to 588 cm^{-1} during the course of chlorination. In contrast, the parallel mode at 523 cm^{-1} (not observed before 5 min reaction) shifts only slightly though the intensity increases noticeably over the course of the reaction. This mode has been previously assigned to be

a near-surface phonon weakly coupled to the Si–Cl bending mode.[10, 76] It is clear that the vibrational shifts may be useful as an indicator for the coverage dependence of the reaction, although the mechanism cannot be understood without looking deeper into the nature of the shifts.

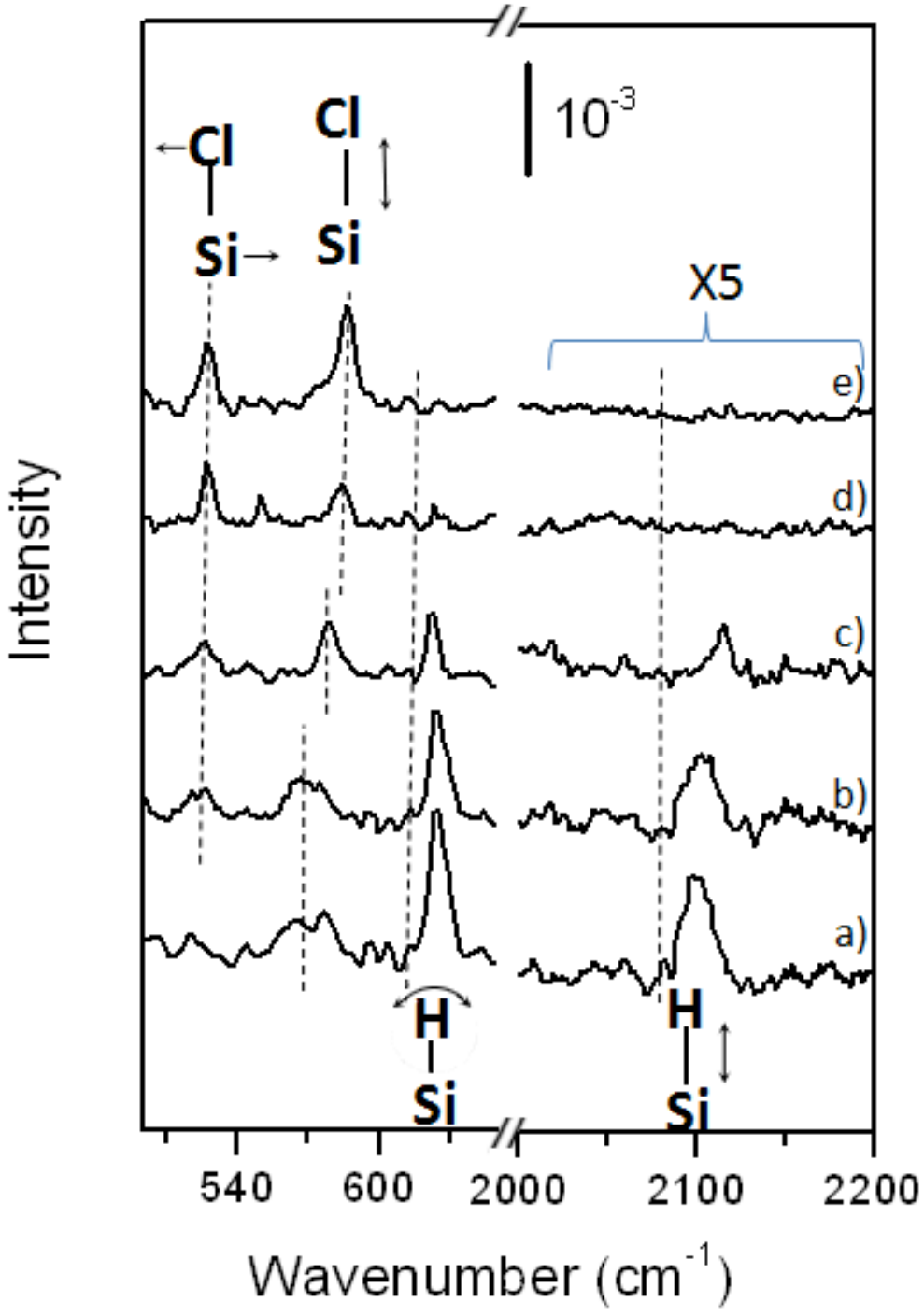

Figure 1.4.3. Transmission IR spectra of a H-Si(111) surface exposed to chlorine for a) 3min, b) 5 min, c) 10 min, d) 20 min and e) 30 min. All spectra are referenced to the initial oxidized silicon surface.

Table 1.4.1. The experimentally observed frequencies and intensities as a function of the chlorine exposure time. The percent hydrogen coverage is determined using the Si–H Bend due to screening of the Si–H stretch which varies with chlorine coverage. The Si–H Bend area is references to the initial value of 0.026 cm^{-1}. Intensity is measured in arbitrary units. (Courtesy of the Chabal Group UT Dallas)

Mode	Time, min.	Frequency, cm^{-1}	Intensity	Hydrogen Coverage, %
Si–H Stretch	3	2097	0.0020 ± 0.0002	–
	5	2102	0.0015 ± 0.0002	–
	10	2109	0.0007 ± 0.0001	–
	20	–	–	–
	30	–	–	–
Si–H Bend	3	625	0.0130 ± 0.0010	50
	5	625	0.0090 ± 0.0010	35
	10	623	0.0032 ± 0.0005	12
	20	623	0.0010 ± 0.0002	4
	30	–	–	–

Geometric Parameters

The surfaces functionalized with single atoms, either H or Cl, have the simplest geometry. They share all of the common features of the unreconstructed Si(111) surface. The primary geometric parameter is the Si–H or Si–Cl bond distance, 1.506 Å and 2.110 Å, respectively, for complete termination. The calculated distance between surface sites is ~ 3.9 Å. The van der Waals radius of hydrogen is 1.20 Å and 1.75 Å for chlorine. Since the distance between surface sites is larger than the sum of the van der Waals radii (2.4 Å

or 3.5 Å) there is little steric repulsion between surface groups. This is also true for all the mixed coverage surfaces.

The point group symmetry of the chlorine and hydrogen terminated surfaces is locally C_{3v} for each surface site. If only the adsorbate atoms and the first layers are considered the system is part of the high symmetry *p*6*m* wallpaper group. While the wallpaper symmetry of many adsorbates gives more information than the local point group, there is no particular insight to be gained for this simple system. The cluster models for these adsorbates as extracted from the PBC calculations are close to the C_{3v} point group within numerical noise.

When the hydrogen passivated Si(111) surface is chlorinated, the coverage of the surface will gradually shift from complete hydrogen coverage to complete chlorine coverage. During this reaction intermediates will be formed that are Cl/H mixtures with some surface sites being terminated with chlorine and others terminated with hydrogen. Assuming a random substitution process (i.e., a lack of adatom island formation and site vacancies), the surface coverage morphologies at a particular coverage can be predicted. The highly symmetric nature of the surface (C_{3v} for complete coverage) results in a limited number of possible morphologies.

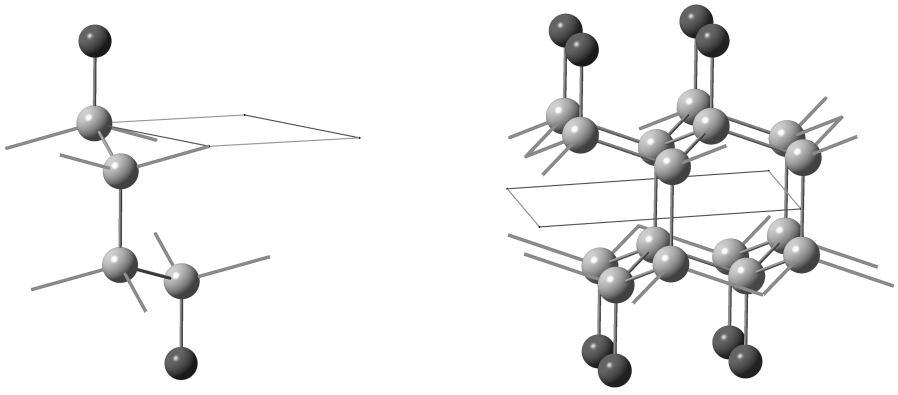

Si(111)-Cl PBC Unit Cell

Si(111)-Cl PBC Supercell

Figure 1.4.4. Comparison of the one surface site unit cell versus the four surface site supercell, boxes represent translation vectors along the unit cell axis. The chlorine atoms are represented by dark spheres and the silicon atoms by grey spheres.

In order to understand coverage dependence of the vibrations we have used a four surface site PBC model, figure 1.4.4. Within this model there are three possible intermediate structures: the dilute chlorine case, the dilute hydrogen case, and the case with equal hydrogen and chlorine. The dilute chlorine case has one silicon surface atom terminated with chlorine with the three remaining surface sites terminated by hydrogen. This model reflects a surface with 25% chlorine coverage. The bond distances at the surface are again the key parameters for the system. The Si–H bond distance is 1.502 Å while the silicon-chlorine bond distance is 2.144 Å, a difference from complete coverage

of 0.004 Å for hydrogen and 0.034 Å for chlorine. It is known that small changes (~ 0.01 Å) in bond distance can result in significant shifts of vibrational frequencies. The origin and implications of these shifts are discussed below. The length mismatch between the Si–Cl and Si–H bonds gives a slight increase in the distance between the hydrogen and chlorine atoms (0.05 Å larger than the distance between surface sites).

The local symmetry of the 25% chlorine coverage is interesting. The symmetry of the chlorine surface sites is locally C_{3v} if the surface layer is considered. However, the local symmetry for the hydrogen is reduced to C_{2v} symmetry. The symmetry for the extended surface is best considered using wallpaper symmetry. Since the lattice has both chlorine and hydrogen in different proportions, the resulting structure has a lower symmetry. Using the four-site unit cell the *cm* symmetry of the motif can be seen. The corresponding supercell, figure 1.4.5, shows rows of hydrogen terminated surface sites. In between these hydrogen rows are rows with alternating chlorine and hydrogen-terminated surface sites.

The geometry of 75% chlorine coverage is considered the concentrated chlorine surface. The model is the same as the 25% coverage if hydrogen and chlorine are interchanged. The only significant differences are the bond lengths from the surface. For the PBC geometries the silicon-chlorine bond distance is 2.199 Å while the silicon-hydrogen distance is 1.496 Å. These are a shift of 0.009 Å and 0.010 Å from the complete coverage from chlorine and hydrogen respectively. The distance between the hydrogens and the chlorines is slightly larger, 4.00 Å, due to the changes in the silicon-hydrogen and silicon-chlorine bond distances.

The final coverage type of surface coverage is when there are an equal number of equal hydrogen and chlorine adsorbates. This surface represents the midpoint of the reaction at uniform coverage. It is important to remember that this is an idealized surface where coverage occurs evenly. For the PBC models there is only one possible unique arrangement of the atoms at the four sites. However, when both sides of the slab are considered there are multiple possible configurations. For this study we have used the configuration with the lowest energy. This surface coincides with the most symmetric model.

The key geometric parameter is again the silicon-adsorbate bond distances. The silicon-chlorine bond is 2.130 Å and the silicon-hydrogen bind is 1.498 Å. The shifts from the complete coverage are 0.020 Å for the chlorine and 0.008 Å for the hydrogen. These shifts are significant and will be discussed below. The intermolecular distance between chlorine and hydrogen is 3.99 Å. As is true for the other mixed hydrogen/chlorine surfaces there is no steric hindrance in monolayer formation. The PBC model has less symmetry than the other models described thus far. The unit cell has C_{2v} symmetry and the extended surface has the *p2* wallpaper space group. The four unit supercell shows alternating bands of chlorine and hydrogen on the surface, figure 1.4.5.

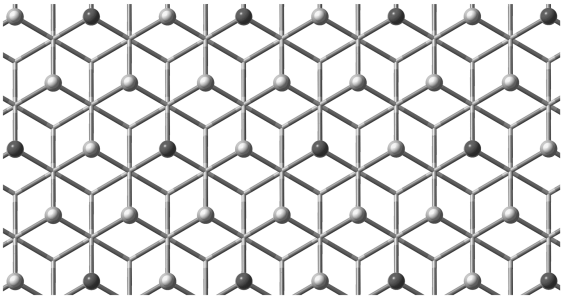

Si(111)-H/Cl 75% H 25% Cl

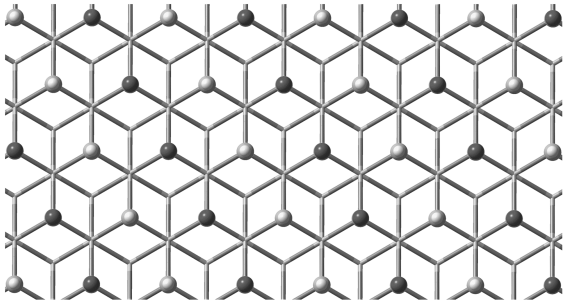

Si(111)-H/Cl 50% H 50% Cl

Figure 1.4.5. The surface at different intermediate coverages showing the banding patterns of the chlorines repeated on the surface. The chlorine atoms are represented by dark spheres, silicon atoms by grey spheres and hydrogen atoms are shown as white spheres.

Vibrational Frequencies

In order to unravel the vibrations of mixed adsorbate surfaces we have carefully considered the vibrations of infinite as well as finite systems. The uniform adsorbate model is simple containing only one surface site per unit cell while the mixed coverage surfaces have four surface atoms per unit cell. To ensure the numerical stability of our technique, we first determined the frequencies of the uniform adsorbates with a single atom unit cell as well as with a four-atom supercell. As can be seen in table 1.4.2**,** when the single site and four site frequencies are compared, there is excellent agreement. The close agreement indicates that the computed numerical frequencies are stable and have a precision of a few cm^{-1}. The comparison to experimental work is also very good for the Si(111)–H and Si(111)–Cl uncorrected harmonic vibrations. The Si–Cl stretch is underestimated by a modest amount (~ 35 cm^{-1}) while the Si–H stretch is overestimated by a similar amount. The calculated hydrogen bending modes are very close to the

observed experimental values. Our theoretical results are in keeping with previous theoretical values by Ricca and Musgrave[68] that place the Si–Cl stretch at 555 cm^{-1} using cluster models with an additive correction factor derived from other cluster-experimental differences (uncorrected value of 538 cm^{-1}). In a purely theoretical study similar to ours, Juarez et al. used a different model chemistry (PBE/6-21G(d,p) with anharmonic corrections to derive a value of 577 cm^{-1}.[74] The result also gives us confidence in our earlier assumption[61, 69] in the validity of the Γ-point approximation for calculated frequencies.

Table 1.4.2. A comparison PBC models of the unit cell and supercell (containing four unit cells) frequencies for the chlorine and hydrogen terminated Si(111)-1×1 surface.

Adsorbate	**Mode**	**Supercell Frequency, cm^{-1}**	**Unit Cell Frequency, cm^{-1}**	**Experiment [a] Frequency, cm^{-1}**
Chlorine	Si–Cl Stretch	554	555	584
	Phonon-Bend	491	491	527
Hydrogen	Si–H Stretch	2118	2123	2083
	Si–H Bend	628	628	626

a from Refs 10 & 76.

Table 1.4.3. A comparison of the PBC frequencies for the mixed chlorine/hydrogen Si(111)-1×1 surface at 0, 25, 50, 75 & 100% coverage. All PBC results include four unit cells. All frequencies below are shown in wavenumbers, cm^{-1}.

Mode	**100% Cl**	**75% Cl**	**50% Cl**	**25% Cl**	**0% Cl**
Si–Cl Stretch	554	540	520	498	–
Si–H Stretch	–	2160	2152	2137	2118
Si–H Bend	–	635	630, 642	609, 632	628
Phonon-Bend	491	487	486	485	–

We have assigned the vibrational frequencies of the mixed coverage surfaces using the four-site PBC cluster described above. As mentioned earlier, we have three possible intermediate structures: concentrated hydrogen and dilute chlorine, equal hydrogen and chlorine, and dilute hydrogen and concentrated chlorine. To evaluate the relationship between our calculated and experimental spectra we must first analyze the calculated spectra. In general, there is a significant shift in the stretching frequencies with coverage while the bending modes show only a modest shift. In particular, the spectra show the large shifts with surface coverage for the silicon-chlorine and silicon-hydrogen stretching frequencies, table 1.4.3. The calculated silicon-hydrogen stretching frequency shifts from 2160 cm^{-1} at 25% coverage to 2118 cm^{-1} at 100% coverage, a range of 42 cm^{-1}. Juarez *at al*. obtained a shift of 33 cm^{-1} over this range using a different model chemistry (PBE/6-21G(d,p)) and surface model.[74] The silicon-chlorine stretching frequency shifts from 495 cm^{-1} at 25% coverage to 554 cm^{-1} at 100% coverage, a range of 59 cm^{-1}, which is also close to the shift from Juarez et al. of 61 cm^{-1}.[74] The relationship between surface coverage and shift over the range can be approximated as

linear, figure 1.4.6. If we assume the error in our cluster frequencies is uniform over the range studied we can assume the shifts will be of similar magnitude in the experimental frequencies. While the reported experimental results are qualitatively consistent with the theoretical predictions it may be difficult to establish a quantitative relationship within the observed signal to noise. It is clear that the Si–H stretching frequency shifts up significantly with chlorine coverage in the experimental spectrum. Similarly, it can be seen that the Si–Cl stretch also shifts up in frequency with chlorine coverage. Both shifts are clearly large, of order tens of cm^{-1}. It should be mentioned that the calculations have been performed using small unit cells assuming a uniform coverage. Experimentally, nonlinear behavior is possible due to effects such as island formation and site vacancies (H abstraction not immediately followed by Cl deposition). More detailed experimental measurements and a detailed knowledge of the abstraction reaction may be needed for a full assessment. It is possible to state that our calculations do reproduce the experimentally observed trend and are comparable to the experimental frequencies at high coverage. We believe it is possible from these values to draw conclusions about surface coverage. Similar well-ordered behavior can be seen with other systems, which are not uniform such as bimetallic alloys.[78, 79]

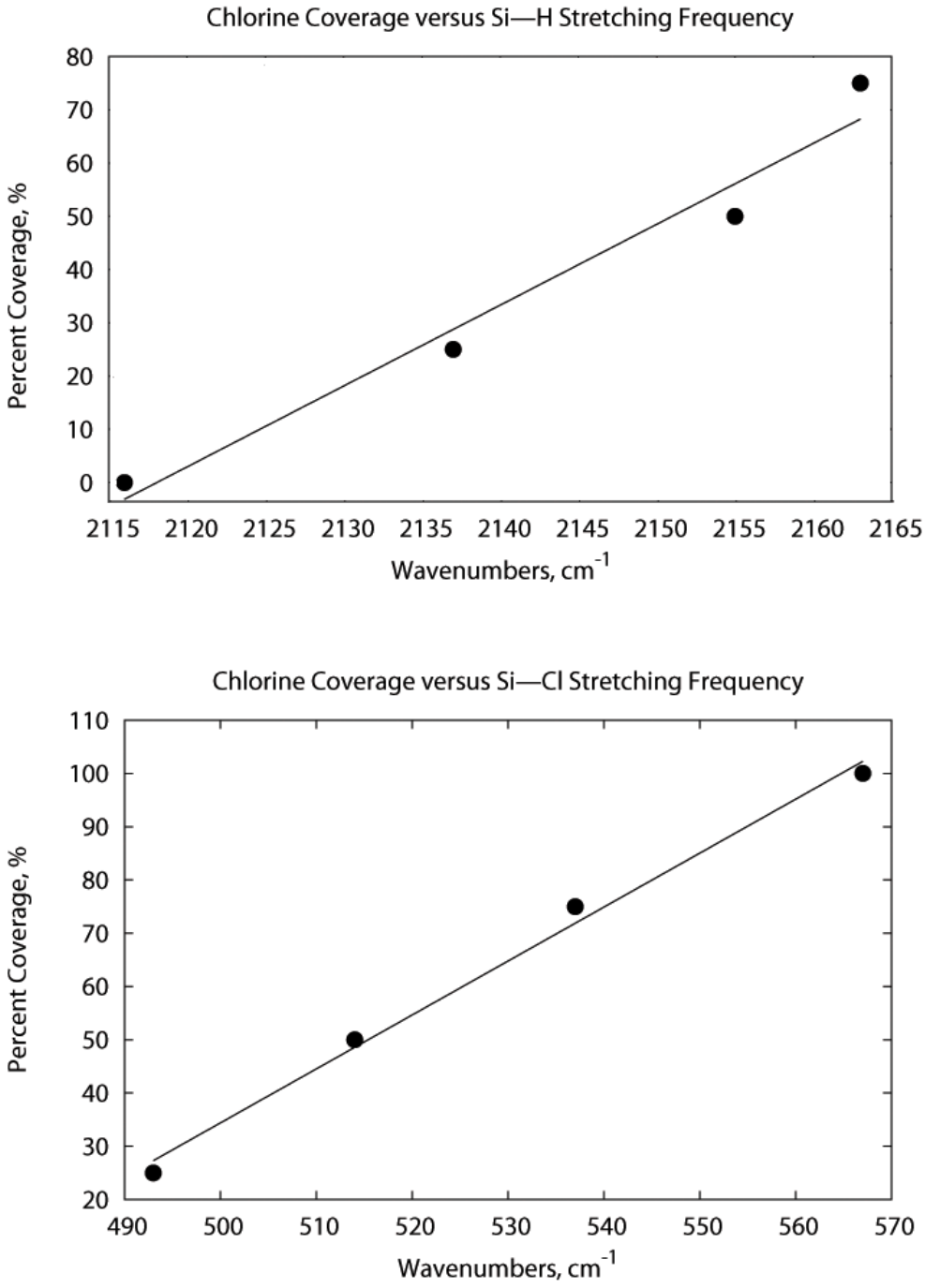

Figure 1.4.6. The correlation between the percent coverage for the Si–H (top) and Si–Cl (bottom) surfaces and the calculated vibrational frequencies. Black lines indicate a linear best fit for the surface.

It is interesting that the bending modes do not shift significantly with a change in coverage. Unlike the bond lengths that are coverage dependent, the bond angles are insensitive to coverage. Thus the bending modes involving hydrogen (at 626 cm^{-1} for monolayer hydrogen coverage) shift by only a few cm^{-1}. In the case of the chlorine related mode (at 527 cm^{-1} for monolayer chlorine coverage), again the shift is small since it is dominated by the near-surface phonon mode with significantly smaller chlorine contributions.

Using frequency shifts to measure surface coverage was suggested by Hammaker et al.[80] for uniform adsorbates on metal surfaces. In the case of chlorinating the Si(111) hydrogen terminated surface the simplest and most direct method is to measure the Si–Cl stretching frequency. Unfortunately, direct measurement of Si–Cl stretching frequency may be difficult. The mode occurs too close to the phonon region for unambiguous assignment[10] in most spectra. The silicon-hydrogen stretching mode is well above the phonon region, sharp and well separated. We, therefore, propose that the surface coverage of chlorine can be related to the shift of the silicon-hydrogen stretching mode to determine chlorine coverage. This method can be used not only to determine chlorine coverage but is most likely possible for any surface with similar morphology and structure, e.g., fluorine, bromine, iodine.

Cluster Models

We have also generated cluster models from the PBC optimized structures to perform the vibrational analysis. In all cases, we use the seven surface atom cluster described earlier. For the case of complete hydrogen coverage or complete chlorine

coverage, this results in a symmetric C_{3v} cluster geometry. The cluster models generated from the 25% chlorine coverage PBC structure present some problems. For a seven surface site cluster there are multiple possible geometries. For 25% coverage the number of chlorines on the surface can be either one or two with two chlorines being closer to the actual ratio of 0.25. In addition, there are two possible sites that are not symmetrically equivalent, either the center of the cluster or on the outer ring. While many isomers are possible, they are not all analogues to the extended PBC structure. Since we are interested in the infinite systems we have decided to use clusters that replicate the wallpaper group as close as possible. In this case the single chlorine in the center and the two chlorines that are *para* to one another are the only allowable configurations. Similarly, the case with 75% chlorine coverage is exactly analogous with the interchange of chlorines and hydrogens.

The 50% coverage models also have multiple possibilities. Since there are seven sites it is only possible to form clusters that are ratios of three or four to seven. In keeping with the same philosophy as the previous models only those models which reproduce the correct wallpaper group were used. There are two unique configuration of the surface with four hydrogens and three chlorines or vice versa, each with C_s symmetry.

The cluster models can also be used to derive vibrational frequencies, particularly for the important stretching modes. In each case, the collective vibrations can be clearly identified and correlate closely with the computed PBC modes. As mentioned above, the seven site cluster models have two structures that approximate each of the intermediate coverage levels. The presented frequencies are the average of both frequencies. The PBC and cluster frequencies can be seen in table 1.4.4. In all cases the silicon-adsorbate

stretching modes are very similar for both the PBC and cluster calculations. The MAD is ~ 3 cm^{-1} which is in excellent agreement between the PBC and cluster vibrations.

Table 1.4.4. The shifts in stretching frequency for the H/Cl-Si(111)-1×1 surface with decreasing coverage on one species relative to the other. The clusters contain seven adsorbates and the PBC models have four surface layers.

Coverage	Origin	Mode	
		Si–Cl Stretch, cm^{-1}	Si–H Stretch, cm^{-1}
100%	PBC	554	2118
	Cluster	551	2116
75%	PBC	534	2137
	Cluster	537	2137
50%	PBC	514	2152
	Cluster	514	2155
25%	PBC	491	2160
	Cluster	493	2163

Origin of the frequency shifts

The simple nature of the adsorbates in the mixed coverage surface allows us to carefully consider the underlying physical/chemical effects responsible for the frequency shifts. The possible reasons for adsorbate interactions shifting frequencies have been enumerated by Platero et al.[81] as follows: dynamic effects such as (1) "through-space" dipole-dipole coupling,[80, 82, 83] (2) "through-solid" vibrational coupling,[84] (3) vibrational coupling via image charge interactions,[82] or static effects such as (4) chemical or inductive effects,[82] (5) electrostatic interactions.[85] For the current work we can

immediately discard possibilities 2 and 3. The through-orbital overlap between the different adsorbates is small and image charge effects due to the adsorbates are not likely for the Si(111) surface. We therefore need to examine interactions 1, 4 and 5. Dipole-dipole coupling between nearest-neighbor and further dipoles is important for the stretching vibrations perpendicular to the surface. This effect is larger for the surface vibrations involving chlorine and smaller for hydrogen stretching vibrations. The effects of dipole-dipole interactions would be expected to shift the frequencies higher for the stretching modes. Consequently, the silicon-chlorine stretch (and the silicon-hydrogen stretch to a smaller extent) would be expected to shift higher with increased chlorine or hydrogen coverage.

To investigate the electrostatic interaction (5) of the adsorbates we have calculated the NBO charges on the atoms for the different coverages that we have studied. Calculated NBO charges do not show large differences as a function of coverage and we do not expect significant effects at the typical distances between adsorbates, ~ 4.0 Å. This result is expected from chemical intuition. The final possibility is an inductive or chemical effect. These effects are the result of changes in the electronic structure of the system due to the species and bond types present. In this case the very electronegative chlorine atoms would be expected to have an electron withdrawing effect on the surface silicon atom. The effect is then felt through the silicon-silicon bonds of the system to the silicon bonded to the hydrogen adsorbate. The silicon is made slightly more positive. The slightly more positive silicon binds to the weakly negative hydrogen more strongly shifting the vibrational frequency higher. The effect increases with increasing concentration of chlorine. The bonds in question are polar but strongly covalent,

rationalizing the small effect. The Si–H distance ranges from 1.506 Å for a complete hydrogen monolayer to 1.496 Å for the dilute hydrogen-concentrated chlorine surface. The trend of the Si–H bond distance decreasing with an increase of chlorine substitution is also seen in the case of small molecules. If chlorines are added to silane to create chlorosilane, dichlorosilane, and trichlorosilane, the Si–H bond distance decreases from 1.494 Å for silane to 1.480 Å for trichlorosilane (BLYP/6-31G(d,p) model chemistry). The surface contains more bonds in between the chlorine adsorbate and the silicon-hydrogen bond indicating a slightly weaker effect. The relationship of the bond lengths to frequency shifts for the surface species can be seen to be linear, figure 1.4.7. These small bond length changes have a large effect on vibrational frequencies. It is also possible the lone pairs of the chlorine are interacting with the surface, but for the case of chlorine we believe the inductive effect is dominant.

Overall, we would expect dipole-dipole and inductive effects to dominate the frequency shifts. In the mixed coverage surface containing H and Cl, since the dipole-dipole effects between hydrogen atoms are small, the significant shift on the Si–H stretching modes due to neighboring chlorines is mostly due to inductive effects. Both the inductive effect and dipole coupling shift the Si–H stretching frequency higher. As the percentage of hydrogen increases the dipole coupling will blue-shift the Si–H stretching frequency slightly higher. Increasing chlorine concentration will result in a significant blue-shift of the stretching frequency. It is thus interesting to note that the Si–H frequency *decreases* with increasing hydrogen coverage (table 1.4.4). The key to understanding the observed effect is to realize that *as hydrogen coverage increases chlorine coverage decreases*. The large blue-shift caused by chlorine is lost at a greater

rate than the slight blue-shift from dipole coupling is accumulated. The net result is a decrease in frequency compared to the surface with dilute hydrogen. The Si–H stretching frequency of a complete monolayer would still be higher than that of an isolated Si–H stretch on the surface.

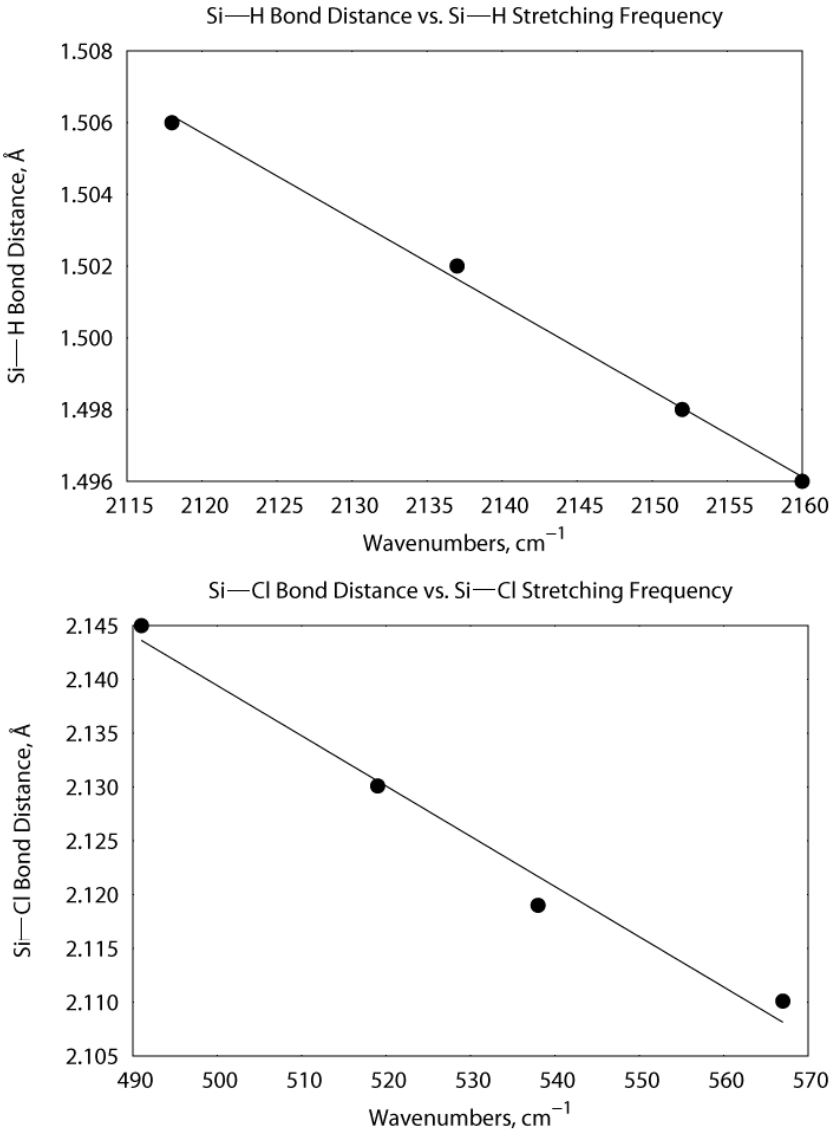

Figure 1.4.7. The correlation between the calculated bond length and frequencies for the Si–H (top) and Si–Cl (bottom) stretches on the Si(111). The solid black line is a linear fit to the data.

Conclusions

Using quantum chemical calculations combined with surface infrared spectroscopy (Courtesy of the Chabal Group UT Dallas) we have assigned the vibrations of the mixed adsorbate Si(100)-H/Cl surface. Significant shifts in the Si–H and Si–Cl stretching frequencies are found as a function of coverage while the bending modes are shifted only slightly. We have also shown the technique of determining infinite vibrations from finite cluster models using the method of collective vibrations[61, 69] is valid for the stretching vibrations of mixed cluster adsorbates. Our results suggest that Si–H stretching shifts can be used as a probe for chlorine coverage during the reaction of chlorine precursors with the hydrogen terminated Si(111) surface. Finally, an analysis of coverage dependence suggests that an inductive effect is the dominant origin of the resulting stretching frequency shifts.

1.5 Trends for Mixed Halide Terminated Surfaces

Silicon is a critically important material that is widely used by the semiconductor industry.[3, 86] While most semiconductor devices currently use the Si(100) surface due to the existing technological infrastructure, the Si(111) surface has also received considerable attention. The unit cell of the unpassivated Si(111) surface is complex with a 7×7 reconstruction. When the surface is exposed to atomic hydrogen the surface becomes remarkably simple with a 1×1 unreconstructed surface.[7] This nearly atomically flat surface is an ideal starting point for uniform functionalization. The current paradigm for semiconductor manufacturing may reach its limit around the year 2020.[87, 88] Leading up to this eventuality, new innovations in designing novel functionalized surfaces are clearly important.

Recently there has been interest in functionalizing the Si(111) surface using organic molecules to explore the development of new devices.[9-18, 25, 26, 31, 32, 46-48, 50, 54-56, 59, 63-66, 70, 74, 89-93] One of the techniques used to achieve functionalization is a surface Grignard reaction which was first attempted in 1996[11] but has received renewed interest in the last few years.[9, 11, 17, 33, 59, 68, 71, 73, 94] In this technique, halide is substituted for the hydrogen to create a X/Si(111) (X=F, Cl, Br & I).[10, 29, 60, 93, 95] Subsequently the surface is alkylated by creating a silicon-carbon bond using the Grignard reagent. During the initial halide substitution there is a mixed coverage surface, partially covered with hydrogen and partially covered with a halogen. This surface can be used to answer two important questions. First, is it possible to track the percent coverage of the halide on the surface? Second, what is the effect of varying numbers of neighboring hydrogens and halides on the surface structure and vibrational frequencies? Both questions rest upon the idea that the neighboring groups can exert a measurable influence upon one another. These effects

can be measured using surface vibrational spectroscopy to determine the stretching frequencies of the adsorbates.[6, 96] The use of electronic structure theory makes it possible to examine the structural changes occurring at various percentages of halide and hydrogen coverage.

Recently several reports have examined these questions using either electronic structure calculations[74] or a combination of electronic structure calculations and surface vibrational spectroscopy[97] for mixed chlorinated/hydrogen Si(111) surfaces. These studies show that neighboring chlorines shift the surface vibrational frequencies by polarizing the silicon-adsorbate bond. The effect is nearly linear with coverage giving an indication that it is possible to determine the coverage using the surface vibrational shifts during the reaction. In this report we have sought to extend these results for the group 17 elements (F, Cl, Br & I). Using electronic structure calculations we consider the shift in vibrational frequency versus coverage for the silicon-adsorbate and discuss the origin of the shifts. These results are compared to the experimental frequencies for the partial coverage (~ 30%) of fluorine. We then draw some general conclusions about the mixed coverage hydrogen/halogen surfaces.

Computational Details

Functionalized Si(111) surface were modeled using periodic boundary conditions. Unit cells were constructed by choosing the smallest repeating group of the bulk crystal that replicates the proper surface geometry of the two-dimensional slab. The Si(111) surface is relatively simple allowing for a single unique atom per surface layer. To obtain models suitable for mixed coverage the single unit cell models were replicated once along each translation vector to create a four unit cell model, figure 1.5.1. Overall the unit

cell contains Si_{4n} silicon atoms with n equal to the number of layers. Due to the lack of strain on Si(111) surface termination, we have previously seen that as few as four layers are sufficient to give reliable results. As a consequence of symmetry, the number of layers must be an even integer to maintain upper and lower surfaces. In cases of uniform coverage, one surface is terminated with hydrogen while the opposite side is terminated with a halide. In cases of mixed coverage we have mirrored the upper and lower surfaces. Using these models it is possible to have halide coverage percentages of 0, 25, 50 & 75% (while the remainder of the surface is terminated with hydrogen).

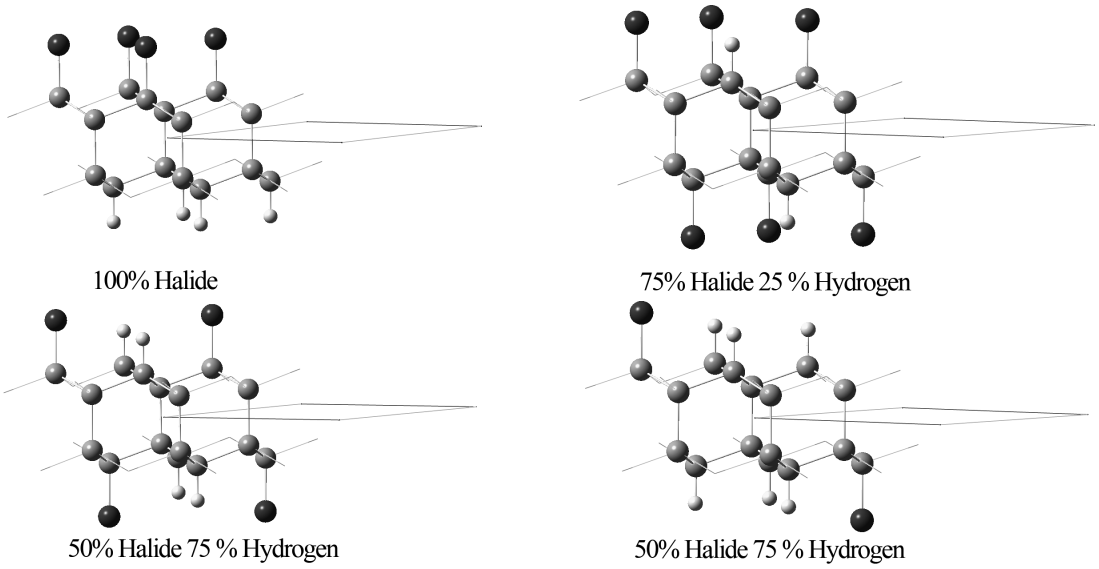

Figure 1.5.1**.** Ball and stick model of the four-site PBC models used for the study. Large dark spheres represent the halides, large lighter spheres represent the silicon surface and the small spheres represent hydrogen atoms. The lines show the translation vectors.

We have used the gradient-corrected BLYP density functional (B88 exchange functional with the Lee, Yang and Parr correlation functional) along with the Pople-style 6-31G(d,p) basis set (BLYP/6-31G(d,p) model chemistry) to investigate all the systems in this study.[35-38, 75] This model chemistry has been used in several previous studies on periodic systems. While other popular hybrid functionals such as B3LYP are more widely used, we have not seen a significant difference in previous studies.[61, 69, 97] A notable difference is the Si–Si bond distance which is known to be systematically too long by 0.04 Å with the BLYP/6-31G(d,p) model chemistry.[61, 69, 97] However, the BLYP functional is substantially more economical for PBC calculations that were performed using the implementation of Kudin et al.[39-41]

Currently the use of analytic force constants is not yet widely implemented for PBC in most popular quantum chemical programs. To obtain PBC force constants at the Γ-point (wave vector k=0) we have used numerical second derivatives as in our previous studies.[61, 69, 97] The analytic forces were numerically differentiated in Cartesian space (step size of 0.001 Å) using the symmetric finite difference method. The forces constants were mass weighted, diagonalized and scaled to give vibrational frequencies (scaled eigenvalues of the force constant matrix) and the normal modes (the corresponding eigenvectors). While this method does not compute the phonon dispersions, it has been sufficient to assign infrared spectra for a number of similar systems. All calculations were done with a modified version of the Gaussian development suite of programs.[42]

Results and Discussion

Geometric parameters

The geometries for the functionalized Si(111) surfaces we have studied are straightforward. The distance between top layer surface atoms is ~ 4 Å. This distance easily permits the formation of a complete monolayer for all the uniform and mixed adsorbates considered in this study. The largest adsorbate is iodine with a van der Waals radius of 1.98 Å.[98] The bonds formed by all the single atom adsorbates are normal to the plane of the surface. Therefore, when considering the surface adsorbate geometries there is only one significant parameter for the uniform surfaces and three for the mixed coverage surfaces. The uniform adsorbate parameter is the silicon-adsorbate distance. The parameters for the mixed coverage surface consist of the two silicon-adsorbate distances along with the wallpaper symmetry group that contains information about the periodic arrangements at each surface site.

Uniform adsorbates present the simplest case. The Si–H bond length is 1.506 Å and the Si–X bond distances are 1.647 Å for X=F, 2.110 Å for X=Cl, 2.259 Å for X=Br, and 2.572 Å for X=I. The distances are all slightly longer than the corresponding values observed with small molecules (H_3SiX, X=H, F, Cl, Br &I) using the same model chemistry by ~0.01 Å showing an effect of the surface on the silicon-adsorbate distance. The wallpaper symmetry gives an indication of the long range adsorbate order of the surface. The uniform adsorbates transform as the symmetry of the surface, i.e., local C_{3v} symmetry at each adsorbate site. The wallpaper symmetry is *p6m* if the lower layer

silicon atoms are ignored.[99] While the uniform adsorbate case is simple, the wallpaper symmetry is important for mixed-coverage adsorbates (*vide infra*).

Using a model with four possible surface sites, there are three possible percentages of *partial* halide coverage, 25, 50 and 75%. The model of the surface with 25% halide coverage contains three hydrogens and one halide. At 50% there are two hydrogens and two halides and at 75% coverage there is one hydrogen among three halides. While these surfaces are simple, understanding the key geometrical parameters of the surface is critical to the vibrational shifts.

The 25% halide coverage has two important distance parameters, the Si–X (X=F, Cl, Br & I) and Si–H bond distances. The local symmetry at each site is reduced to the C_{2v} symmetry group. Ignoring the lower layers silicon atoms the wallpaper symmetry is *cm*. If we consider the extended system shown in figure 1.5.2 the surface symmetry group forms a pattern consisting of solid rows of hydrogen and a second row with alternating hydrogen and halide. This structure is the inverse of the 75% halide coverage with the same symmetry group. It is worth noting that using a four site model the different arrangements of the adsorbates all form the same wallpaper space group and are equivalent by symmetry.

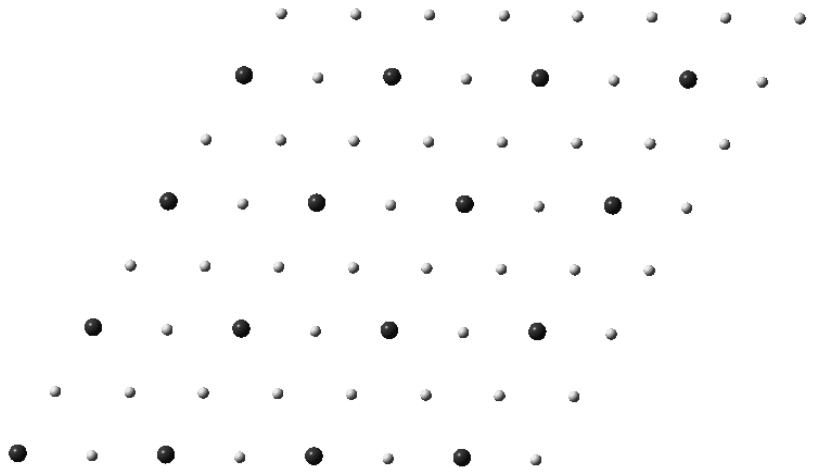

Figure 1.5.2**.** A top down view of the adsorbate pattern on the surface showing the *cm* wallpaper symmetry group. The large dark spheres are the halide atoms and the smaller spheres are the hydrogen atoms.

The Si–X bond distances at 25% halide coverage are X=F 1.660 Å, X=Cl 2.144 Å, X=Br 2.287 Å, and X=I 2.544 Å. The differences in bond lengths from the surfaces with complete termination are 0.013 Å for the fluorine, 0.034 Å for chlorine, 0.028 Å for bromine and 0.059 Å for the iodine adsorbate. The difference shows the effect of adding halides to the surface on the Si–X bond distance. The reasons for bond length shifts due to surface interactions have been previously examined in detail.[80-84, 97] Three possible sources of the difference are crowding of the adsorbates, an inductive effect, and an effect via interaction of the adsorbate lone pairs with the silicon-surface bonds. The adsorbate-adsorbate distances are larger than the sum of the van der Waals radii for all of the

adsorbates and the bonds lengths of the adsorbates are uniform. If the effect is due to increased crowding of the adsorbates, it is likely that additional geometrical relaxations such as unequal bond lengths or tilting of the adsorbates away from each other will be seen. The inductive effect would affect the bond lengths but would die off going down the period from fluorine to iodine. The effect of a lone pair, on the other hand, would increase down the period as polarizability increases. Our analysis suggests that the effect is due to a combination of both an inductive effect and an interaction of the loan pair of the adsorbate with the surface (*vide infra*). The intensity of the effects move in opposition to one another (inductive effect decreases down the period while the lone pair effect increases down the period) but both decrease the Si–X bond length. It is worth noting these interactions are fairly weak resulting in a slight shift of the bond distance.

The Si–H bond distances at 25% halide coverage show a clear trend. As shown in table 1.5.1 the bond lengths decrease from the complete hydrogen coverage. The largest shift is for iodine where the Si–H bond distance changes from 1.506 Å (0%) to 1.497 Å (50%). A similar pattern is observed for the other adsorbates. The origins of these bond length changes and their implications on the silicon-hydrogen stretching frequencies are discussed below.

Table 1.5.1. The Si–H bond lengths, Å at several percentages of halide coverage for fluorine, chlorine, bromine and iodine adsorbates on the Si(111) surface.

	Si–H Bond Lengths, Å			
Halide	0% Halide	25% Halide	50% Halide	75% Halide
Fluorine	1.506	1.504	1.501	1.499
Chlorine	1.506	1.502	1.498	1.496
Bromine	1.506	1.501	1.498	1.495
Iodine	1.506	1.500	1.497	—

At 75% halide coverage the symmetry group is the same as for 25% coverage. The bond lengths are, however, considerably different. The Si–X bond lengths are longer than for the case of 25% coverage. The values for the Si–X bond lengths are X=F 1.651 Å, X=Cl 2.119 Å, X=Br 2.266 Å, and X=I 2.524 Å. The magnitude of the changes in bond length are consistent with the effects discussed above. Changes to the Si–H bond lengths are shown in table 1.5.1 and also follow the pattern discussed above for 25% coverage.

The final set contains an equal amount of halide and hydrogen adsorbates. The wallpaper space group for this surface ignoring the lower layer silicon atoms is *p2*. The extended surface has alternating rows of hydrogens and halides. Other arrangements of halides and hydrogen on the surface using the same unit cell give the same wallpaper symmetry group. The bond distances for the Si–X bond lengths are intermediate between those of 25% coverage and 75% coverage, X=F 1.655 Å, X=Cl 2.130 Å, X=Br 2.275 Å. The Si–H bond lengths are shown in table 1.5.1 have the pattern, which would be expected from the values at other percentages of halide coverage.

Vibrational Frequencies

The vibrational spectra of surfaces with uniform coverage are the simplest to consider and offer a reference for comparison. If only modes involving the adsorbate are considered, these spectra have a single perpendicular-polarized mode that is the silicon-adsorbate stretching mode. The values for the Si–X stretching frequencies (X=F, Cl, Br & I) are shown in table 1.5.2 and the Si–H stretching frequency in table 1.5.3. The silicon-halide stretching frequencies are shifted higher than for the corresponding substituted silanes. The bond lengths for the surface atoms are correspondingly shorter than in the substituted silanes. The surface Si–H stretching frequency is lower than that of silane (D_3Si–H isotopic substituted form to avoid vibrational coupling) with a longer bond length. These results show a slight stabilizing effect of the surface for the silicon-halide bond and a slight destabilizing effect for the silicon-hydrogen bond. The experimental frequencies for the hydrogen and chlorine covered surface have been reported.[97] We have previously compared these values to our computed results[97] and shown very good agreement. While there is a slight overestimation of the stretching modes by ~30 cm^{-1}, this is expected since the frequencies were calculated using the harmonic approximation. The good agreement for the H/Cl system gives confidence to the reliability of the computed results for the fluorine, bromine, and iodine species that have, to our knowledge, not been well studied experimentally.

Table 1.5.2. The Si–X stretching frequency, cm^{-1} at different percentages of halide coverage on the Si(111) surface, the remaining sites are terminated by hydrogen.

	Si–X Stretching Frequency, cm^{-1}			
Mode	100% Halide	75% Halide	50% Halide	25% Halide
Si–F	861	843	825	807
Si–Cl	554	537	514	499

Table 1.5.3. The Si–H stretching frequency, cm^{-1} for the four halides at different percentages of halide coverage on the Si(111) surface.

	Si–H Stretching Frequency, cm^{-1}			
Halide	0% Halide	25% Halide	50% Halide	75% Halide
Fluorine	2118	2128	2139	2145
Chlorine	2118	2137	2152	2160
Bromine	2118	2138	2157	2168
Iodine	2118	2141	2159	—

The vibrational spectra of the mixed coverage surfaces are more interesting. There are significant shifts of the Si–X (X= F, Cl, Br & I) and Si–H vibrational frequencies as the percentage of halide coverage on the surface changes. If we first examine the Si–X stretching frequencies on the H/Si(111) with varying concentrations of halide, the frequencies decrease with decreasing halide coverage. This is shown for X=F and Cl in table 1.5.2. This change in stretching frequencies is approximately linear with respect to

coverage for fluorine and chlorine, though some saturation effect is seen. The stretching frequencies for the surfaces partially covered with bromine and iodine also show a similar effect. However, since these frequencies occur below the phonon threshold (below 500 cm^{-1}), there are difficulties in assigning clear-cut isolated Si–Br and Si–I stretching modes in this region due to substantial phonon coupling and hence these frequencies are not listed. It is interesting that, in all cases, there is a roughly linear shift in the Si–X bond length with coverage.

While it is possible to experimentally characterize Si–F and Si–Cl stretches on the Si(111) surface, it is difficult to characterize larger halides due to the phonon coupling mentioned above. Recently it has been proposed to use the Si–H stretching frequency to monitor the halide coverage on the surface.[74, 97] Thus, it is important to calibrate the relationship of the silicon-hydrogen stretching shifts with the surface coverage for the different halides.

The silicon-hydrogen stretching frequencies increase by tens of wavenumbers with the increase in halide coverage that is reflected in the bond length changes discussed previously (table 1.5.1). The relationship between the Si–H bond length and frequency is approximately linear, figure 1.5.3. There is a slight dependence on the local environment of the hydrogen that slightly affects the slope of the bond length versus frequency relationship that has been previously noted.[97]

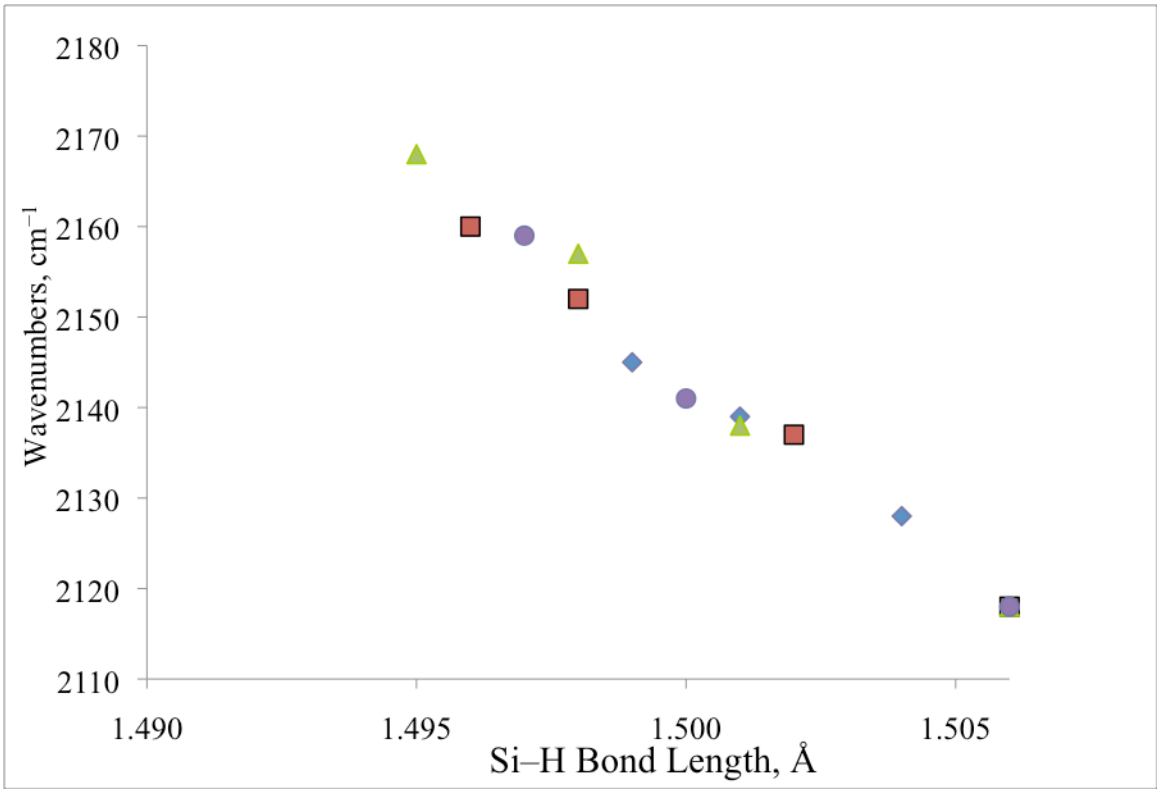

Figure 1.5.3**.** The Si–H bond lengths in Å plotted against the Si–H stretching frequency in cm^{-1}. The bond lengths and frequency have a linear relationship when considering only one halide, showing a slight dependence on the local environment, fluorine =♦, chlorine=■, bromine=▲ and iodine= ●.

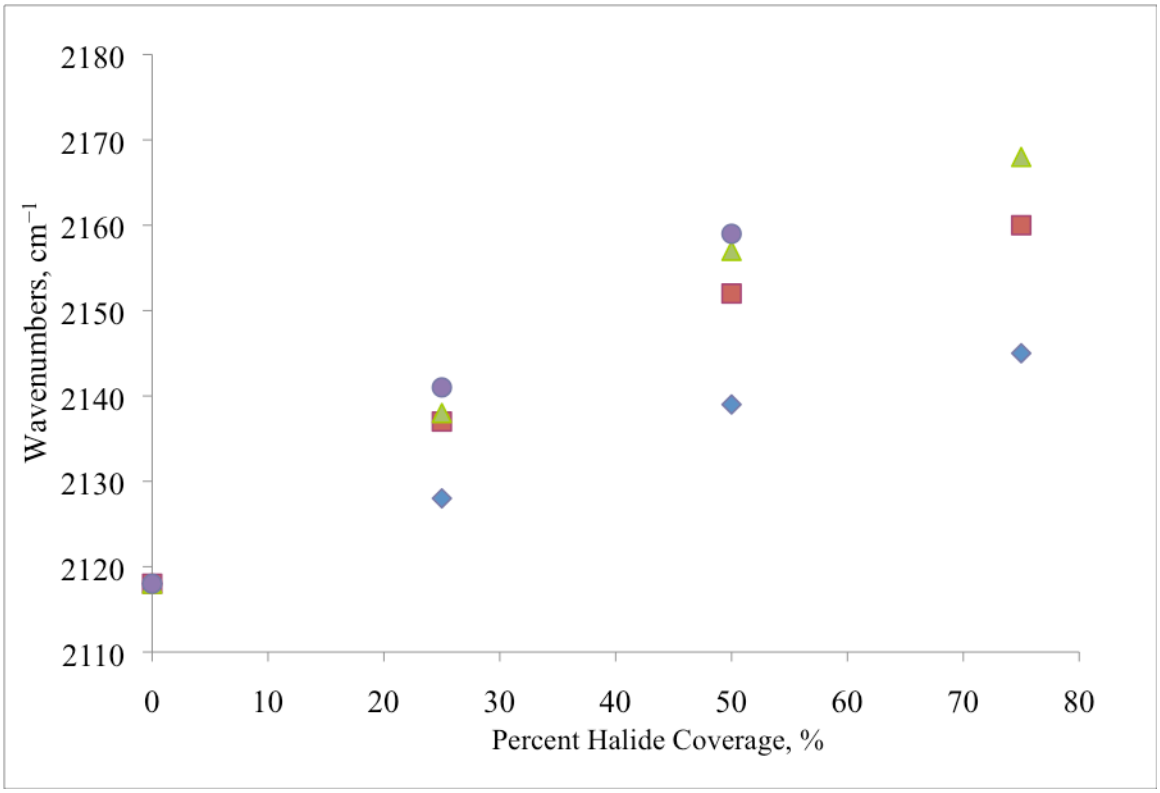

Figure 1.5.4**.** The Si–H stretching frequencies in cm^{-1} plotted against the percentage of halide coverage, fluorine =♦, chlorine=■, bromine=▲ and iodine= ●.

If the effects of particular halides are considered, several trends emerge. First considering partial fluorine and partial hydrogen termination, it can be seen from figure 1.5.4 that the Si–H stretching frequencies increase linearly with increasing fluoride coverage from 2118–2145 cm^{-1} over a range or 27 cm^{-1}. This rate of increase is the smallest for all of the halides calculated. The chlorine surface shows a similar increase in frequency. However, the rate of increase is larger than for fluorine and occurs over a larger range, 2118–2160 cm^{-1}. Under close inspection the frequencies level off slightly, possibly indicating a saturation of the effects that are driving the frequency increase. This tapering off is also seen with bromine that increases at a slightly higher rate than chlorine. Finally iodine shows both the largest rate increase with increased coverage and the

largest tapering off. The rate of increase has been previously characterized for chlorinated surface by our group[97] and by Juarez et al.[74]

The origin of the frequency shift has been proposed to be an inductive effect for the chlorinated surface.[74] When the trend for all halides is examined it is clear that an inductive effect alone is insufficient to explain the trend. The inductive effect would increase the frequency as previously described but would be strongest for fluorine and drop off for less electronegative halides. Since the blue shift in Si–H stretching increases for less electronegative halides and is largest for iodine, another property is partly responsible for the increase in the Si–H frequency in addition to electronegativity. As the halide size increases they become much more polarizable. This increase in polarizability results in the possibility of halide lone pairs donating electron density into the surface. This donation strengthens the silicon-halide bond while slightly destabilizing the surface silicon-silicon bonds. Indirectly this allows a stronger interaction with the silicon-adsorbates, slightly strengthening the Si–H bond and increasing the frequency. The lone pair effect combined with the inductive effect, previously described,[74] significantly affects the frequencies. The inductive effect is linear with coverage and is expected to be highest for fluorine (Pauling electronegativity of 3.98) and will decrease down the period to iodine (Pauling electronegativity of 2.66). The lone pair donation is non-linear. The lone pair effect is expected to have a large initial effect and then reach saturation quickly as halide coverage increases. This effect is highest for iodine, which is the most polorizable, and decreases up the period. The frequency shift for fluorine is likely to be almost entirely an inductive effect and shows a linear increase with coverage. The shift of iodine is likely to have a substantial contribution from the lone pair effect. In order to

probe slightly deeper into the lone pair effect we have performed calculations on halide substituted trisilanes ($XSiD_2SiD_2SiD_2H$) substituted with deuterium to eliminate spurious vibrational coupling. These small molecules follow the same pattern observed for the surface between different halides.

In our previous work it was difficult to calibrate the method using experimentally known percentages of halide coverage.[97] Instead, we were able to track the increase in halide Si–H stretching frequencies at specific time interval exposures to chlorine precursors.[97] In this work, wet chemistry on atomically smooth H–Si(111) surface has been performed to investigate the influence of atoms bonded to the neighboring silicons on the observed Si–H stretching frequencies. Figure 1.5.5 shows the transmission FTIR spectra in the Si–H stretching region for the silicon surface at several steps of the modification process, referenced to the initial oxidized silicon. Exposing the atomically smooth H–Si(111) surface to solutions of neat anhydrous methanol or ethanol at 65 °C leads to the replacement of approximately 30% of the initial Si–H (determined by the integration of the Si–H stretching band) by $Si–OCH_3$ or $Si–OC_2H_5$, respectively. In both cases, complete monolayer termination is not possible due to the steric interactions between the relatively bulky surface methoxy and ethoxy groups.

The Si–H stretching mode is shifted from the initial frequency (2083 cm^{-1}) to a lower value (2079 cm^{-1}) due to average reduction of the Si–H dipole-dipole interactions.[100] The $–OCH_3$ group can then be replaced with fluorine to form a silicon–fluorine bond by immersion of the methoxy-terminated surface in HF(*aq*) solution. Figure 1.5.5 shows the effect of the progressive exchange of the methoxy groups by the fluorine atoms on a flat Si–H surface with ~30% $Si–OCH_3$ coverage. The discrete shifts

in the frequencies from 2079 with no immersion to 2084, 2087 and 20n2 cm^{-1} after 30, 120 and 180 s HF immersion, corresponding to the replacement of the methoxy-terminated surface with fluorine atoms. The final blue shift of the Si–H on the ~30% Si–F surface is 13 cm^{-1}. The calculated results indicate that at 30% coverage the Si–H blue shift should be 11 cm^{-1}. This remarkable agreement shows the robust nature of the relationship between halide coverage and frequency. When fluorine atoms are replaced by hydroxyl groups by immersion into water, the Si–H stretching frequencies red shift again to the same position as that of the flat Si–H surface with ~30% Si–OCH_3 or Si–OC_2H_5 coverage, highlighting the effect of the fluorine atoms compared to O–R groups on the Si–H stretching frequency.

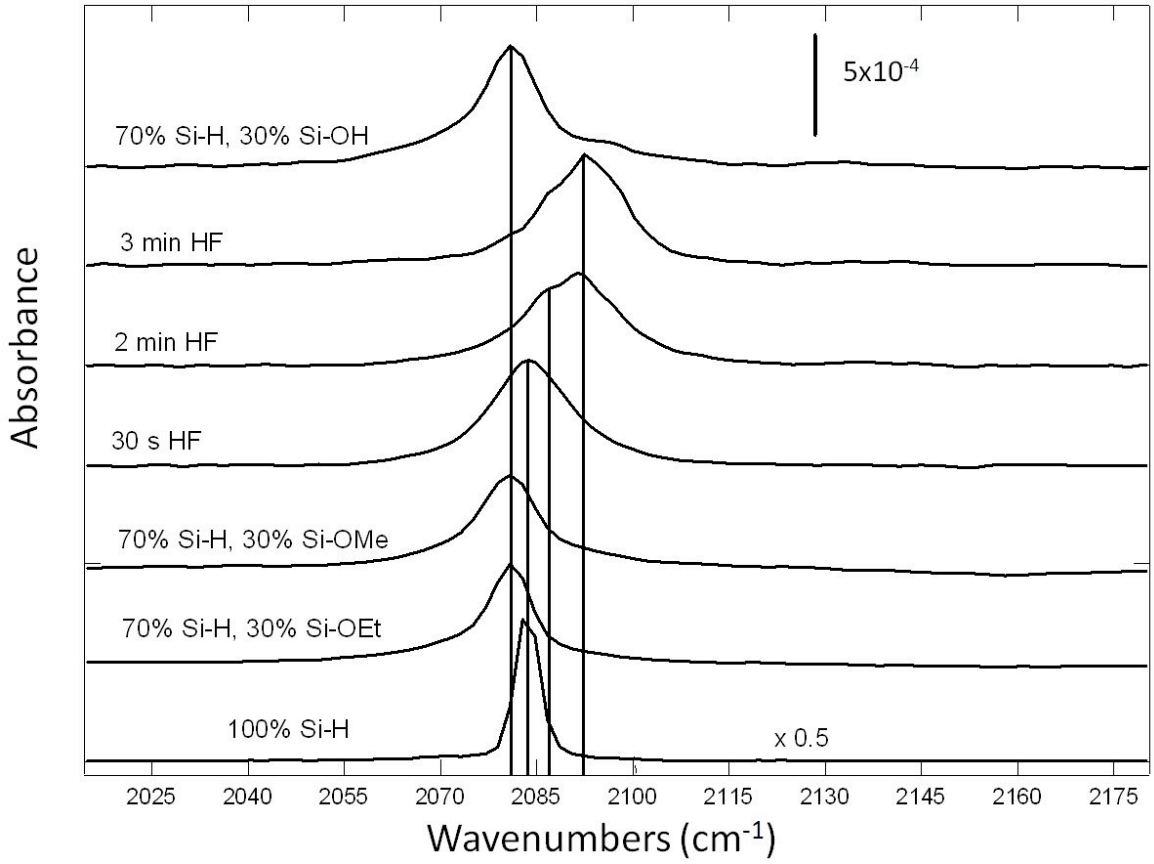

Figure 1.5.5. Transmission infrared spectra of flat silicon surfaces referenced to oxidized silicon surfaces. From bottom to top: freshly hydrogenated silicon, after reaction with ethanol (leading to 70% SiH, 30% $SiOC_2H_3$) and methanol (leading to 70% Si–H, 30% $SiOCH_3$). After sequential treatment in 49% HF(aq) for t=30 s, 120 s and 180 s (leading to 70% Si–H, 30% Si–F), and after immersion in water (leading to 70% Si–H, 30% Si–OH).(Courtesy of the Chabal Group UT Dallas)

It is interesting that the methoxy surface does not show a shift due to lone pair donation. Oxygen does contain lone pairs that should shift the spectra in a similar manner as the halides. Using methoxy functionalized trisilanes it is possible to understand why

this may be the case. By choosing the trisilanes which best reproduce the geometry of the surface and calculating the frequencies of the trans and gauche geometries one can calculate the splitting due to orientation of the methoxy group. In the trans configuration when the lone pairs of the oxygens point towards the hydrogen of interest the lone pair donation of the oxygen strengthens the Si–H bond (1.487 Å), increasing the frequency. If the lone pair of the oxygen is oriented away from the hydrogen of interest the bond is weakened (1.490 Å), decreasing the frequency. This clearly shows a lone-pair effect due to the hydroxyl (or methoxy) group on a neighboring Si–H bond. The key to understanding why this is not present on the surface is the surface geometry. On the surface there are two equivalent orientations of the methoxy groups. In both orientations a methoxy group lone pair will face towards some hydrogen and away from others. Therefore, the effect is nearly cancelled by both positive and negative frequency shifts from neighboring methoxy groups. An effect of this type is not possible for halides that are spherical.

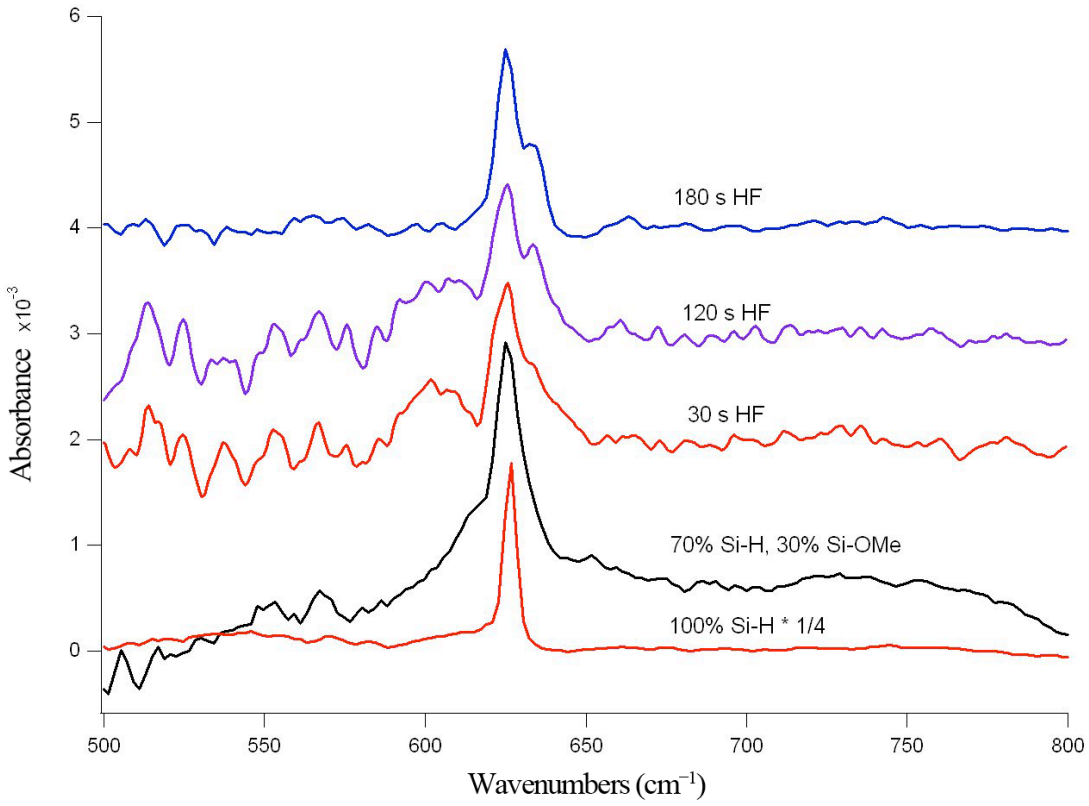

Figure 1.5.6. Transmission IR-spectra silicon surfaces referenced to oxidized silicon surfaces showing the region typically associated with the Si–H bending modes. From bottom to top: 100% hydrogenated silicon, after 30% $–OCH_3$ coverage, after sequential treatment in 49% HF(aq) for t=30 s, 120 s and 180 s (leading to 30% Si–F coverage). (Courtesy of the Chabal Group UT at Dallas)

In previous studies the Si–H *bending modes* were observed not to shift after 30% coverage of $–OCH_3$.[76, 97] In our current work, we also do not observe bending mode shifts for the surface with 30% methoxy coverage. Upon fluorination of the surface a shoulder is observed in the region of the Si–H bending mode, figure 1.5.6. The most likely attribution of this feature is to a split in the bending modes due to the lower symmetry of

the 30% Si–F surface. The experimental splitting for the peaks is ~17 cm^{-1}. The calculated spectrum does show a splitting for the bending modes but the lack of intensity data makes it difficult to make definitive assignments. The splitting of the Si–H bending vibrations for the 50% fluorine/50% hydrogen coverage is approximately 15 cm^{-1} for analogous modes. The splitting is due to the lower symmetry of the system that makes the surface directions nonequivalent. However, the close agreement is probably fortuitous since the coverage in the calculations is not the same as in the experiments. It is interesting that a similar splitting of 15-22 cm^{-1} is calculated for the other halogenated surfaces also. More work is necessary to understand the dependence of the splitting on the adsorbate-coverage, and why the splitting is observed for partially halogenated surfaces but not for partially methoxy covered surface.

Conclusions

We have investigated the geometries and frequencies of Si(111)-1×1 surface with mixed halide and hydrogen coverage. We have also characterized the relationship between the ν(Si–H) mode and the percentage of halide coverage. The ν(Si–H) mode blue-shifts with increasing halide coverage. The relationship is linear for fluorine and approximately linear for chlorine and bromine. At high coverage, chlorine, bromine and iodine show some saturation of the effects. The calculated values were calibrated by experimentally characterizing a ~30% fluorine surface which showed excellent agreement with the predicted values. Our proposed explanation for the origin of the shifts is a combination of an inductive effect that is highest for fluorine and declines down the period along with a lone pair donation to the silicon surface that is highest for iodine and decreases up the period.

1.6 Adsorbate–Phonon Coupling

Chemical modification of silicon surfaces using organic molecules provides a possible route to highly ordered semiconductor devices containing novel functionality. Much of the current literature[3, 9, 13, 14, 26, 27, 29, 30, 47, 50, 53, 55, 56, 76, 91, 97] in this area has concentrated on functionalization of the Si(111) surface using a two step alkylation/chlorination technique followed by reaction of the surface with a Grignard reagent.[11, 18, 31-33, 46, 60, 63] In order to achieve well–ordered layers it is necessary to begin with as close to an atomically flat surface as possible. An ideal starting point is the H-passivated Si(111) surface obtained by buffered HF (or NH_4F) etching.[7] This process creates an almost atomically flat surface that is ideal for further functionalization described above.[8, 9, 22, 25, 28, 32, 33, 46, 54, 56-60, 62] The structure of the hydrogen-passivated surface, therefore, has far reaching implications for silicon surface functionalization.

Determination of surface structure is a difficult task that is best accomplished using a combination of theory and experiment. In particular, surface infrared vibrational spectroscopy combined with quantum chemical cluster calculations has been used successfully as a probe of surface structure[61, 69, 97, 101] for both Si(100) and Si(111) surfaces. For example, the structure of the methylated Si(111) surface has been determined from HREELS (high resolution electron energy loss spectroscopy),[32, 46] surface vibrational spectroscopy,[33] and was supported by theoretical calculations.[61] The structures of the water dissociation products on Si(100) have also been extensively characterized using a combination of theoretical predictions and experimental observations.[101] In many such studies, the structural assignments are confirmed using isotopic substitution reactions, e.g., D_2O substituted for H_2O.[101] Using a force constant

analysis, it is possible to predict the shift of the hydrogen vibrational modes on deuterium substitution and then confirm the results by observation.

In this work we have interpreted Fourier transform infrared (FTIR) spectroscopy along with gradient-corrected density functional theory and two-dimensional periodic boundary conditions to determine the frequency shifts of deuterated versus hydrogenated Si(111) surfaces. Indeed, the experimental observation of a blue shift of the Si–H bending mode upon deuterium substitution suggests that the nature of the surface vibrational spectrum on such atomically perfect surfaces is more complex than originally thought. The theoretical calculations reveal that, when adsorbate bending vibrations (e.g., Si–D bending mode) are in the vicinity but lower than selected surface phonon modes, a coupling takes place that substantially affects the surface phonon spectrum. In the case of deuterium, it leads to an increase of a phonon mode at ~ 537 cm^{-1}, i.e., at a frequency seemingly too high for a pure Si–D bending mode.

Computational Details

Surfaces are intrinsically complex systems whose large size and rigid structure present challenges to cluster-based modeling. To overcome these problems we have used periodic boundary conditions (PBC) to simulate the effect of an infinite system on a unit cell. The PBC implementation of Kudin and Scuseria[39-41], which uses atom-centered basis functions, was used for all energy calculations and geometry optimizations.

As previously mentioned, the ground state structure of the hydrogen or deuterium passivated Si(111) surface is the bulk structure with a single adsorbate atom per surface dangling bond.[7] This simple structure reduces the number of atoms in the unit cell to one

unique atom per layer. It is thus possible to use a larger number of layers to model the system. In our case we have used ten layers in addition to the upper and lower surface adsorbate atoms resulting in twelve atoms per unit cell, figure 1.6.1. The model was then completely optimized without constraints using the gradient-corrected BLYP density functional (composed of the B88 exchange functional[35] and the Lee-Yang-Parr correlation functional[37]) with the 6-31G(d,p)[38] polarized double-zeta basis set. While hybrid functionals such as B3LYP that include exact exchange are generally more accurate than their GGA counterparts, they are far less cost effective for periodic systems of this type. We have shown in previous studies that BLYP/6-31G(d,p) model provides a reliable description of the vibrational properties for these similar systems.[10, 76]

There are no readily available analytic second derivatives for PBC. Therefore, in order to calculate the harmonic vibrational frequencies the analytically obtained forces were numerically differentiated using symmetric displacements of the Cartesian coordinates with a step size of 0.001 Å. This procedure results in a Cartesian force constant matrix that is then mass-weighted and diagonalized to obtain the vibrational frequencies (eigenvalues) and normal modes (eigenvectors). The resulting frequencies are fully periodic but do not include phonon-dispersions resulting in Γ–point only frequencies. The consequences of this approximation have been previously described.[76] Assignments were then made using these computed vibrational frequencies without any other corrections. All calculations were performed using a modified version of the Gaussian Development Version suite of programs.[42]

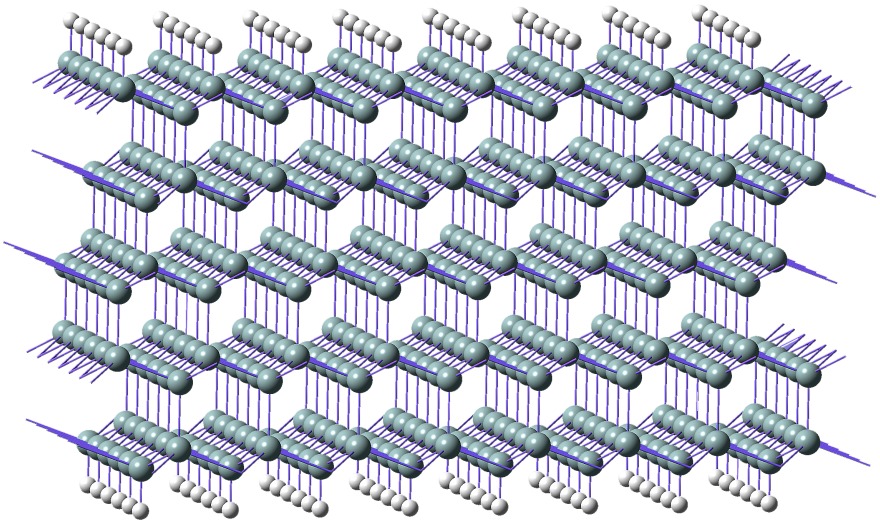

Figure 1.6.1. The ten layer two-dimensional PBC model of the H-terminated Si(111) surface with the larger spheres representing silicon atoms and the small spheres representing hydrogen atoms.

Results and Discussion

The geometry of the hydrogen passivated Si(111) surface is simple in form. While the structure of the unpassivated Si(111) surface is a complex 7x7 reconstruction under ultra-high vacuum conditions, hydrogen passivation from a wet-chemical preparation results in the formation of a nearly perfect 1x1 monolayer on the surface[7] with a hydrogen atom satisfying the single dangling bond present at each surface silicon. The

PBC geometry optimization was accomplished using the BLYP functional that has given reliable geometries in past studies.[61, 69, 97] It should be noted that the bond distances from the BLYP optimized geometry (2.40 Å for the Si–Si distance and 1.50 Å for Si–H) are slightly longer then the observed values (e.g., the bulk value silicon–silicon distance is 2.35 Å). This 2% increase in bond length has been previously discussed.[61]

It is expected that if a hydrogen atom is replaced with a deuterium the associated vibrational frequencies will shift to lower values based on the difference in the reduced mass of the total atoms participating in the vibrational mode. Under the approximation that the potential energy surface does not change with isotopic substitution, the nature of the shift, *for modes that are dominated by hydrogen motion*, can be predicted by taking the square root of the ratio of the masses, i.e., $1/\sqrt{2}$ or approximately 0.707 for hydrogen to deuterium. This result is expected for both Si–H stretch and Si–H bend due to the light mass of hydrogen. The actual shift may vary slightly due to the influence of cubic and quartic terms in the potential energy as well as the contribution of other heavier atoms in the vibration. Using these values, the predicted isotopic shifts are a validation of the surface spectral assignments.

Table 1.6.1. The experimental and calculated values for the infrared vibrational mode of the hydrogen- and deuterium-terminated Si(111) surface in wavenumbers, cm^{-1}.

Mode	Si–H Calc	Si–H Obs	Si–D Expected[a]	Si–D Calc	Si–D Obs
Stretching	2120	2083	1499	1525	1516
Bending	628	626	444	412	n/o
Coupling	476[b]	n/o	n/a	519	537

[a]The expected values are calculated by multiplying the observed Si-H values by $1/\sqrt{2}$ (~0.707).
[b]The hydrogen-phonon coupling is weak and can be considered almost a pure phonon mode. For this reason, there is very little change in either the intensity or frequency of this mode for the H/Si(111) or O_x/Si(111) surfaces, and hence no difference in absorption is observed.
n/o stands for not observed out of the noise.

The infrared absorption spectra of H- and D-terminated Si(111)–(1×1) shown in figure 1.6.2 confirm that the Si–H stretch mode (ν_{Si-H} = 2084 cm^{-1}) detectable with 74° incidence (spectrum b), and the Si–H bend (δ_{Si-H} = 626 cm^{-1}), detectable with 10° incidence, are polarized perpendicular and parallel to the surface, respectively. With near normal incidence (~ 10°), the electric field is essentially parallel to the surface and therefore cannot excite perpendicular modes, such as the Si–H stretch. Upon deuteration of the Si(111)–(1×1) surface, the Si–D stretch is observed at 1514 cm^{-1} (figure 1.6.2 d) as expected. However, a strong and sharp mode is also observed at 537 cm^{-1} (figure 1.6.2 c and d), well above the expected Si–D bending mode (~ 450 cm^{-1}). The theoretical assignment of the modes for the hydrogen and deuterium terminated surface is shown in table 1.6.1, with schematics of the modes drawn in figure 1.6.3. While all surface phonon modes were inspected, *only those modes that have a non-negligible (displacement less than 0.1 amu^{½} Bohr) contribution from the hydrogen/deuterium* are listed. The calculated hydrogen stretching mode is seen at 2120 cm^{-1} in the calculated spectrum. The higher-

than-expected accuracy of the theoretical value relative to the experimentally observed value can be attributed partly to the cancellation of the opposing effects of anharmonicity and bond length overestimation. The deuterium spectrum is shifted to 1514 cm^{-1} in the experimental spectrum (figure 1.6.2 a) and 1525 cm^{-1} in the theoretical spectrum (table 1.6.1, diagram in figure 1.6.3 a). The Si–D experimental stretching mode is seen only for an incidence angle of 74° (figure 1.6.2 d) and not for 10° (figure 1.6.2c). The deuterated surface must be atomically flat with a monodeuteride termination. The experimentally observed frequency of the Si–D stretch is slightly red shifted relative to previous measurements for an atomically smooth D/Si(111) surface.[102] This red shifting implies the presence of some surface bound impurities that reduce the dipole coupling between neighboring Si–D species.[98-101] The FTIR spectra of our D/Si(111) sample also demonstrate the presence of a small amount of oxidation (approximately 3% of the Si-O-Si longitudinal optical and transverse optical mode areas observed after an SC1/SC2 clean of the native oxide surface) relative to the initial oxide-free H/Si(111) surface, and this is consistent with this reduction in dipole coupling. These observed Si-D stretching frequencies are very close to the expected shift from simple mass arguments, which are 1499 cm^{-1} and 1473 cm^{-1} based on the calculated and experimental frequencies for Si–H respectively. All these observations are consistent with the well-understood behavior associated with the silicon-hydrogen stretching mode at 2083 cm^{-1}.

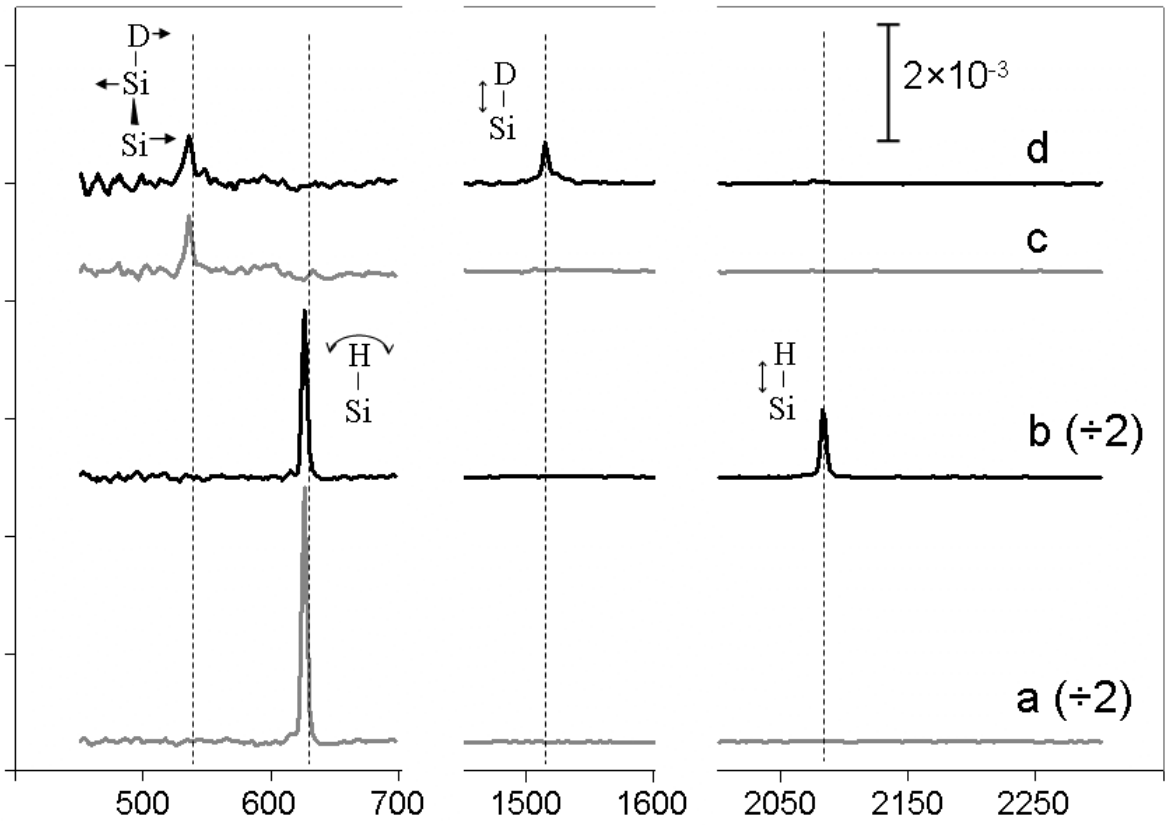

Figure 1.6.2. FTIR spectra of the atomically smooth H/Si(111) surface with an infrared-light incidence angle of a) 10° or b) 74° off normal, and the atomically smooth D/Si(111) surface with incidence angles of c) 10° or d) 74° off normal. For clarity, the intensities of spectra a) and b) have been divided by a factor of 2 relative to the scale provided. (Courtesy of the Chabal Group at UT Dallas)

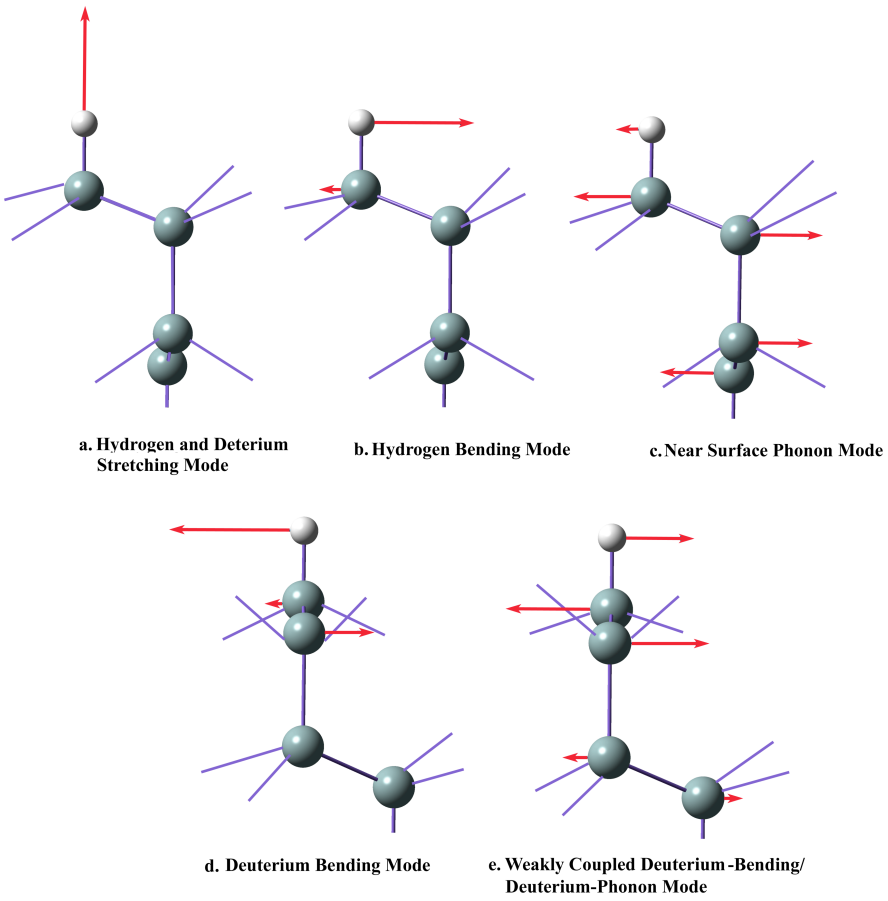

Figure 1.6.3. A schematic of the local atomic motions in the key vibrations considered in this study. The atomic displacements (indicated by the length of the arrows) are scaled relative to one another.

The bending mode is both more complicated to assign and more interesting. The experimental value for the hydrogen bending mode has been assigned at 626 cm^{-1}. The dipole for the Si–H bending motion is oriented parallel to the surface and is, hence, observed at both angles of incidence. The assignment is consistent with the calculated value of 628 cm^{-1}. While the computed errors for bending modes are typically smaller,

the nearly perfect agreement in this case results from a fortuitous cancelation of the inherent error of the BLYP functional with the neglect of anharmonicity. At first glance the deuterium spectrum gives puzzling results. The expected shift by a factor approximately 0.707 places the vibration inside the phonon region at 444 cm^{-1} where it may not be easily experimentally observed due to detector limitations. However, a clearly observed feature at 537 cm^{-1} (figures 1.6.2 and 1.6.4**),** is observed at both 74° and 10° off normal, implying that the mode is oriented parallel to the surface. If this peak corresponds to the deuterium bending it would indicate the vibrational frequency decreases *far less* than expected. Since this occurrence is rather unlikely we investigated the possibility the mode is not the deuterium bending mode. Considering that the surface has few defects there are a limited number of other possibilities. For example, the surface may also contain phonon modes that have significant intensity. But since the observed absorbance spectrum is the difference of two single beam spectra, the phonon modes should be the same in each surface and would be expected to cancel. If it is a phonon mode it must therefore be a mode of significantly different intensity relative to the H/Si(111) or O_x/Si(111) reference surfaces. Another possibility is the coupling of the deuterium bending mode with the near-surface phonon modes. This phenomenon (i.e., coupling of near surface phonons with surface adsorbate atoms) has been seen in several previous studies.[56, 65, 93] For this mechanism to be in accordance with the data, the coupling of the near-surface phonon modes with the adsorbate bending must change with the mass change.

When the normal modes (eigenvectors) of the calculated deuterium adsorbate spectrum are examined in the lower frequency region, the deuterium bending mode is

seen at 412 cm^{-1}, relatively close to the expected value of 444 cm^{-1}. This mode is dominated by deuterium motion (~ 90%) with only a modest vibrational coupling with the phonons in this region of the spectrum. This is clearly analogous to the hydrogen bending mode calculated at 628 cm^{-1} (table 1, diagram in figure 3b) and observed at 626 cm^{-1}. This mode is clearly *not* the mode that corresponds to the observed mode at 537 cm^{-1}. A closer inspection of the computed frequencies reveals the presence of another mode at 519 cm^{-1} (table 1.6.1, diagram in figure 1.6.3 e) that corresponds to weak coupling between the near-surface phonons and the deuterium bending. Unlike the mode at 412 cm^{-1}, (table 1.6.1, diagram in figure 1.6.3 d) this mode is mostly dominated by the opposing motion of the first two layers of silicon atoms with a significantly smaller contribution of deuterium bending motion, and is polarized parallel to the surface (as observed experimentally). There is a weaker contribution of the deeper silicon layers. A similar phonon mode can also be seen for hydrogen at 476 cm^{-1} (table 1.6.1, diagram in figure 1.6.3 c), although the coupling to the hydrogen-bend motion is significantly weaker. It is clear that the coupling is stronger for deuterium, resulting in a higher intensity for deuterium, making it observable for the latter.

We suggest the following explanation for the observations. In the case of deuterium, the frequency of the intrinsic deuterium bending mode (expected around 440 cm^{-1}, table 1.6.1) is slightly lower in frequency than the intrinsic near-surface phonon mode that occurs around 480–500 cm^{-1}. The coupling to the phonon from the lower frequency Si–D bend shifts the phonon mode to higher frequency (computed at 519 cm^{-1}, table 1, diagram in figure 1.6.3 e) and allows it to be detectable. In the case of hydrogen, the intrinsic bending mode (~ 620 cm^{-1}, table 1.6.1, diagram in figure 1.6.3 b) is

significantly higher in frequency than the near-surface phonon modes. The coupling is much weaker due to the lighter mass of hydrogen as well as the larger intrinsic frequency difference, and shifts the phonon mode slightly lower in frequency.

Overall, in the case of hydrogen, the observed mode at 626 cm^{-1} is mostly composed of Si–H bending while in the case of deuterium, the observed mode at 537 cm^{-1} is mostly composed of phonon motion. The differences arise from the fact that on going from H to D, the intrinsic bend moves from *above* the phonon region to *below* the phonon region. Our computational studies show that the point at which the qualitative nature of the mode changes, i.e., the point at which the intrinsic modes are equal in frequency, occurs for adsorbate atoms having masses around 1.6 amu.

The observation of such an adsorbate-coupled near surface phonon mode can also be seen for the chlorine-terminated surface at 527 cm^{-1} and for the methyl-terminated surface at 522 cm^{-1}.[61, 69] The intrinsic bending mode for both of these adsorbates is also lower in frequency than the intrinsic phonon mode. The fact that the mode shifts only slightly with the adsorbate (e.g., D vs. Cl) is consistent with a mode composed mostly of a phonon whose frequency blue shifts slightly, but sufficiently high enough, with different adsorbate atoms to be observable. We predict that a similar mode is likely to be seen for other monovalent adsorbates on the unreconstructed Si(111)–1×1 surface with a mass greater than that of deuterium. From this combined theoretical and experimental evidence, we can assign the 537 cm^{-1} mode of the D-Si(111) surface to near-surface phonons weakly coupled to the deuterium-bending mode. If it is possible to examine the spectrum at lower frequencies, we believe the deuterium bending mode would appear around 400 cm^{-1}, as expected. Nevertheless these observations confirm that the simple

isotopic exchange from hydrogen to deuterium leads to a considerable difference in the degree of coupling between the subsurface phonons and the surface adsorbates.

Figure 1.6.4 demonstrates that the Si–D coupled phonon and bending mode can be observed for other Si–D containing surfaces even when it is dispersed among different adsorbate species. The spectra in figure 1.6.4 result from the exposure of atomically smooth H–Si(111) to 65 °C solutions of neat anhydrous CH_3OH, CH_3OD, and CD_3OD. In these cases, approximately 30% of the initial Si–H is removed and replaced with either $Si–OCH_3$ or $Si–OCD_3$. This replacement occurs randomly across the surface, rather than in phase separated domains, based on the red shift in the Si–H stretching mode.[91] The surfaces that result from this chemistry retain their initial atomically smooth nature as evidenced by the orientation of the resulting modes (both $Si–OCH_3$ and Si–H related), and to the absence of any detectable dihydride or monohydride step modes. Despite the difference in chemistry of the surface sites (70% Si–D, and ~30% $Si–OCH_3$ or $Si–OCD_3$), the coupled Si–D bending and near surface phonon modes are almost the same intensity relative to the smooth deuterated surface (*vide supra*). The fact that the coupling of the intrinsic bending modes of the surface adsorbates to the phonon mode does not shift with surface coverage was also seen in other computational studies of small clusters when one of the seven surface deuterium atoms was replaced with a methyl group. Since the mode is mostly comprised of phonon motion that is *weakly* coupled to the surface adsorbate, it can be understood that it may not shift significantly due to relatively minor surface-coverage changes in the adsorbate atoms. In order for this to be the case, the splitting between the near surface phonon mode coupled to a deuterium or methyl adsorbate is not large, in accordance with the observed spectra.

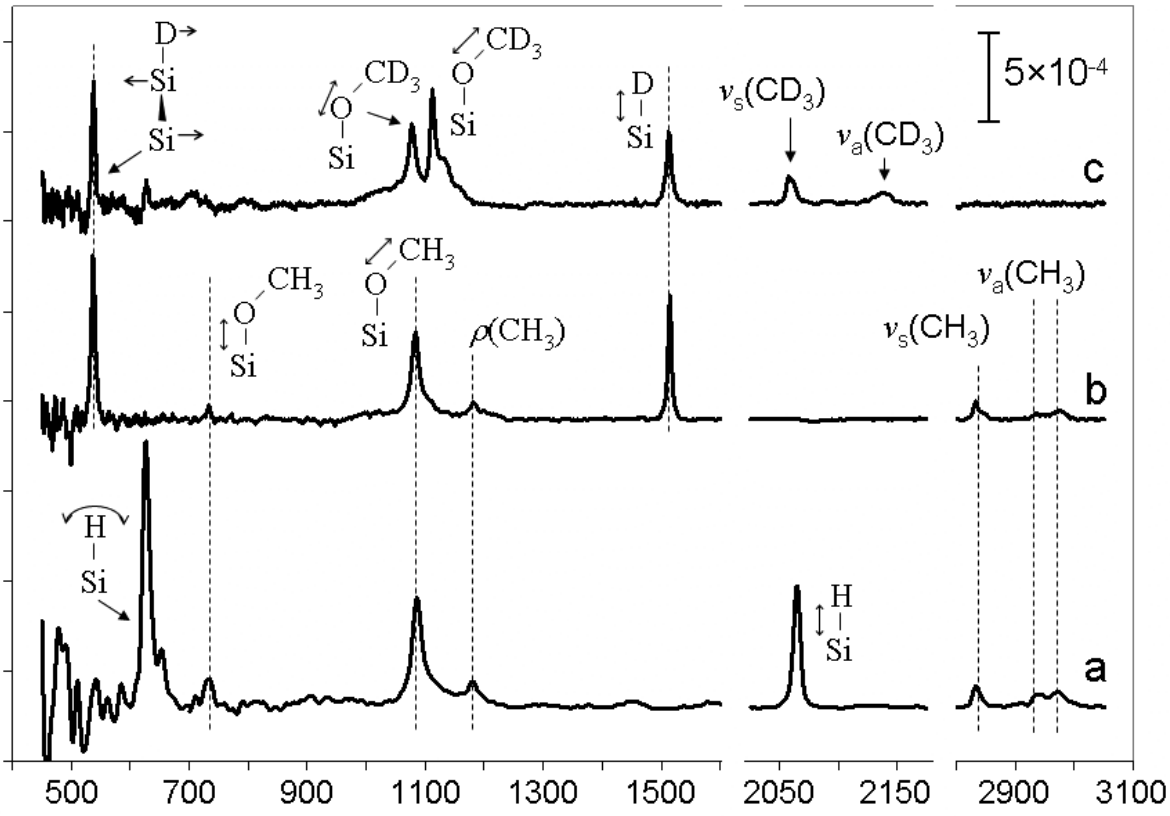

Figure 1.6.4. FTIR spectra for H/Si(111) surfaces after a 3-hour exposure to a 65 °C solution of either a) CH_3OH, b) CH_3OD, or c) CD_3OD. Reaction with CH_3OH or CH_3OD produced similar amounts of surface-bound Si–OCH_3 species (i.e., similar peak areas were observed for the CH_3 stretching modes at 2832 cm^{-1}, 2940 cm^{-1}, and 2970 cm^{-1}, for the CH_3 umbrella modes at 1190 cm^{-1}, for the modes at 1085 cm^{-1}, which are comprised of a C–O stretch coupled with a CH_3 bending motion, and for the Si–O stretching modes at 735 cm^{-1}). The Si-H stretching (2083.7 cm^{-1}) and Si–H bending (626 cm^{-1}) modes were, however, only observed on surfaces reacted with CH_3OH. For surfaces reacted with either CH_3OD or CD_3OD, no detectable Si–H modes were observed, and only the Si–D (1512 cm^{-1}), Si–Si–D coupled phonon and bending mode (537 cm^{-1}) were observed. The isotopic exchange of the remaining Si–H sites (approximately 70% of a monolayer) after reaction with either CH_3OD or CD_3OD has

been observed previously[91] and is ascribed to either a step-flow or direct-exchange mechanism. Reaction of H/Si(111) with CD_3OD produces a similar amount of Si–D surface coverage relative to CH_3OD, but spectral features attributing to the formation of $Si–OCD_3$ sites are observed (CD_3 stretching peaks at 2068 cm^{-1}, 2216 cm^{-1}, and 2224 cm^{-1}, a coupled CD_3 umbrella and C–O stretching mode at 1112 cm^{-1}, a coupled Si–O–C stretch and a CD_3 bending mode at 1078 cm^{-1}, and Si–O stretching peaks at 735 cm^{-1}). Very little observable subsurface oxidation was observed after any of these reactions. For clarity, the spectral regions of 450-700 cm^{-1} and 2000-2200 cm^{-1} have been reference relative to the native oxide surface, while the spectral regions of 700-1600 cm^{-1} and 2800-3050 cm^{-1} have been referenced relative to the freshly-etched H/Si(111) surface. (Courtesy of the Chabal Group UT Dallas)

Conclusions

To summarize, we have investigated the spectrum of the deuterated and hydrogen-terminated Si(111) surface using theoretical and experimental techniques. To explain the unexpected presence of a sharp vibrational mode around 535 cm^{-1} for deuterated, chlorinated and methylated Si(111)-(1×1) surfaces, it was necessary to consider the coupling of near-surface phonons with the bending mode of the surface. This phenomenon resulted in a shift in the ordering of the expected vibrational modes when hydrogen was replaced by deuterium. We have assigned the vibrational modes of both surfaces and have offered a simple explanation for the appearance of this phonon mode on Si(111)-(1×1) surfaces containing adsorbates heavier than hydrogen.

1.7 Si–H Vibrations of the Si(100) Surface

When thinking of the importance of various materials one could not question the primacy of silicon to the microelectronic industry.[7, 8, 10, 19, 21, 42, 66, 102] While the Si(100) surface has been instrumental for most key developments in microelectronics due to its small number of defects, several other materials systems have shown significant promise, e.g., the Si(111)-1×1 reconstruction,[1, 57, 98] the Ge(100)-2×1 surface,[7, 8, 42] and compound semiconductors such as gallium arsenide or indium phosphide.[103-106] While silicon may lose its preeminent place as the material of choice for semiconductors, future devices are still likely to be built upon silicon substrates. As the limits of current technologies are reached the need to understand silicon surface reactivity will become ever more critical. To drive forward basic research in this area we must understand the structure of the silicon surface at the atomic scale. An understanding of surface structure allows for the prediction of novel chemistry on such surfaces. For example, surface morphology has been shown to control chemistry on the surface, e.g., radical-initiated chain reactions of organic molecules on the hydrogen-terminated Si(100)-2×1 surface.[103]

While much is understood about the bare, hydrogen terminated, and oxidized silicon surfaces, many problems of surface characterization still exist. Characterization of surfaces is difficult due to their complex nature. Among the many techniques used to explore surface structure one of the most successful is Fourier transform infrared spectroscopy (FTIR),[6] most especially when used in conjunction with quantum chemical calculations.[62, 92, 108, 109] The combination of these methods has yielded significant returns for many systems including the hydrogen terminated Si(111) and Si(100) surfaces.[56, 62, 65, 72, 92, 93, 96, 99-101, 108-115] Detailed experimental information is available for the flat hydrogen terminated Si(111) surface and the 9º miscut vicinal Si(111) surface. Likewise, the 2×1,

3×1 reconstructions of the Si(100):H surface along with the dihydride-terminated (1×1) surface have been carefully studied. More recently a bowtie feature has been identified as the dihydride dimer feature on Si(100):H.[45, 102, 116, 117] Each of these reconstructions results in a different set of vibrational frequencies that can be analyzed to yield the surface structure. Additional features may arise in the experimental spectra from the predominant defects on the surface. Finally, when lower frequency regions of the spectra are investigated, reliable quantum chemical calculations are essential for interpreting surface spectra since complex vibrational coupling makes the assignment of experimental modes particularly difficult.[104]

To our knowledge no comprehensive quantum chemical study of the Si–H vibrational modes *on a variety of surfaces using a uniform level of theory* has yet been performed. One reason may be the lack of a single coherent method for calculating all of the vibrations. While defect sites are most easily studied with cluster models, uniformly terminated surfaces are best calculated using periodic boundary conditions (PBC). The sensitivity of vibrations to the local geometry means that cluster models should be precisely calibrated. While a hydrogen-terminated single-dimer (Si_9H_{12}–based) model has been used by many groups in interpreting spectra and exploring reactivity on Si(100) surfaces, this model has not been calibrated with high quality periodic calculations. Such calibrations are now possible since PBC structures and vibrational frequencies can be calculated using the same level of theory, and could be rigorously compared to the cluster results. Recently we have evaluated the use of cluster models for approximating PBC numerical frequencies.[56, 65, 72, 93] This allows us to understand the validity of the structures and vibrational frequencies obtained with cluster models. In addition, it gives us a way to

explore surfaces which cannot easily be calculated using cluster models, such as the Si(100) dihydride-terminated surface that has substantial steric interactions.

In this paper we describe the geometries and assign the vibrational spectra of the hydrogen terminated Si(111):H flat surface, the 9º miscut Si(111) surface, the Si(100) 2×1, 3×1 and 1×1 reconstructions, along with the bowtie Si(100) defect. The Si(111) surfaces and the Si(100)-2×1 and 3×1 reconstructions are calculated using PBC as well as cluster models. In particular, the same model chemistry (identical density functional and Gaussian basis set) is used to make direct comparisons. Additionally, the Si(100):D frequencies are computed for the 2×1 and 3×1 reconstructions. The dihydride terminated Si(100) (1×1) surface and the vicinal 9º miscut Si(111):H surface are calculated using PBC. Finally, the bowtie defect (dihydride dimer) that is a local feature is treated with appropriate cluster models.

Computational Details

For each type of surface we have chosen the most appropriate modeling technique based on the nature of the surface, reconstruction, or defect. We will discuss our logic and then describe the details of each model. The goals for the Si(100):H (1×1) dihydride-terminated surface and the vicinal 9º miscut Si(111) surface is simply to calculate the geometry and assign the spectra. The geometry of the Si(100):H (1×1) surface is simple and calculated using a single unit cell PBC model. However, the severe crowding of the 1×1 surface frustrates the use of cluster models making the PBC model the appropriate choice. In previous work we have modeled the more complicated stepped Si(111) surface using a cluster model.[100, 101] We now use more robust PBC models to see if we can validate our previous conclusions. The important Si(100)-2×1 and Si(100)-3×1

reconstructions are modeled with both PBC and cluster models. The use of cluster models to calculate surface vibrations has been *de rigueur* for many years because of their success in modeling reactivity. It is our goal to determine the validity of such models by comparing high quality PBC results to cluster models for both the Si(100)-2×1 and Si(100)-3×1 reconstructions. The final structure is the bowtie defect found on the Si(100) surface. Since this structure occurs only at isolated sites on the surface where long range interactions are absent, we have used a small cluster to model this defect.

A uniform model chemistry has been used on all the systems with the same functional and basis set to ensure compatibility. We have employed the B88 gradient-corrected exchange functional along with the Lee, Yang and Parr correlation functional using a Pople-style double zeta 6-31G(d,p) basis set[30-33, 71] (model chemistry of BLYP/6-31G(d,p)). We have shown this model chemistry to give excellent frequency assignments in the past.[56, 65, 72, 93] While hybrid functionals such as B3LYP tend to be slightly more accurate, PBC calculations using such functionals are prohibitively expensive. The only major shortfall of the BLYP/6-31G(d,p) model is the Si–Si bond lengths which are typically too long by ~ 2% (0.04-0.05 Å). This deviation is systematic and does not negatively affect the quality of our results. PBC optimizations were carried out using the implementation of Kudin and coworkers.[34-36] Slab 2D models and linear 1D models using this implementation do not require 3D unit cells with a vacuum space resulting in a modest cost-saving per calculation.

All PBC models were constructed from ideal crystal structures that were subsequently modified to represent the appropriate surface, reconstruction, or defect. The simplest PBC model is the flat Si(111):H surface, figure 1.7.1. All of the surface silicons

are bound to single hydrogen atoms and the surface does not reconstruct. Instead the Si(111) plane terminates in the bulk crystalline structure with little or no strain. The PBC model can be constructed with one unique silicon atom per layer. The upper and lower surfaces are mirror images of one another. This simple structure allows us to make the model deep enough (eight layers or more between surfaces) to yield converged results. Similar models were also constructed for the dihydride-terminated Si(100)-1×1 surface. However, in this case the surface layer has a different orientation, and each surface silicon is bound to two terminating hydrogens resulting in substantial steric repulsions (*vide infra*), figure 1.7.2.

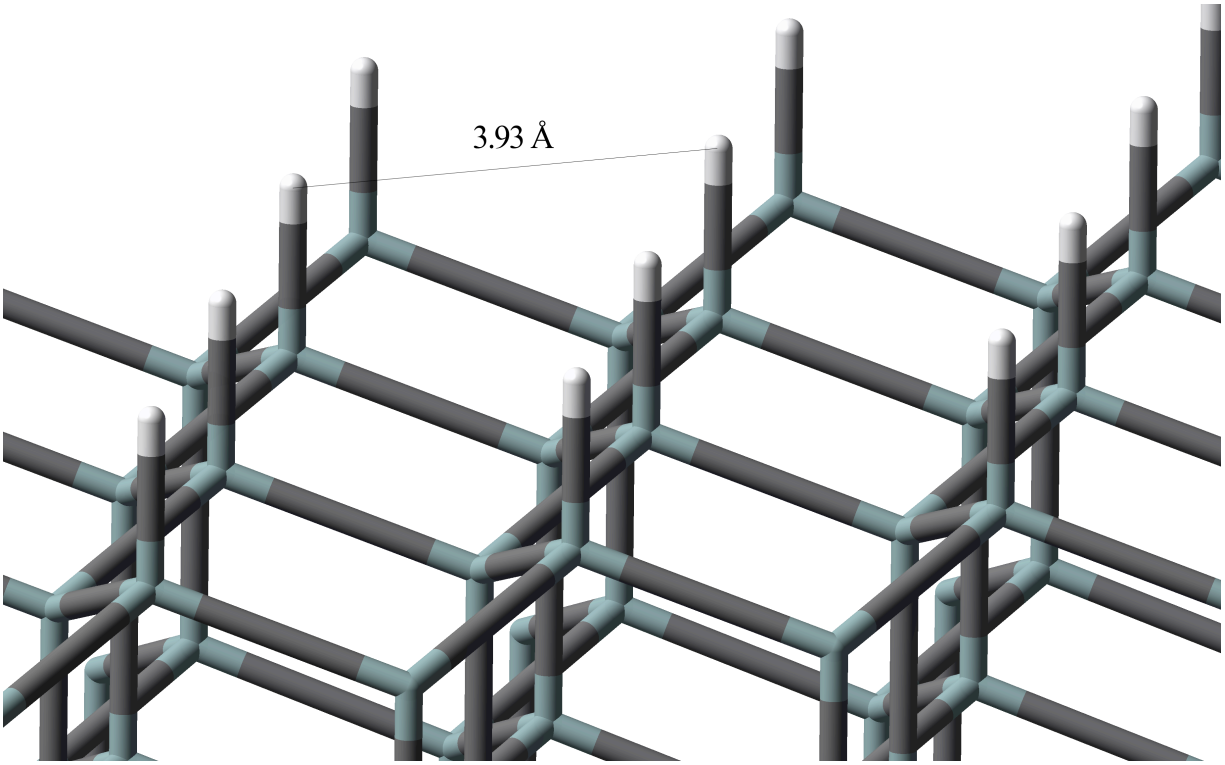

Figure. 1.7.1. The structure of the hydrogen terminated Si(100)-1×1 surface optimized using BLYP/6-31G(d,p) and PBC. White bars indicate hydrogen, blue-green bars indicate silicon, and grey bars indicate bonds. The supercell shown contains 12 unit cells.

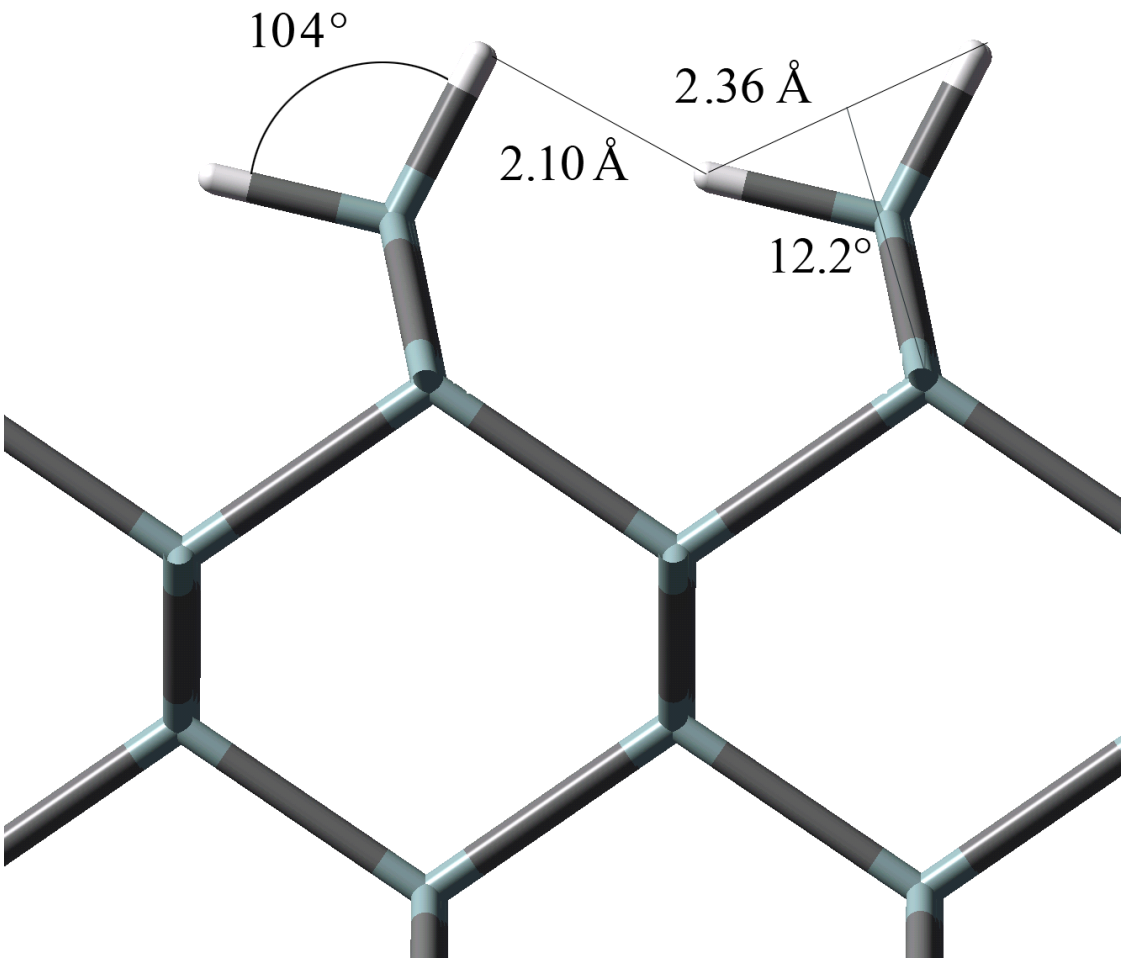

Figure 1.7.2. The structure of the canted dihydride of the Si(100)-1×1 surface, optimized using 10 layer PBC (two unit cells shown). White bars indicate hydrogen, blue-green bars indicate silicon, and grey bars indicate bonds.

The remaining models are more complicated. The Si(100)-2×1 surface has a larger unit cell with two surface atoms per surface layer. Due to the offset needed to model this reconstruction, two layers must be added at a time to conserve symmetry. These factors results in larger models compared to the Si(100)-1×1 surface. The reconstruction forms a chemical bond between adjacent surface silicon atoms resulting in a strained dimer.[105] While it is known the bare surface is buckled, the hydrogen-

terminated surface is flat. The unit cell for the PBC model for the H-terminated surface with a mirrored top and bottom surface can be seen in figure 1.7.3 a. To understand the effect of depth on convergence, we have investigated models with two, four and ten layers between the surface dimers. Several cluster models were also used to test the convergence of the calculated vibrations. The cluster models used correspond to the single dimer Si_9H_{12} model, two dimer models in the same row ("along" dimer row model) $Si_{15}H_{20}$, two dimer models in adjacent rows ("across" dimer row model) $Si_{21}H_{29}$, and the four-dimer cluster model $Si_{35}H_{40}$. All of the models use the PBC geometry in accordance with previous studies.[56, 65, 72, 93] The resulting dangling backbonds were terminated with hydrogen (Si–H=1.47 Å) in accordance with well established procedure.[34]

The PBC models for the Si(100)-3×1 surface are more complex than the 2×1 surface. The reconstruction leaves alternating rows of dimers and single dihydride silicon atoms. There are three atoms per surface layer and layers must again be added in pairs, due to the nature of the reconstruction, making these models computationally expensive, figure 1.7.3 b. These cluster models mimic the same pattern as the 2×1 cluster models. The models ranged from the smallest with one dimer and one dihydride, $Si_{15}H_{22}$, the across and along dimer models each with two dimers and two dihydrides, $Si_{36}H_{48}$ and $Si_{25}H_{32}$, a four dimer two dihydride model, $Si_{45}H_{52}$, and finally a square four dimer four dihydride model, $Si_{65}H_{76}$. All other parameters are the same for as for the Si(100)-2×1 surface.

The final models are for the 9º miscut vicinal Si(111) surface and the bowtie Si(100) defect. The unit cell for the miscut Si(111) surface contains twenty silicon atoms

and fourteen hydrogen atoms. This structure is shown in figure 1.7.4 a. Unlike the other PBC models used in this study, the periodicity is 1D rather than 2D. The nature of the kink makes the use of fully two-dimensional periodic models prohibitively expensive. The terminating hydrogens are frozen at the angles corresponding to those of the silicon atoms they are replacing. The imposed constraints allow for smaller models. Finally, the bowtie defect can be calculated using cluster models. This model was made by constructing a structure containing three dimers across rows and splitting the central dimer giving a stoichiometry of $Si_{37}H_{42}$. The model can be seen in figure 1.7.4 b. As in other cluster models, terminating hydrogens are frozen (Si–H distance of 1.47 Å). Convergence with cluster depth was tested to ensure the adequacy of PBC models, table 1.7.1.

Table 1.7.1. The frequencies of different PBC models for the Si(100)-2×1:H showing convergence with the number of layers. The units of all frequencies are in wavenumbers, cm^{-1}.

Si(100)-2×1:H	Single Dimer Stretch Frequency	
	Symmetric	Asymmetric
Four Layers	2110	2095
Ten Layer	2112	2095

We have calculated the PBC frequencies by numerical differentiation of the analytic forces and the cluster frequencies via the analytic force constants. While analytic force constants are usually preferable to numerical differentiation of the forces, in this case the finite difference method presents an embarrassingly parallel workload.[106] We

have taken advantage of the parallelization of the PBC force evaluations to speed up our calculations. The numerical frequencies used a two-point finite difference method (displacement of 0.001 Å) to yield the force constants. The force constant matrix is then mass-weighted and diagonalized to give the normal modes (eigenvectors) and the frequencies (eigenvalues). The frequencies were appropriately scaled to yield the results in wavenumbers, cm^{-1}. Cluster vibrational frequencies were calculated analytically, and spurious vibrational coupling between surface hydrogens and terminating hydrogens is eliminated by isotopic substitution. In general, the BLYP/6-31G(d,p) model gives harmonic frequencies that are in good agreement with experimentally observed frequencies. This is fortuitous and is partly due to cancellation of systematic errors from two opposing factors - the tendency of BLYP/6-31G(d,p) to give bond lengths that are slightly too long and the neglect of anharmonicity.

It is customary in quantum chemical calculations to scale computed harmonic frequencies to correct for known systematic errors. However, as mentioned above, the scale factor for BLYP/6-31G(d,p) is very close to unity. Nevertheless, we have scaled all computed frequencies with the exception of the 1D PBC by 0.9945[107] and obtain results in good agreement with experiment. The 1D PBC calculations that were performed subject to additional constraints (*vide supra*) seem to require a slightly different scale factor (0.9884) that was obtained by matching the high frequency stretching mode to well-characterized experimental data. Calculations were performed with a modified development version of the Gaussian suite of programs.[42]

Results and Discussion

In this section we discuss the results for the individual surfaces that we have investigated in detail. The well characterized periodic systems (H/Si(111), H/Si(100)-2×1, and H/Si(100)-3×1) are discussed first. This is followed by the more sterically hindered surfaces (canted Si(100) dihydride, and the stepped vicinal Si(111) surface). Finally, the bowtie defect which is a local defect on a Si(100) surface is discussed.

Hydrogen Terminated Si(111) surface

Before passivation the Si(111) surface has a large complex unit cell, forming a 7×7 reconstruction under ultrahigh vacuum conditions. After hydrogen passivation the surface reconstruction is eliminated to form a nearly perfect unreconstructed surface that terminates in the bulk crystalline geometry.[7] This resulting surface has one hydrogen atom per surface site and has very little strain. Periodic systems containing 4, 6, and 10 layers have been studied and yield very similar results. The simple nature of the surface suggests that there should be only two characteristic adsorbate vibrations: a perpendicular stretching mode and a parallel bending mode (doubly degenerate). Both modes have been well characterized experimentally and theoretically in the case of hydrogen. However, the system has shown surprising complexity in the case of deuterium due to a coupling between the adsorbate bending mode and a near-surface phonon mode. These results have been described previously and we summarize them briefly below.[76]

Table 1.7.2. A comparison of the PBC and experimental frequencies of the Si–X (X=H or D) for the passivated Si(111) surface.

Si(111):H/D Surface

	Frequencies, cm^{-1}	
Mode	PBC	Expt.[36]
Si–H Stretch	2105	2083
Si–H Bend	626	626
Si–H Phonon	472	n/o
Si–D Stretch	1517	1515
Si–D Bend	409	n/o
Si–D Phonon	515	536

n/o indicates not observed

The hydrogen and deuterium modes are listed in table 1.7.2. The stretching modes appear at 2105 cm^{-1} (calculated) and 2083 cm^{-1} (observed) for hydrogen, and at 1517 cm^{-1} (calculated) and 1515 cm^{-1} (observed) for deuterium. The high frequency of the mode and the results on isotopic substitution clearly allow for unambiguous description of the stretching mode. The same is not true for the bending mode. In the case of hydrogen, the bending mode appears at 626 cm^{-1} (calculated) and 626 cm^{-1} (observed), the perfect agreement being clearly fortuitous. After deuterium substitution the mode would be expected to shift by $1/\sqrt{2}$ or ~ 0.707 to ~ 440 cm^{-1} which is presently outside of the experimentally observable range. However, there is a parallel-polarized mode observed in infrared experiments at 536 cm^{-1}, much higher than expected for the silicon-

deuterium bend. This mode has been assigned to a weakly coupled phonon mode.[76] The nature of this mode and the difference between hydrogen and deuterium are interesting. The pure silicon-deuterium bending mode is calculated at 409 cm^{-1}, close to the value expected from simple mass considerations. The silicon-hydrogen and silicon-deuterium bending modes are both coupled to phonon modes but the silicon-hydrogen bending mode (626 cm^{-1}) is significantly *above* the frequency of surface phonons and the silicon-deuterium bending mode (409 cm^{-1}) is *below* the frequency of the near surface phonons. Therefore the silicon-hydrogen coupling to the phonon results in a small phonon red shift while the silicon-deuterium coupling to the phonon results in a larger phonon blue shift. Since the intrinsic phonon frequency is outside of the observable region in such difference spectra, the blue shift for deuterium pushes it into the observable region. Our previous theoretical study has shown the mass at which the silicon-adsorbate bending and phonon mode are equal is ~1.6 amu. We suggest that all well-ordered adsorbates with a mass above hydrogen will have such a coupled mode close to the phonon region ~ 500-550 cm^{-1} on the Si(111)-1×1 surface.

Hydrogen Terminated Si(100)-2×1 Surface

The Si(100)-2×1 reconstruction is a stable, well-characterized surface and has been analyzed in detail in many previous studies.[90, 108, 109, 115, 120-123] As can be seen in figure 1.7.3 a, the most salient feature of the 2×1 reconstruction is the presence of dimer rows on the surface with each dimer consisting of two silicon monohydrides bonded to each other (i.e., two hydrogens per surface dimer). The calculated Si–Si dimer bond distance is 2.45 Å for the single-dimer, ten-layer PBC optimization. This is about 0.06 Å

longer than the optimal Si–Si distance at the same level of theory, indicating the presence of significant surface strain.

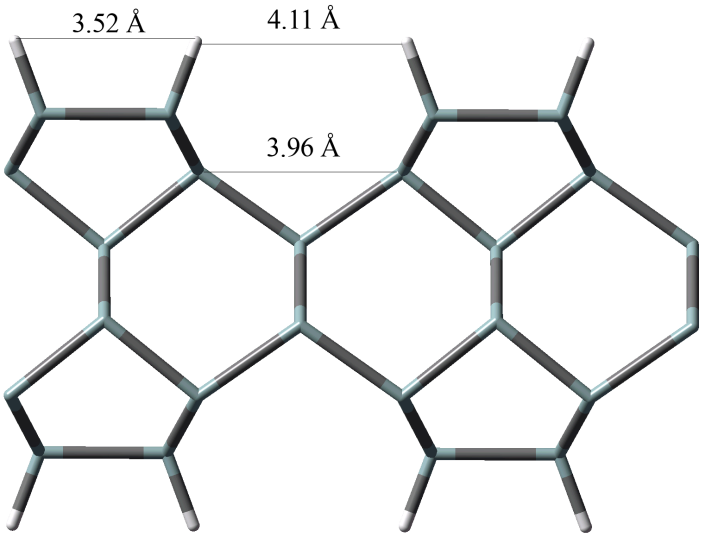

(a)

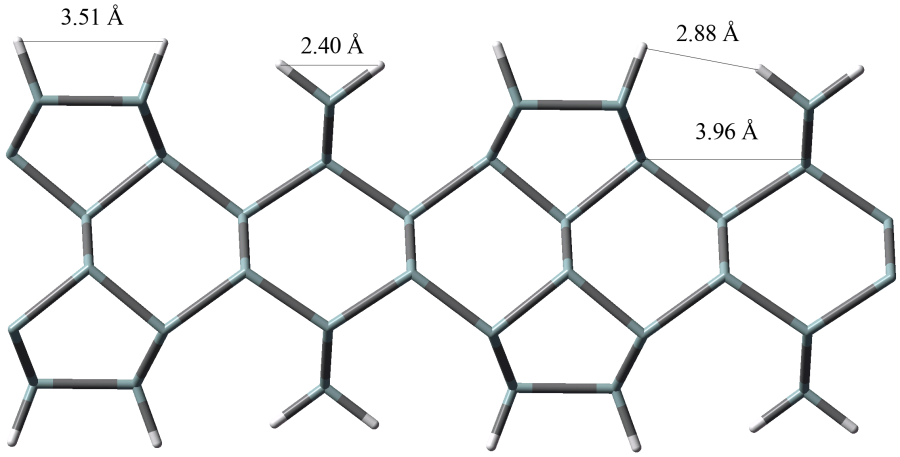

(b)

Figure 1.7.3. The side view of the PBC model for the **(a)** Si(100)-2×1 and **(b)** Si(100)-3×1 surfaces each showing two unit cells. Top and bottom surface are mirrored to avoid unphysical relaxation. White bars indicate hydrogen, blue-green bars indicate silicon, and grey bars indicate bonds.

To probe deeper into our PBC models we have optimized PBC unit cells with four and ten intermediate layers between surface dimers. The geometries as well as the vibrational frequencies obtained using the two models are quite close. The average deviation in the calculated frequencies is 2 cm^{-1} with a maximum deviation of 4 cm^{-1}. In particular, the maximum difference for the stretching frequencies is only 2 cm^{-1} (table 1.7.1). These differences show the values are fairly well converged with model depth.

A comparison between the calculated frequencies using PBC and cluster models of the hydrogen terminated Si(100)-2×1 surface is shown in table 1.7.3 with schematics of the modes in figure 1.7.5 a. To aid in this analysis, we have also carried out 1D PBC calculations for both directions, (a) along the dimer row and (b) across dimer rows. These values are also listed in table 1.7.3. The clusters and PBC models have an excellent correspondence for the Si–H stretching modes. The maximum difference is 6 cm^{-1} for the symmetric stretching mode between the PBC and the single dimer model. It is interesting to note that the splitting between the symmetric and asymmetric stretching frequencies increases from 8 cm^{-1} (single dimer model) to 15 cm^{-1} (2-dimensional PBC). This is principally due to the weak coupling between the neighboring oscillators that pushes the collective symmetric stretching mode up by a few cm^{-1}. As expected, the splittings obtained with the larger cluster models and 1-dimensional PBC are intermediate. Overall, definitive predictions of the stretching frequencies can be made using relatively small cluster models.

Table 1.7.3. Comparison of cluster models of increasing size with the PBC models for the Si(100)-2×1 reconstruction for both hydrogen and deuterium substitution.

2×1 Reconstruction							
Mode		**Cluster Model**					
	PBC	**1 Dimer**	**2 Dimer Along Row**	**1D PBC Along row**	**2 Dimer Across Row**	**1D PBC Across**	**4 Dimer**
				Hydrogen Frequencies, cm^{-1}			
Symmetric Stretch	2110	2104	2106	2108	2105	2107	2107
Asymmetric Stretch	2095	2096	2097	2098	2096	2096	2096
Rock (b_2)	629	657	657	654	649	634	648
Wag (b_1)	618	656	651	631	652	646	648
Twist (a_2)	618	648	646	631	642	632	630
Symmetric Bend (a_1)	604	629	631	631	620	607	624
				Deuterium Frequencies, cm^{-1}			
Symmetric Stretch	1520	1515	1516	–	1516	–	1517
Asymmetric Stretch	1508	1508	1509	–	1508	–	1508

The agreement between the bending modes of the cluster and the PBC results is not close. It is clear that the bending modes are not well converged for these models. The

deviation from the PBC and single dimer frequencies ranges from 25-40 cm^{-1}. The in-plane modes (symmetric bend and rock, a_1 and b_2 within C_{2v} symmetry) have a deviation of 25 and 28 cm^{-1}, while the out-of-plane modes (wag and twist, b_1 and a_2 within C_{2v} symmetry) have deviations of 38 and 30 cm^{-1}. Among these, the rock and wag modes are expected to have high intensities that can be observed experimentally.

In all cases, the single dimer frequencies are higher than the corresponding PBC values. It is clear that the coupling between different dimers is responsible for this frequency shift. The larger cluster models as well as the 1D PBC models are useful in interpreting this further. To illustrate this, let us consider two examples: (a) the in-plane rocking mode, and (b) out-of-plane wagging mode. The in-plane rocking mode is expected to couple strongly "across dimers" and only weakly "along dimers". This is consistent with the small calculated shift of 3 cm^{-1} on going from a single dimer model to 1D PBC (along dimers), and a larger shift of 23 cm^{-1} on going to the 1D PBC value (across dimers). Conversely, the out-of-plane wagging mode is expected to couple strongly along dimers and only weakly across dimers. This is again consistent with the smaller calculated shift of 10 cm^{-1} on going from a single dimer model to 1D PBC (across dimers), and a larger shift of 25 cm^{-1} on going to the 1D PBC value (along dimers). The frequency shifts on going from single dimer to 2-dimer cluster models are also qualitatively consistent with this analysis though the results are still far from reaching the corresponding 1D PBC results. Overall, even the four-dimer cluster model still shows substantial deviations from the full 2D PBC results, demonstrating the limitations of cluster models in this case.

The deuterated surface shows the same pattern for the stretching modes as the hydrogen terminated surface. There is a good agreement between the cluster and PBC models, and there is an increase in the splitting between the symmetric and asymmetric stretching modes on going from the single dimer model to PBC. The bending modes fall below the phonon bands precluding a definitive analysis.

Hydrogen Terminated Si(100)-3×1 Surface

In this reconstruction both dimer (monohydride) silicons and dihydride silicons are formed on the surface. The surface has dimer rows with dihydride rows in between. The surface is found at saturation coverage in the narrow temperature range between 360 and 400 K. Overall, the experimental spectra are more complex than for the 2×1 reconstruction and will be discussed below.[108, 109] The dimer silicon rows are 4.6 Å from the dihydride silicon rows. The nearest hydrogen-hydrogen distances are 3.9 Å along the rows and 2.9 Å between the dimer hydrogen and the dihydride hydrogen. This large spacing, that is larger than the sum of their van der Waals radii, allows for complete coverage without significant steric strain, figure 1.7.3 b. For this particular study we investigated PBC and cluster models including only four layers of bulk atoms. However, as seen earlier for the 2×1 surface, the frequencies should be adequately converged to enable a careful analysis. The cluster models contained up to four dimers and four dihydrides. The upper and lower surfaces of both models are mirrored to avoid unphysical relaxation. The mirrored cluster contains no symmetry for the local groups. The only other symmetry is the C_2 symmetry resulting for the mirrored upper and lower surfaces. The Si–Si dimer bond distance is very similar to that calculated for the 2×1

surface: 2.46 Å for the 3×1 vs. 2.45 Å for the 2×1 surface. The interaction of the dimers with the dihydride hydrogens is fairly weak.

Table 1.7.4. The Si–H vibrations of the Si(100)-3×1 reconstruction using both PBC and cluster models. The vibrations for hydrogen and deuterium are compared.

Si(100):H 3×1 Reconstruction					
Mode	PBC	Cluster Model			
		1 Dimer + 1 Dihydride	2 Dimer + 2 Dihydride Along	2 Dimer + 2 Dihydride Across	4 Dimer + 2 Dihydride Square
		Hydrogen Frequencies, cm^{-1}			
Dihydride Asymmetric Stretch	2126	2135	2137	2132	2129
Dihydride Symmetric Stretch	2122	2123	2124	2120	2116
Dimer Symmetric Stretch	2106	2106	2107	2106	2109
Dimer Asymmetric Stretch	2097	2098	2099	2099	2101
Dihydride Scissor	905	904	905	904	902
Dihydride Wag	648	690	680	672	667
Dimer Rock	636	650	648	641	642
Dimer Wag	613	633	636	633	637
Dimer Twist	613	641	623	627	620
Dihyride Twist	605	637	626	627	633
Dimer Symmetric Bend	607	626	617	612	615
		Deuterium, Frequencies, cm^{-1}			
Dihydride Asymmetric Stretch	1536	1542	1543	1540	1538
Dihydride Symmetric Stretch	1522	1520	1521	1519	1515
Dimer Symmetric Stretch	1514	1516	1516	1515	1520
Dimer Asymmetric Stretch	1509	1510	1509	1509	1519
Dihydride Scissor	654	653	654	652	651

The frequencies of the Si(100)-3×1 surface are a combination of the Si(100)-2×1 dimer (monohydride) vibrations and silicon dihydride vibrations, table 1.7.4. The dimer modes are analogues to the Si(100)-2×1 modes though they occur slightly higher on the 3×1 surface. The interaction of the dimer monohydride hydrogens and the dihydride hydrogens in quite weak as evidenced by the relatively small changes in the dimer hydrogen-stretching modes. The dihydride modes appear much higher in the spectrum than the dimer stretches at 2126 and 2122 cm^{-1} for the asymmetric and symmetric stretching modes, respectively. This splitting between the asymmetric and symmetric frequencies increases significantly to 14 cm^{-1} upon deuteration.

The results found with the clusters are consistent with the PBC results for the stretching modes as in the case of the 2×1 surface seen earlier. The overall mean absolute deviation between PBC and cluster models for all the stretching frequencies (including deuterated species) is only 3-4 cm^{-1}. The maximum deviation between the PBC and cluster results for the stretching modes is 11 cm^{-1} for the dihydride asymmetric stretch. The agreement for the symmetric stretch is much better within a smaller range of 1-6 cm^{-1}. The dimer monohydride frequencies are in essentially perfect agreement between cluster models and PBC.

The bending modes occurring below 1000 cm^{-1} are more difficult to assign with the exception of the dihydride scissor mode found at 905 cm^{-1}. Modes in the region of the spectra around 900 cm^{-1} are characteristic of surface dihydride species. The next six bending modes occur over a range of 42 cm^{-1} and many of them have contributions from both monohydride and the dihydride. Using the PBC models it is possible to characterize the bending modes, and we have labeled them with their dominant contributions in table

1.7.3. With the exception of the dihydride rock, which is in the phonon region (not listed), the remaining frequencies occur between 600 and 650 cm^{-1}. The dihydride wag is the highest among these modes (648 cm^{-1}) and should be seen experimentally.

The dimer modes can be compared between 2×1 and 3×1 surfaces. As for the 2×1 surface the twist has a_2 symmetry and therefore IR inactive. The dimer rocking mode found in the 3×1 surface is separated from the wag by 23 cm^{-1} compared to only 11 cm^{-1} in the pure 2×1 surface. The increase in splitting is a result of the rocking mode shifting up slightly in response to the crowding from the adjacent dihydride while the wag is shifted down slightly relative to 2×1. As for the 2×1 surface, the calculated cluster model bending frequencies again have significant differences from the corresponding PBC values. The agreement between the clusters and the PBC does not improve significantly from the single dimer to four dimer model showing a very slow convergence of the frequencies with cluster size. While we have not performed a more thorough analysis of the convergence with increasing cluster size, it is clear that relatively small errors can potentially result in qualitatively incorrect assignments using cluster models.

The shifts upon deuterium substitution for the stretching modes and the dihydride scissor are well reproduced in the cluster models, table 1.7.3. There is not a marked difference in the frequencies or the frequency splitting with increased cluster size. The dimer modes occur at slightly higher values in the 3×1 surface.

Dihydride Terminated Si(100)-1×1 Surface

The structure of the dihydride surface is highly strained relative to the other Si(100) surfaces, figure 1.7.4 a. If the top layer silicon atoms are held at the ideal

crystalline positions and hydrogenated, the interlayer hydrogen-hydrogen distance is 1.4 Å, which is far less than the sum of their van der Waals radii of 2.4 Å. When the geometry is relaxed to relieve the surface strain, the surface structures tilt and become canted as seen previously in other studies.[110] In our calculations the dimer tilts by 12.2° from the plane of the ideal crystalline positions. The titling increases the distance between hydrogens of adjacent dimers to 2.10 Å, which is still within the van der Waals radii of the hydrogens. The dihydride silicons deviate from the ideal tetrahedral arrangement by a significant amount with an optimized H–Si–H angle of 104°. However, even with the tilting to the canted structure and deviation from tetrahedral angle, some steric strain still exists. In previous reports using plane wave calculations,[111, 112] tight binding molecular dynamics,[113, 114] and Gaussian orbital calculations,[113, 114] the corresponding values for these parameters differ significantly in some cases. The largest deviations are the tilt from the normal angle that has been reported as high as 15°.

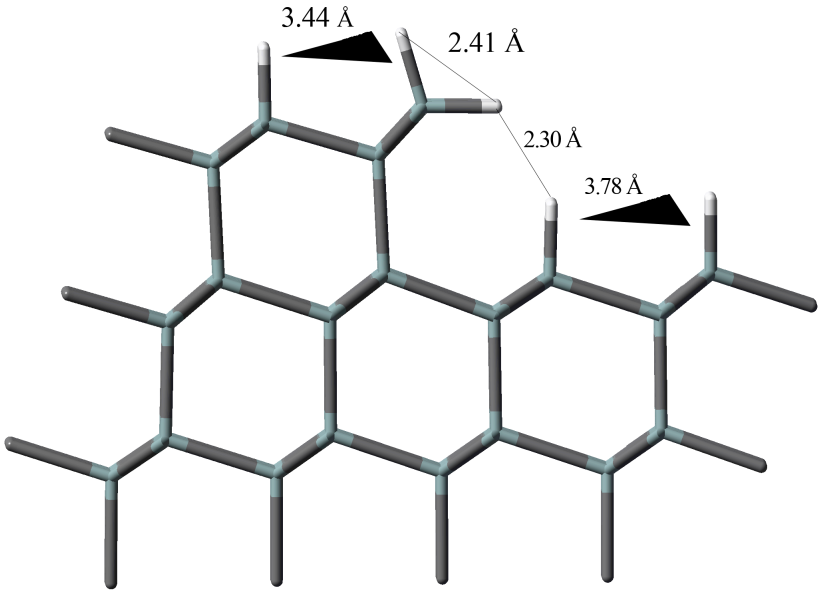

(a)

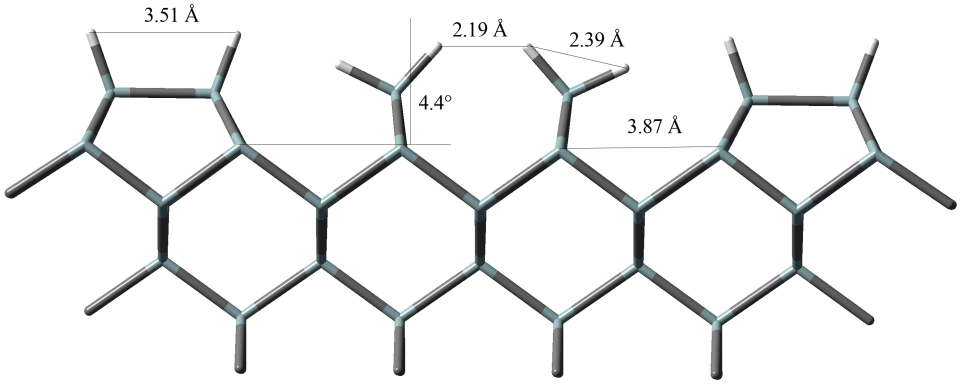

(b)

Figure 1.7.4. (a) The 1D PBC model of the Si(111) surface with a step edge in the ($\bar{1}\,\bar{1}\,2$) direction. Wedges indicate the bonds are not in line with one another. **(b)** The Si(100) bowtie surface defect optimized with a cluster model. In both models terminating hydrogens are not shown. White bars indicate hydrogen, blue-green bars indicate silicon, and grey bars indicate bonds.

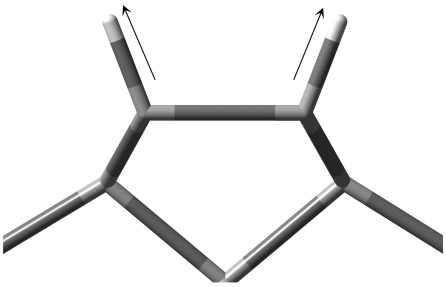

Symmetric Stretch

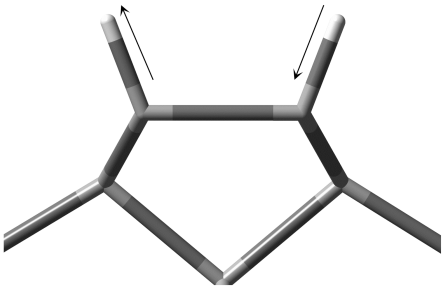

Asymmetric Stretch

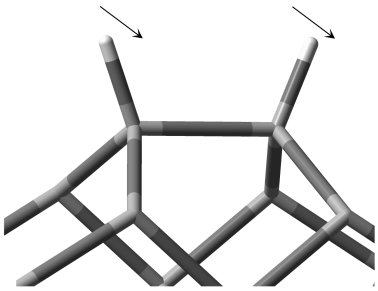

Wag

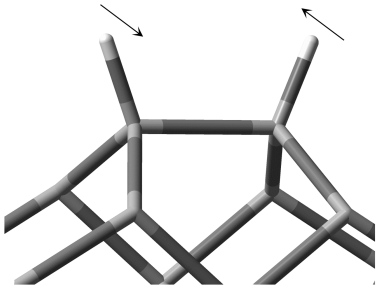

Twist

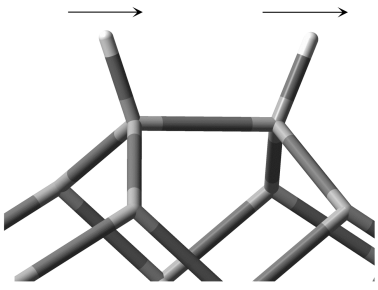

Rock

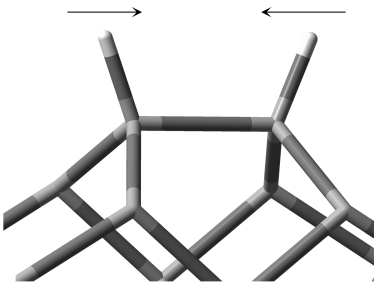

Symmetric Bend

(a)

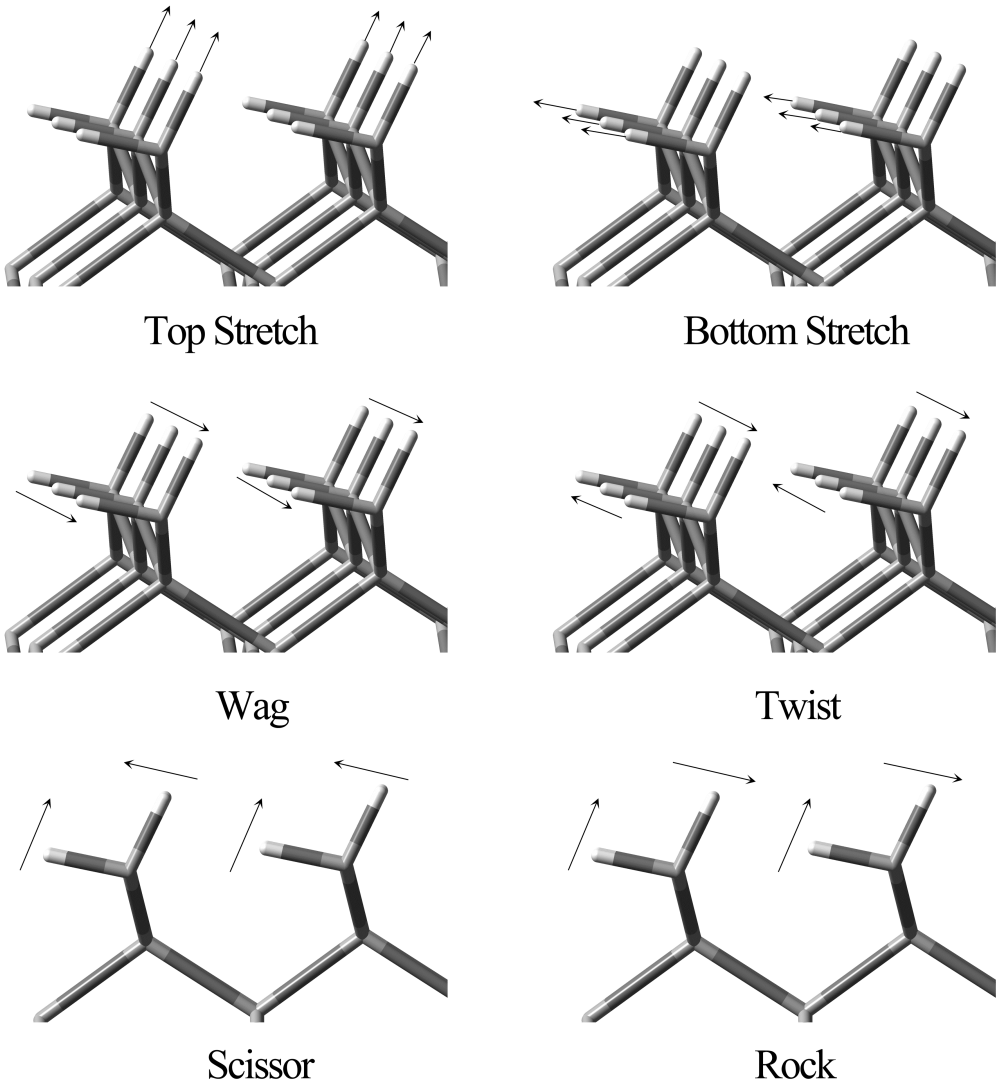

(b)

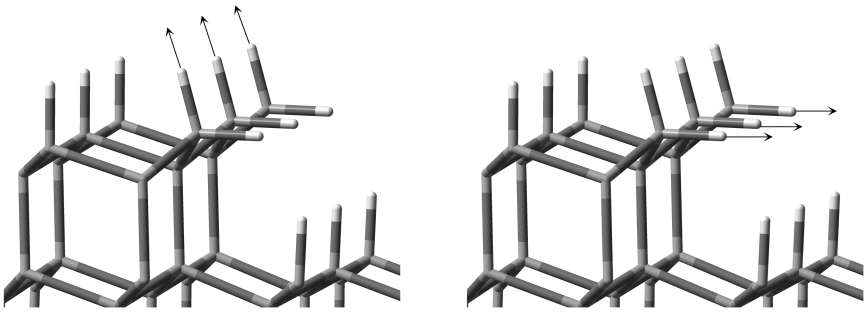

(c)

Figure 1.7.5. The vibrational models of the (a) Si(100)-2×1 surface, (b) the Si(100)-1×1 surface and (c) the Si(111) surface with a step edge in the ($\bar{1}\ \bar{1}$ 2) direction. Arrows indicate displacement vectors. For (b) & (c) three unit cells are shown while only one unit cell is shown in (a).

The silicon dihydride vibrational modes are shown in figure 1.7.5 b. The highest frequency modes clearly correspond to the Si–H stretching motions. If the tilting angle is zero, they give symmetric and asymmetric stretching vibrations. If the tilting angle is nonzero the modes are split. When the tilting is large, they separate into top and bottom Si–H stretching modes. In addition, there are the lower frequency scissor, wag, twist and rocking modes. The calculated stretching and bending frequencies are listed in column 2 of tables 5 & 6. Crowding of the adjacent dihydrides shifts the frequency of the stretching modes to higher frequencies. Since only a moderate relief of strain is possible, we would expect these modes to be much higher than the dihydride stretching modes in the Si(100)-3×1 reconstruction. This is indeed the case as indicated by the calculated top stretch (2147 cm^{-1}) and bottom stretch (2175 cm^{-1}) frequencies that are much higher than the

symmetric and asymmetric stretching modes of the 3×1 dihydride that occur at 2126 cm^{-1} and 2122 cm^{-1}, respectively. The dihydride scissor mode at 941 cm^{-1} is also higher than that seen in the 3×1 dihydride by 31 cm^{-1}, a shift that can again be attributed to crowding. Interestingly, the dihydride twist now occurs about 46 cm^{-1} lower than that for the 3×1 dihydride though the shift for the wag is much smaller.

Table 1.7.5. A comparison of the Si–H stretching modes for the Si(111) Step edge, the Si(100)-1×1, 2×1, 3×1 reconstructions and the bowtie defect. The following terminology is used: BS (bottom Stretch), TS (Top Stretch), As (Asymmetric Stretch), and SS (Symmetric Stretch). In previous studies the Si(100) dimer has been referred to as the coupled monohydride.

Si–H Stretching Modes	**Frequencies, cm^{-1}**				
Mode	**1×1[a]**	**2×1[a]**	**3×1[a]**	**Bowtie[b]**	**Edge[a]**
Uncoupled Dihydride BS	2175	–	–	–	–
Uncoupled Dihydride TS	2147	–	–	–	–
Dihydride Top SS	–	–	–	2175	–
Dihydride Top AS	–	–	–	2156	–
Crowded Dihydride BS	–	–	–	–	2135
Dihydride Bottom AS/SS	–	–	–	2136	–
Coupled Dihydride AS	–	–	2126	–	–
Coupled Dihydride SS	–	–	2122	–	–
Dimer SS	–	2110	2106	2114	–
Step Edge Dihydride TS	–	–	–	–	2100
Dimer AS	–	2095	2097	2105	–
Crowded Monohydride	–	–	–	–	2106

[a] Values from PBC calculations

[b] Values from cluster calculations

Table 1.7.6. The Si–H bending modes for the Si(111) step edge, the Si(100)-1×1, 2×1, 3×1 reconstructions and the bowtie defect. The dimer has previously been described as a coupled monohydride.

Si–H Bending Modes	**Frequencies, cm^{-1}**				
Mode	**1×1[a]**	**2×1[a]**	**3×1[a]**	**Bowtie[b]**	**Edge[a]**
Dihydride Scissor	936	–	905	923	905
Dihydride Scissor	–	–	–	903	–
Dihydride Wag	643	–	648	676	646
Dimer Rock	–	630	636	647	–
Dimer Twist/Wag	–	614	613	629	–
Dihyride Twist	559	–	605	610	598
Dimer Symmetric Bend	–	602	607	613	–
Dihyride Rock	382	–	399	333	372

a Values from PBC calculation

b Values from cluster calculation

Previous studies of this surface have computed vibrational frequencies using several techniques: density functional perturbation theory method with plane wave basis (DFPT-PW),[111] a layer force constant approach using Gaussian orbitals,[111] Γ-point frequencies using DFT and a slab model,[114] and DFT tight binding.[113, 114] The dihydride Si–H top stretch has a range of 2098 cm^{-1} to 2163 cm^{-1} depending on the method used. The range of the down stretch depends even more strongly on the method used. Our results clearly show that the top stretch is lower in frequency, and are in agreement with results from a previous study using Gaussian orbital basis sets.[111] Results from DFPT-PW show the top Si–H stretch is higher than the bottom Si–H stretch. This result seems inconsistent with the idea that crowding of the hydrogens in the canted structure will compress the bond and result in a blue shifted frequency. Part of the observed variations may be due to differences in the predicted dihydride tilt angle, 12° in the current work

versus ~15° for the plane wave calculations. While more work is needed to understand the differences between the calculations, we believe that our calculated values using reliable methods and well-converged geometries are consistent with the physics of the surface.

The complete dihydride terminated surface has not yet been experimentally characterized definitively. Some experimental evidence for the presence of a dihydride-covered surface comes from symmetric etching of the silicon surface using ultrapure water.[127, 128] This is examined in more detail in below.

Bowtie Defect on the Si(100) Surface

The bowtie defect suggests an interesting origin for some of the observed Si–H vibrational modes. This structure, observable using scanning tunneling microscopy, was thought to be the segregation of dopant pairs.[115] Recently, Bellec et al.[115] have reassigned this structure as the dihydride dimer defect.[116] The defect occurs when a Si(100)-2×1 dimer bond is broken and the dangling bonds are passivated to form two dihydride silicons in between dimers. The two canted dihydrides in the bowtie defect are tilted away from one another to relieve the strain from overcrowding. The distance between the top hydrogens on the dihydride is only 2.19 Å and they are directed toward one another. The distance is 0.09 Å longer than the shortest hydrogen-hydrogen distance of the complete dihydride surface. In the canted dihydride the distance is from the top hydrogen of one silicon and the bottom hydrogen on the adjacent surface silicon. The tilt angle is less than that for the dihydride surface at 4.4° from normal. The distance of the dimers allows for a more relaxed structure than the complete dihydride but less relaxed then the

dihydride in the 3×1 reconstruction. The dimer geometry is almost unchanged with a slight shortening of the Si–H distance in relation to the 2×1 reconstruction.

While no experimental frequencies have been reported we will review the theoretical results for these structures. The frequencies of the double dihydride defect follow a predictable pattern (tables 5 and 6). The top dihydride hydrogens are coupled to give symmetric and asymmetric stretching frequencies of 2175 cm^{-1} and 2156 cm^{-1}. The stretching modes (symmetric and asymmetric) of the bottom dihydride hydrogens occur at 2136 cm^{-1}. The significant overlap in the stretching frequencies between the bowtie and the complete dihydride structure indicates the presence of substantial strain in both. However, the bowtie spectrum should have three features in the higher frequency region (compared to 2 features for the complete dihydride) though it may not be observable if it has a low concentration on the surface. The relative frequencies between the bowtie reconstruction, complete dihydride, and the 3×1 dihydride can be rationalized in terms of the changes in bond length due to steric interactions between adjacent hydrogens. The dimer stretching frequencies are also shifted up in the bowtie, though by a lesser amount, relative to the 2×1 and 3×1 surfaces. The scissor modes for the bowtie structure are significantly lower than is seen in the complete dihydride and closer to the values for the 3×1 surface. The most interesting feature of the scissor mode is the splitting into symmetric and asymmetric modes. The higher symmetric mode occurs below the complete dihydride and above the 3×1 reconstruction.

Stepped Vicinal Si(111):H 9º Surface

The stepped edge surface is a vicinal surface formed from the Si(111) surface miscut by 9º.[100, 101, 111, 112, 130] The miscut leaves a step edge in the ($\bar{1}\,\bar{1}\,2$) direction. The structure is formed in a repeating pattern on the surface. The structure, seen in figure 1.7.4 a, contains a dihydride silicon at the edge in between the Si(111) surfaces. This is known to be a surface with substantial steric interactions. This is principally due to the short distance between the dihydride hydrogens in the upper terrace and the monohydride in the lower surface (~1.4 Å in the absence of structural relaxation). This leads to a significant tilt of the dihydride away from its ideal orientation to minimize the resulting steric repulsion. The relaxation from normal for the step edge dihydride is 20º as seen in our previous work using cluster models. After relaxation, the dihydride is 3.44 Å from the nearest Si(111) monohydride on the upper terrace and 2.30 Å from the monohydride in the lower terrace.

The computed PBC frequencies of the step edge dihydride can be seen in the last column of table 1.7.5 for the stretching modes and table 1.7.6 for the bending modes. The tilting of the dihydride produces a relaxed top hydrogen atom and a crowded bottom hydrogen atom interacting with the monohydride on the Si(111) terrace below the ledge. The top hydrogen appears at 2103 cm^{-1} and is the lowest dihydride stretch seen for the complete dihydride (1×1), 3×1 or bowtie defect surface. The bottom stretch is significantly blue shifted in the spectrum to 2135 cm^{-1} but occurs well below that on the 1×1 surface and the bowtie defect. The splitting for the PBC model is 35 cm^{-1} which is in very close agreement with experimentally observed value of 30 cm^{-1}. These PBC results give further validation our previous work using small cluster models. The bending modes

provide us with a little more insight into the nature of the strain. The scissor mode is shifted up due to the strain on the bottom hydrogen. The dihydride wag is comparable to the 1×1 and 3×1 surfaces and lower than the bowtie defect indicating relatively little interaction in the wag. The twist is close to the 3×1 value and the rock is intermediate between the 1×1 and 3×1 surfaces. Overall, we can conclude that the strain is intermediate between the 3×1 and 1×1 surfaces and is due to the interaction between the bottom hydrogen and the lower terrace Si(111) monohydride. Finally the crowded monohydride on the terrace below the ledge is blue shifted ~ 20 cm^{-1} to 2106 cm^{-1} relative to the monohydride stretch of the flat Si(100) surface.

Comparison to Experiment

Many experimental studies investigating vibrational spectra on silicon surfaces have been performed in the last few years. It order to apply our calculations to practical spectra we have reexamined the following FTIR studies of hydrogen terminated Si(100) surfaces. The first study is by Weldon et al.[104] who formed the hydrogen terminated surface by exposure to atomic hydrogen. This work contains spectra of the 3×1 and 2×1 reconstructions. The second study by Faggin et al.[117] formed the surface by etching the silicon surface with ultrapure water over long time periods. The work shows spectra for a more complicated surface of hillocks containing various reconstructions. The third study contains the vibrational modes observed on the vicinal H/Si(111) surface.[118] We discuss the assignments for these spectra from the theoretical predictions discussed above.

Table 1.7.7. Assignments for the vibrational frequencies of the Si(100) surface exposed to atomic hydrogen without annealing. The original assignment refers to Ref 104 and the new assignment refers to the preset work.

Si(100) Exposed to atomic H		
Frequency, cm^{-1}	Original Assignment	New Assignment
2140	Strained Si–H_2 Stretch	Strained Dihydride Species
2123	Strained/Unstrained Si–H_2 Stretch	3×1 Dihydride Symmetric/Asymmetric Stretch
2110	Strained/Unstrained Si–H_2 Stretch	3×1 Dimer Symmetric Stretch
2102	2×1 Dimer Stretch	2×1 Dimer Symmetric/3×1 Asymmetric Stretches
2091	2×1 Dimer Stretch	2×1 Dimer Asymmetric Stretch
2065	Not Assigned	Not Assigned
914	Strained Si–H_2 Scissor	Strained Dihydride Scissor
900	Unstrained Si–H_2 Scissor	3×1 Dihydride Scissor
668	Not Assigned	Strained Dihydride Wag
656	Strained/Unstrained Si–H_2 Wag	3×1 Dihydride Wag
638	2×1 Dimer Rock	2×1 Dimer Rock
619	2×1 Dimer Wag	2×1 Dimer Wag

The 3×1 spectrum of Weldon et al.[104] is shows a number of interesting features. The surface is not a complete 3×1 surface but instead contains both 2×1 and 3×1 domains. As result the spectrum contains peaks from both species making clear-cut

assignment of peaks difficult. In table 1.7.7 we have reassigned the 3×1 spectra. The highest frequency at 2140 cm^{-1} was originally assigned to the dimer dihydride, now identified as the bowtie defect feature. According to our calculations the modes found in the bowtie feature would place some of the dihydride stretching mode much higher in the spectrum than is seen in the spectrum at 2147-2175 cm^{-1} while others would be in the region of the observed peak at 2136 cm^{-1}. The lack of these modes besides the mode at 2140 cm^{-1} indicates the bowtie feature is probably not a significant feature on the surface. While we have not calculated any frequencies in this region for the 2×1 and 3×1 structures, we believe the mode at 2140 cm^{-1} to be a dihydride with more strain than the 3×1 dihydride but less than that found in the bowtie reconstruction and the 1×1 surface. In the past, some higher frequency modes in this range were assigned to trihydride species. Calculations on the trihydride species have shown that its frequency is significantly blue shifted relative to the dihydride species (~ 20 cm^{-1}) for isolated molecules.[67]

Table 1.7.8. The frequencies measured after etching of the Si(100) with ultrapure water over a period of days. The original assignment refers to Ref 117 and the new assignment refers to the preset work.

Si(100) etched using ultrapure water		
Frequency, cm^{-1}	Original Assignment	New Assignment
2137	Strained Canted Si–H_2 Asymmetric Stretch	Strained Dihydride Bottom Stretch
2116	Strained Canted Si–H_2 Symmetric Stretch	3×1 Dihydride Symmetric Stretch
2110	Relaxed Canted Si–H_2 Asymmetric Stretch	3×1 Dimer Symmetric Stretch
2104	Not Assigned	2×1 Dimer Symmetric Stretch
2092	Relaxed Canted Si–H_2 Symmetric Stretch	Strained Dihydride Top Stretch

Two modes found at 2123 cm^{-1} and 2110 cm^{-1} were originally assigned as resulting from both strained and/or unstrained dihydrides on the surface. The mode at 2123 cm^{-1} must be a dihydride since it is out of the range of dimer monohydride stretching frequencies. From our PBC calculations we can see the strained dihydride species are significantly blue shifted. We, therefore, believe the feature seen at 2123 cm^{-1} represents the unstrained 3×1 dihydride stretches. The feature at 2110 cm^{-1} is split from the 2123 cm^{-1} by 13 cm^{-1}, close to the calculated splitting of 16 cm^{-1} between the 3×1 dimer monohydride symmetric stretch and the dihydride stretching frequencies. We therefore assign the mode at 2110 cm^{-1} to the 3×1 dimer monohydride symmetric stretch.

The mode at 2100 cm^{-1} and 2091 were assigned to the 2×1 dimer stretches with the symmetric stretch higher than the asymmetric stretch, which is in accordance with our calculated values. The mode at 2065 cm^{-1} is interesting. Dimer monohydride, 3×1 monohydride, or dihydride Si–H stretches do not appear in this region. It may be due to some local defect or a kink site on the surface.

Modes appearing in the region from 350 cm^{-1} to 900 cm^{-1} are assigned to bending modes. The highest of these modes are seen at 914 and 900 cm^{-1}, and are clearly due to dihydride bending modes. The mode at 900 cm^{-1} is close to the calculated value of 905 cm^{-1} for the 3×1 dihydride scissor mode, and agrees with its original assignment as an unstrained dihydride. The mode at 914 cm^{-1} was assigned to a strained dihydride scissor mode that appears quite plausible. The lower frequency modes seen around 650 cm^{-1} can be assigned to the wagging and rocking modes of the 3×1 dihydride and 2×1 dimer monohydride. The low frequency modes at 619 and 638 cm^{-1} can be assigned to the dimer wag and rock, respectively. The mode seen at 656 cm^{-1} can best be assigned as the 3×1 dihydride wag. The higher frequency mode at 668 cm^{-1} is tentatively assigned as a strained dihydride wag that was not previously calculated. Overall, the assignments indicate a surface containing both 2×1 and 3×1 domains with a small amount of strained dihydride species that contribute at higher frequencies.

The second spectrum we investigate is that of Si(100) etched with ultrapure water to produce a surface covered with hillocks with various facets. On the tops of the hillocks, the authors propose a model including the presence of relaxed and canted dihydride species. In these species the geometry of the silicon dihydride will have a variety of tilt angles. There will be a minority of species with a 0° tilt angle with C_{2v}

symmetry. At the edges of the hillocks the dihydrides can cant away from each other to minimize the strain more than dihydrides in the interior of the hillocks. Structures in between the central and edge dihydrides will have an intermittent tilt angle. While the extent of tilt is not known, there will be a range of tilting by the dihydrides depending on the crowding.

This surface gives a vibrational spectrum containing many modes in the Si–H stretching region. The conjecture is the valleys between the hillocks correspond to the strained Si(100)-1×1 surface and the plateaus of the hillocks correspond to a relaxed Si(100)-1×1 surface. While it is normally impossible to assign such modes, Faggin et al.[117] have used a clever decomposition method based on surface symmetry to separate the *x*– and *z*–polarized modes of the *p*–polarized light. The resulting spectrum contains seven *z*–polarized modes perpendicular to the surface. In order to validate their ideas we have examined their vibrational assignments using our current calculations. Two of these modes are assigned to monohydrides on the Si(111) facet (2081 cm^{-1}) and the Si(110) facet (2089 cm^{-1}) which seems reasonable. The remaining five modes are assigned in table 1.7.8. It is these assignments that we will examine further. The highest frequency mode occurs at 2137 cm^{-1} and was assigned to the strained dihydride asymmetric stretch in the valleys between the hillocks. In our calculations, the strained dihydride species appear much higher in the spectrum above 2150 cm^{-1}. We believe another possible assignment is a strained dihydride other than the 1×1 reconstruction. The exact nature of the reconstruction is impossible to determine without further experimental evidence. However, we think it is likely that the surface structure is a mixture of 2×1 and 3×1 domains with dihydrides in several environments. If our conjecture is correct the

remaining modes can be reassigned. The mode at 2116 cm^{-1} was originally assigned to the symmetric stretch of the strained dihydride but is closer to the 3×1 symmetric stretching mode calculated at 2106 cm^{-1} for the 3×1 surface. This blue-shifted mode behaves as is expected for a dimer symmetric stretch in a crowded environment. The mode at 2110 cm^{-1} can be assigned to the 3×1 dimer symmetric stretch. The mode at 2104 cm^{-1} was not assigned in the experimental spectrum. We believe this mode belongs to a slightly strained symmetric stretching mode of the 2×1 reconstruction. This mode was ruled out by in previous studies because it was not believed to shift significantly in the spectra. However, our calculations show that the symmetric stretch of the 2×1 reconstruction shifts over a range from 2107-2114 cm^{-1} depending on the environment. The final mode was assigned to the relaxed dihydride symmetric stretch. We believe this mode is close to the stretching of the top hydrogen of a dihydride. If our assignments are correct the surface structure is more likely mixture of 2×1 and 3×1 domains with dihydrides in several environments.

The vicinal H/Si(111) surface with the step-edge along the $<\bar{1}\,\bar{1}\,2>$ direction has been well characterized.[118] Three sharp vibrational modes are seen at 2096, 2103, and 2136 cm^{-1}, all significantly higher than the terrace mode at 2084 cm^{-1}. The calculated 1D-PBC values are in excellent agreement. The calculated modes occur at 2100, 2106, and 2135 cm^{-1} and correspond to step-edge dihydride top stretch, crowded monohydride stretch, and crowded dihydride stretch. In particular, the internal splitting between the two crowded modes (~ 30 cm^{-1}) is in excellent agreement with the observed value. Finally, the mode observed[119] at 655 cm^{-1} can be assigned to the dihydride wag mode

calculated at 646 cm^{-1}. The overall good agreement of this well-characterized surface lends confidence to the accuracy of our PBC frequencies.

Conclusions

Using PBC and cluster models we have characterized the vibrational spectra of the hydrogen terminated Si(111) and Si(100) surfaces. Specifically, we have characterized the Si(100) 2×1 and 3×1 reconstructions, the Si(100) pure dihydride, the Si(100) bowtie defect, the Si(111) flat surface and finally the Si(111) 9º miscut surface. We have validated the PBC models and shown the correspondence between the cluster and PBC frequencies. The use of cluster models was validated for the stretching modes of the 2×1 and 3×1 reconstructions but not for the lower frequency bending modes. The isotopic shifts of the 2×1 and 3×1 were presented. Finally, we reassigned the previous experimental spectra using newer data. These new assignments give us a new interpretation of the surface structure of surface exposed to atomic hydrogen and ultrapure water. We believe our results will be useful as a benchmark for interpreting novel spectra on the Si(100) surface and reassigned difficult or ambiguous past spectra.

References

1. McQuarrie, D. A.; Simon, J. D., *Physical Chemistry A Molecular Approach*. University Science Books: Sauasalito, CA, 1997; p 1360.

2. Szabo, A.; Ostlund, N. S., *Modern Quantum Chemistry Introduction to Advanced electronic Structure Theory*. First Ed. Revised ed.; Mineola, NY, 1982; p 466.

3. Sze, S. M., *The Physics of Semiconductor Devices*. 2nd ed.; Wiley-Interscience: New York, 1981; p 880.

4. Goldstein, A.; Aspray, W., *Facets New Perspectives on the History of Semiconductors*. IEEE Center for the History of Electrical Engineering: New Brunswick, NJ, 1997; p 318.

5. Jung, Y. S.; Akinaga, Y.; Jordan, K. D.; Gordon, M. S., An ab initio study of the structure of two-, three- and five-dimer silicon clusters: An approach to the Si(100) surface. *Theor Chem Acc* **2003,** *109* (5), 268-273.

6. Hirschmugl, C. J., Frontiers in infrared spectroscopy at surfaces and interfaces. *Surf. Sci.* **2002,** *500* (1-3), PII S0039-6028(01)01523-0.

7. Higashi, G. S.; Chabal, Y. J.; Trucks, G. W.; Raghavachari, K., Ideal Hydrogen Termination of the Si-(111) Surface. *Applied Physics Letters* **1990,** *56* (7), 656-658.

8. Webb, L. J.; Lewis, N. S., Comparison of the electrical properties and chemical stability of crystalline silicon(111) surfaces alkylated using grignard reagents or olefins with Lewis acid catalysts. *Journal of Physical Chemistry B* **2003,** *107* (23), 5404-5412.

9. Rivillon, S.; Chabal, Y. J., Alkylation of silicon(111) surfaces. *J. Phys. IV* **2006,** *132*, 195-198.

10. Rivillon, S.; Chabal, Y. J.; Webb, L. J.; Michalak, D. J.; Lewis, N. S.; Halls, M. D.; Raghavachari, K., Chlorination of hydrogen-terminated silicon(111) surfaces. *Journal of Vacuum Science & Technology A* **2005,** *23* (4), 1100-1106.

11. Bansal, A.; Li, X. L.; Lauermann, I.; Lewis, N. S.; Yi, S. I.; Weinberg, W. H., Alkylation of Si surfaces using a two-step halogenation Grignard route. *Journal of the American Chemical Society* **1996,** *118* (30), 7225-7226.

12. Bansal, A.; Li, X. L.; Yi, S. I.; Weinberg, W. H.; Lewis, N. S., Spectroscopic studies of the modification of crystalline Si(111) surfaces with covalently-attached alkyl chains using a chlorination/alkylation method. *Journal of Physical Chemistry B* **2001,** *105* (42), 10266-10277.

13. Bent, S. F., Organic functionalization of group IV semiconductor surfaces: principles, examples, applications, and prospects. *Surf. Sci.* **2002,** *500* (1-3), 879-903.

14. Bent, S. F., Attaching organic layers to semiconductor surfaces. *Journal of Physical Chemistry B* **2002,** *106* (11), 2830-2842.

15. Bent, S. F., Surface patterning: Silicon falls into line. *Nature Nanotechnology* **2008,** *3* (4), 185-186.

16. Buriak, J. M., Organometallic chemistry on silicon and germanium surfaces. *Chemical Reviews* **2002,** *102* (5), 1271-1308.

17. Fidelis, A.; Ozanam, F.; Chazalviel, J. N., Fully methylated, atomically flat (111) silicon surface. *Surf. Sci.* **2000,** *444* (1-3), L7-L10.

18. Hurley, P. T.; Nemanick, E. J.; Brunschwig, B. S.; Lewis, N. S., Covalent Attachment of Acetylene and Methylacetylene Functionality to Si (111) Surfaces: Scaffolds for Organic Functionalization while Retaining Si-C Passivation of Si (111) Surface Sites. *Journal of the American Chemical Society* **2006,** *128*, 9990-9991.

19. Lercel, M. J.; Whelan, C. S.; Craighead, H. G.; Seshadri, K.; Allara, D. L., High-resolution silicon patterning with self-assembled monolayer resists. *J. Vac. Sci. Technol. B* **1996,** *14* (6), 4085-4090.

20. Lin, Z.; Strother, T.; Cai, W.; Cao, X. P.; Smith, L. M.; Hamers, R. J., DNA attachment and hybridization at the silicon (100) surface. *Langmuir* **2002,** *18* (3), 788-796.

21. Niwa, D.; Inoue, T.; Fukunaga, H.; Akasaka, T.; Yamada, T.; Homma, T.; Osaka, T., Electrochemical behavior of methyl- and butyl-terminated Si(111) in aqueous solution. *Chem. Lett.* **2004,** *33* (3), 284-285.

22. Rohde, R. D.; Agnew, H. D.; Yeo, W.; Bailey, R. C.; Heath, J. R., A Non-Oxidative Approach toward Chemically and Electrochemically Functionalizing Si(111). *Journal of the American Chemical Society* **2006,** *128*, 9518-9525.

23. Strother, T.; Cai, W.; Zhao, X. S.; Hamers, R. J.; Smith, L. M., Synthesis and characterization of DNA-modified silicon (111) surfaces. *Journal of the American Chemical Society* **2000,** *122* (6), 1205-1209.

24. Sugimura, H.; Okiguchi, K.; Nakagiri, N.; Miyashita, M., Nanoscale patterning of an organosilane monolayer on the basis of tip-induced electrochemistry in atomic force microscopy. *J. Vac. Sci. Technol. B* **1996,** *14* (6), 4140-4143.

25. Takeuchi, N.; Kanai, Y.; Selloni, A., Surface reaction of alkynes and alkenes with H-Si(111): A density functional theory study. *Journal of the American Chemical Society* **2004,** *126* (48), 15890-15896.

26. Yates, J. T., A new opportunity in silicon-based microelectronics. *Science* **1998,** *279* (5349), 335-336.

27. Haick, H.; Hurley, P. T.; Hochbaum, A. I.; Yang, P.; Lewis, N. S., Electrical Characteristics and Chemical Stability of Non-Oxidized, Methyl-Terminated Silicon Nanowires. *Journal of the American Chemical Society* **2006,** *128*, 8990-8991.

28. Solares, S. D.; Michalak, D. J.; Goddard, W. A.; Lewis, N. S., Theoretical investigation of the structure and coverage of the Si(111)-OCH3 surface. *Journal of Physical Chemistry B* **2006,** *110* (16), 8171-8175.

29. Solares, S. D.; Yu, H. B.; Webb, L. J.; Lewis, N. S.; Heath, J. R.; Goddard, W. A., Chlorination-methylation of the hydrogen-terminated silicon(111) surface can induce a stacking fault in the presence of etch pits. *Journal of the American Chemical Society* **2006,** *128* (12), 3850-3851.

30. Hunger, R.; Fritsche, R.; Jaeckel, B.; Jaegermann, W.; Webb, L. J.; Lewis, N. S., Chemical and electronic characterization of methyl-terminated Si(111) surfaces by high-resolution synchrotron photoelectron spectroscopy. *Physical Review B* **2005,** *72* (4), 045317.

31. Yu, H. B.; Webb, L. J.; Ries, R. S.; Solares, S. D.; Goddard, W. A.; Heath, J. R.; Lewis, N. S., Low-temperature STM images of methyl-terminated Si(111) surfaces. *Journal of Physical Chemistry B* **2005,** *109* (2), 671-674.

32. Yamada, T.; Inoue, T.; Yamada, K.; Takano, N.; Osaka, T.; Harada, H.; Nishiyama, K.; Taniguchi, I., Detection of C-Si covalent bond in CH3 adsorbate formed by chemical reaction of

CH3MgBr and H : Si(111). *Journal of the American Chemical Society* **2003,** *125* (26), 8039-8042.

33. Webb, L. J.; Rivillon, S.; Michalak, D. J.; Chabal, Y. J.; Lewis, N. S., Transmission infrared spectroscopy of methyl- and ethyl-terminated silicon(111) surfaces. *Journal of Physical Chemistry B* **2006,** *110* (14), 7349-7356.

34. Raghavachari, K.; Halls, M. D., Quantum chemical studies of semiconductor surface chemistry using cluster models. *Mol. Phys.* **2004,** *102* (4), 381-393.

35. Becke, A. D., Density-Functional Exchange-Energy Approximation with Correct Asymptotic-Behavior. *Phys. Rev. A* **1988,** *38* (6), 3098-3100.

36. Becke, A. D., Density-Functional Thermochemistry .3. the Role of Exact Exchange. *Journal of Chemical Physics* **1993,** *98* (7), 5648-5652.

37. Lee, C. T.; Yang, W. T.; Parr, R. G., Development of the Colle-Salvetti Correlation-Energy Formula into a Functional of the Electron-Density. *Physical Review B* **1988,** *37* (2), 785-789.

38. Hariharan, P. C.; Pople, J. A., Influence of Polarization Functions on Molecular-Orbital Hydrogenation Energies. *Theor. Chim. Acta* **1973,** *28* (3), 213-222.

39. Ayala, P. Y.; Kudin, K. N.; Scuseria, G. E., Atomic orbital Laplace-transformed second-order Moller-Plesset theory for periodic systems. *Journal of Chemical Physics* **2001,** *115* (21), 9698-9707.

40. Kudin, K. N.; Scuseria, G. E., A fast multipole algorithm for the efficient treatment of the Coulomb problem in electronic structure calculations of periodic systems with Gaussian orbitals. *Chemical Physics Letters* **1998,** *289* (5-6), 611-616.

41. Kudin, K. N.; Scuseria, G. E.; Schlegel, H. B., A redundant internal coordinate algorithm for optimization of periodic systems. *Journal of Chemical Physics* **2001,** *114* (7), 2919-2923.

42. M. J. Frisch, G. W. T., H. B. Schlegel, G. E. Scuseria, M. A. Robb, J. R. Cheeseman, J. A. Montgomery, Jr., T. Vreven, K. N. Kudin, J. C. Burant, J. M. Millam, S. S. Iyengar, J. Tomasi, V. Barone, B. Mennucci, M. Cossi, G. Scalmani, N. Rega, G. A. Petersson, H. Nakatsuji, M. Hada, M. Ehara, K. Toyota, R. Fukuda, J. Hasegawa, M. Ishida, T. Nakajima, Y. Honda, O. Kitao, H. Nakai, M. Klene, X. Li, J. E. Knox, H. P. Hratchian, J. B. Cross, V. Bakken, C. Adamo, J. Jaramillo, R. Gomperts, R. E. Stratmann, O. Yazyev, A. J. Austin, R. Cammi, C. Pomelli, J. W. Ochterski,; P. Y. Ayala, K. M., G. A. Voth, P. Salvador, J. J. Dannenberg, V. G. Zakrzewski, S. Dapprich, A. D. Daniels, M. C. Strain, O. Farkas, D. K. Malick, A. D. Rabuck, K. Raghavachari, J. B. Foresman, J. V. Ortiz, Q. Cui, A. G. Baboul, S. Clifford, J. Cioslowski, B. B. Stefanov, G. Liu, A. Liashenko, P. Piskorz, I. Komaromi, R. L. Martin, D. J. Fox, T. Keith, M. A. Al-Laham, C. Y. Peng, A. Nanayakkara, M. Challacombe, P. M. W. Gill, B. Johnson, W. Chen, M. W. Wong, C. Gonzalez, and J. A. Pople *Gaussian Development Version*, Revision E.05; Gaussian, Inc.: Wallingford CT, 2004.

43. Heyd, J.; Scuseria, G. E., Efficient hybrid density functional calculations in solids: Assessment of the Heyd-Scuseria-Ernzerhof screened Coulomb hybrid functional. *Journal of Chemical Physics* **2004,** *121* (3), 1187-1192.

44. Heyd, J.; Scuseria, G. E., Assessment and validation of a screened Coulomb hybrid density functional. *Journal of Chemical Physics* **2004,** *120* (16), 7274-7280.

45. Heyd, J.; Scuseria, G. E.; Ernzerhof, M., Hybrid functionals based on a screened Coulomb potential. *Journal of Chemical Physics* **2003,** *118* (18), 8207-8215.

46. Yamada, T.; Kawai, M.; Wawro, A.; Suto, S.; Kasuya, A., HREELS, STM, and STS study of CH3-terminated Si(111)-(1x1) surface. *Journal of Chemical Physics* **2004,** *121* (21), 10660-10667.

47. Filler, M. A.; Bent, S. F., The surface as molecular reagent: organic chemistry at the semiconductor interface. *Prog. Surf. Sci.* **2003,** *73* (1-3), 1-56.

48. Bansal, A.; Lewis, N. S., Stabilization of Si photoanodes in aqueous electrolytes through surface alkylation. *Journal of Physical Chemistry B* **1998,** *102* (21), 4058-4060.

49. Haick, H.; Hurley, P. T.; Hochbaum, A. I.; Yang, P.; Lewis, N. S., Electrical Characteristics and Chemical Stability of Non-Oxidized, Methyl-erminated Silicon Nanowires. *Journal of the American Chemical Society* **2006,** *128*, 8990-8991.

50. Lopinski, G.; Wayner, D.; Wolkow, R., Self-directed growth of molecular nanostructures on silicon. *Nature* **2000,** *406*, 48-51.

51. Cicero, R. L.; Linford, M. R.; Chidsey, C. E. D., Photoreactivity of unsaturated compounds with hydrogen-terminated silicon(111). *Langmuir* **2000,** *16* (13), 5688-5695.

52. Effenberger, F.; Gotz, G.; Bidlingmaier, B.; Wezstein, M., Photoactivated preparation and patterning of self-assembled monolayers with 1-alkenes and aldehydes on silicon hydride surfaces. *Angew. Chem.-Int. Edit.* **1998,** *37* (18), 2462-2464.

53. Haber, J. A.; Lauermann, I.; Michalak, D.; Vaid, T. P.; Lewis, N. S., Electrochemical and electrical behavior of (111)-oriented Si surfaces alkoxylated through oxidative activation of Si-H bonds. *Journal of Physical Chemistry B* **2000,** *104* (43), 9947-9950.

54. Linford, M. R.; Chidsey, C. E. D., Alkyl Monolayers Covalently Bonded to Silicon Surfaces. *Journal of the American Chemical Society* **1993,** *115* (26), 12631-12632.

55. Linford, M. R.; Chidsey, C. E. D., Surface functionalization of alkyl monolayers by free-radical activation: Gas-phase photochlorination with Cl-2. *Langmuir* **2002,** *18* (16), 6217-6221.

56. Linford, M. R.; Fenter, P.; Eisenberger, P. M.; Chidsey, C. E. D., Alkyl Monolayers on Silicon Prepared from 1-Alkenes and Hydrogen-Terminated Silicon. *Journal of the American Chemical Society* **1995,** *117* (11), 3145-3155.

57. Terry, J.; Linford, M. R.; Wigren, C.; Cao, R. Y.; Pianetta, P.; Chidsey, C. E. D., Determination of the bonding of alkyl monolayers to the Si(111) surface using chemical-shift, scanned-energy photoelectron diffraction. *Applied Physics Letters* **1997,** *71* (8), 1056-1058.

58. Terry, J.; Linford, M. R.; Wigren, C.; Cao, R. Y.; Pianetta, P.; Chidsey, C. E. D., Alkyl-terminated Si(111) surfaces: A high-resolution, core level photoelectron spectroscopy study. *J. Appl. Phys.* **1999,** *85* (1), 213-221.

59. Nemanick, E. J.; Hurley, P. T.; Webb, L. J.; Knapp, D. W.; Michalak, D. J.; Brunschwig, B. S.; Lewis, N. S., Chemical and electrical passivation of single-crystal silicon(100) surfaces through a two-step chlorination/alkylation process. *Journal of Physical Chemistry B* **2006,** *110* (30), 14770-14778.

60. Webb, L. J.; Nemanick, E. J.; Biteen, J. S.; Knapp, D. W.; Michalak, D. J.; Traub, M. C.; Chan, A. S. Y.; Brunschwig, B. S.; Lewis, N. S., High-resolution X-ray photoelectron spectroscopic studies of alkylated silicon(111) surfaces. *Journal of Physical Chemistry B* **2005,** *109* (9), 3930-3937.

61. Ferguson, G.; Raghavachari, K., The Emergence of collective vibrations in cluster models: Quantum chemical study of the methyl-terminated Si(111) surface. *Journal of Chemical Physics* **2006,** *125* (15), 154708.

62. Michalak, D. J.; Rivillon, S.; Chabal, Y. J.; Estéve, A.; Lewis, N. S., Infrared Spectroscopic Investigation of the Reaction of Hydrogen-Terminated, (111)-Oriented, Silicon Surfaces with Liquid Methanol. *Journal of Physical Chemistry B* **2006,** *110*, 20426-20434.

63. Yu, H. B.; Webb, L. J.; Solares, S. D.; Cao, P. G.; Goddard, W. A.; Heath, J. R.; Lewis, N. S., Scanning tunneling microscopy of ethylated Si(111) surfaces prepared by a chlorination/alkylation process. *Journal of Physical Chemistry B* **2006,** *110* (47), 23898-23903.

64. Bergerson, W. F.; Mulder, J. A.; Hsung, R. P.; Zhu, X. Y., Assembly of organic molecules on silicon surfaces via the Si-N linkage. *Journal of the American Chemical Society* **1999,** *121* (2), 454-455.

65. Wayner, D. D. M.; Wolkow, R. A., Organic modification of hydrogen terminated silicon surfaces. *Journal of the Chemical Society-Perkin Transactions 2* **2002,** (1), 23-34.

66. Wolkow, R. A., Controlled molecular adsorption on silicon: Laying a foundation for molecular devices. *Annu. Rev. Phys. Chem.* **1999,** *50*, 413-441.

67. Chabal, Y. J.; Higashi, G. S.; Raghavachari, K.; Burrows, V. A., INFRARED-SPECTROSCOPY OF SI(111) AND SI(100) SURFACES AFTER HF TREATMENT - HYDROGEN TERMINATION AND SURFACE-MORPHOLOGY. *J. Vac. Sci. Technol. A-Vac. Surf. Films* **1989,** *7* (3), 2104-2109.

68. Ricca, A.; Musgrave, C. B., Theoretical study of the Cl-passivated Si(111) surface. *Surf. Sci.* **1999,** *430* (1-3), 116-125.

69. Ferguson, G. A.; Raghavachari, K., Collective vibrations in cluster models for semiconductor surfaces: Vibrational spectra of acetylenyl and methylacetylenyl functionalized Si(111). *Journal of Chemical Physics* **2007,** *127*.

70. Hines, M. A., In search of perfection: Understanding the highly defect-selective chemistry of anisotropic etching. *Annu. Rev. Phys. Chem.* **2003,** *54*, 29-56.

71. Cao, P. G.; Yu, H. B.; Heath, J. R., Scanning tunneling microscopy and spectroscopy of wet-chemically prepared chlorinated Si(111) surfaces. *Journal of Physical Chemistry B* **2006,** *110* (47), 23615-23618.

72. Okubo, T.; Tsuchiya, H.; Sadakata, M.; Yasuda, T.; Tanaka, K., An organic functional group introduced to Si(111) via silicon-carbon bond: a liquid-phase approach. *Applied Surface Science* **2001,** *171* (3-4), 252-256.

73. Eves, B. J.; Lopinski, G. P., Formation and reactivity of high quality halogen terminated Si(111) surfaces. *Surf. Sci.* **2005,** *579* (2-3), 89-96.

74. Juarez, M. F.; Patrito, E. M.; Paredes-Olivera, P., Quantum Mechanical Investigation of the Influence of the Local Environment on the Vibrational Properties of Hydrogenated Si(111). *Journal of Physical Chemistry C* **2009,** *113* (2), 681-690.

75. Miehlich, B.; Savin, A.; Stoll, H.; Preuss, H., Results Obtained with the Correlation-Energy Density Functionals of Becke and Lee, Yang and Parr. *Chemical Physics Letters* **1989,** *157* (3), 200-206.

76. Ferguson, G. A.; Raghavachari, K.; Michalak, D. J.; Chabal, Y., Adsorbate-surface phonon interactions in deuterium-passivated si(111)-(1 x 1). *Journal of Physical Chemistry C* **2008,** *112* (4), 1034-1039.

77. Weinhold, F.; Carpenter, J. E., The Structure of Small Molecules. Plenum: New York, 1988; p 227.

78. Bardi, U., THE ATOMIC-STRUCTURE OF ALLOY SURFACES AND SURFACE ALLOYS. *Reports on Progress in Physics* **1994,** *57* (10), 939-987.

79. Chen, J. G.; Menning, C. A.; Zellner, M. B., Monolayer bimetallic surfaces: Experimental and theoretical studies of trends in electronic and chemical properties. *Surface Science Reports* **2008,** *63* (5), 201-254.

80. Hammaker, R. M.; Francis, S. A.; Eischens, R. P., INFRARED STUDY OF INTERMOLECULAR INTERACTIONS FOR CARBON MONOXIDE CHEMISORBED ON PLATINUM. *Spectrochimica Acta* **1965,** *21* (7), 1295-&.

81. Platero, E. E.; Coluccia, S.; Zecchina, A., DIPOLE COUPLING AND CHEMICAL-SHIFTS IN CO OVERLAYERS ADSORBED ON NIO. *Surf. Sci.* **1986,** *171* (3), 465-482.

82. Mahan, G. D.; Lucas, A. A., COLLECTIVE VIBRATIONAL MODES OF ADSORBED CO. *Bulletin of the American Physical Society* **1978,** *23* (3), 334-334.

83. Persson, B. N. J.; Ryberg, R., Vibrational interaction between molecules adsorbed on a metal surface. The dipole-dipole interaction. *Physical Review B (Condensed Matter)|Physical Review B (Condensed Matter)* **1981,** *24* (12), 6924-70.

84. Moskovits, M.; Hulse, J. E., FREQUENCY-SHIFTS IN SPECTRA OF MOLECULES ADSORBED ON METALS, WITH EMPHASIS ON INFRARED-SPECTRUM OF ADSORBED CO. *Surf. Sci.* **1978,** *78* (2), 397-418.

85. Griffin, G. L.; Yates, J. J. T., Adsorption studies of H[sub 2] isotopes on ZnO: Coverage-induced IR frequency shifts and adsorbate geometry. *The Journal of Chemical Physics* **1982,** *77* (7), 3744-3750.

86. Massoud, H. Z. P., E.H.; Helms, C.R. In *Proceedings of Third International Symposium on the Physics and Chemistry of Si02 and the Si Si02 Interface (ISBN 1 56677 151 X)*, Proceedings of Third International Symposium on the Physics and Chemistry of Si02 and the Si Si02 Interface (ISBN 1 56677 151 X), Los Angeles, CA, USA, 5-10 May; Massoud, H. Z.; Poindexter, E. H.; Helms, C. R., Eds. Electrochem. Soc: Los Angeles, CA, USA, 1996; p xv+780 pp.

87. Bourianoff, G. I.; Gargini, P. A.; Nikonov, D. E., Research directions in beyond CMOS computing. *Solid-State Electron.* **2007,** *51* (11-12), 1426-1431.

88. Jakubowski, A.; Lukasiak, L., CMOS evolution. Development limits. *Mater. Sci.* **2008,** *26* (1), 5-20.

89. Ferguson, G. A.; Than, C. T. L.; Raghavachari, K., Line Growth on the H/Si(100)-2 x 1 Surface: Density Functional Study of Allylic Mercaptan Reaction Mechanisms. *Journal of Physical Chemistry C* **2009,** *113* (43), 18817-18822.

90. Juarez, M. F.; Soria, F. A.; Patrito, E. M.; Paredes-Olivera, P., Influence of subsurface oxidation on the structure, stability, and reactivity of grafted Si(111) surfaces. *Journal of Physical Chemistry C* **2008,** *112* (38), 14867-14877.

91. Lopinski, G., Organics on silicon; single molecules, nanostructures and monolayers. *International Journal of Nanotechnology* **2008,** *5* (9-12), 1247-1267.

92. Lopinski, G. P.; Wayner, D. D. M.; Wolkow, R. A., Self-directed growth of molecular nanostructures on silicon. *Nature* **2000,** *406* (6791), 48-51.

93. Rivillon, S.; Amy, F.; Chabal, Y. J.; Frank, M. M., Gas phase chlorination of hydrogen-passivated silicon surfaces. *Applied Physics Letters* **2004,** *85* (13), 2583-2585.

94. Alerhand, O. L.; Allan, D. C.; Mele, E. J., DIPOLE ACTIVITY OF SURFACE PHONONS ON SI(111)2X1. *Physical Review Letters* **1985,** *55* (24), 2700-2703.

95. Michalak, D. J.; Rivillon, S.; Chabal, Y. J.; Esteve, A.; Lewis, N. S., Infrared spectroscopic investigation of the reaction of hydrogen-terminated, (111)-oriented, silicon surfaces with liquid methanol. *Journal of Physical Chemistry B* **2006,** *110* (41), 20426-20434.

96. Chabal, Y. J.; Hines, M. A.; Feijoo, D., Characterization of Silicon Surfaces and Interfaces by Optical Vibrational Spectroscopy. *J. Vac. Sci. Technol. A-Vac. Surf. Films* **1995,** *13* (3), 1719-1727.

97. Ferguson, G. A.; Rivillon S.; Chabal, Y.; Raghavachari, K., The Structure and Vibrational Spectrum of the Si(111)−H/Cl Surface. *Journal of Physical Chemistry C* **2009,** *113* (52), 21713–21720.

98. Bondi, A., VAN DER WAALS VOLUMES + RADII. *J. Phys. Chem.* **1964,** *68* (3), 441-&.

99. Cotton, F. A., *Chemical Applications of Group Theory*. 3rd ed.; Wiley Interscience: 1990.

100. Jakob, P.; Chabal, Y. J.; Raghavachari, K., THE ROLE OF KINKS IN THE SI-H VIBRATIONAL-SPECTRUM OF VICINAL SI(111)-[(1)OVER-BAR(1)OVER-BAR-2] SURFACES. *J. Electron Spectrosc. Relat. Phenom.* **1993,** *64-5*, 59-66.

101. Raghavachari, K.; Chabal, Y. J.; Struck, L. M., Vibrational interactions at surfaces: H2O on Si(100). *Chemical Physics Letters* **1996,** *252* (3-4), 230-235.

102. Luo, H. H.; Chidsey, C. E. D., D-Si(111)(1x1) surface for the study of silicon etching in aqueous solutions. *Applied Physics Letters* **1998,** *72* (4), 477-479.

103. Hossain, M. Z.; Kato, H. S.; Kawai, M., Self-directed chain reaction by small ketones with the dangling bond site on the Si(100)-(2 x 1)-H surface: Acetophenone, a unique example. *Journal of the American Chemical Society* **2008,** *130* (34), 11518-11523.

104. Weldon, M. K.; Queeney, K. T.; Gurevich, A. B.; Stefanov, B. B.; Chabal, Y. J.; Raghavachari, K., Si-H bending modes as a probe of local chemical structure: Thermal and chemical routes to decomposition of H2O on Si(100)-(2x1). *Journal of Chemical Physics* **2000,** *113* (6), 2440-2446.

105. Chabal, Y. J.; Raghavachari, K., SURFACE INFRARED STUDY OF SI(100)-(2X1)H. *Physical Review Letters* **1984,** *53* (3), 282-285.

106. Foster, I., *Designing and Building Parallel Programs, by*. Addison-Wesley: 1995; p 381.

107. Scott, A. P.; Radom, L., Harmonic vibrational frequencies: An evaluation of Hartree-Fock, Moller-Plesset, quadratic configuration interaction, density functional theory, and semiempirical scale factors. *J. Phys. Chem.* **1996,** *100* (41), 16502-16513.

108. Angot, T.; Bolmont, D.; Koulmann, J. J., High resolution electron energy loss spectroscopy study of the Si(001)3x1 hydrogenated surface. *Surf. Sci.* **1996,** *352*, 401-406.

109. Chabal, Y. J.; Raghavachari, K., NEW ORDERED STRUCTURE FOR THE H-SATURATED SI(100) SURFACE - THE (3X1) PHASE. *Physical Review Letters* **1985,** *54* (10), 1055-1058.

110. Jakob, P.; Chabal, Y. J.; Raghavachari, K., The Role of Kinks in the SIi-H Vibrational-Spectrum of Vicinal Si(111)-[(1)Over-Bar(1)Over-Bar2] Surfaces. *J. Electron Spectrosc. Relat. Phenom.* **1993,** *64-5*, 59-66.

111. Freking, U.; Kruger, P.; Mazur, A.; Pollmann, J., Surface phonons of Si(001)-(1X1) dihydride. *Physical Review B* **2004,** *69* (3).

112. Noda, H.; Urisu, T., Assignments of bending and stretching vibrational spectra and mechanisms of thermal decomposition of SiH2 on Si(100) surfaces. *Chemical Physics Letters* **2000,** *326* (1-2), 163-168.

113. Tagami, K.; Sasaki, N.; Tsukada, M., A tight-binding study of chemical interaction of nanotube tip with Si(001) surface. *Journal of the Physical Society of Japan* **2000,** *69* (12), 3937-3942.

114. Tagami, K.; Tsuchida, E.; Tsukada, M., First-principles study of vibrational spectra on dihydride-terminated Si(001)/H surfaces. *Surf. Sci.* **2000,** *446* (1-2), L108-L112.

115. Bellec, A.; Riedel, D.; Dujardin, G.; Rompotis, N.; Kantorovich, L. N., Dihydride dimer structures on the Si(100):H surface studied by low-temperature scanning tunneling microscopy. *Physical Review B* **2008,** *78* (16).

116. Buehler, E. J.; Boland, J. J., Identification and characterization of a novel silicon hydride species on the Si(100) surface. *Surf. Sci.* **1999,** *425* (1), L363-L368.

117. Faggin, M. F.; Green, S. K.; Clark, I. T.; Queeney, K. T.; Hines, M. A., Production of highly homogeneous Si(100) surfaces by H2O etching: Surface morphology and the role of strain. *Journal of the American Chemical Society* **2006,** *128* (35), 11455-11462.

118. Raghavachari, K.; Jakob, P.; Chabal, Y. J., STEP RELAXATION AND SURFACE STRESS AT H-TERMINATED VICINAL SI(111). *Chemical Physics Letters* **1993,** *206* (1-4), 156-160.

119. Caudano, Y.; Thiry, P. A.; Chabal, Y. J., Investigation of the bending vibrations of vicinal H/Si(111) surfaces by infrared spectroscopy. *Surf. Sci.* **2002,** *502*, 91-95.

Chapter Two

Reactivity of Silicon (100) Surfaces

2.1 Introduction

As previously discussed silicon may soon lose its preeminent position as the most widely used material in semiconductor device manufacture. The central reason is that the intrinsic limits of silicon and silicon-based materials will be reached around the year 2020 as device dimensions shrink to ever-smaller sizes.[1-3] An example of an intrinsic limit is the use of the native silicon-oxide as the dielectric layer in silicon-based devices. Silicon-oxide was an excellent material as the dielectric layer for many years until device dimensions reached a point at which the tunneling current through the dielectric was too

high. Newer high-κ dielectric materials were devised to overcome these limitations, i.e., oxynitrides and hafnium-based dielectrics. [4-6] It has thus far been possible to overcome this limitation within the current paradigm. In the future this is not likely. The limitations of the current paradigm may result in a shift towards molecular-scale devices that are fabricated by patterning surfaces. A natural substrate for such devices is the silicon surface. Both a massive industrial infrastructure and the rich scientific literature make this substrate an excellent candidate. While it may be possible to imagine other materials with superior properties one must ask the following question. Is it worth the effort to replicate the knowledge and infrastructure or can we modify silicon to have these properties? In some cases the answer is certainly yes but it may cases, perhaps the bulk of cases, the answer is likely no. Therefore, the study into the functionalization of silicon is critical to extend device fabrication.

A possible method of modifying silicon for molecular-scale devices is the use of nanopatterning molecules on the surface using chemical techniques. One of the major advantages of this method is the large number of species and reactions that can be exploited. Organic functionalization of silicon surfaces has already produced interesting results. The first step of nanopatterning research is therefore to understand how molecules of interest chemisorb on a surface in order to exploit this reactivity to produce predictable and reproducible patterns. The patterns can then be manipulated to form either nanoscale devices or interconnects for those devices. Using such a process nanoscale circuits could be constructed from a relatively small number of molecules. Once this hurdle is overcome it may be possible to drive the field towards single

molecule devices. These promises are as yet unrealized. The field is in still in its nascent stages and much of the basic work has yet to be explored.

Two major challenges in this field are how molecules react with the surface and what techniques can be used to form patterns. Understanding the reactivity of many species is challenging. If a bare Si(100) is used the "diradical character" of the surface makes it very reactive. This reactivity would only allow device construction in ultra-high vacuum to avoid contamination of the surface. The reactivity of many molecules on silicon surfraces has been studied. Much theoretical and experimental research in this area is ongoing. While it is useful to consider these cases of molecular reactivity with bare silicon surface, the high reactivity of the bare surface may necessitate passivation of the surface prior to functionalization. The current manufacturing techniques of silicon devices use an oxidized surface but direct functionalization would require a uniform non-oxidized surface. For the Si(100) surface any application that must occur outside of ultra-high vacuum conditions requires passivation. For the Si(111) surface passivation can be used to create the nearly atomically flat unreconstructed H/Si(111) surface. These passivated surfaces are much less reactive. As previously mentioned, the lower reactivity prevents oxidation but complicates surface chemistry. The surface must, therefore, be activated to initiate useful chemistry. One method for overcoming this limitation is the creation of dangling bonds on the surface. Surface sites with dangling bonds are far more reactive than passivated sites. It is also possible to use heat, UV exposure, atomic hydrogen or an STM tip to active the surface. Another very clever innovation by the Teplyakov group at Delaware is the use of dehydrative cyclocondensation to functionalize a passivated surface.[7] While the understanding of single molecule reactivity

is important, another consideration is the scale of necessary reactions to create useful molecular circuits. If molecules were assembled one-by-one the assembly process involving a single macroscale device could only be done on a galactic time scale. Patterning techniques involving passivated surfaces will therefore require self-assembly.

In this work we have studied the reaction of Lewis acids with the bare Si(100)-2×1 to understand if the molecules undergo a [2+2] cycloaddition or if they degrade on the surface. This work was motivated by previous experimental work that supported [2+2] cycloaddition, an important discovery if correct. We have also studied the radical chain reactions of allylic mercaptan (ALM) on the Si(100)-2×1 surface and the subsequent reactions of acetone, styrene and a second ALM. Finally we have examined the reactions of atomic hydrogen with the water and ammonia exposed Si(100)-2×1 surface.

2.2 Interaction of Lewis Acids with the Si(100) Surface

Silicon and germanium are widely recognized as the most important materials used in the semiconductor industry. While new technologies based on other semiconductors are being developed, future microelectronics devices will be based on heterogeneous integration into silicon and germanium substrates.[1-6] To continue the march towards better technology it is necessary to have a fundamental understanding of the chemical reactivity on these surfaces at the molecular level. One of the most broadly explored areas to date is the functionalization of the Si(100)-2×1 and Ge(100)-2×1 surfaces with hydrocarbons.[7-10] Another important area of semiconductor surface functionalization is surface cycloaddition reactions. Cycloaddition mechanisms have been reported on silicon[11-14] and on the germanium surface.[15-20]

Surface addition mechanisms often involve the reaction of a Lewis base or Lewis acid with the Si(100)-2×1 or Ge(100)-2×1 surfaces. In the case of a Lewis base such as NH_3, the mechanism proceeds by the nucleophilic center (up, electron rich) of the Lewis base interacting with the electrophilic (down, electron deficient) silicon or germanium surface dimer atom. The Lewis base can then form a dative bond with the surface. If the Lewis base contains hydrogens, the base will dissociate into a non-cyclic surface species, e.g., NH_3 will interact with silicon to form $H_2N–Si–Si–H$.[5] Trimethylamines initially interact similarly but the $N–CH_3$ bonds do not dissociate.[8] For comparison, the Lewis acid BH_3, has been theoretically found to weakly interact with the silicon surface via the electron rich surface dimer atom and dissociate without a barrier.[9] The Lewis acid BF_3 was also shown to experimentally dissociate on the silicon surface.[10] These results indicate analogous mechanisms for Lewis acids and Lewis bases reacting with the

Si(100)-2×1 surface. If the surface is first reacted with the Lewis base, trimethylamine (TMA), and then with the Lewis acid, boron trifluoride, BF_3, an adduct forms on the surface.[10] Presumably, the surface species is a Lewis acid-base pair datively bound through the boron-nitrogen bond.

In an interesting recent report, Jung et al.[11] reported the first reaction of a Lewis acid with the Ge(100)-2×1 surface. They interpreted their observations in terms of the formation of a *cyclic structure* on the germanium surface. In the product, the aluminum is bound to a germanium dimer atom and the chlorine is bound to the other germanium atom of either the same dimer or the adjacent dimer in the same row. Figure 2.2.1 a shows the silicon analogue for the case involving two atoms from the same dimer. This behavior is very different from that of Lewis bases, such as amines, that are known to form dative-bonded complexes on the Ge(100)-2×1 surface. In addition, there seems to be a fundamental difference between the reactivity of BF_3 on the Si(100)-2×1 (dissociative addition) and $AlCl_3$ on the Ge(100)-2×1 surface (cyclic product). Jung et al.[11] proposed an explanation for the different mechanisms using valence shell electron pair repulsion (VSEPR) theory. The hypothesis is that $AlCl_3$ is planar with a reported (20%) π–bonding character between the aluminum and chlorine atoms.[12] The $AlCl_3$ molecule orients such that the Al interacts with the nucleophilic up Ge atom and a Cl interacts with the electrophilic down Ge atom. Instead of dissociating, it undergoes a [2+2] *cycloaddition reaction* breaking the metal-halide and surface dimer partial π–bonds forming a four-membered ring with Ge–Al and Ge–Cl σ–bonds.[11] According to this model, the covalent metal-halogen bond is intact at room temperature and is broken only on annealing to a higher temperature (380 K). While the experimental results represent a

significant advancement to the literature of reactions on semiconductor surfaces, our theoretical results reported in this paper show some significant differences in the mechanistic understanding of reactions of Lewis acids on the Ge(100)-2×1 surface.

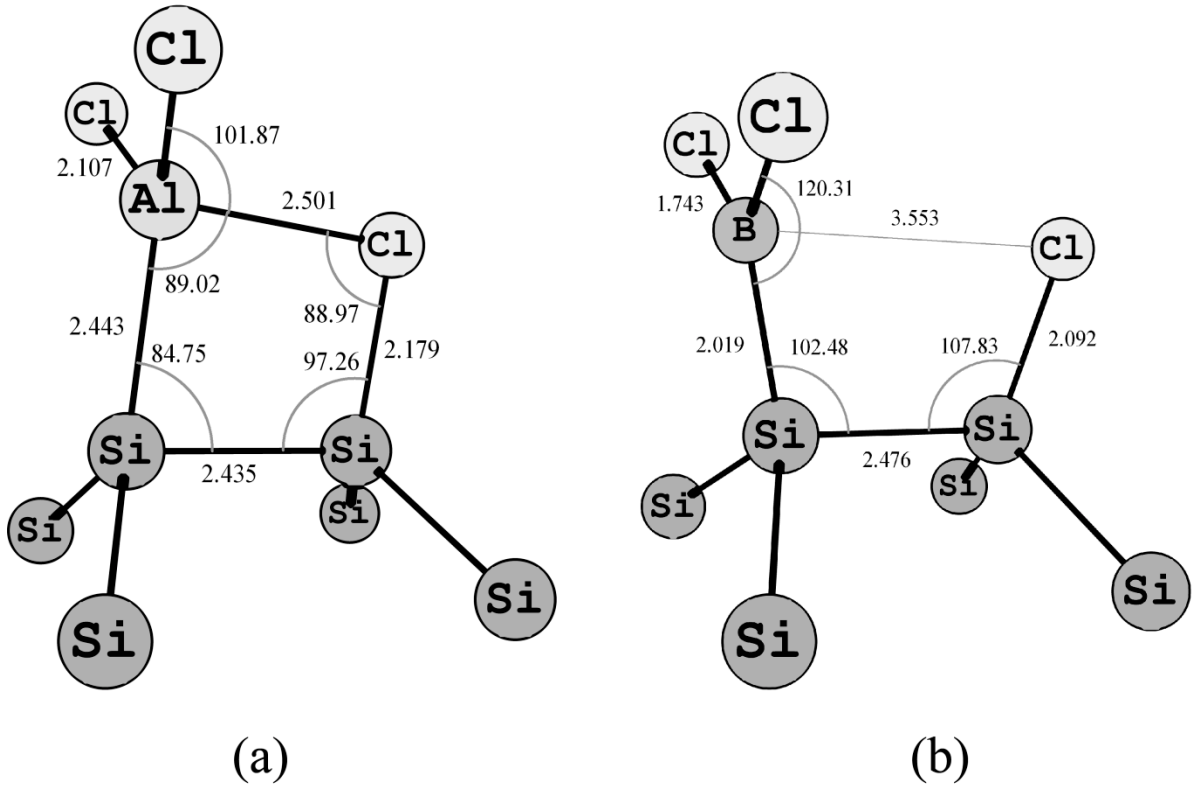

Figure 2.2.1. Geometric parameters for some of the Lewis Acids adsorbed on the Si_9 cluster, the aluminum trichloride (a) forms a cyclic structure on the surface with a bond between the aluminum and chlorine, the boron trichloride (b) dissociates on the surface.

In this section, we have considered the possible reactions and products of Lewis acids of the form MX_3 (M = B, Al or Ga, and X = F, Cl, Br or H) with the Si(100)-2×1 and Ge(100)-2×1 surfaces using Møller-Plesset[13] second order perturbation theory in

order to understand their surface reactivity. Several hypotheses are examined to see if they correspond with the experimentally available data. After careful consideration we have arrived at an explanation which reconciles the reactivity of Si(100)-2×1 and Ge(100)-2×1 surfaces with Lewis acids and bases showing how a dissociated product is formed with BF_3 while a cyclic structure is formed with $AlCl_3$. Our mechanism is consistent with all known previous experimental and theoretical studies.[11-14, 17, 22, 24, 27-29]

Computational Details

The models used for the Si(100)-2×1 and Ge(100)-2×1 surfaces were the Si_9H_{12} and Ge_9H_{12} dimers used extensively throughout the literature.[14] We have also performed calibration of our results using the $Si_{15}H_{16}$ clusters, which are composed of two silicon dimers in a single row of the Si(100)-2×1 surface. These models contain a single surface dimer excised from the surface. Dangling bonds are terminated with hydrogen in accordance with well-established procedures.[14] Hybrid density functional theory using Becke's three parameter electron exchange functional with the Lee-Yang-Parr correlation functional[31, 32] (B3LYP) and Møller-Plesset second order perturbation theory[13, 15] (MP2) were used with the standard 6-31+G(d,p) basis set (double–ζ basis set with added polarization functions on all the atoms and diffuse functions on all the non-hydrogen atoms).[16] Overall model chemistries are either B3LYP/6-31+G(d,p) or MP2/6-31+G(d,p). The minimum energy geometries reported were carried out using the MP2 model chemistry with either C_S symmetry or C_1 symmetry. All calculations were carried out using a development version of the Gaussian quantum chemistry software package.[17]

Results and Discussion

To understand the reactivity of the bare silicon and germanium surfaces, the reactions and products of Lewis acids with the type MX_3 (M = B, Al or Ga, and X = F, Cl, Br or H) were computed on the Si(100)-2×1 and Ge(100)-2×1 surfaces. As expected and as seen in Table 2.2.1, Lewis acids containing hydrogen do not form cyclic structures. Interestingly, boron does not form cyclic structures with either halides or hydrogen on silicon and germanium surfaces. The product of BCl_3 reacting with the silicon surface via dissociative addition is shown in figure 2.2.1 b. All of the Lewis acids containing aluminum or gallium with halides (F, Cl or Br) form cyclic structures. For comparison, surface geometric parameters at the MP2/6-31+G(d,p) level are shown in Table 2.2.2. We will first develop an understanding of the reason for the formation of cyclic structures followed by a short explanation of why certain species do not form cyclic structures.

Table 2.2.1. The formation of the surface structures for the adsorbed metal halide and metal hydride Lewis acids on the Si(100)-2×1 and Ge(100)-2×1 surfaces.

	Lewis Acid Surface Products			
Surface-Metal	**Fluorine**	**Chlorine**	**Bromine**	**Hydrogen**
Si–B	Dissociated	Dissociated	Dissociated	Dissociated
Si–Al	Cyclic	Cyclic	Cyclic	Dissociated
Si–Ga	Cyclic	Cyclic	Cyclic	Dissociated
Ge–B	Dissociated	Dissociated	Dissociated	Dissociated
Ge–Al	Cyclic	Cyclic	Cyclic	Dissociated
Ge–Ga	Cyclic	Cyclic	Cyclic	Dissociated

Table 2.2.2. The geometric parameters for the metal halides bound to the Si(100)-2×1 and Ge(100)-2×1 surfaces, bond distances in Å and angles in degrees. Y are surface atoms, X is a halide and M is a metal atom.

	Species		Bond Distances, Å				Bond Angles, °	
Surface	**Metal**	**Halide**	**Y–Y**	**Y–M**	**Y–X**	**M–X**	**Y–Y–X**	**Y–Y–M**
Silicon	Boron	Fluorine	2.47	2.03	1.66	3.42	106	103
		Chlorine	2.48	2.02	2.09	3.55	108	102
		Bromine	2.47	3.40	2.26	3.49	107	100
	Aluminum	Fluorine	2.43	2.45	1.78	1.96	92	76
		Chlorine	2.43	2.44	2.18	2.50	97	85
		Bromine	2.44	2.43	2.34	2.67	97	89
	Gallium	Fluorine	2.43	2.40	1.73	2.15	94	78
		Chlorine	2.41	2.38	2.13	2.79	101	89
		Bromine	2.42	2.38	2.31	2.88	100	91
Germanium	Boron	Fluorine	2.51	2.06	1.81	3.22	103	98
		Chlorine	2.52	2.05	2.20	3.42	105	99
		Bromine	2.51	2.03	2.37	3.46	105	99
	Aluminum	Fluorine	2.49	2.49	2.00	1.88	89	76
		Chlorine	2.49	2.47	2.34	2.37	93	84
		Bromine	2.49	2.45	2.47	2.57	88	94
	Gallium	Fluorine	2.48	2.43	1.92	2.05	89	79
		Chlorine	2.48	2.42	2.28	2.64	95	89
		Bromine	2.48	2.48	2.43	2.76	96	91

The four hypotheses we have considered here are: physisorption or weak interactions holding the molecule to the surface, dative bonding between the metal in MX_3 and the surface atom, [2+2] cycloaddition proposed by Jung et al.,[11] and finally breaking of the metal–halide covalent bond as in the case of dissociative addition but with the formation of a metal–halide dative bond. Our method will be to consider the structural and bonding nature of the products formed from the starting materials. Each hypothesis will be analyzed based on the computed results. Once the most probable theoretical explanation is discovered, we will show how it explains the experimental observations.

We first consider the possibility of physisorption on the surface. If the metal–halide Lewis acids are physically bound to the surface they will not have covalent bonding interactions. The physisorption molecule would be attracted to the surface by noncovalent interactions in a way that maximizes the interactions affecting only the orientation of the molecule on the surface. For the case of $AlCl_3$ physisorbed to the Si(100)-2×1 surface the slightly positive aluminum would be attracted to the electron rich silicon dimer atom and the slightly negative chlorine atom would be attracted to the electron rich silicon dimer atoms. Significant changes to geometry of the $AlCl_3$ molecule and to the surface structure would not be expected leaving the molecule intact and surfaces unmolested. Our observations show significant changes to the bond lengths of the Lewis acids as well as passivation of the surface dangling bonds at the sites where the Lewis acids are bound. Therefore we can easily rule out this possibility.

The second hypothesis is analogous to the reaction of the Lewis base, trimethylamine, with the Si(100)-2×1 surface. However, the initial step in the reaction

corresponds to the interaction of a Lewis acid, not a base. The metal–halide Lewis acid datively bonds to the surface by the lone pair of the up surface dimer atom donating into the empty *p*–orbital of the metal atom. The halide atom can then donate electrons into the empty surface orbital of the down dimer atom forming a second dative bond with the surface. The feasibility of the reaction is based on the asymmetric charge of the buckled dimer.[18] These interactions would result in a species that is bound to the surface along dimer bonds. Furthermore, the metal–halide bond along the dimer will be slightly elongated (~ 0.1 Å) due to the interaction with the surface. Otherwise no serious structural changes are expected. To explore the plausibility of this mechanism, we will examine the cyclic structure formed by $AlCl_3$ reacting with the Si(100)-2×1 surface (figure 2.2.1 a). The Al–Cl bond length along the surface dimer is almost 0.4 Å larger than the two other Al–Cl bonds in $AlCl_3$ demonstrating that the molecule is no longer intact i.e., Al–Cl covalent bond along the dimer is broken. Rather, such an elongated distance corresponds to what is expected for an Al–Cl dative bond (*vide infra*). In addition, the $AlCl_3$ unit is no longer planar or near-planar whereas the $AlCl_2$ unit is nearly planar with the surface silicon atom (indicating covalent bond formation with the surface). Also, if this mechanism is correct the down surface silicon atom involved in the second dative bond would be expected to become more planar.[5, 8] The geometric effect is absent for the down silicon atom in our calculations. A final definitive way to characterize the nature of the Si–Cl bond is to estimate its bond energy. Using appropriate gas phase species at the MP2 level, the covalent bond energy (102 kcal/mol) is more than an order of magnitude larger than the dative bond energy (8 kcal/mol). The energy of the Si–Cl bond on the surface is 99 kcal/mol, clearly indicating a covalent bond

and not a dative bond. From bond energies and the geometric evidence we can conclude that the mechanism is implausible. Similar results can be seen for the remaining cyclic structures, ruling out this possibility.

The next hypothesis is the cycloaddition mechanism as proposed by Jung et al.[11] for the reaction of $AlCl_3$ with the Ge(100) surface. We will examine their proposal not only for $AlCl_3$ on germanium but for all of the cyclic Lewis acid species seen in Table 2.2.1. The surface dimer has a buckled morphology with an electrophilic (down, electron deficient) atom and a nucleophilic (up, electron rich) atom. The electronic structure of the surface dimers is relatively complex but can be thought of as having a polar double-bonded nature. The hypothesis of Jung et al.[11] is that $AlCl_3$ is planar with a reported (20%) double bond character between the aluminum and chlorine atoms.[12] The reaction proceeds via the concerted interactions of a chlorine with the down germanium atom and the aluminum with the up germanium atom. Instead of dissociating, it undergoes a [2+2] cycloaddition reaction breaking the Al–Cl and surface dimer partial π–bonds forming a four-membered ring with Ge–Al and Ge–Cl σ–bonds.[11] Cycloaddition has previously been observed for cyclooctadiene on the germanium surface.[19] According to this model, the covalent metal-halogen bond is intact at room temperature. However, evaluation of the bond strength of this Al–Cl interaction (parallel to the surface dimer) shows it to be < 10 kcal/mol. A typical covalent Al–Cl bond strength is ~ 100 kcal/mol and can clearly be ruled out. Thus a simple cycloaddition process involving the loss of two π–bonds and the formation of two σ–bonds is not consistent with the calculations.

The final hypothesis is a dissociative addition reaction accompanied by the formation of a weak dative bond leading to a cyclic product. Unlike the cycloaddition

mechanism, the metal-halogen covalent bond is broken in this case. However, as in the case of the cycloaddition mechanism, two σ–bonds are formed, one between the metal and the surface and the other between the halide and the surface. Again using $AlCl_3$ as our example, initially the aluminum interacts with the up dimer atom and the chlorine atom interacts with the down atom. One of the Al–Cl bonds break and a covalent bond forms between the up dimer atom and the Al and between the down dimer atom and the Cl from the broken Al–Cl bond. If considered simplistically, this picture could be thought to form a dissociative addition product ($Cl_2Al–Ga–Ga–Cl$). Instead, the $AlCl_2$ group rotates such that a new interaction occurs between a lone pair of the chlorine attached to the surface and the empty *p*–orbital of the aluminum resulting in a cyclic structure containing an aluminum–chlorine dative bond. The bond distance, the orientation, and the bond strength (*vide infra*) of this bond confirm this picture.

To analyze the interactions further, we performed additional series of calculations. Using gas phase molecular analogues, e.g., $H_3Al•••Cl–SiH_3$, the strength of the dative bond is estimated to be ~ 8 kcal/mol, consistent with its calculated length. In addition, if we twist the dihedral angle around the Al by 10º such that the empty Al *p*–orbital is not pointing towards the Cl, the resulting structure opens out demonstrating that it is a weak directional dative bond. The calculated bond lengths are also entirely consistent with this picture. For example, the Si–Cl distance for the dative bond in figure 2.2.1 a (2.501 Å) is about 0.4 Å longer than the covalent distance (2.107 Å), typical for such systems. A similar trend is seen for the other cyclic structures. Finally, the estimated strength as indicated above (< 10 kcal/mol) is not consistent with a covalent bond but only consistent with a dative bond. However, the interaction is sufficiently strong that in all cases

involving halogens and Al or Ga, no other minima were found. In particular, no loosely bound surface complex was found but transformed without a barrier into the dative bonded cyclic structures as in figure 2.2.1 a. The same result was found by Konecny and Doren[20] for the dissociation of BH_3 on silicon.

Significant differences were found for some Lewis acids. As expected, the metal–hydrides of aluminum, gallium and boron form open dissociated structures due to their lack of lone pairs and would therefore not be expected to form dative-bonded cyclic structures. Interestingly, the boron–halides BF_3, BCl_3 and BBr_3 also do not form cyclic structures. We interpret this as resulting from the fact that the energy stabilization from forming the dative bond is less than the strain energy imposed on forming cyclic structures.

The experimental evidence also supports this conclusion. Cao and Hamers[10] have shown that BF_3 dissociates without dative bonding on the silicon surface, a result our calculations support. If cycloaddition occurs on the germanium surface, it would also be expected to occur on the silicon surface which has even more dative bonding character than the germanium surface. In the same work it was shown that if TMA reacts with the silicon surface followed by BF_3 a datively bound complex is formed. To test if similar dative bonds will form with other groups containing lone pairs, we optimized structures where the Cl atom attached to the surface is replaced by NH_2, PH_2, AsH_2, OH, SH or SeH groups. In every case cyclic structures were found showing that such dative bonding is likely to occur for many different species. Our results indicate that if Lewis acids are placed on the surface with adjacent Lewis bases cyclic structures would be expected in most instances.

To determine the effect of additional dimers on the structure of Lewis acids on the silicon surface we have investigated the structure of $AlCl_3$ on the silicon surface using $Si_{15}H_{16}$ models. The structure of the $AlCl_3$ molecule was examined bonding across two dimers and on one dimer with an adjacent dimer attached. The $AlCl_3$ across a dimer row showed a similar structure to the $AlCl_3$ molecule after reacting with a single dimer. The Al—Cl covalent bond is broken and has been replaced with a weak dative bond. The largest differences result from the changes in bond length of the Al—Cl weak dative bond which is 2.4 Å. The distance is 0.1 Å less than the same species on the single dimer. The origin of the difference is from the relaxation allowed when going from a four member ring in the single dimer structure to a five membered ring when the structure is reacted across two dimers. Our conclusions remain valid for the $AlCl_3$ bond across two dimers. The $AlCl_3$ bound to a single dimer with the adjacent dimer included in the model has only slight differences from the single dimer model. The bond angles are unchanged and the key parameter of the Al—Cl weak dative bond distance is changed by 0.02 Å. The Si—Cl bond distance is lengthened by 0.01 Å and the Si—Al bond distance is unchanged. These small differences do not change our previous conclusions and indicate that a single dimer model captures the full complexity of the system in this case.

Limitations of DFT

Thus far, we have discussed all the results from MP2/6-31+G(d,p) model. We also performed detailed calculations with the B3LYP/6-31+G(d,p) model. However, the results were erratic when compared to the MP2 model chemistry, particularly when comparing open dissociated structures vs. datively bonded cyclic structures. In particular, dative bond dissociation energies were uniformly lower at the B3LYP level compared to

MP2. Calibration using small molecular systems showed that the MP2 results are much closer to the binding energies at the G3 level. Specifically, GaF_3 and $GaCl_3$ were predicted not to form cyclic structures with DFT while MP2 predicts only cyclic structures. Additionally, both open and datively bonded minima were found for $AlCl_3$ on the silicon surface with an activation barrier of less than 1 kcal/mol. In retrospect, it is not surprising that the MP2 model chemistry is more reliable for these weak datively bound species.

Conclusions

After carefully examining the evidence for each of the hypothesis we conclude that the cyclic structures on germanium are formed via a surface–metal and surface–halide covalent bond formation, breaking of the metal–halide covalent bond and formation of a weak metal–halide dative bond. The evidence does not support [2+2] cycloaddition-like reactions as proposed by Jung et al.[11] We predict that most donor–accepter species on the silicon and germanium surface will form weakly bound cyclic structures. Systems that have lone pairs but do not form cyclic structures are due to weak bonding between the metal and the donor species. In our case the only species for which this condition is true are boron–halides. In addition to presenting a very parsimonious explanation our proposed mechanism rationalizes not only the reactions of Lewis acids but also conforms to the current understanding of the reactivity of Lewis bases on group IV semiconductor surfaces.

2.3 Line Growth of ALM on the Si(100) Surface

While much of the early focus of silicon surface chemistry has been centered on structure and its basic chemistry, attention has recently shifted to organic monolayers using the reactivity of the surface with small organic molecules.[2, 7-10, 16, 38-42] The reason for the change is rapid miniaturization of feature size. In a few short years, silicon will reach its intrinsic limits forcing a paradigm shift in the microelectronics industry to maintain Moore's Law.[1, 4-6] While silicon may no longer be used as the preeminent material for device fabrication, its available technological infrastructure may maintain silicon as the substrate upon which future devices will be built. This new use is likely to drive future research in silicon-based technologies.

One of the most interesting areas of recent advancement has been the use of self-assembled molecular lines.[27, 43-63] These lines may serve as molecular wires directly, as in the case of styrene.[19, 40, 50, 54, 58, 59] For other molecules it may be possible to later modify the lines to become molecular wires.[21] These molecular wires are envisioned to link together molecular scale devices on a silicon substrate. The growth mechanism for these lines is a radical chain reaction starting at a radical site created either by a surface defect or by inducing a defect site using an STM (Scanning Tunneling Microscope) tip.[63, 64] The surface radical is transferred to the adsorbate molecule which then abstracts a second hydrogen atom from an adjacent surface site creating a stable adsorbate and a second radical site for another molecule to react. To date these lines have been grown for a variety of molecules on the H/Si(111)-1×1 and H/Si(100)-2×1 surfaces.[22] The initial growth mechanism has been experimentally characterized. For the present work we focus on the growth of molecular lines on the important H/Si(100)-2×1 surface.

In general, molecular lines must be grown preferentially in two directions to produce useful interconnects. The H/Si(111)-1×1 surface is uniform making this goal more challenging. The intrinsic directional anisotropy of the Si(100)-2×1 surface (local C_{2v} symmetry) provides the necessary two directions for line growth. Lines can be grown either along a dimer row or across a dimer row. Many molecules have been shown to grow along dimer rows: styrene, vinylferrocene, long-chain (n ≥ 8) alkenes, and 2,4 dimethylstyrene.[46, 47, 50-56, 63, 65] The corresponding mechanism of growth along dimer rows has been well explained in several studies.[50, 52, 58, 59, 62, 63, 66, 67] While both ALM and acetophenone have been observed to grow across dimer rows on the H:Si(100)-2×1 surface only ALM grows exclusively across dimer rows.[50, 54, 55] Acetophenone has been observed to grow both across and along dimer rows on the H:Si(100)-2×1 surface with a proposed mechanism of selectivity due to chirality.[54, 55] The complete mechanism of ALM line growth has not been conclusively explained. This mechanism is important beyond the immediate usefulness of ALM molecular lines. Since ALM is not likely to be an excellent molecular wire understanding the mechanism is critical to exploiting across dimer radical chain reactions.

The first proposed mechanism for across dimer growth was proposed by Hossain et al.[23] who also reported the initial experimental observations. According to this mechanism, the molecule follows the chain-reaction mechanism. The mechanism requires an intra-dimer hydrogen migration (known to be a high barrier reaction) to explain the experimentally observed distance between surface features. STM images show the features across dimers are at a distance of 7.7 Å. This distance is very close to the calculated distance between dimer silicon atoms across a row of ~ 7.6-7.7 Å. The

barrier to hydrogen migration is much higher than the barriers for the other steps involving the reacting structures. This high barrier makes preferential growth across a dimer row unlikely. A second relatively high barrier reaction (~ 7 kcal/mol higher than the separated reactants) is the 1,3-hydrogen shift moving the radical from the carbon atom to the sulfur atom. This barrier would most likely result in desorption of allylic mercaptan from the surface.

To overcome the problems presented by both of these barriers Choi and Cho have proposed an alternate mechanism.[24] In the Choi and Cho mechanism, the high barriers are avoided by a complex pathway. This mechanism proceeds in the same fashion as the original mechanism with respect to ALM deposition but requires a series of rearrangements (*vide infra*) ending in *the elimination of molecular hydrogen and the creation an ALM bridge* between the dimers. The mechanism explains the stability of the resulting product (stable to 650 ºC) and avoids the high barriers of the hydrogen migration and the 1,3-hydrogen shift. The mechanism is novel because it suggests the possibility of molecular hydrogen elimination and the formation of the bridge across the dimers. A problem with this explanation is raised by a clever experiment conducted previous to the study by Dogel et al.[25] In this experiment trimethylene sulfide was reacted with *p*- and *n*-type H:Si(100)-2×1 surfaces to create either a surface carbon-silicon bond with a sulfur radical or a sulfur-silicon bond with a carbon radical (verified by high resolution electron energy loss spectroscopy and density functional calculations). *Both* of these structures grow in a square wave pattern showing no preference for either across or along dimer growth. Since the intermediate of the *n*-type H/Si(100)-2×1 surface with the sulfur radical is identical to the intermediate formed by the mechanism proposed by Choi

and Cho, it is not clear why the same intermediates would result in substantially different reactivities.

Another alternative was presented in the work of Pei et al.[26] In this mechanism the deposition is postulated to occur *through a branched structure* where the surface radical reacts with the medial carbon of the double bond to create a primary radical. The hydrogen transfer becomes a 1,4 shift rather than a 1,3 shift with a correspondingly lower barrier. Unfortunately, the mechanism fails to show the exclusivity of the across dimer abstraction with the difference between across dimer and along dimer hydrogen abstraction being ~ 1 kcal/mol. This point was not explored in detail in the Choi and Cho mechanism.[24]

In this work we propose a mechanism that begins with the bridged structure proposed by Pei et al.[26] and ends with the elimination/bridge formation mechanism products. We will discuss the detailed mechanism starting from the separated reactants leading to a bridged structure formed via molecular hydrogen elimination. We compare these reactions to the direct migration mechanism starting from a branched structure using the same model for across dimer growth with hydrogen migration.

Computational Details

The Si(100)-2×1 surface is made of dimer rows separated by troughs giving the surface an intrinsic directional anisotropy. This structure increases the number of atoms needed to model the surface using clusters. For reactions across dimer rows a minimum of two dimers must be used making the smallest possible model the $Si_{23}H_{27}$, figure 2.3.1. The cluster model has previously proven reliable for studying the chemical reactivity on this system.[14] While using such clusters to model surfaces, the cluster must be properly

constrained to mimic the extended surface. As is appropriate, the broken backbonds generated during the excision of the cluster are terminated with hydrogen atoms. Silicons below the third layer and hydrogens below the second layer are frozen in accordance with previous studies.[14] The validity of these constraints is examined below. While it is usual to include four layers for models of this type we have included a fifth to avoid problems of proximate terminating hydrogens.

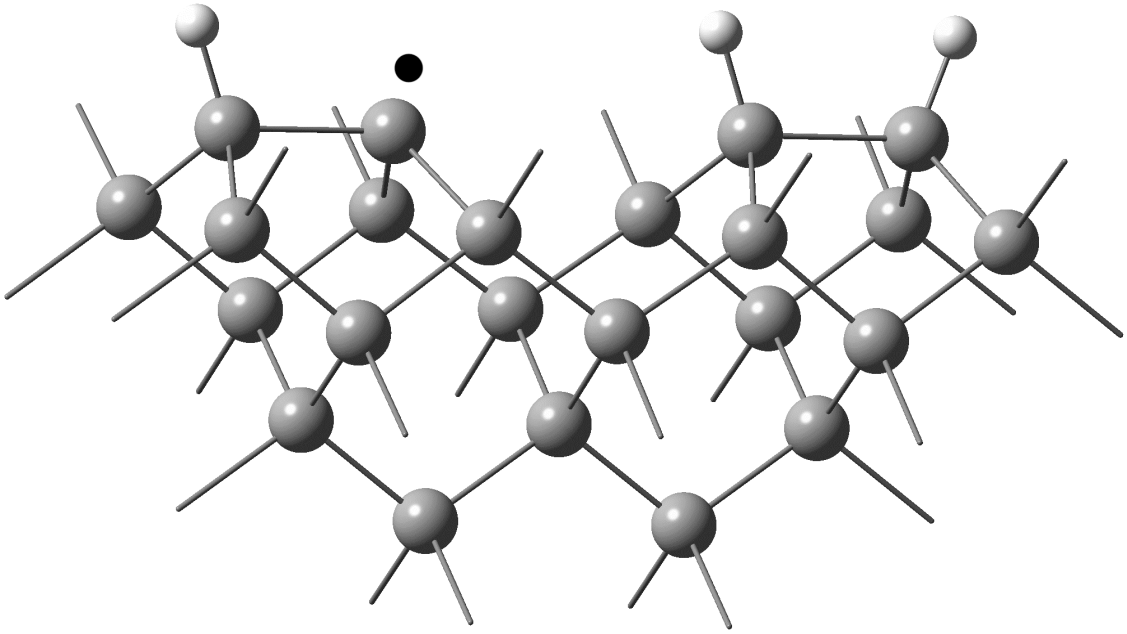

Figure 2.3.1. The $Si_{23}H_{27}$ model used to represent two Si(100)-2×1 dimers across a row. White spheres are hydrogens, grey spheres are silicons and the solid black dot marks the radical site. Terminating hydrogens are omitted for clarity.

The hybrid density functional theory using Becke's three-parameter exchange functional with the Lee-Yang-Parr correlation functional (B3LYP) has been show to give good results in past studies.[31, 32, 34, 68, 69] It was used in conjunction with a Pople style

double-ζ basis set with added polarization functions for both hydrogen and heavy atoms as well as diffuse functions on heavy atoms: overall model chemistry is B3LYP/6-31+G(d,p). Some previous studies have shown an underestimation of barrier heights using hybrid density functional theory, specifically B3LYP. These underestimations could lead to qualitatively incorrect conclusions. We have avoided the need to correct values by *making comparisons only among reactions of the same type between competing mechanisms*. The nature of the minima and transition states were confirmed with analytic second derivative calculations. All calculations were carried out with the Gaussian development suite of programs.[17]

Results and Discussion

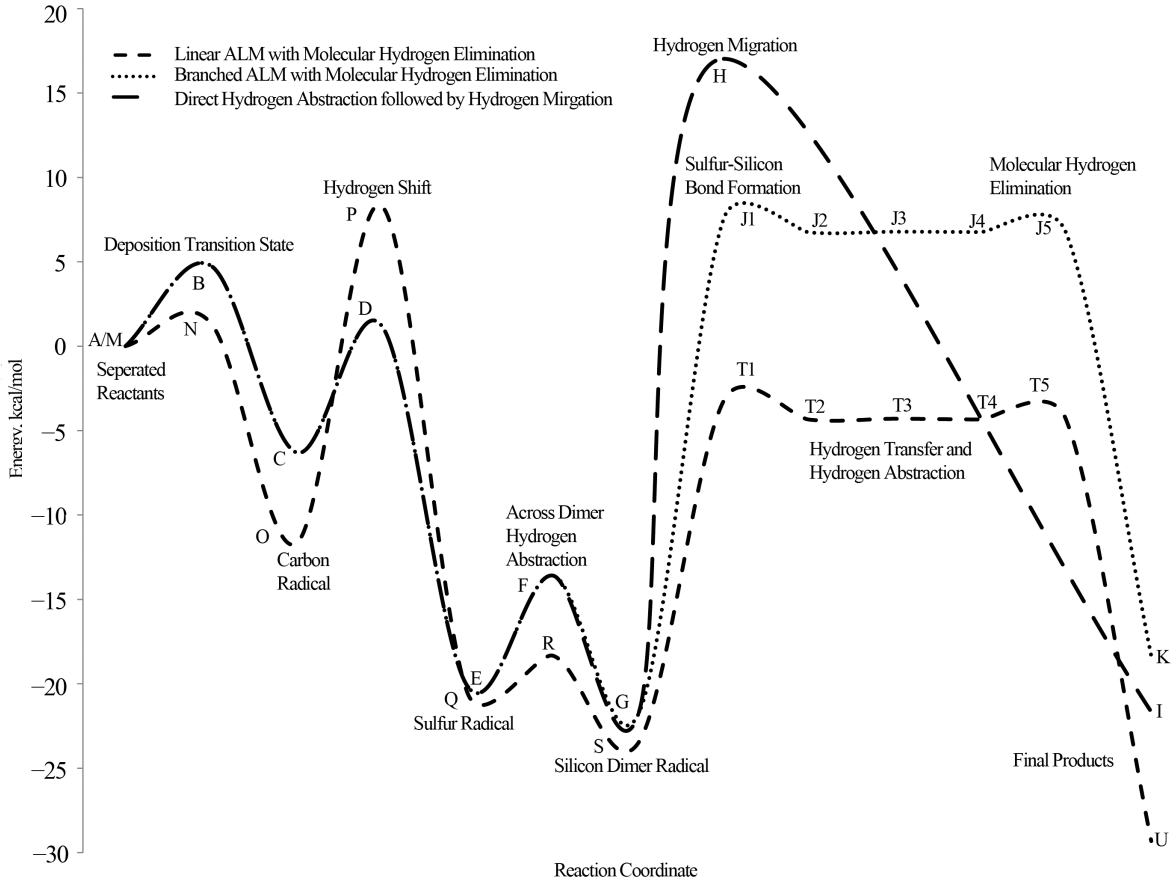

Figure 2.3.2. A comparison of the reactions pathways for the three pathways of ALM reacting across dimer rows on the Si(100)-2×1 surface.

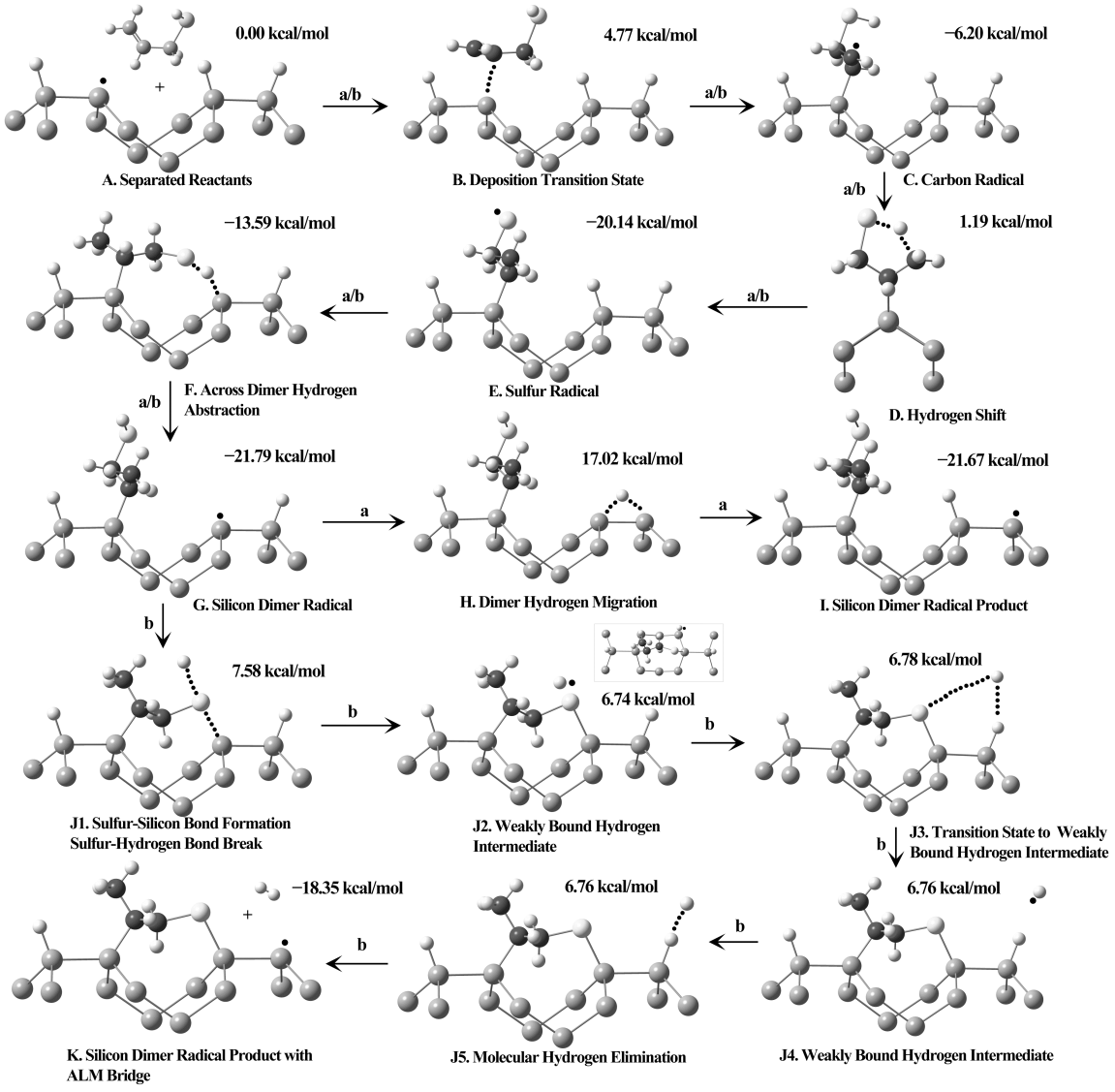
0.00 kcal/mol
A. Separated Reactants
a/b
4.77 kcal/mol
B. Deposition Transition State
a/b
−6.20 kcal/mol
C. Carbon Radical
a/b
1.19 kcal/mol
D. Hydrogen Shift
a/b
−20.14 kcal/mol
E. Sulfur Radical
a/b
−13.59 kcal/mol
a/b
F. Across Dimer Hydrogen Abstraction
−21.79 kcal/mol
G. Silicon Dimer Radical
a
17.02 kcal/mol
H. Dimer Hydrogen Migration
a
−21.67 kcal/mol
I. Silicon Dimer Radical Product
b
7.58 kcal/mol
J1. Sulfur-Silicon Bond Formation
Sulfur-Hydrogen Bond Break
b
6.74 kcal/mol
J2. Weakly Bound Hydrogen Intermediate
b
6.78 kcal/mol
b
J3. Transition State to Weakly Bound Hydrogen Intermediate
6.76 kcal/mol
J4. Weakly Bound Hydrogen Intermediate
b
6.76 kcal/mol
J5. Molecular Hydrogen Elimination
b
−18.35 kcal/mol
K. Silicon Dimer Radical Product with ALM Bridge

(a)

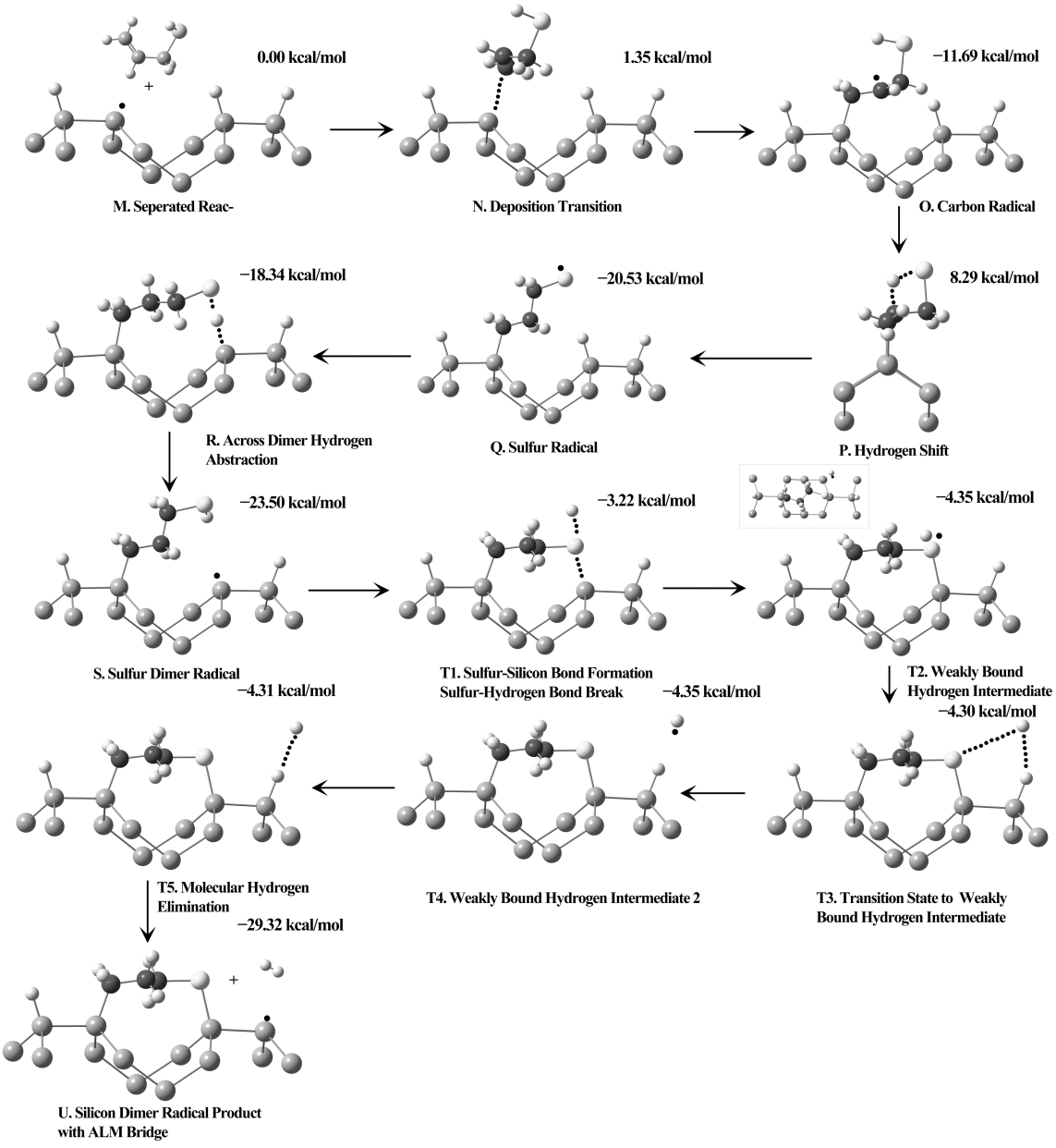

(b)

Figure 2.3.3. Intermediates and transition states along the reaction paths for the deposition of ALM with a branched adsorbate (a) and a linear adsorbate (b). Lower layers not shown for clarity. Grey spheres are silicon, black spheres are carbon, small white spheres are hydrogen and large white spheres are sulfur. Black dots mark radical and dotted black lines trace transition states. Paths are differentiated in (a) as a/b, a & b.

Comparison of different mechanisms is challenging. We will first review the mechanism of sulfur radical formation that is common to every mechanism,[45, 50, 61] We show the reaction profiles for the different mechanisms in figure 2.3.2, and the sequence of reaction steps in figure 2.3.3 (a) path a/b for the branched adsorbate and figure 2.3.3 (b) for the linear adsorbate. The ALM molecule can potentially react with a silicon-dangling bond with either the terminal carbon or medial carbon of the double bond. If it reacts with the former it will produce a secondary radical and the latter will produce a primary radical. The primary radical can be stabilized through hyperconjugation with the silicon surface making it more stable than would be thought from simple considerations of radical stability. The deposition barrier for the secondary radical product is 3.4 kcal/mol lower than the barrier for the primary radical product. Thus, the secondary radical product is kinetically favored. The secondary radical is also thermodynamically favored by 5.4 kcal/mol. At this point in the reaction both species have a carbon radical, and can convert via a 1,3-hydrogen shift for the secondary radical (leading to a linear sulfur radical) or a 1,4-hydrogen shift for the primary radical (leading to a branched sulfur radical). The 1,3-shift is predictably much higher in energy (8.3 kcal/mol barrier) than the 1,4 shift (1.2 kcal/mol barrier) due to a more strained transition state. The resulting stability of the sulfur radicals is close, 20.1 kcal/mol for the branched form vs. 20.5 kcal/mol for the linear form. However, from the calculated reaction profile it is more likely the linear structure would desorb from the surface rather than react further to form the sulfur radical. From this evidence we believe it is unlikely that linearly adsorbed sulfur radical is formed. A similar conclusion was reached by Pei et al.[26] and Choi and Cho.[24] Using a different model Pei et al.[26] found a difference of 2.35 kcal/mol for the

branched versus linear using an ONIOM model without constraints. The Choi and Cho mechanism[24] is substantially different than the other two. In this mechanism, after deposition the secondary carbon radical is formed. The secondary carbon radical abstracts a hydrogen atom *from the dimer in the same row* creating a satisfied adsorbate and a dangling bond on the surface. The resulting silicon radical in the same dimer row is stable by ~ 27 kcal/mol below the separated reactants. The mechanism proceeds by the surface-dangling bond abstracting the hydrogen from the sulfur at the end of the ALM adsorbate thus creating the sulfur radical. The sulfur radical formed in this mechanism is metastable and quickly reacts.

Considering the mechanisms thus far, the Choi and Cho mechanism[24] is energetically the most attractive while the branched and linear hydrogen shifting mechanisms provide a simpler explanation. There are several questions to consider, however. The formation of the silicon dimer radical is an opportunity for deposition by a second ALM molecule. While it is true that hydrogen abstractions are lower in energy than adding a second ALM, the silicon surface radical is quite stabile. It is, therefore, not clear that a second ALM molecule would not react to form a line along the dimer row in some cases. Experimentally, square wave or along-row line growth has *never* been observed. If we consider only the linear and branched ALM molecules for the same mechanism, figure 2.3.3 a vs. figure 2.3.3 b, it is clear the branched structure is preferred over the linear structure. The high barrier to the 1,3-shift would favor desorption over reaction to form the sulfur radical.

Further reactions are necessary to form stable products. Each proposed mechanism follows a similar path for the next step in the reaction. The sulfur radical

abstracts the silicon dimer hydrogen in the *adjacent* row. The barrier for the reaction is below that of the starting reactants by 13.6 kcal/mol for the branched structure and 18.3 kcal/mol for the linear structure. These low barriers indicate a very facile reaction to form the silicon radical. The barrier for the branched structure from the sulfur radical is 6.5 kcal/mol, and the barrier for the linear structure is 2.2 kcal/mol. The silicon radical formation is exothermic by 1.7 kcal/mol and 3.0 kcal/mol for the branched and linear structures, respectively. Since the sulfur radical and the silicon radical are both stable, they can potentially interconvert unless further reactions occur. It is likely the oscillation between the silicon surface radical and the sulfur radical is the bottleneck resulting in a low probability of reaction observed by Hossain et al.[21] The study by Pei et al.[26] reported the exothermicity of the branched structure to be 8.1 kcal/mol, and Choi and Cho[24] reported a corresponding value of 14.5 kcal/mol for the linear structure. The variance of the findings is most likely due to differences in the model chemistries and surface models used. It is worth noting that the reaction of this intermediate with a free ALM molecule is possible but unlikely due to the steric hindrance of the site by the adsorbed molecule. Once the silicon radical state is achieved the reaction proceeds by very different means for each of the proposed models.

The original model of Hossain et al.[21] and the branched variation of Pei et al.[26] both follow a similar mechanism. We will only discuss the branched mechanism. Once the silicon radical is created it is possible for the hydrogen on the opposite side of the dimer to migrate across the dimer bond forming a structure with a site open for a second ALM molecule to continue the radical chain reaction mechanism. Hydrogen migration across a dimer is a high barrier process that is not facile. Steckel et al.[27] have calculated

the barrier for intra-dimer hydrogen migration to be 40 kcal/mol using density functional calculations and cluster models. This result is in accordance with our calculated barrier of 38.8 kcal/mol for hydrogen migration in the case of the branched structure. The barrier is far too high for any possible reaction. The barrier calculated by Choi and Cho was 31.8 kcal/mol.[24] Interestingly, their calculated barrier is ~ 2 kcal/mol higher than the separated reactants, much lower than our calculated value of 17 kcal/mol. Such a high barrier makes desorption a more likely possibility. One could also consider the possibility hydrogen tunneling through the barrier. Preliminary calculations of excited vibrational states show an exceedingly small probability of tunneling. We conclude formation of the final silicon radical via hydrogen migration is not viable.

To avoid the high barrier it is necessary to conceive a lower barrier process that forms the products. According to the mechanism of Choi and Cho[24] the sulfur forms a bond with the silicon from the *adjacent* row and molecular hydrogen is eliminated in a *concerted* reaction. The second hydrogen forming the molecular hydrogen comes from the far silicon of the adjacent dimer. The resulting product is a bridging structure with a sulfur silicon bond and a silicon dimer radical ~ 7.6 Å from the reaction site. The reported barrier is 24.9 kcal/mol that is 4.8 kcal/mol below the separated reactants. The reaction avoids the high barrier and forms a very interesting product. The bridged structure provides another piece of the puzzle by proffering an explanation for the high stability observed by Hossain et al.[21] ALM lines were observed not to desorb and were stable up to 650 K. The bridged structure contains both carbon-silicon and sulfur-silicon bonds both of which are strong covalent bonds. Additionally, the elimination of molecular hydrogen removes any possibility of back reaction as observed for styrene.

After many attempts we were unable to locate a concerted transition state for the stated reaction. Instead we explore a multi-step process starting from the silicon radical and ending in the bridged structure with accompanying molecular hydrogen elimination. The hydrogen transfer mechanism begins with the sulfur forming a bond with the surface silicon and the sulfur-hydrogen bond breaking. The hydrogen forms a weakly bound complex with the sulfur atom. The hydrogen then transfer to a weakly bound complex with the remaining dimer hydrogen through a well characterized transition state. The hydrogen can then abstract the dimer hydrogen giving the molecular hydrogen product and leaving the silicon radical. We have characterized the pathway for both the linear and branched adsorbates.

The linear adsorbate shows a lower energy pathway. The sulfur-silicon bond formation (accompanied by the sulfur-hydrogen bond breaking) has a barrier of 20.3 kcal/mol and is 3.2 kcal/mol below the starting reactants. In this transition state the sulfur-silicon bond is 2.22 Å, close to the sulfur-silicon bond distance of 2.17 Å and the sulfur-hydrogen distance is 2.0 Å which is much higher than the 1.3 Å of the thiol bond indicating a late transition state involving a mostly formed sulfur-silicon bond and a mostly broken sulfur-hydrogen bond. In the weakly bound intermediate the sulfur-hydrogen distance is 2.6 Å which indicates a weak complex. The hydrogen transfer and hydrogen abstraction are essentially barrierless (< 0.1 kcal/mol) and the formation of the products is highly exothermic (25 kcal/mol) indicating that if the initial barrier to form the sulfur-silicon bond is overcome, the reaction will proceed to the product with little chance of back reaction. The barrier for the hydrogen abstraction is likely to be

underestimated but the errors are systematic for structures of the same type and will not affect our conclusions.

The branched structure is considerably more strained than the linear structure. The energy difference of the branched and linear transition states is ~ 10 kcal/mol. The source of this difference is found in the distance between the dimers and the size of the adsorbed ALM molecule. The Si–Si distance between dimers is 5.3 Å for the bare surface 5.3 Å for the surface with the bridging linear adsorbate and 5.1 Å for the branched bridging adsorbate. The linear adsorbate fits well in the inter-dimer distance with a length of 4.2 Å from the carbon to the sulfur in a direct line. The branched adsorbate is shorter by one carbon-carbon bond length inducing strain in the system. The branched ALM closer induces strain in the surface silicon dimer increasing the intradimer distance from 2.48 Å (linear) to 2.54 Å (branched). The surface bonds are strong allowing for some deformation without breaking. To test if the strain in the system is principally responsible for the differences between the linear and branched reactions, the constraints on the third and lower layer atoms were removed. Interestingly, the branched reaction barriers for hydrogen transfer and abstraction shift down by ~9 kcal/mol, and are within 2 kcal/mol of the corresponding values for the linear reactions. This test shows the differences are due to the strain induced by the shorter branched molecule. However, the geometry of the cluster is unphysically deformed after the constraints are removed showing the decrease in energy is too great. Using intermediate constraints, we estimate that the true energy of the hydrogen transfer and elimination is likely 2-3 kcal/mol lower. Calculations using larger structures are ongoing to determine the accurate value of the strain induced by the branched structure.

Considering the energetics of the entire reaction pathways of the branched and linear mechanisms in figure 2.3.2, there are two possible conclusions. The rate determining steps are either the hydrogen shift following deposition (linear) or the hydrogen transfer and abstraction (branched). Between the two reactions the hydrogen shift following deposition for the linear structure is slightly higher by 0.7 kcal/mol over the hydrogen transfer and abstraction of the branched pathway. Since the hydrogen transfer and abstraction energies are likely to be too high due to our constraints, we believe they the difference should be in the range of 3-4 kcal/mol. From this evidence, we can conclude that the branched reaction path would be the more likely pathway. If we have overestimated the effects of the strain and the barriers are much closer, it is possible both branched and linear structures can form.

Finally, we note that our proposed mechanism differentiates between the reactions of ALM and trimethylene sulfide on the H/Si(100)-2×1 surface. Experimentally,[25] it is known that while ALM reacts exclusively across dimer rows, trimethylene sulfide reacts via a square wave pattern. Some of the previously proposed mechanisms[49, 50] for ALM and trimethylene sulfide reacting with the H/Si(100)-2×1 surface go through a common intermediate (linear sulfur radical). One would expect the common intermediates to lead to the same product formation, in conflict with the experimental observations. In our mechanism, the pathways do not share common intermediates and would be expected to react differently. We plan to pursue a more detailed study of such reactions along with those of other reactive molecules in the future.

Conclusions

We have explored the reaction paths of ALM reacting across dimer rows, calculating the entire reaction paths with well-characterized transition states. We have calculated the formation of the product via intra-dimer hydrogen migration starting from a branched adsorbate, as well as the formation of the inter-dimer bridge with hydrogen elimination starting from either a branched or linear adsorbate. We have ruled out the possibility of intra-dimer hydrogen migration. From our reaction profiles it is possible the products formed are branched bridged structures, or a combination of branched and linear bridged structures. Our proposed reaction pathway differentiates between ALM and trimethylene sulfide on the Si(100)-2×1 surface since the pathways do not have common intermediates.

2.4 Line Growth Perpendicular to ALM Lines on Si(100) Surface

A promising research direction to circumvent the future limitations of silicon-based devices is the direct functionalization of surfaces to create molecular-scale devices.[10, 40, 44-47, 49-58, 60-66, 71-74] A small number of molecules (possibly a single molecule) could be used to form a nanoscale device. Some of the fundamental work geared towards this goal has been focused on the chemistry of organic molecules with silicon surfaces. While there is still much work to be done in this area, some initial progress has been achieved by exploiting the surface chemistry of organic molecules to form nanoscale patterns on the silicon surface.[2, 7-9, 12, 16, 39, 41-43, 75]

The nascent field of silicon surface nanopatterning has many unanswered questions. One of the most difficult questions is how to make complex patterns. Some of the techniques used to functionalize silicon have been the Grignard reaction,[2, 71, 76] reactions at defect sites[44, 45, 49-56, 61, 65, 66, 71] and dehydrative cyclocondensation reactions.[28] Reactions at defect sites offer a powerful strategy for exploring the science of functionalization, particularly the reaction of olefins or carboxyl groups with surface dangling bonds. This technique was first discovered by Lopinski et al. for the reaction of styrene on Si(100) surfaces.[29] The dangling bonds may be the result of incomplete hydrogen-passivation of the surface or may be created on the surface by a Scanning Tunneling Microscope (STM) tip. The chemistry for this class of reactions follows a chain reaction-type mechanism; a surface silicon radical reacts with a carbon-carbon or oxygen-carbon double bond to create a silicon-carbon[40, 46, 47, 50, 51, 53, 56, 58, 72] or a silicon-oxygen bond[52, 53, 55, 57] between the molecule and the surface, this shifts the radical site to the adsorbed molecule that then reacts with an adjacent surface silicon, shifting the

radical back to the surface. This chemistry has been shown to occur with a number of molecules and also demonstrated not to occur for other related molecules.

These molecular scale lines are envisioned to act as interconnects for nanoscale devices. In some cases, e.g., styrene, a line of adsorbed molecules acts as a wire while in other cases, i.e., long-chain alkanes, further modification would be required.[30] To make interconnects on a surface, predictable growth in at least two distinct directions is required. The directional anisotropy of the Si(100)-2×1 surface makes this possible.[40, 45, 50, 52-55, 58, 59, 61, 66, 71] Most molecules, e.g., styrene and acetone, grow preferentially "along" dimer rows on the of the Si(100)-2×1 surface.[40, 50, 52-55, 58, 59, 66] A few molecules are known to grow "across" dimer rows including allylic mercaptan (ALM) and acetophenone;[45, 50, 54, 55, 61, 71] of these only ALM grows *exclusively* across dimer rows. The mechanism for growth of molecules along dimer rows has been well-established.[31] For across dimer growth several initial mechanisms have been proposed with our proposed mechanism explaining the key experimental observations.[45, 61, 71] This mechanism proposes that the initial reaction of ALM occurs to form a primary carbon radical and results in a bridged structure across dimer rows linked by a silicon-sulfur bond, figure 2.4.1 a. The formation of a primary carbon radical was first proposed by Pei et al.[26] Our proposed bridged product is similar to one suggested previously by Choi and Cho though some of the details are different (branched in our model vs. linear in their model).[24] One point that is not fully understood in our previous work is if the branched ALM adsorbates would be too strained to form a line on the surface. An alternate possibility would be a line of branched ALMs interspersed with linear ALMs to relieve the strain. If this were the case we would expect ALM lines composed of both branched

and linear bridging ALM molecules. This consideration leaves open the possibility that the terminating ALM molecule could be either branched or linear.

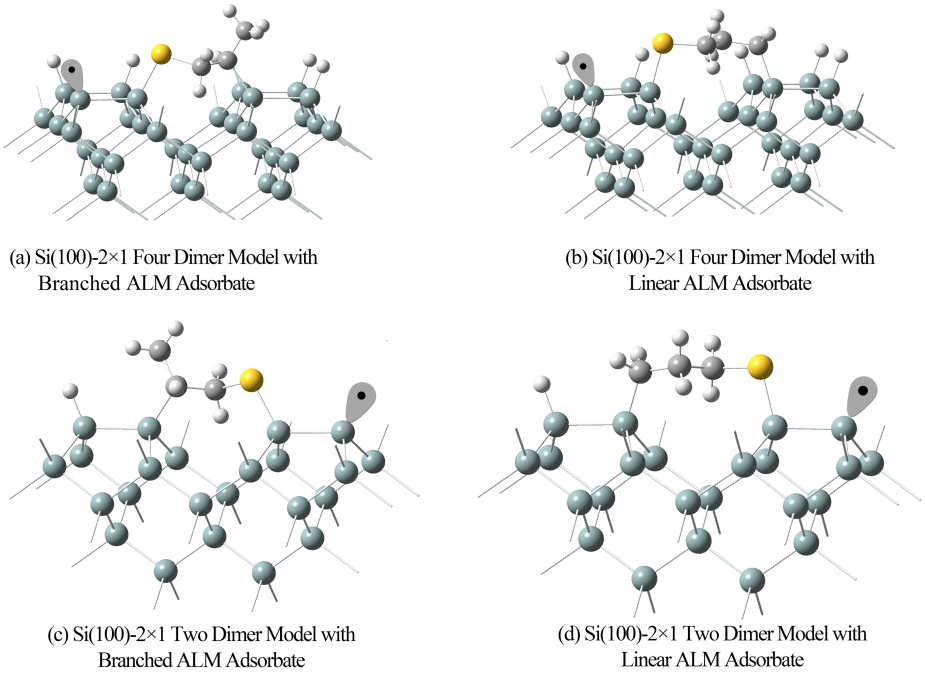

Figure 2.4.1. The models used in this study containing four surface dimers (top) and two surface dimers (bottom). Branched ALM adsorbates (a) and (c) are shown on the left and linear ALM adsorbates (b) and (d) are shown on the right. The light blue spheres represent silicon, the small white spheres represent hydrogen, the gray spheres represent carbon, and the yellow spheres represent sulfur. Radicals are shown with grey orbitals containing black dots.

Another important problem is the reactivity of dangling bonds on the surface. At the terminal site of such a chain reaction, dangling bonds still exist.[46, 48, 49, 53, 59, 63] At the end of styrene lines these radicals can result in reverse reactions effectively "unzipping" the line from the surface.[32] Radicals at the end of ALM lines have been shown to react

with acetone and grow a line perpendicular to the ALM line but not with styrene or dimethylstyrene (DMS). Interestingly, an interaction is observed between dimethylstyrene (DMS) and the silicon radical at the end of the ALM line but no subsequent line growth is observed.[50, 51, 56]

From these observations we would like to consider two important questions. Both concern the reactivity of the dangling bond at the terminal point of an ALM line on the Si(100)-2×1 surface. The first question that we address is how the initial reactivity of a second ALM molecule affected by the first ALM on the surface. The second question is why it is possible to grow acetone but not styrene at the end of an ALM line. To answer these questions we have examined the reactivity of ALM, acetone and styrene at the terminal dangling bond site with an adjacent ALM adsorbate. The reaction mechanisms for the initial reaction of ALM on the Si(100)-2×1 surface have been proposed by several groups but not yet verified.[21, 24, 26, 33] For reactions occurring at the terminal site of the ALM line there are two possible starting points, the branched or the linear ALM adsorbate, figure 2.4.1. Since the efficacy of the initial mechanism has not yet been determined and it is possible that linear ALMs may exist within a line of branched ALMs we have examined the reactions for both branched and linear structures.

Computational Details

The structure of the Si(100)-2×1 surface is well-known.[34] The 2×1 reconstruction gives a series of dimer rows separated by troughs, figure 2.4.1. To model this surface we have used several clusters. The critical points of the reactions pathway reactions (true minima and transition states) of ALM with the Si(100)-2×1 surface requires a $Si_{23}H_{27}$ cluster model containing two surface dimers, figure 2.4.1. This smaller model is possible

since the deposition and rearrangement reactions (*vide infra*) do not occur along the dimer rows. For the acetone and styrene reactions on the surface we use the larger $Si_{35}H_{32}$ model, figure 2.4.1. This model contains four dimers which is large enough to model the hydrogen abstraction along dimer rows. Cluster models similar to these have been used in the past and were reliable for a variety of different chemistries. When constructing cluster models the truncated bonds are terminated with hydrogen. To mimic the extended surface and to avoid unphysical relaxation, hydrogen atoms below the second layer and silicons below the third layer are frozen in their ideal crystal positions during optimization in accordance with well-established procedure.[14] In order to reduce the forces from proximate hydrogens a fifth layer of silicon was added to the two-dimer model. The fifth layer was not added to the four-dimer model to because the benefit of avoiding proximate hydrogens was outweighed by the increase in computational cost of adding more heavy atoms to the cluster.

To maintain computational tractability with accuracy we have used hybrid density functional theory with Becke's three-parameter exchange functional along with the Lee-Yang-Parr correlation functional (B3LYP). While deficiencies have been noted with hydrogen abstractions the performance for systems of this type (hydrogen abstraction via a carbon or oxygen radical) has been sufficient. The basis set used in our model chemistry is the Pople-style double-ζ basis set with polarization functions on all the hydrogen and heavy atoms. This gives an overall model chemistry of B3LYP/6-31G(d,p).[16, 35-37] Transition states and minima were characterized using analytic second derivatives. Calculations were performed using the Gaussian suite of programs.[17]

Results and Discussion

First we compare and contrast reactions of ALM at radical sites on the hydrogen-passivated surface to those on surfaces containing branched and linear ALM adsorbates. The reaction of the first ALM across the silicon dimer bond creates a bridge with a silicon-sulfur bond, figure 2.4.1 a and 2.4.1 c. The largest change after forming the bridged structure involves the silicon dimer bond distance. The silicon dimer bond of the passivated surface is 2.47 Å and the distance between dimers is 5.32 Å (surface containing a single radical). After the reaction of ALM forming a liner structure, the silicon dimer distance is increased slightly (at the dimer forming the silicon-carbon bond) to 2.48 Å and the distance between dimers is reduced slightly by 0.01 Å. A branched ALM adsorbate is a much larger perturbation to the bond distances with silicon dimer distance of 2.53 Å and a interdimer distance of 5.05 Å (difference of 0.27 Å from reference). It is clear that part of the strain caused by the shorter branched structure merely extends the dimer bonds and would not be expected to cause significant buckling of the surface as previously thought.[33]

Several of the reaction paths for a second ALM molecule reacting on the Si(100)-2×1 surface starting from the surface with an adsorbed ALM are shown in figure 2.4.2. There are four possible reaction pathways for the second ALM: reaction at a linear ALM adsorbate site to form either a branched or linear ALM adsorbate (linear-linear and linear-branched) or reaction at a branched ALM site to create either a linear or branched ALM adsorbate (branched-linear and branched-branched). The proposed reaction sequence closely follows the previously established mechanism.[31] We have calculated the initial reaction steps up to the formation of the sulfur radical. The reaction proceeds by

the interaction of the olefin functional group with the surface radical to form a carbon radical on the ALM and a carbon-silicon bond. The carbon radical can then rearrange to form a sulfur radical which subsequently reacts with the adjacent dimer. The reactions following the sulfur radical formation require much larger models that we plan to investigate in the future.

As can be seen from the reaction profiles in figure 2.4.2, the radical formation at either the linear or branched adsorbate is little perturbed by the presence of the initial ALM molecule. The largest variance of the reactions between surfaces with adsorbates and those without is the initial deposition barrier. This could be expected since the largest perturbation to the structure is to the length of the dimer bonds. The smallest differences in deposition energy are for the linear-linear and branched-linear reactions. These are within 1–2 kcal/mol of the deposition without an adsorbate. Since the bonds are very slightly perturbed for the linear adsorbate we would not expect to see a significant difference. The reactions at branched sites have slightly more variance but are not significantly different from the reactions without ALM adsorbates. From these results several inferences can be made. The adsorbed ALM does not significantly stabilize the adsorption of a second ALM. While it is possible that there may be an effect with longer lines, studies with larger models are needed to explore this. The strain induced by a branched adsorbate does not significantly destabilize the initial deposition of a second molecule.

The reactions of styrene and acetone with radical sites on the Si(100)-2×1 have been extensively studied.[21, 29, 31, 38-40] These molecules are known to react at defect sites on the hydrogen passivated Si(100)-2×1 surface but only acetone reacts at the end of

ALM lines on the Si(100)-2×1 surface. The reaction of styrene follows a pathway where the initial reaction is the loss of a double bond and formation of a silicon-carbon bond. The carbon radical then abstracts a hydrogen from a site along the dimer row to create a silicon surface-radical. Acetone contains no olefin group; therefore it reacts through the carbon-oxygen double bond to form a silicon-oxygen bond and a carbon radical. The radical can then abstract a hydrogen from a neighboring dimer; as is the case with styrene only along dimer growth has been observed.[32, 41-43]

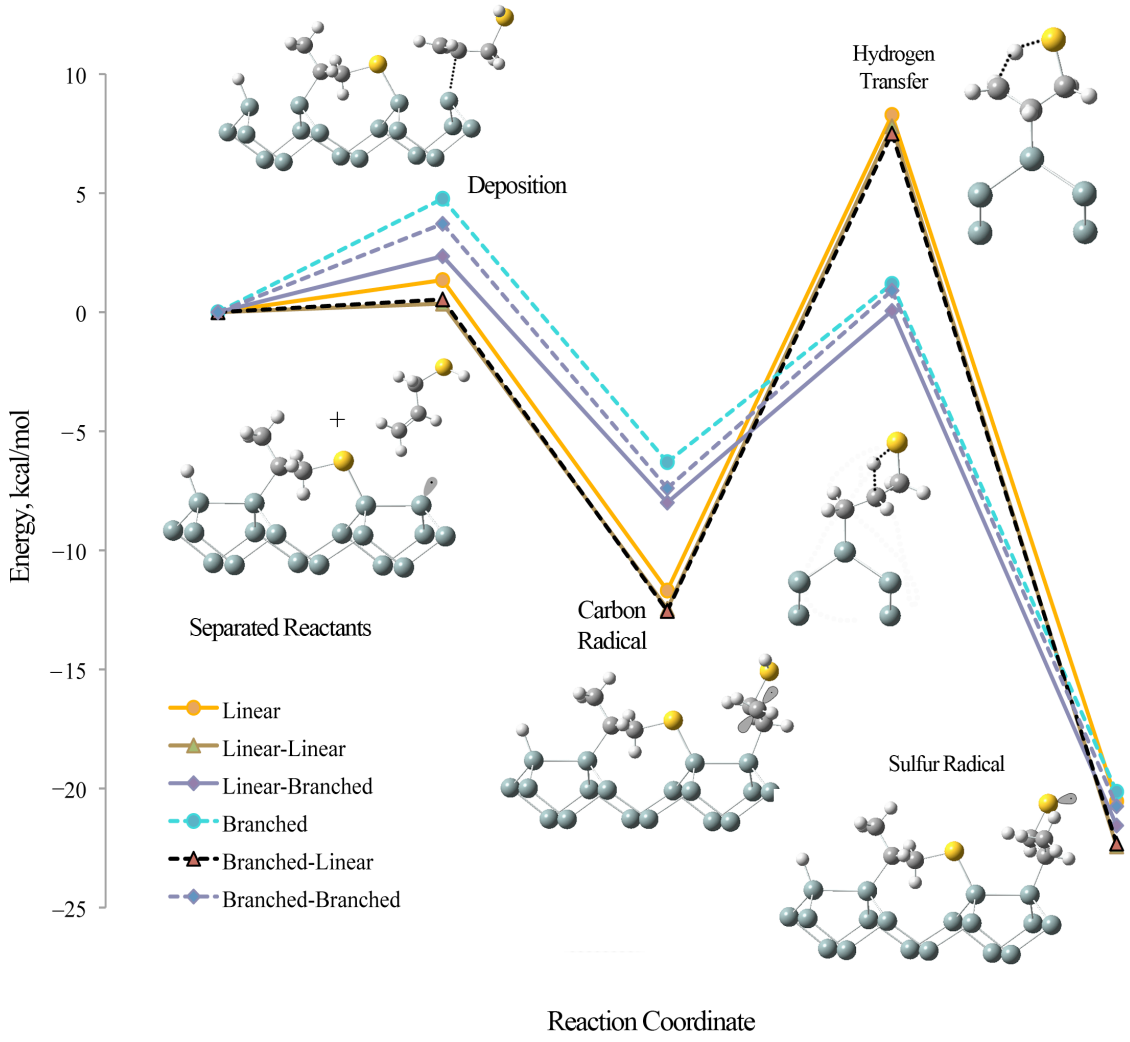

Figure 2.4.2. Reaction coordinate of a second ALM reacting on the Si(100)-2×1 surface. Only the reaction path of an ALM forming a branched adsorbate reacting next to a branched adsorbate is shown with the exception of the hydrogen transfer step that is shown for both branched and linear adsorbate reactions. Lower layer hydrogen and silicon atoms omitted for clarity. The light blue spheres represent silicon, the small white spheres represent hydrogen, the gray spheres represent carbon, and the yellow spheres represent sulfur. Radicals are shown with grey orbitals containing black dots, and black dotted lines are bonds breaking and forming during a reaction.

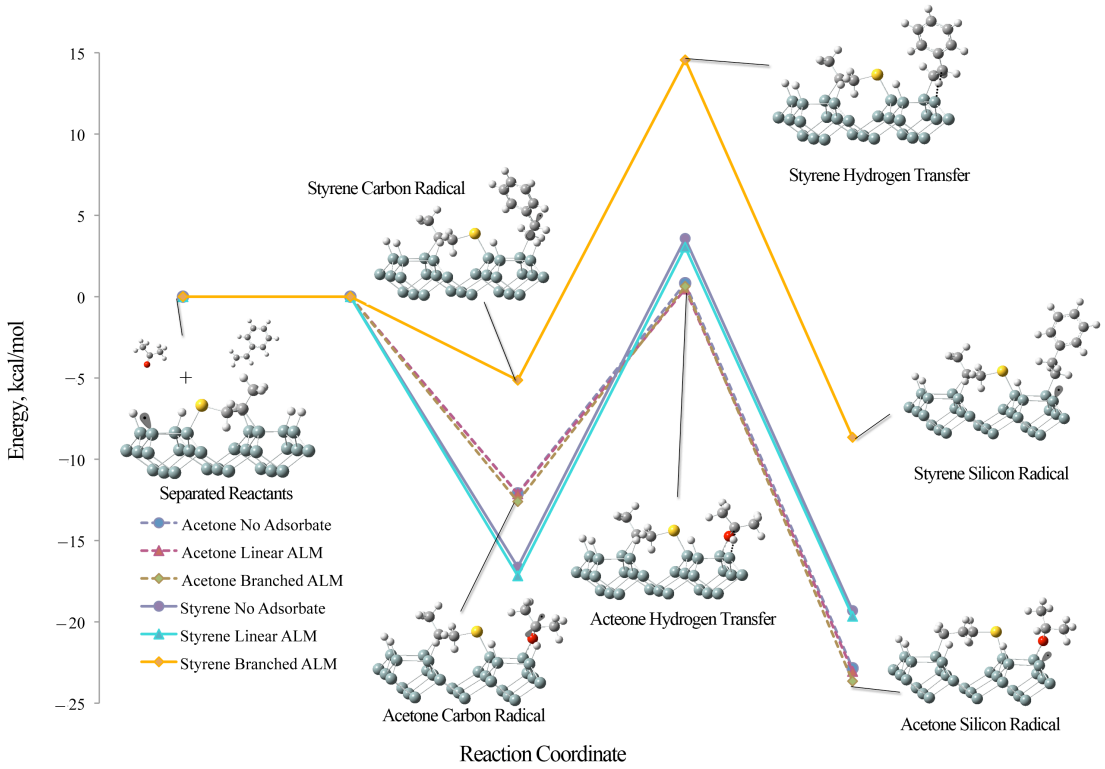

Figure 2.4.3. Reaction coordinate of styrene and acetone reacting on the Si(100)-2×1 surface at the end of an ALM line. Only some of the structures are shown, i.e., the acetone and styrene products with the branched ALM adsorbate. Reactions and structures with linear ALM are analogous. Lower layer hydrogen and silicon atoms omitted for clarity. The light blue spheres represent silicon, the small white spheres represent hydrogen, the gray spheres represent carbon, and the yellow spheres represent sulfur. Radicals are shown with grey orbitals containing black dots, and black dotted lines are bonds breaking and forming during a reaction.

As can be seen in figure 2.4.3, the reaction of styrene is affected by the adjacent ALM molecule for branched ALM but not for linear ALM. Acetone is unaffected by adjacent adsorbates. This provides an interesting explanation for the experimental

observations of styrene versus acetone growth at the end of ALM lines on the Si(100)-2×1 surface.[38] The growth of acetone lines is the same since the electronic and structural perturbation of the ALM does not affect the stability of subsequent abstraction. From these results one would predict styrene may adsorb to the surface but would be much more likely to desorb rather than to undergo a hydrogen abstraction reaction if it is adjacent to a branched ALM. If the terminal ALM is linear then styrene would react almost as if no ALM were present. STM observations show an interaction of styrene with the end of an ALM line (formation of an "S" feature) but no line growth.[38] These calculations along with the STM observation support our proposal of a branched bridging ALM adsorbate at the end of an ALM line. With these results it is not possible to rule out interspersed linear bridging adsorbates. It can be concluded that these would be as reactive as a silicon radical on the hydrogen-passivated surface with styrene.

It has been shown previously that the reactivity of styrene is controlled by the stability of the adsorbed molecule.[31] This conclusion is based on the low barrier to adsorption. In fact, the barrier for the reaction of the carbon-carbon and carbon-oxygen double bonds with the silicon radical is, in most instances, a few kcal/mol.[44, 45] The relative energies of the forward and reverse reaction barriers is the most important factor in determining line growth on the Si(100)-2×1. The highest barrier for acetone and styrene is the hydrogen abstraction along the dimers rows. Acetone adsorbates with the silicon radical of the hydrogen-passivated surface are less stable than the corresponding styrene adsorbates by ~4 kcal/mol, but have a very low overall barrier to reaction, < 1 kcal/mol. A possible source of this reactivity is due to the weakly stabilizing effect of the electronegative oxygen next to the carbon radical. Moreover, the oxygen does not

significantly destabilize the transition state for hydrogen abstraction. These factors are relatively unaffected by the partially broken silicon dimer bond on the branched ALM adsorbate. Styrene radicals, on the other hand, are stabilized on the surface by radical delocalization through the phenyl ring and through hyperconjugation of the radical with the surface silicon. This is unaffected by the linear ALM adsorbate which changes the silicon dimer only slightly. However, the stability of the adsorbed styrene is significantly affected by the adjacent branched ALM on the surface by ~10 kcal/mol. The source of the destabilization is the partially broken silicon dimer bond. A similar effect may be present for other carbon-carbon double bonds reacting at a radical site with the same chemistry, i.e., carbon radical formation with immediate hydrogen abstraction. This is not the case for the reaction of a second ALM since it rearranges to form the sulfur radical before hydrogen abstraction.

We have calculated the reaction pathways of ALM, styrene and acetone at the radical site adjacent to a bridging ALM on the Si(100)-2×1 surface. Our results indicate that the reactivity of ALM and acetone are unchanged when reacting with a silicon radical adjacent to an ALM adsorbate. Styrene reactivity is affected only if the terminal ALM is a branched adsorbate. In this case the styrene is destabilized by ~10 kcal/mol and would not be expected to undergo further reaction. This final observation is in accordance with the experimental observation that styrene interacts with the radical at the end of an ALM line but does not form a molecule line. Acetone and ALM will react at the radical site at a rate similar to that observed without the ALM adsorbate.

2.5 Oxidation and Nitridation of Si(100) Surface

Silicon interfaces including the Si/SiO_2 and Si/Si_3N_4 are an important area of research.[6, 8, 46-58] These materials have been studied due to their use as gate dielectric layers for microelectronics devices such as the field-effect transistors. Newer hafnium based materials have shown to be more suitable properties as dielectrics[59] for microelectronics devices. Research on these interfaces is important from two perspectives: first after the limits of the current silicon paradigm are reached[1-3] future devices are still likely to be built upon silicon giving both silicon and silicon interfaces continuing technological importance; and second the large body of knowledge for silicon makes it a very interesting system for fundamental surface science research.

Controlled fabrication of ultrathin layers of silicon oxide or silicon nitride is an interesting starting point for surface functionalization. In order to form these layers it is necessary to have very precise control over oxygen or nitrogen layer formation. A well-ordered surface can be expected to have much more stable and reproducible properties than a disordered surface. While direct exposure of silicon to atmospheric oxygen rapidly forms an oxide layer,[4] controlled oxide layer growth may be possible using different chemistries.

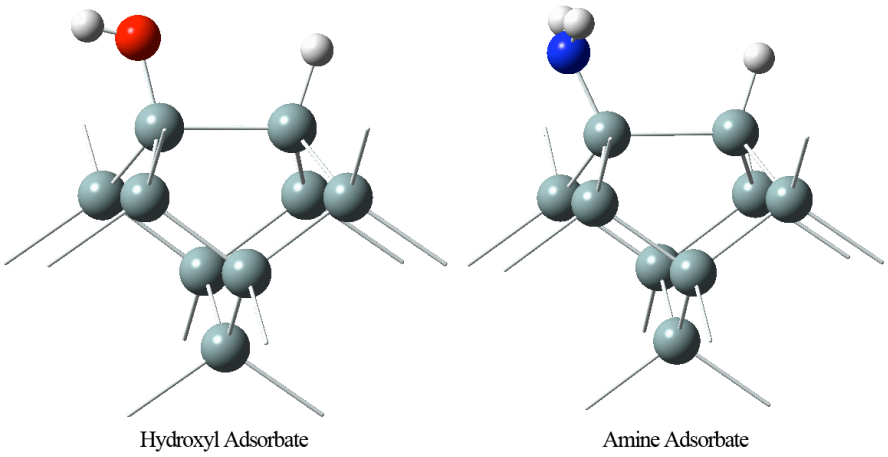

Figure 2.5.1. Si_9H_{12} clusters shown with the dissociation products of wet-oxidation (left) with a hydroxide and silicon dimer monohydride or amination (right) with an amine group and a silicon dimer monohydride. The color key is grey-blue atoms silicon, white atoms are hydrogen, red atom is oxygen and dark blue atom is nitrogen. Termination hydrogens are omitted for clarity.

A potential first step in controlled oxidation or amination could be to expose the bare Si(100)-2×1 surface to small amounts of water or ammonia in ultra-high vacuum. These molecules are known to dissociatively chemisorb on the surface to form the structures seen in figure 2.5.1.[9, 60] The surface hydroxide and amine groups can then be induced to insert into the surface forming an ultrathin layer. As shown in figure 2.5.2, on the Si(100)-2×1 surface it is possible to insert into either the dimer bond or the silicon-silicon backbond. Insertion into the dimer bond is unique and creates the most ordered surface. Insertion into the backbond results in the possibility of more complex processes such as multiple adsorbate-insertions on a single dimer and no insertion on other dimers.

Such a surface is expected to be significantly more disordered. It is therefore much more desirable to induce preferential insertion into the dimer bond.

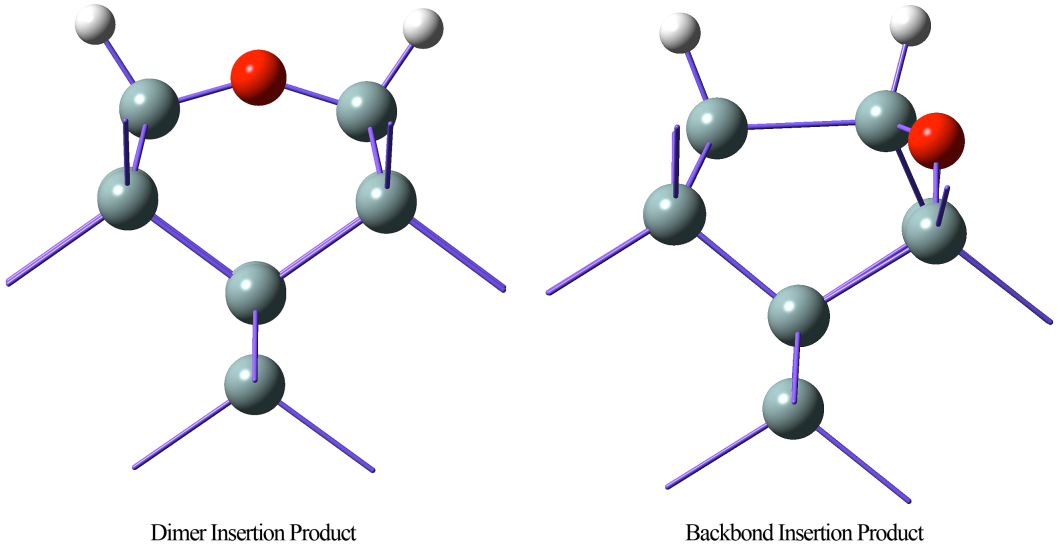

Figure 2.5.2. Products of oxygen insertion into the dimer bond (left) and backbond (right). Structures for nitrogen are analogous except for one additional hydrogen on the nitrogen.

A possible way of inducing insertion starting from the structures in figure 2.5.1 is thermal annealing.[58] The results of these experiments show non-selective insertion into the silicon surface to form disordered structures. Therefore, thermal annealing of wet-oxidized silicon gives an inhomogenous surface which is not ideal for forming ultrathin oxide layers.[58] Another means for forming ultrathin oxide layers is to use chemical control. This was accomplished by Weldon et al.[58] exposing the wet-oxidized Si(100)-2×1 surface to atomic hydrogen. The atomic hydrogen drives the reaction of the hydroxyl group with the silicon surface by creating radicals on the surface via hydrogen abstraction to create molecular hydrogen. Weldon et al.[58] used surface infrared spectroscopy to

characterize the atomic hydrogen-exposed surfaces. The results indicate a preference for dimer bond insertion over backbond insertion that yields a more well-ordered surface. This observation is significant and gives significant insight as to the possible mechanism. A proposed mechanism was the atomic hydrogen abstracts a hydrogen atom from the hydroxyl oxygen resulting in an oxygen radical that preferentially inserts into the dimer bond.[58] The formation of ultrathin nitrogen layers could potentially occur in a similar fashion. Ammonia is known to degrade in a manner similar to water on the Si(100)-2×1 surface. The resulting amine can then insert into the silicon surface. Previous studies by Widjaja and Musgrave indicate that the mechanism of thermal nitrogen insertion is more complicated than that of oxygen, requiring hydrogen diffusion and desorption to achieve insertion.[4, 6, 8, 61, 62] Exposure to atomic hydrogen may induce preferential insertion creating a more ordered surface in a manner similar to oxygen.

In order to fully exploit this pathway to ultrathin oxygen or nitrogen layers it is necessary to fully understand the reaction of atomic hydrogen with the hydroxide, amine and monohydride silicon and the subsequent chemistry of the resulting radicals. In order to model this chemistry we must first develop a method for effectively modeling the most significant steps in these reaction paths, viz. the hydrogen abstraction reactions. It is well known that popular density functionals tend to give very poor results even for the simplest hydrogen abstraction reaction, i.e., the $H_2 + H\cdot$ reaction.[63] In particular, this problem has been observed with one of the most popular of density functionals, B3LYP. The origin of the poor barrier heights is attributed to the presence of self-interaction error (SIE). This problem comes from the improper treatment of electronic exchange (and correlation) in approximate density functionals.[63]

There have been many attempts to overcome this problem such as the method of Perdew and Zunger[64] and an improvement on the Perdew-Zunger self-interaction correction by scaling techniques.[65] Recently new classes of functionals have been developed that attempt to systematically correct the known failings of density functionals including SIE. An example is the M06 class of functionals of Zhao and Truhlar.[43, 66, 67] These are general purpose functionals which have been shown to decrease the errors from SIE and correct barrier heights in addition to fixing several other known deficiencies.[68] Specifically we have tested the M06 functional to determine how well it reproduces hydrogen abstraction reaction barriers for main group elements.

We have compared the radical abstraction reaction barrier heights from small molecules containing one heavy atom for the first three rows of groups 14-17, with the exception of fluorine, using model chemistries M06, B3LYP and CCSD(T)//MP2 using identical basis sets. Our goal is not to perform an exhaustive search of many functionals to get heroically correct results but instead to discover an efficient practical method for obtaining reliable results that can then be applied for more complex surface reactions. While some of the reactions investigated are part of the training set used to parameterize of M06, many others are not. We also compared abstractions from some silicon cluster models to represent surfaces to ensure consistency of our results from small molecules to clusters. The M06 functional was then used to characterize the reactions of atomic hydrogen with the functionalized Si(100)-2×1 surface and to model its subsequent reactivity.

Computational Details

To maintain computational efficiency and calculate all models at the same level of theory we have used small cluster models in our study to represent the silicon surface. The Si_9H_{12} model is representative of an excised silicon dimer from the Si(100)-2×1 surface and is the smallest unit which accurately reproduces the surface. Dangling bonds at excision points were capped with hydrogens in accordance with well-established procedure.[14] To avoid unphysical relaxations the third and fourth layer silicon and hydrogens were constrained.[14]

The reaction energetics were determined using two density functionals; the popular B3LYP functional composed of the B88 electron exchange functional and the Lee-Yang-Parr correlation functional[35-37], and the general purpose M06 functional of Zhao and Truhlar.[43, 67, 68] As is customary, transition states and minima were verified with second derivative calculations. To calibrate the models, we performed geometry optimizations of the minima and transition states using second-order Møller–Plesset perturbation theory, MP2.[13] and then performed single point CCSD(T)[69] (coupled-cluster singles and doubles with perturbative triples corrections) calculations at these geometries. All calculations used the standard Pople-style polarized double-zeta 6-31G(d,p) basis set for the top two layers of atoms and the adsorbates while a smaller 6-31G basis set was used for the lower layer constrained atoms.[16] All calculations are corrected to include the effects of zero-point vibrations. Calculations were performed with a development version of the Gaussian suite of programs.[17]

Results and Discussion

Density Functional Comparison

Table 2.5.1. Errors for the hydrogen abstraction barrier of the reaction of atomic hydrogen with main group small molecules ($H_xX + H\bullet \rightarrow H_2 + \bullet XH_x$ with X=C, Si, Ge, N, P, As, O, S, Se, Cl and Br) for B3LYP and M06 density functionals compared to CCSD(T)//MP2 calculations.

	Activation Barrier Errors, kcal/mol	
Reaction	B3LYP	M06
$H\bullet + H_4C \rightarrow H_2 + \bullet CH_3$	8.80	4.84
$H\bullet + H_4Si \rightarrow H_2 + \bullet SiH_3$	6.83	2.96
$H\bullet + H_4Ge \rightarrow H_2 + \bullet GeH_3$	5.25	2.03
$H\bullet + H_3N \rightarrow H_2 + \bullet NH_2$	10.15	4.94
$H\bullet + H_3P \rightarrow H_2 + \bullet PH_2$	4.96	1.93
$H\bullet + H_3As \rightarrow H_2 + \bullet AsH_2$	3.70	1.50
$H\bullet + H_2O \rightarrow H_2 + \bullet OH$	10.73	4.07
$H\bullet + H_2S \rightarrow H_2 + \bullet SH$	5.74	2.30
$H\bullet + H_2Se \rightarrow H_2 + \bullet SeH$	4.36	1.49
$H\bullet + HCl \rightarrow H_2 + \bullet Cl$	7.25	3.18
$H\bullet + HBr \rightarrow H_2 + \bullet Br$	4.94	1.52
MAE	6.61	2.80

As is easily seen in table 2.5.1, there is a clear failure of B3LYP in predicting barrier heights for hydrogen abstraction reactions. The B3LYP activation barriers for the hydrogen abstraction are underestimated uniformly from 19.73 kcal/mol for the $H\bullet + H_2O$

$\rightarrow H_2 + \bullet OH$ reaction to 3.70 kcal/mol for the $H\bullet + H_3As \rightarrow H_2 + \bullet AsH_2$ reaction with a mean absolute deviation (MAD) for the entire test set of 6.61 kcal/mol when compared to CCSD(T)//MP2. The errors for three reactions involving carbon, nitrogen and oxygen are particularly large, while only bromine, selenium and arsenic are below 5 kcal/mol. Out of eleven reactions, B3LYP predicted five barriers below the starting reactants when zero-point corrections are included. While the barriers are slightly positive without zero-point corrections, the failure is evident. Several other barriers were near zero. These results show that B3LYP is clearly not an appropriate functional to use for these type of systems.

The M06 functional performs quite well for the reactions in this study. The MAD of 2.28 kcal/mol for the eleven main group hydrogen abstraction reactions that is 4.33 kcal/mol less than the error of the B3LYP model chemistry using the same basis set. The maximum error was 4.94 kcal/mol for the hydrogen abstraction from nitrogen (very close to the error of 4.84 kcal/mol for hydrogen abstraction from carbon). It is interesting to note that carbon is included in the training set (HTBH3838/04 database)[68] used to calibrate the M06 functional, though other reactions not part of the training set have better performance. The smallest errors in the hydrogen abstraction reactions are for the reactions with arsenic, selenium and bromine (1.50, 1.49 and 1.52 respectively). Most other reactions are within a few kcal/mol of these reactions. The absolute error decreases down a group, e.g., from a 4.84 kcal/mol error for carbon to 2.03 kcal/mol error for germanium. The barrier heights follow the same trend. The overall errors are excellent compared to B3LYP. The spread of underestimation is small with no outliers indicating the method is consistent from system to system. There is a slight increase in the error as a percentage of barrier height down a group. While the underestimation is significant, the

results are qualitatively correct, indicating it is possible to use M06 to understand the chemistry of hydrogen abstraction reactions for main group elements of small molecules.

Table 2.5.2. Benchmarking the cluster calculations against for B3LYP and MP2 against CCSD(T)//MP2 values for the hydrogen abstraction reactions and the insertion of the NH_2 group into the silicon backbond.

		CCSD(T)//MP2	M06	B3LYP
Pathway	**Reaction Coordinate**	**Relative Energy, kcal/mol**	**Relative Energy, kcal/mol**	**Relative Energy, kcal/mol**
Amine Hydrogen Abstraction	HSi–Si(H)N--H--H	16.19	10.35	5.96
Dimer Hydrogen Abstraction	H--H--Si–$SiNH_2$	4.79	2.77	0.00
Surface Radical/Backbond Insertion	•Si–Si–N(H_2)--Si + H_2	49.56	44.11	46.44

To test the use of M06 for silicon cluster models we have compared the results of CCSD(T)//MP2 to M06 for hydrogen abstraction reactions from nitrogen adsorbates and from silicon atoms both on the Si(100)-2×1 surface. The results in table 2.5.2 show good agreement with the small molecule calculations. The B3LYP error is still catastrophic with an underestimation of 10.23 kcal/mol compared to the reference calculation (compared to 10.15 kcal/mol for the small molecule). The error in the M06 hydrogen abstraction barrier from the amine functional group is 5.85 kcal/mol compared to 4.94 kcal/mol for the small molecule. These results also show a significant improvement over the B3LYP results. The silicon abstraction results are an interesting comparison since the barrier for hydrogen abstraction from silicon is much lower than for hydrogen abstraction

from nitrogen. The B3LYP gives a *barrier-less transition state* while the CCSD(T)//MP2 barrier height is 4.79 kcal/mol. The M06 barrier of 2.02 kcal/mol. While it might be reasonable to suggest a 3.5 kcal/mol (MAE for M06) additive correction factor to the barrier heights for hydrogen abstraction reactions, we have reported values for M06 in this study that are uncorrected.

If we examine the thermochemistry of the products, both B3LYP and M06 perform well without significant error. Barrier heights for reactions which do not involve hydrogen abstractions reactions are underestimated by a smaller percentage for both B3LYP and M06 with M06 performing very well compared to CCSD(T)//MP2. It is likely the errors for these systems would be reduced with larger basis set but our goal for this study was to determine the efficacy of the general purpose M06 functional with a reasonably compact basis set. All indications are that M06 gives excellent results, which are superior to B3LYP. The following discussion for the atomic hydrogen-induced oxidation and amination uses the M06 functional for all calculations.

B. Surface Reactions

The initial reactions to consider for the formation of ultrathin oxide or nitride layers on silicon are the hydrogen abstraction reactions. When considering the reactions of atomic hydrogen with the hydroxide- or amine-terminated silicon surface, the two possible reaction sites are: the hydrogen on the functional group and the hydrogen on the monohydride silicon of the dimer bond. They will lead to the formation of H_2 along with the creation of a radical on the functional group or silicon. While there are other silicon sites that would produce side reactions, they would not lead to insertion products. In this

work we restrict ourselves to explore the pathways leading to oxygen and nitrogen insertion products.

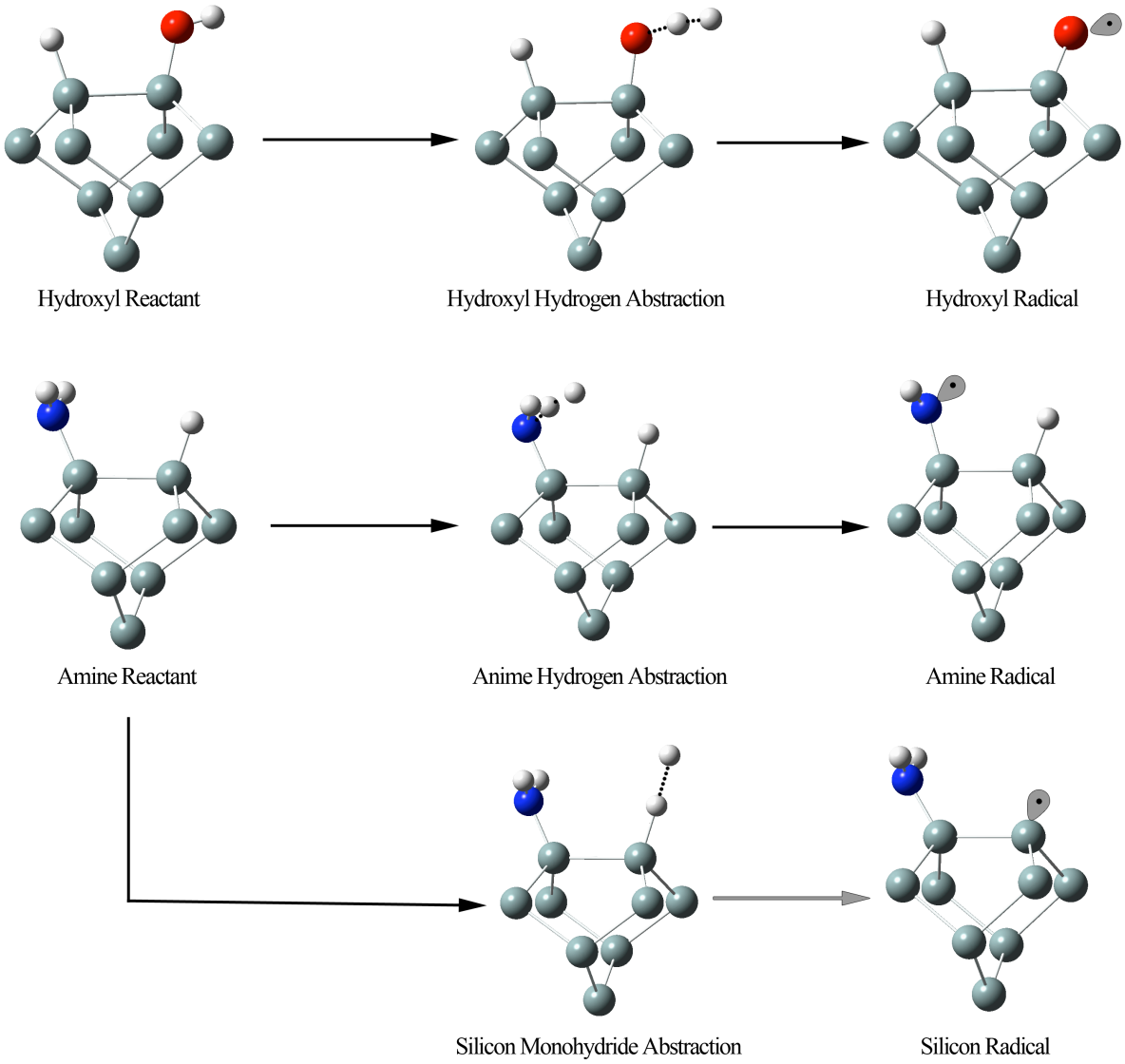

Figure 2.5.3. Initial hydrogen abstraction reactions for the reaction of atomic hydrogen with the wet-oxidized or aminated Si(100)-2×1 surface. The silicon monohydride abstraction is shown for the aminated surface only and analogous reaction exists for the wet-oxidized surface. See figure 2.5.1 for color key.

Table 2.5.3. The initial hydrogen abstraction reactions for the wet-oxidized and aminated Si(100)-2×1 surfaces.

Pathway	Coordinate	Relative Energy, kcal/mol
Hydroxyl Hydrogen Attack	HSi–SiOH + H	0.0
	HSi–SiO--H--H	11.9
	HSi–SiO• + H_2	0.3
Dimer Hydrogen Attack with Hydroxyl Group	HSi–SiOH + H•	0.0
	H--H--Si–SiOH	3.8
	•Si–SiOH + H_2	−20.8
Amine Hydrogen Attack	HSi–$SiNH_2$ + H•	0.0
	HSi–Si(H)N--H--H	10.4
	HSi–Si(H)N• + H_2	−9.4
Dimer Hydrogen Attack with Amine Group	HSi–$SiNH_2$ + H•	0.0
	H--H--Si–$SiNH_2$	2.8
	•Si–$SiNH_2$ + H_2	−21.7

Formation of the function group radical occurs via atomic hydrogen abstraction creating a nitrogen or oxygen radical, figure 2.5.3 and table 2.5.3. The atomic hydrogen interacts with a functional group breaking the hydrogen–oxygen or hydrogen–nitrogen bond and forming molecular hydrogen. The formation of the radical is exothermic

relative to the surface plus atomic hydrogen for the nitrogen radical and very slightly endothermic for the oxygen radical, ~0.3 kcal/mol. The source of the reduced stability in the oxygen radical is due to the stronger nature of the original O–H bond relative to the N–H bond. The oxygen radical seems to show a weak "double bond" as evidenced by the silicon–oxygen bond distance that decreases from 1.673 Å in the reactant to 1.603 Å in the oxygen radical product. The barrier for the abstraction from the adsorbate is 10.3 kcal/mol for the amine and 11.9 kcal/mol for oxygen.

The silicon radical is formed when the atomic hydrogen abstracts the hydrogen from the silicon dimer monohydride, figure 2.5.3. Silicon monohydride hydrogen abstraction is exothermic regardless of the adsorbate. The barriers to abstraction are slightly less for oxygen than nitrogen by 1 kcal/mol but both barriers are much smaller than the abstraction barriers of the functional groups. The differences are small relative to the functional group hydrogen abstractions. It is clear the silicon–hydrogen bond is much weaker than either the O–H or the N–H bonds. From these results we would expect the formation of a silicon radical at a much greater rate than functional group radical formation for both hydroxylated and aminated surfaces. However, we will explore the insertion reactions of functional group radicals for comparison with previous results.

Insertion of the oxygen radical into the Si(100)-2×1 surface has been studied previously.[53, 54, 70] The two possible pathways are the insertion of oxygen into the backbond or dimer bond on the silicon surface.[58] The thermodynamic stability of the oxygen inserted into the silicon dimer bond and the backbond on bare surfaces was explored in studies by Stevanov and Raghavachari[53, 54] and Teraishi et al.[70] These studies indicate the product of oxygen insertion into the dimer bond is more thermodynamically

favorable then insertion into the dimer backbond, ~ 14 kcal/mol and ~ 8 kcal/mol for Teraishi et al.[70] using semi-empirical methods, and Stevanov and Raghavachari using hybrid-density functional theory.[53, 54] This indicates that dimer insertion would be observed more than the backbond insertion if thermodynamic stability is the primary factor. Considering the reaction barriers allows us to make a definitive judgment on the nature of the reaction. We will first consider the oxygen radical reactions followed by the silicon radical reactions.

The reaction paths for the oxygen radical inserting into the dimer bond and the backbond to form bridging oxygen products are shown in figure 2.5.4 a (bottom) and table 2.5.4. Preferential insertion into the dimer bond was suggested in earlier work.[58] However, the energetics of insertion show almost identical barriers between dimer bond and backbond insertions, 22.5 kcal/mol and 22.6 kcal/mol, respectively. As noted earlier, insertion into the dimer bond is more exothermic (by ~5 kcal/mol, table 2.5.4) due to the lower strain induced by the bridging oxygen in the dimer bond. This reaction step leaves a radical on the silicon that could combine with a free atomic hydrogen to form the final oxygen-inserted product. Overall, the kinetics of the reaction suggests that the creation of an oxygen radical would be nonselective for subsequent insertion.

Table 2.5.4. The insertion reactions for functional group and surface radicals on the the-oxidized and aminated Si(100)-2×1 surfaces reacted after reaction with atomic hydrogen.

Pathway	**Coordinate**	**Relative Energy, kcal/mol**
Surface Radical Hydroxyl Dimer Insertion	•Si–SiOH + H_2	0.0
	•Si--O(H)Si + H_2	39.6
	•Si–O(H)Si + H_2	24.7
Surface Radical Hydroxyl Backbond Insertion	•Si–SiOH + H_2	0.0
	•Si–Si–O(H)--Si + H_2	45.7
	•Si–Si–O(H)–Si + H_2	38.7
Radical Hydroxyl Group Dimer Bond Insertion	HSi–SiO• + H_2	0.0
	HSi--O•Si + H_2	22.5
	Si–O–Si + H_2	−25.3
Radical Hydroxyl Group Backbond Insertion	HSi–SiO• + H_2	0.0
	HSi–Si–O•--Si + H_2	22.6
	HSi-Si(•)–O–Si + H_2	−20.0
Surface Radical Amine Dimer Insertion	•Si–$SiNH_2$ + H_2	0.0
	•Si--$N(H_2)$Si + H_2	43.8
	•Si–$N(H_2)$Si + H_2	27.1
Surface Radical Amine Backbond Insertion	•Si–$SiNH_2$ + H_2	0.0
	•Si–Si–$N(H_2)$--Si + H_2	44.1
	•Si–Si–$N(H_2)$–Si + H_2	31.4
Radical Amine Group Dimer Bond Insertion	HSi–Si(H)N• + H_2	0.0
	HSi--N•Si + H_2	10.5
	Si–N–Si + H_2	−27.8
Radical Amine Group Backbond Insertion	HSi–SiN• + H_2	0.0
	HSi–Si-N•--Si + H_2	18.1
	HSi–Si(•)–N–Si + H_2	−25.3

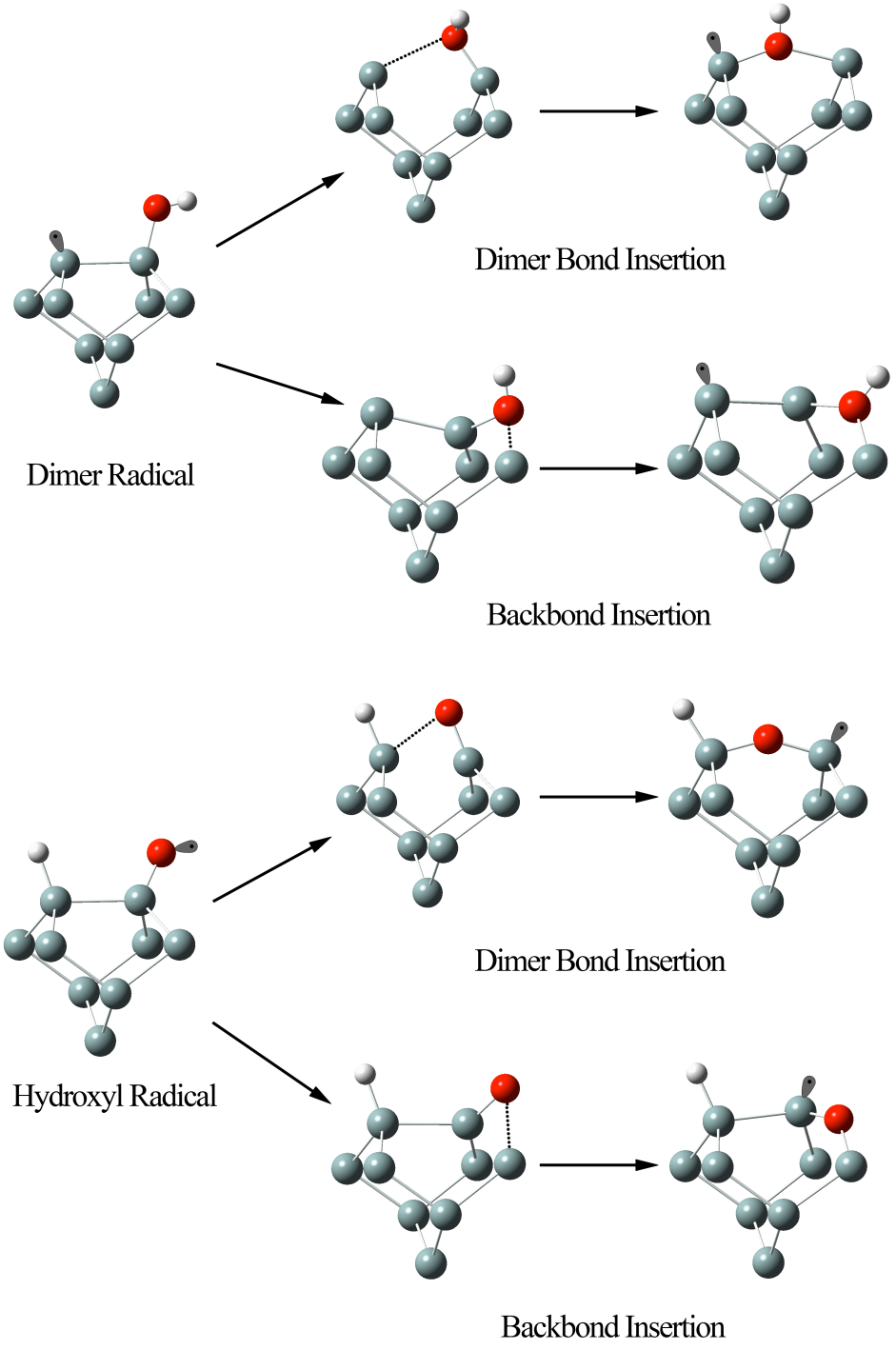
Dimer Bond Insertion
Dimer Radical
Backbond Insertion
Dimer Bond Insertion
Hydroxyl Radical
Backbond Insertion

(a)

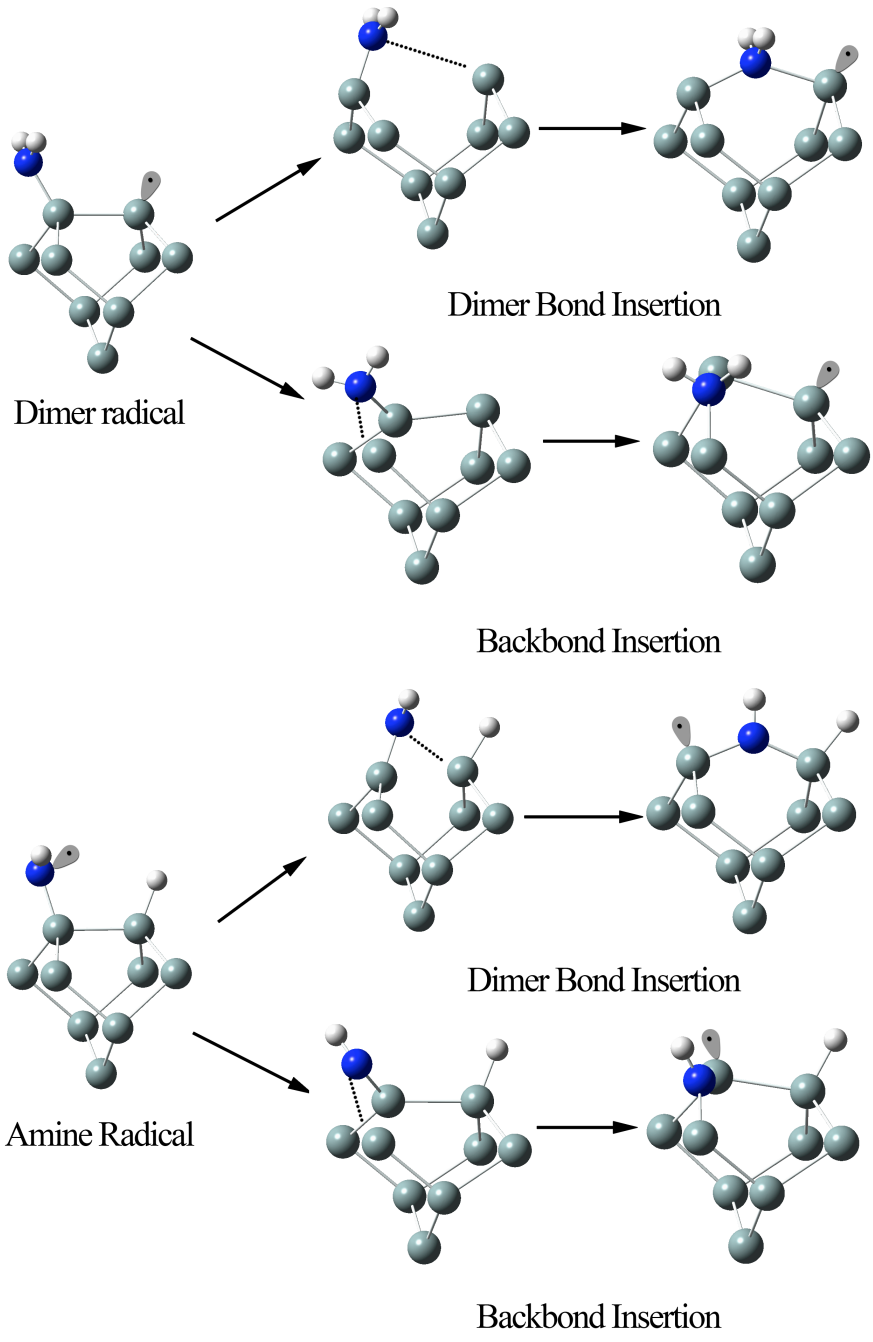

(b)

Figure 2.5.4. Oxygen radical and hydroxyl insertion reactions into the dimer bond or backbond (a). Amine radical and amine insertion reactions into the dimer bond and back bonds (b). Radical are only shown in the reactants and products. See figure 2.5.1 for color key.

If a silicon radical is created, it is possible for the hydroxyl group to insert into the dimer or backbonds, figure 2.5.4 a (top) and table 2.5.4. The insertion of the hydroxyl has a higher barrier, as expected. The hydroxyl inserts in the same manner as the oxygen radical except that the product is a three coordinate oxygen species. This transient species (intermediate) is not very stable and would be expected to react either quickly via hydrogen migration or molecular hydrogen elimination via a free atomic hydrogen to give a silicon radical that will be passivated by atomic hydrogen to yield the final product.[54] A key observation from our results (table 2.5.4) is that the calculated barrier for dimer insertion is 6.1 kcal/mol lower than for backbond insertion.[71] This difference would give a significant preference for more dimer-inserted products than backbond-inserted products.

In a previous computational study of thermally induced insertion of nitrogen starting from an aminated surface, it was found that the amine was much more likely to desorb from the surface rather than insert into either the dimer bond or backbond.[6] Insertion of the amine group into the dimer and backbond without creating any radical was a high barrier process that showed no selectivity of insertion into the backbond and the dimer bond.[6] In order for a reaction to occur, hydrogen desorption from the surface was suggested as an assisting step. Desorption of the silicon dimer hydrogen is equivalent to hydrogen abstraction of the silicon monohydride hydrogen.

The aminated surface provides the same types of hydrogen abstraction reactions as the hydroxylated surface. The nitrogen radical can insert into the dimer or backbond forming a nitrogen bridging species, figure 2.5.4 b (bottom). While there are several possible reactions for the nitrogen radical, we have restricted ourselves to reactions

analogous to those considered earlier for oxygen. The energetics of the reactions, table 2.5.4, shows a very significant difference between dimer bond and backbond insertion barrier with the dimer bond favored by 7.6 kcal/mol. The difference in energy is due to the steric hindrance of inserting into the backbond. The resulting structures are within 3 kcal/mol of one another. Thus, if the nitrogen radical is created, dimer insertion will dominate the reaction. After insertion the remaining dangling bonds will be passivated by free atomic hydrogen to yield the final products.

The silicon radical has opposite results. The barriers to insertion are not significantly different for dimer and backbond insertion, less than 1 kcal/mol with a slightly more stable backbond inserted product. Thus, if a silicon radical is created, nitrogen insertion will occur without preference for the dimer bond or backbond. If these results are compared to those of Widjaja and Musgrave, the barrier for amine insertion into the dimer bond with a silicon radial (44.04 kcal/mol using a different model chemistry, B3LYP with a larger basis set) is nearly identical to our results of 44.1 kcal/mol.[6] The resulting species is a quaternary amine that can lead to the final product by hydrogen migration followed by atomic hydrogen passivation. The insertion process itself is quite endothermic which may indicate a higher percentage of back reactions.

There is a large difference between the oxygen and nitrogen reactions with the surface. If the surface is hydroxylated, it has a preference for dimer insertion if a silicon radical is created. If the surface is aminated, it has a preference for dimer insertion if a nitrogen radical is created. Since it is most likely that silicon radicals will be formed on hydroxylated and aminated Si(100)-2×1 surfaces, the wet-oxidized surface will have a

strong preference for dimer bond insertion while the aminated surface will have no selectivity.

V. Conclusions

We have explored the use of atomic hydrogen to induce preferential insertion into the silicon dimer bond on the Si(100)-2×1 surface. To study the hydrogen abstraction reactions the broadly applicable M06 functional of Zhao and Truhlar[43, 66-68] was compared to the popular B3LYP functional for hydrogen abstraction reaction of main group elements and for silicon cluster models. In all cases the M06 functional performed consistently and was superior to B3LYP. Atomic hydrogen can abstract hydrogen from the functional group (hydroxide or amine) or from the dimer silicon monohydride. The silicon–hydrogen bond of the dimer monohydride is significantly weaker than the oxygen–hydrogen or nitrogen–hydrogen bonds indicating a silicon radical on the dimer is the most likely to form. The subsequent oxygen insertion is affected by the silicon radical that induces preferential insertion into the dimer bond. Insertion of the amine group is unaffected by the silicon radical and does not have an insertion preference. If the functional group radicals are formed the preference is reversed. The oxygen radical has no preference for insertion into either the dimer bond or backbond while amine radicals have a preference for the dimer bond. Our results suggest atomic hydrogen is possibly a viable method for inducing preferential oxygen insertion into the dimer bond to form ultrathin oxide layers but not for nitrogen insertion.

References

1. Bourianoff, G. I.; Gargini, P. A.; Nikonov, D. E., Research directions in beyond CMOS computing. *Solid-State Electron.* 2007, *51* (11-12), 1426-1431.

2. Jakubowski, A.; Lukasiak, L., CMOS evolution. Development limits. *Mater. Sci.* 2008, *26* (1), 5-20.

3. Zhirnov, V. V.; Cavin, R. K.; Hutchby, J. A.; Bourianoff, G. I., Limits to binary logic switch scaling - A Gedanken model. *PROCEEDINGS OF THE IEEE* 2003, *91* (11), 1934-1939.

4. Widjaja, Y.; Musgrave, C. B., Atomic layer deposition of hafnium oxide: A detailed reaction mechanism from first principles. *Journal of Chemical Physics* 2002, *117* (5), 1931-1934.

5. Widjaja, Y.; Musgrave, C. B., A density functional theory study of the nonlocal effects of NH3 adsorption and dissociation on Si(100)-(2 x 1). *Surf. Sci.* 2000, *469* (1), 9-20.

6. Widjaja, Y.; Musgrave, C. B., Ab initio study of the initial growth mechanism of silicon nitride on Si(100)-(2×1) using NH3. *Physical Review B (Condensed Matter and Materials Physics)* 2001, *64* (20), 205303/1-9.

7. Leftwich, T. R.; Madachik, M. R.; Teplyakov, A. V., Dehydrative Cyclocondensation Reactions on Hydrogen-Terminated Si(100) and Si(111): An ex Situ Tool for the Modification of Semiconductor Surfaces. *Journal of the American Chemical Society* 2008, *130* (48), 16216-16223.

8. Mui, C.; Wang, G. T.; Bent, S. F.; Musgrave, C. B., Reactions of methylamines at the Si(100)-2x1 surface. *Journal of Chemical Physics* 2001, *114* (22), 10170-10180.

9. Konecny, R.; Doren, D. J., Adsorption of water on Si(100)-(2x1): A study with density functional theory. *Journal of Chemical Physics* 1997, *106* (6), 2426-2435.

10. Cao, X. P.; Hamers, R. J., Formation of a surface-mediated donor-acceptor complex: Coadsorption of trimethylamine and boron trifluoride on the silicon (001) surface. *Journal of Physical Chemistry B* 2002, *106* (8), 1840-1842.

11. Jung, S. J.; Youn, Y. S.; Lee, H.; Kim, K. J.; Kim, B. S.; Kim, S., Cycloaddition on ge(100) of the Lewis acid AlCl3. *Journal of the American Chemical Society* 2008, *130* (11), 3288-+.

12. Aarset, K.; Shen, Q.; Thomassen, H.; Richardson, A. D.; Hedberg, K., Molecular structure of the aluminum halides, Al2Cl6, AlCl3, Al2Br6, AlBr3, and AlI3, obtained by gas-phase electron-diffraction and ab initio molecular orbital calculations. *Journal of Physical Chemistry A* 1999, *103* (11), 1644-1652.

13. Møller, C.; Plesset, M. S., Note on an Approximation Treatment for Many-Electron Systems. *Physical Review* 1934, *46* (7), 618.

14. Raghavachari, K.; Halls, M. D., Quantum chemical studies of semiconductor surface chemistry using cluster models. *Mol. Phys.* 2004, *102* (4), 381-393.

15. Leininger, M. L.; Allen, W. D.; Schaefer Iii, H. F.; Sherrill, C. D., Is M[o-slash]ller--Plesset perturbation theory a convergent ab initio method? *The Journal of Chemical Physics* 2000, *112* (21), 9213-9222.

16. Hariharan, P. C.; Pople, J. A., Influence of Polarization Functions on Molecular-Orbital Hydrogenation Energies. *Theor. Chim. Acta* 1973, *28* (3), 213-222.

17. M. J. Frisch, G. W. T., H. B. Schlegel, G. E. Scuseria, M. A. Robb, J. R. Cheeseman, J. A. Montgomery, Jr., T. Vreven, K. N. Kudin, J. C. Burant, J. M. Millam, S. S. Iyengar, J. Tomasi, V. Barone, B. Mennucci, M. Cossi, G. Scalmani, N. Rega, G. A. Petersson, H. Nakatsuji, M. Hada, M. Ehara, K. Toyota, R. Fukuda, J. Hasegawa, M. Ishida, T. Nakajima, Y. Honda, O. Kitao, H. Nakai, M. Klene, X. Li, J. E. Knox, H. P. Hratchian, J. B. Cross, V. Bakken, C. Adamo, J. Jaramillo, R. Gomperts, R. E. Stratmann, O. Yazyev, A. J. Austin, R. Cammi, C. Pomelli, J. W. Ochterski,; P. Y. Ayala, K. M., G. A. Voth, P. Salvador, J. J. Dannenberg, V. G. Zakrzewski, S. Dapprich, A. D. Daniels, M. C. Strain, O. Farkas, D. K. Malick, A. D. Rabuck, K. Raghavachari, J. B. Foresman, J. V. Ortiz, Q. Cui, A. G. Baboul, S. Clifford, J. Cioslowski, B. B. Stefanov, G. Liu, A. Liashenko, P. Piskorz, I. Komaromi, R. L. Martin, D. J. Fox, T. Keith, M. A. Al-Laham, C. Y. Peng, A. Nanayakkara, M. Challacombe, P. M. W. Gill, B. Johnson, W. Chen, M. W. Wong, C. Gonzalez, and J. A. Pople *Gaussian Development Version*, Revision E.05; Gaussian, Inc.: Wallingford CT, 2004.

18. Takahasi, M.; Nakatani, S.; Ito, Y.; Takahashi, T.; Zhang, X. W.; Ando, M., SURFACE X-RAY-DIFFRACTION STUDY ON THE SI(001)2X1 STRUCTURE. *Surf. Sci.* 1995, *338* (1-3), L846-L850.

19. Prayongpan, P.; Stripe, D. S.; Greenlief, C. M., Cycloaddition-like reactions at germanium (100) surfaces: Adsorption and reaction of 1,5-cyclooctadiene. *Surf. Sci.* 2008, *602* (2), 571-578.

20. Konecny, R.; Doren, D. J., Adsorption of BH3 on Si(100)-(2x1). *Journal of Physical Chemistry B* 1997, *101* (51), 10983-10985.

21. Hossain, M. Z.; Kato, H. S.; Kawai, M., Fabrication of interconnected 1D molecular lines along and across the dimer rows on the Si(100)-(2 x 1)-H surface through the radical chain reaction. *Journal of Physical Chemistry B* 2005, *109* (49), 23129-23133.

22. McNab, I. R.; Polanyi, J. C., Patterned atomic reaction at surfaces. *Chemical Reviews* 2006, *106* (10), 4321-4354.

23. Hossain, M. Z.; Kato, H. S.; Kawai, M., Controlled fabrication of 1D molecular lines across the dimer rows on the Si(100)-(2 x 1)-H surface through the radical chain reaction. *Journal of the American Chemical Society* 2005, *127* (43), 15030-1.

24. Choi, J. H.; Cho, J. H., Growth Mechanism of a 1D Molecular Line across the Dimer Rows on H-Terminated Si(001). *Physical Review Letters* 2009, *102* (16), 166102.

25. Dogel, S. A.; DiLabio, G. A.; Zikovsky, J.; Pitters, J. L.; Wolkow, R. A., Experimental and theoretical studies of trimethylene sulfide-derived nanostructures on p- and n-type h-silicon(100)-2 x 1. *Journal of Physical Chemistry C* 2007, *111* (32), 11965-11969.

26. Pei, Y.; Ma, J.; Zeng, X. C., Effects of Radical Site Location and Surface Doping on the Radical Chain-reaction on H-Si(100)-(2 x 1): A Density Functional Theory Study. *Journal of Physical Chemistry C* 2008, *112* (41), 16078-16086.

27. Steckel, J. A.; Phung, T.; Jordan, K. D.; Nachtigall, P., Concerted use of slab and cluster models in an ab initio study of hydrogen desorption from the Si(100) surface. *Journal of Physical Chemistry B* 2001, *105* (18), 4031-4038.

28. Leftwich, T. R.; Teplyakov, A. V., Chemical manipulation of multifunctional hydrocarbons on silicon surfaces. *Surface Science Reports* 2008, *63* (1), 1-71.

29. Lopinski, G.; Wayner, D.; Wolkow, R., Self-directed growth of molecular nanostructures on silicon. *Nature* 2000, *406*, 48-51.

30. Piva, P. G.; DiLabio, G. A.; Pitters, J. L.; Zikovsky, J.; Rezeq, M.; Dogel, S.; Hofer, W. A.; Wolkow, R. A., Field regulation of single-molecule conductivity by a charged surface atom. *Nature* 2005, *435*, 658-661.

31. Kang, J. K.; Musgrave, C. B., A quantum chemical study of the self-directed growth mechanism of styrene and propylene molecular nanowires on the silicon (100) 2X1 surface. *Journal of Chemical Physics* 2002, *116* (22), 9907-9913.

32. Hossain, M. Z.; Kato, H. S.; Kawai, M., Competing forward and reversed chain reactions in one-dimensional molecular line growth on the Si(100)-(2 x 1)-H surface. *Journal of the American Chemical Society* 2007, *129*, 3328-3332.

33. Ferguson, G. A.; Than, C. T. L.; Raghavachari, K., Line Growth on the H/Si(100)-2 x 1 Surface: Density Functional Study of Allylic Mercaptan Reaction Mechanisms. *Journal of Physical Chemistry C* 2009, *113* (43), 18817-18822.

34. Sze, S. M., *The Physics of Semiconductor Devices*. 2nd ed.; Wiley-Interscience: New York, 1981; p 880.

35. Becke, A. D., Density-Functional Exchange-Energy Approximation with Correct Asymptotic-Behavior. *Phys. Rev. A* 1988, *38* (6), 3098-3100.

36. Becke, A. D., Density-Functional Thermochemistry .3. the Role of Exact Exchange. *Journal of Chemical Physics* 1993, *98* (7), 5648-5652.

37. Lee, C. T.; Yang, W. T.; Parr, R. G., Development of the Colle-Salvetti Correlation-Energy Formula into a Functional of the Electron-Density. *Physical Review B* 1988, *37* (2), 785-789.

38. Hossain, M. Z.; Kato, H. S.; Kawai, M., Selective chain reaction of acetone leading to the successive growth of mutually perpendicular molecular lines on the Si(100)-(2x1)-H surface. *Journal of the American Chemical Society* 2007, *129*, 12304-12309.

39. Kirczenow, G.; Piva, P. G.; Wolkow, R. A., Linear chains of styrene and methylstyrene molecules and their heterojunctions on silicon: Theory and experiment. *Physical Review B* 2005, *72* (24).

40. Zikovsky, J.; Dogel, S. A.; Haider, A. B.; DiLabio, G. A.; Wolkow, R. A., Self-directed growth of contiguous perpendicular molecular lines on H-Si(100) surfaces. *Journal of Physical Chemistry A* 2007, *111* (49), 12257-12259.

41. Hossain, M. Z.; Kato, H. S.; Kawai, M., Self-directed chain reaction by small ketones with the dangling bond site on the Si(100)-(2 x 1)-H surface: Acetophenone, a unique example. *Journal of the American Chemical Society* 2008, *130* (34), 11518-11523.

42. Hossain, M. Z.; Kato, H. S.; Kawai, M., Valence States of One-Dimensional Molecular Assembly Formed by Ketone Molecules on the Si(100)-(2 x 1)-H Surface. *Journal of Physical Chemistry C* 2009, *113* (24), 10751-10754.

43. Zhao, Y.; Truhlar, D. G., Exploring the Limit of Accuracy of the Global Hybrid Meta Density Functional for Main-Group Thermochemistry, Kinetics, and Noncovalent Interactions. *J. Chem. Theory Comput.* 2008, *4* (11), 1849-1868.

44. DiLabio, G. A.; Piva, P. G.; Kruse, P.; Wolkow, R. A., Dispersion interactions enable the self-directed growth of linear alkane nanostructures covalently bound to silicon. *Journal of the American Chemical Society* 2004, *126* (49), 16048-16050.

45. Kruse, P.; Johnson, E. R.; DiLabio, G. A.; Wolkow, R. A., Patterning of vinylferrocene on H-Si(100) via self-directed growth of molecular lines and STM-induced decomposition. *Nano Letters* 2002, *2* (8), 807-810.

46. Hellman, O. C.; Vancauwenberghe, O.; Herbots, N.; Olson, J.; Culbertson, R. J.; Croft, W. J., Structure and Properties of Silicon-Nitride and SIXGE1-X Nitride Prepared by Direct Low-Energy Ion-Beam Nitridation. *Materials Science and Engineering B-Solid State Materials for Advanced Technology* 1992, *12* (1-2), 53-59.

47. Ishidzuka, S.; Igari, Y.; Takaoka, T.; Kusunoki, I., Nitridation of Si(100) surface with NH3. *Applied Surface Science* 1998, *130*, 107-111.

48. Keung, A. J.; Filler, M. A.; Porter, D. W.; Bent, S. F., Tertiary amide chemistry at the Ge(100)-2 x 1 surface. *Surf. Sci.* 2005, *599* (1-3), 41-54.

49. Kobayashi, Y.; Ogino, T., Angle-variable infrared external reflection spectroscopy in UHV and its application to the observation of Si-H vibrations on Si(001) substrates with a buried metal layer. *Surf. Sci.* 1996, *368*, 102-107.

50. Peden, C. H. F.; Vandeusen, S. B., Growth-Kinetics of Thermally Nitrided Si(100) by N2H4. *J. Vac. Sci. Technol. A-Vac. Surf. Films* 1987, *5* (4), 2024-2025.

51. Rignanese, G. M.; Pasquarello, A., Nitrogen bonding configurations at nitrided Si(001) surfaces and Si(001)-SiO2 interfaces: A first-principles study of core-level shifts. *Physical Review B* 2001, *63* (7).

52. Slaughter, E. A.; Gland, J. L., N2H4 AND NH3 as Precursors for Silicon-Nitride Thin-Film Growth. *J. Vac. Sci. Technol. A-Vac. Surf. Films* 1992, *10* (1), 66-68.

53. Stefanov, B. B.; Raghavachari, K., Oxidation of Si(100)2x1: thermodynamics of oxygen insertion and migration. *Surf. Sci.* 1997, *389* (1-3), L1159-L1164.

54. Stefanov, B. B.; Raghavachari, K., Pathways for initial water-induced oxidation of Si(100). *Applied Physics Letters* 1998, *73* (6), 824-826.

55. Wang, Z. H.; Urisu, T.; Watanabe, H.; Ooi, K.; Rao, G. R.; Nanbu, S.; Maki, J.; Aoyagi, M., Assignment of surface IR absorption spectra observed in the oxidation reactions: 2H+H2O/Si(100) and H2O+H/Si(100). *Surf. Sci.* 2005, *575* (3), 330-342.

56. Warschkow, O.; Schofield, S. R.; Marks, N. A.; Radny, M. W.; Smith, P. V.; McKenzie, D. R., Water on silicon (001): C defects and initial steps of surface oxidation. *Physical Review B* 2008, *77* (20).

57. Watanabe, H.; Nanbu, S.; Wang, Z. H.; Maki, J.; Urisu, T.; Aoyagi, M.; Ooi, K., Theoretical analysis of the oxygen insertion process in the oxidation reactions of H2O+H/Si(100) and 2H+H2O/Si(100): a molecular orbital calculation and an analysis of tunneling reaction. *Chemical Physics Letters* 2004, *383* (5-6), 523-527.

58. Weldon, M. K.; Queeney, K. T.; Gurevich, A. B.; Stefanov, B. B.; Chabal, Y. J.; Raghavachari, K., Si-H bending modes as a probe of local chemical structure: Thermal and chemical routes to decomposition of H2O on Si(100)-(2x1). *Journal of Chemical Physics* 2000, *113* (6), 2440-2446.

59. Mukhopadhyay, A. B.; Musgrave, C. B.; Sanz, J. F., Atomic layer deposition of hafnium oxide from hafnium chloride and water. *Journal of the American Chemical Society* 2008, *130* (36), 11996-12006.

60. Weldon, M. K.; Queeney, K. T.; Eng, J.; Raghavachari, K.; Chabal, Y. J., The surface science of semiconductor processing: gate oxides in the ever-shrinking transistor. *Surf. Sci.* 2002, *500* (1-3), 859-878.

61. Mui, C.; Widjaja, Y.; Kang, J. K.; Musgrave, C. B., Surface reaction mechanisms for atomic layer deposition of silicon nitride. *Surf. Sci.* 2004, *557* (1-3), 159-170.

62. Widjaja, Y.; Musgrave, C. B., Atomistic mechanism of the initial oxidation of the clean Si(100)-(2x1) surface by O-2 and SiO2 decomposition. *Journal of Chemical Physics* 2002, *116* (13), 5774-5780.

63. Johnson, B. G.; Gonzales, C. A.; Gill, P. M. W.; Pople, J. A., A Density-Functional Study of the Simplest Hydrogen Abstraction Reaction - Effect of Self-Interaction Correction. *Chemical Physics Letters* 1994, *221* (1-2), 100-108.

64. Perdew, J. P.; Zunger, A., Self-Interaction Correction to Density-Functional Approximations for Many-electron Systems. *Physical Review B* 1981, *23* (10), 5048-5079.

65. Vydrov, O. A.; Scuseria, G. E., A simple method to selectively scale down the self-interaction correction. *Journal of Chemical Physics* 2006, *124* (19).

66. Valero, R.; Gomes, J. R. B.; Truhlar, D. G.; Illas, F., Good performance of the M06 family of hybrid meta generalized gradient approximation density functionals on a difficult case: CO adsorption on MgO(001). *J Chem Phys* 2008, *129* (12), 124710.

67. Zhao, Y.; Truhlar, D. G., Density functional for spectroscopy: No long-range self-interaction error, good performance for Rydberg and charge-transfer states, and better performance on average than B3LYP for ground states. *Journal of Physical Chemistry A* 2006, *110* (49), 13126-13130.

68. Zhao, Y.; Truhlar, D. G., Density functionals with broad applicability in chemistry. *Accounts of Chemical Research* 2008, *41* (2), 157-167.

69. Raghavachari, K.; Trucks, G. W.; Pople, J. A.; Headgordon, M., A 5th-Order Perturbation Comparison of Electron Correlation Theories. *Chemical Physics Letters* 1989, *157* (6), 479-483.

70. Teraishi, K.; Takaba, H.; Yamada, A.; Endou, A.; Gunji, I.; Chatterjee, A.; Kubo, M.; Miyamoto, A.; Nakamura, K.; Kitajima, M., Quantum chemical study on the oxidation process of a hydrogen terminated Si surface. *Journal of Chemical Physics* 1998, *109* (4), 1495-1504.

71. We had convergence problems in obtaining the transition state for the dimer insertion. Instead the reported value is that of the second-order saddle point. Since this provides a rigorous upper bound to the transition state energy, the preference for dimer bond insertion is likely to be greater than we report.

Chapter Three

Constrained DFT and Modeling XPS Spectra

3.1 Introduction

Developments in modern electronic structure theory have mostly focused on ground state calculations. Moreover, they work best for solutions that are close to the guess orbitals one starts with. It is common when calculating the ground electronic states of metals to arrive at a solution that is not the ground state but is instead a higher energy *local* minimum. It is certainly possible to calculate electronic excited states using theories such as configuration interaction involving single excitations (CIS), or time-dependent density functional theory (TDDFT).[1] These methods are designed to calculate the excitation energies from of the ground state but are of limited use for finding the

structures and properties of specific electronic excited states. They also have their benefits and pitfalls. For example, the energies of TDDFT long-range charge transfer excited states are severely underestimated and the TDDFT method is known to fail for Rydberg excitations.[1-5] The CIS method can only be used to investigate single electron excitations.[1] Overall, these methods are reliable only for low-lying valence excited states. Other more sophisticated techniques exist such as equation-of-motion coupled cluster, symmetry-adapted cluster configuration interaction, etc., but these methods are generally too computationally expensive for all but small molecules.[1] In this section we would like to concentrate on two particular problems, the first is how to calculate a *particular* electronic state of interest of the SCF equations using an inexpensive single reference method and second is the how to accurately calculate core-ionizations.

Until recently there has not been a widely available *general method* to calculate the energy of a *particular* electronic state of interest. The nature of the self-consistent field (SCF) solution to the Hartree-Fock or DFT equations usually requires that the solution be the lowest energy state of a given symmetry. If a different state is desired, the SCF procedure will still collapse to the wavefunction or density to the lowest *local* minimum. This can be understood from an analysis of the usual SCF procedure.[6]

1. State the molecular specifications and the basis set
2. Calculate necessary quantities, i.e., overlap matrix, core Hamiltonian, etc.
3. Start with an initial guess for the density matrix
4. Calculate the Fock matrix and diagonalize
5. Form a new density matrix from the optimized coefficients
6. Repeat using the new density matrix until there is no change in the density matrix, i.e., convergence is reached

As is evident from this procedure the initial guess of the density matrix is critical to the convergence. If it is possible to bias the guess or to find a constraint that does not allow certain states, many interesting electronic states could be generated. The most natural constraint is the symmetry of the wavefunction. We term this constraint natural because it is implicit in the SCF procedure. The change in the density matrix will transform with the same symmetry as the original density matrix. (Note: it may be possible, for numerical reasons, to have symmetry breaking in the density matrix but this should not be the case if robust numerical algorithms are used). Using this idea it is possible to easily calculate excited electronic states that transform with a different symmetry than the ground state. The symmetry is not limited to the spatial symmetry but also the spin symmetry, i.e., a triplet wavefunction will not optimize to a singlet wavefunction. Using this procedure it is thus possible to solve for some electronic excited states. Another method using a similar idea is the method of maximum overlap (MOM).[7] The MOM method finds a local minimum of the wavefunction (or density) by biasing the guess at every point during the SCF procedure. The form of the bias is in forcing the guess to be close to the desired state and using an alternative SCF procedure. In the usual SCF procedure after solving for the Fock matrix the orbitals are ordered from lowest to highest and the lowest n orbitals are occupied, where n is the number of e^-. The MOM procedure instead occupies the orbitals

that best span the space of the guess orbitals. The method depends on the skill in choosing an appropriate guess. Using this procedure it may be possible to calculate particular electronic states if the quality of the initial guess is reasonable. A method that does not depend on the particular guess orbitals, which may often be difficult to generate, is highly desirable.

One possible way to overcome the limitation of a guess may be to use the constrained DFT method of Wu and Van Voorhis.[2, 3, 8-13] In this method a constraint potential is added to the SCF equation (*vide infra*) using the Lagrangian formalism. The SCF equations are then solved with the addition of the constraint potential. The particular constraint usually applied is the value of the density over a region of a molecule, e.g., for a molecule with regions A and B the charge could be divided up as $A^{+3}B^{-3}$ where the positive charge on region A of the molecule is constrained to +3. CDFT has been shown to fix the problem of charge-transfer excited states that plagues TDDFT. It is overcome by solving for the excited state as a ground state problem that takes advantage of the strength of the underlying DFT formalism. Using this theory is should be possible to find constrained solutions to many states of interest as long as the constraints are applied to different atomic centers or molecular fragments. We have implemented a version of the CDFT code following the formalism of Wu, Yang and Van Voorhis.[2, 3, 8-13] The implementation has been used in illustrative computations of the electronic states of the HeH_2 and Cu_2O_2 test cases. For these molecules three states are possible: the triplet, the singlet and the open-shell singlet (spin multiplicity of one with two unpaired electrons). These cases were solved using several methods and the energy differences compared.

The second problem we have investigated is calculation of core-level ionization spectra. In this problem high-energy photons in the X-ray region of the spectrum are used to ionize the core of an atom or a molecule. This technique is also called X-ray photoelectron spectroscopy (XPS). It is a powerful method for determining the chemical state of an atom in a molecule. In the study of surface chemistry, XPS is an invaluable technique to determine the local chemical environment. The analysis of the local chemical environment involves collecting the ejected electrons. Analysis of the number of electrons at each energy is used to determine the local environment of the element of interest. The kinetic energy of the collected electrons is proportional to the binding energy of the core electron. Consider a photon (in the form of a high-energy X-ray) exciting a core electron from species Y creating a cation Y^+. The energy of the species Y and the photon $h\nu$ must be equal to the energy of the ejected electron and the cation, Y^+.

$$E(Y) + h\nu = E(Y^+) + E(e^-)$$

Where h is the Planck's constant (6.626×10^{-34} Js), and ν is the frequency of the X-ray, and E(Y) represents the energy of the species Y. Assuming the energy of the ejected free electron is kinetic the following relation is true.

$$BE = KE(e^-) - h\nu$$

Where BE is the binding energy of the core electron, i.e., the difference between the energy of the neutral and cationic species ($E(Y) - E(Y^+)$), and $KE(e^-)$ is the kinetic energy of the free electron. If the energy of the photon is known, the binding energy of the species can be determined. In the simple one-electron picture, this binding energy

corresponds to a specific orbital energy of an atom of interest. A schematic of the process is shown in figure 3.1.1.

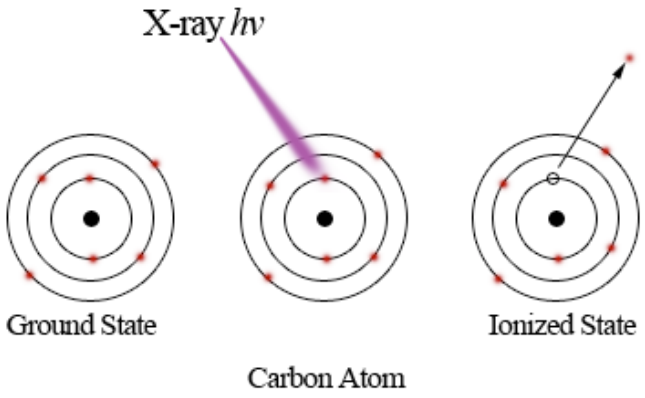

Figure 3.1.1. The schematic for the ionization of a core-level electron by an X-ray photon.

The binding energy is very sensitive to the local chemical environment of an atom in a molecule resulting in characteristic shifts from a reference compound. The interpretation of XPS spectra is not always straightforward, for challenging cases an *ab initio* method of calculating XPS shifts would assist in the interpretation of these spectra.

There are currently a few methods available to calculate XPS spectra. The methods can be classified into two categories, frozen orbital methods and orbital relaxation methods. To understand this classification it is necessary to understand the zero-order approximation to the electron binding energy. Koopmans' theorem states that for the Hartree-Fock single determinant the ionization energy of a system is the negative of the corresponding orbital energy. The orbital energies are explicitly calculated during solutions to the SCF procedure. Therefore, the electronic binding energy measured by X-ray photoelectron spectroscopy should simply be the negative of the orbital energy of the highest core-orbital. Binding energies obtained from Koopmans' theorem are uniformly

too large. The reason for this overestimation is due to the frozen orbital approximation. When a core electron is ionized the remaining orbitals instantaneously relax. This relaxation is not present if the orbitals are frozen making Koopmans' theorem a poor approximation. We will examine two other approximations. The first is the equivalent core (also called the Z+1 method) that approximates orbital relaxation and the second, electron propagator theory, provides a sophisticated electron correlation approach to correct Koopmans' theorem.

The equivalent core method[14] assumes that when the core electron is excited or removed, the relaxation of the orbitals is mainly due to the increased nuclear charge the electrons "feel". This model replaces the core hole on an atom with the filled core of the cation for the atom with one greater atomic number, hence the Z+1 (e.g., nitrogen for carbon). For example, to determine the 1s binding energy of the carbon atom in a CN radical with respect to a reference compound (CH_4), the following scheme is used.

$$CH_4 + CN^{+}* \rightarrow CH_4^{+}* + CN \qquad \Delta E = BE \qquad (1)$$

$$CH_4^{+}* + NN^{+} \rightarrow NH_4^{+} + CN^{+}* \qquad \Delta E = 0 \qquad (2)$$

Adding reactions 1 and 2 gives

$$CH_4 + NN^{+} \rightarrow NH_4^{+} + CN \qquad \Delta E = BE \qquad (3)$$

If the approximation in equation (2) holds, then the *shift* with respect to the reference compound will be correct.

Electron propagator theory (EPT) directly determines the electron binding energies using a Green's function formalism. In standard Hartree-Fock theory the

canonical MOs are calculated as the eigenfunctions of the self-consistent solution to the Fock operator. Analogously the binding energies in propagator theory are the self-consistent solutions to the Dyson equation.[15]

$$\mathbf{G}^{-1}(E) = \mathbf{G}_0^{-1}(E) - \sum(E)$$

The poles of the **G** matrix correspond to the electron-bonding energies. The self-interaction matrix $\sum(E)$ that leads to the self-interaction energy is the correction to Koopmans' theorem. In practice these values are calculated using methods such as the P3 approximation.[16-30]

Another method is the use of effective core potentials (ECP) to mimic core holes. ECPs were originally developed to replace core electrons. These electrons are not believed to be important for chemical bond formation and are omitted for computational expedience.[31-33] An ECP is a potential that is parametrized using a fitting process designed to replace a certain number of core electrons while not adversely affecting the electronic structure of the valence orbitals. ECPs have been used by the plane wave community to mimic the effects of a localized core hole on an element.[31-33] The parameterization is performed by calculating the exact core hole on an atomic center, and then transferring the ECP directly to a system. This method requires the potential be fit for each molecule and while it has given good results it lacks the general applicability that we desire and was not investigated in this work.

In this chapter we have studied the following: the implementation of CDFT within the Gaussian suite of programs, the use of CDFT to solve for the electronic states of Cu_2O_2, and benchmarked the performance of EPT and the Z+1 methods for calculating

core-ionization energies. Our results are divided into three sections with the first two concentrating on CDFT and the latter one dealing with core ionizations.

3.2 CDFT Theory and Implementation

Constrained DFT[2, 3, 8-13] is a method with a great deal of potential. The method is designed to solve the Kohn-Sham formalism of DFT but can arrive at different states than standard Kohn-Sham DFT. The strength of this method is that it calculates a ground state solution under the constraint potential. This solution alleviates some problems experienced when attempting to solve for some electronic states.

This method starts with the standard Kohn-Sham DFT formalism but adds a constraint to the density. This new constraint is applied in a similar manner to the orbital orthogonality constraint of Hartree-Fock or DFT theory, i.e., by using the Lagrange method of undetermined multipliers.

$$\mathcal{L}[\rho, \lambda_c] = E[\rho] + \lambda_c(\sum \int w_c \rho(r) - N)$$

In the above equation, E[ρ] is the energy of the system, λ_c is the undetermined multiplier, w_c is the domain of the constraint, ρ(r) is the electron density and N is the value of the constraint. The domain w_c is determined by the user. The only unknown value is the Lagrangian multiplier λ_c. This value is must be determined self-consistently. As was shown by Wu and Yang and later Wu and Van Voorhis[2, 3, 8-13] the Lagrangian $\mathcal{L}$ is a critical point and a unique maximum.

Under the constraints that $\mathcal{L}$ is stationary and the orbitals are normalized the following equation can be derived.

$$(-\frac{1}{2}\nabla^2 + \upsilon_n(r) + \int \frac{\rho(r')}{|r-r'|}dr' + \upsilon_{xc} + \lambda_c w_c(r))\phi_i = \epsilon_i \phi_i$$

This equation is the same as the standard Kohn-Sham method with the added $\lambda_c w_c(r)$ term from the constraint definition. The $w_c(r)$ term is a predefined input determining the constraint. The λ_c term is determined variationally. The method has been previously applied successfully to a variety of different problems.[2, 3, 8-13]

As is true for systems under Lagrangian constraints the constraint must be holonomic for a solution to exist. The definition of a holonomic constraint is one that may be expressed in the following fashion (Note: a scleronomous constraint).[34]

$$f(r_1, r_2, r_3, ...) = 0$$

For our purposes the variables are the density over the region where the constraint is defined. A charge density over a region forms a holonomic constraint but may have no solution.

The charge density of the core of an atom is a spatial function that has a contribution from many orbitals. A solution will exist if the *orbitals* chosen for the constraint include all of a population in the special region of the core. For example if the 1s orbital is chosen as the core for carbon it is might not possible to satisfy the constraint. The 2s, 2p and other orbitals also contribute to the *spatial* density of the region. Therefore these must be included to satisfy the constraint. This could be fixed simply by including all of the orbitals that have significant spatial overlap but this then changes the spatial region. It could also be fixed by rotating the orbitals (or generating a new set of

orbitals) that do not have overlap in the core region. This solution might, however, be unphysical.

The implementation of CDFT in the Gaussian suite of programs was accomplished by adding a constraint outside of the SCF cycle. In this implementation the SCF equations are first solved using a constraint value of zero. The constrained DFT code is then called and the initial guess for the constraint is applied. The SCF equations are resolved with the added constraint potential. The procedure is iterated until both the orbitals and the constraint reach self-consistency.

The constraint potential is defined over atomic centers. The basis functions on each atom in the constraint domain are determined and the constraint is applied to them using a simple projection matrix. The projection matrix is determined by an electronic population scheme. In our case this is either the Mulliken or Löwdin populations of an atom or group of atoms. Other population schemes, such as Becke's multicenter integration scheme, are equally valid. Presently, we have only implemented two population schemes, Mulliken and Löwdin. In this formalism the projection matrix becomes the dot product of the weight matrix with the overlap matrix. Using the Mulliken population the constraint matrix is one if both basis functions of the overlap matrix element are in the domain of the constraint, one-half if one basis function is in the constraint domain and zero if neither basis function is in the constraint domain. Using the Löwdin populations the weight is determined by the weight matrix as follows.

$$\sum_{\mu \in C} S^{\frac{1}{2}}_{\lambda\mu} S^{\frac{1}{2}}_{\mu\nu}$$

If the constraint is applied outside the SCF, the orbitals are optimized satisfying the orthogonality constraint. Using this as the starting point the Lagrange multiplier that satisfies the constraint can be determined independently. However, there are potential problems. The constraint depends on the orbitals that in turn depend on the constraint. The system is therefore very nonlinear. It could easily be argued that the converged orbitals without the constraint are a poor guess for the starting point to optimize the constraint. Nevertheless this method has been found to be valid though slowly convergent. The first and second derivatives of the constraint are known.[11] Therefore, a robust optimization method such as Newton-Raphson can be used to optimize the constraint after the SCF is converged. This optimized value of the constraint can then be used as the guess for another SCF. The order of operations is as follows.

1. Calculate the SCF energy
2. Initialize the constraint
3. Calculate the SCF with the constraint added
4. Calculate the Lagrangian derivatives
5. Test for convergence
    a. Yes, Exit
    b. No, Go to 6
6. Take a Newton-Raphson Step and update the Lagrangian
7. Go to 3.

The procedure is slightly different if the constraint is applied inside the SCF cycle. The major difference is that the optimization of the Lagrangian occurs at each step in the

SCF determination of the orbitals. The orbitals and the population constraint Lagrange multiplier are simultaneously optimized.

3.3 Electronic States of H_2He and Cu_2O_2 using CDFT

As mentioned earlier constrained density functional theory provides a way to solve for an electronic excited state as a constrained ground state.[2, 3, 8-13] Previously, Van Voorhis and coworkers have used this concept to get exchange coupling constants and to find the solutions for long-range electron transfer parameters.[13] The latter is a notable failure of TDDFT linear response theory.[1, 3-5] This fact is evidence that a constrained ground state is superior to a linear response to the density. If other excited states could also be solved using a constrained ground state solution it might be possible to solve many problems in inorganic chemistry where finding a particular state involving transition metal elements is often very difficult.

For many inorganic systems, e.g. Cu_2O_2, the ground electronic state may be difficult to calculate using conventional methods. Considering the case of an even number of electrons with two center A and B (where A and B are the same element), we can demonstrate why this is the case. The possible spin states are the closed shell singlet, the triplet ↑A — B↑, and finally the open-shell singlet↑A — B↓ where the unpaired electrons have significant spin density on atomic centers A and B. This latter state is referred to as an antiferromagnetically coupled state. This type of coupling also exists for systems with any number of unpaired electrons regardless of spin multiplicity. The open-shell singlet is often times the ground state of a molecule but is rather difficult to find using conventional SCF. The root cause of the problem is that the guess generated for

most systems is much closer to the closed-shell singlet than the open shell singlet. Several techniques exist for overcoming this problem.

One of the most straightforward solutions is to change the guess of the system to be closer to the open-shelled singlet. Since these systems are so called broken-symmetry state (the symmetry of the wavefunction is different from the geometric framework) one possible solution in high symmetry cases is to break the symmetry of the problem by applying an electric field. This generates a broken symmetry wavefunction that is possibly closer to the open-shell state. A second method is to divide the system into fragments with the electronic structure restricted to that of the parent molecule. The fragments can then be reassembled and used as a guess wavefunction that will bias the SCF towards the antiferomagnetic solution. The simplest method is to mix the highest occupied molecular orbital and the lowest unoccupied molecular orbital to destroy the symmetry of the guess. There are many other possibilities all of which follow this theme. The final possibility is to solve for the antiferromagnetic state as a constrained ground state. It is our goal to show that this is possible.

As proof of concept we have used the toy problem H—He—H with the unpaired electrons on the hydrogen atoms. We realize that this is not a very realistic system but it contains the necessary elements to completely understand the problem: several electronic states are possible and the open-shell singlet (antiferromagnetic state) is the ground state. While the natural constraint is to use one unpaired spin on each hydrogen, that is not necessarily the optimal solution. In fact using a constraint on the Mulliken or Löwdin populations it is possible to obtain a range of solutions by constraining the system to different spin densities. However, only one of these spin densities will correspond to the

spin density of the variationally optimized or "real" electronic state. For the system non-minimum spin densities will be above the minimum. Therefore, if it is possible to solve for a number of spin densities around the minimum one can find the spin density of the real system. To accomplish this task we have used the B3LYP/3-21G model chemistry.[35-37] The system was optimized to a linear structure and the constraint is such that the spin density on the hydrogens is equal and opposite. Spin densities of 0.8 to 1.0 a.u. on the hydrogen atoms were used as the constraint. The values were plotted against the energy difference from the minimum energy of the system. In our test case the hydrogen spin density is at 0.85 a.u. with a zero value of the Lagrange multiplier that enforces the constraint, figure 3.3.1.

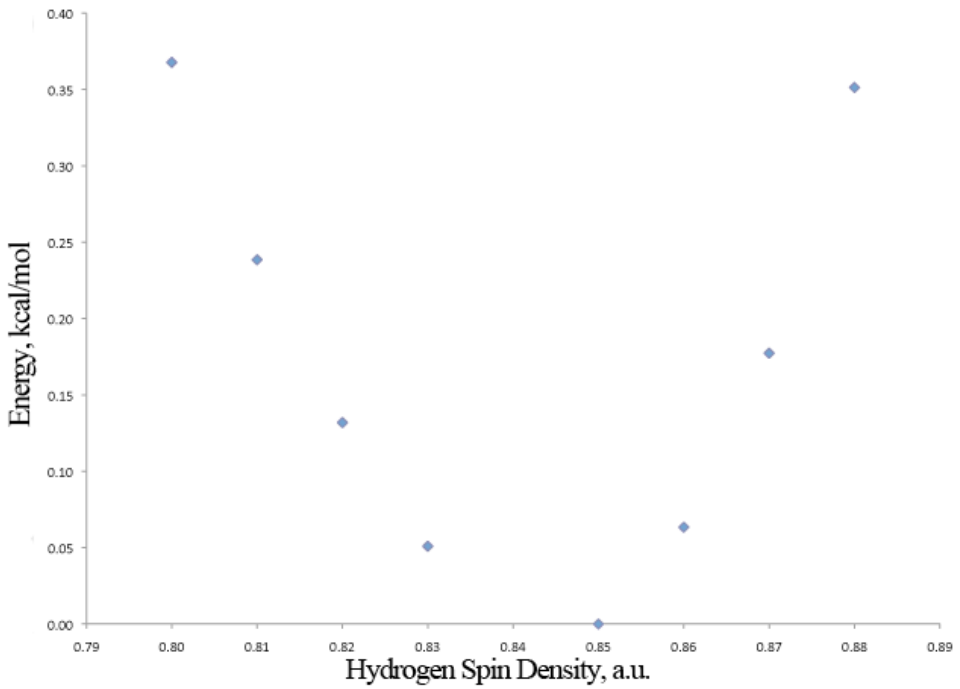

Figure 3.3.1. The energy the open-sell singlet electronic state of HeH_2 molecule optimized to a range of Mulliken spin densities on the hydrogen atoms using CDFT.

If this spin density minimum is compared to that obtained by a direct convergence of the open-shell singlet there is excellent agreement at the spin-density of 0.85 a.u. Since the Lagrange multiplier is zero the total energy is exactly the same. This raises the possibility that if one varies the constraint until a zero Lagrange multiplier is found this point will correspond to an unconstrained solution.

A more practical case is that of Cu_2O_2. For this bimetallic system the ground state is the antiferromagnetically coupled state with two unpaired electrons (open-shell singlet). The spin density accumulates on the copper atoms. It is possible to find the direct solution to this system by manipulating the guess wavefunction. Using CDFT with the B3LYP/sddall model chemistry the spin density on the copper centers was varied between 0.3 a.u. and 0.5 a.u., figure 3.3.2. The minimum energy spin density was at 0.37 a.u., which is the same as the solution using the modified guess wavefunction. At the minimum energy point the constraint value was close to zero. This more practical example again shows the possibility of using CDFT to find particular solutions to for electronic states that mat be difficult to obtain by other means.

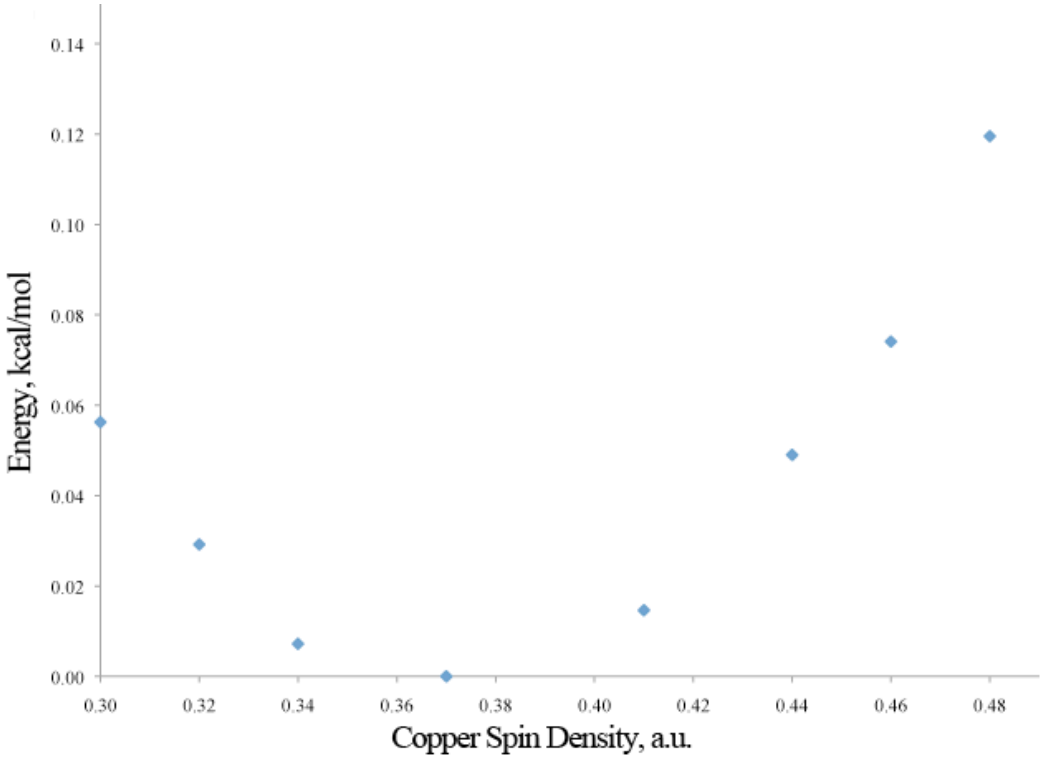

Figure 3.3.2. The Cu_2O_2 molecule energy plotted against the Mulliken spin density on the copper atoms. The different spin densities were found using CDFT.

3.4 Benchmarking Methods for XPS

The methods we have evaluated for calculating approximate core-ionization energies are the equivalent core method and electron propagator theory. The goal of this study is to understand how accurate current methods are for approximating experimentally observed XPS shifts. Our test set is restricted to the first and second row elements of the main group excluding boron and aluminum. It has an emphasis on carbon and silicon. This was specifically chosen to carefully understand the performance of these methods with 1s (carbon) and 2p (silicon) core ionizations. The set includes forty-three small molecules, table 3.4.1. For each molecule the equivalent core and EPT core-ionization energies were compared to experimentally known values. While EPT methods are known to give accurate values for valence ionization energies they have not been extensively explored for core-ionizations. Values within 0.5 eV can be considered good but may not be quantitatively accurate for cases involving small shifts.

Table 3.4.1. The test set for core-level ionization of main group elements.

XPS Test Set			
First Row			
Carbon	Nitrogen	Oxygen	Fluorine
CH_4	NH_3	H_2O	HF
CBr_4	HCN	CO_2	CH_3F
CCl_4	CH_3NH_2	O_2	CHF_3
CF_4	C_5H_5N	N_2O	CF_4
C_2H_4			
CH_3SiH_3			
C_2H_6			
$(CH_3)_2SiH_2$			
$(CH_3SiH_2)_2O$			
$(CH_3SiH_2)_2Se$			
C_6H_6			
C_6F_6			
Second Row			
Silicon	Phosphorous	Sulfur	Chlorine
SiH_3	PCl_3	SF_6	Cl_2
$SiBr_4$	PF_3	H_2S	ClF
CH_6Si			Cl_2
Si_2H_6			CCl_4
$SiCl_4$			ClF
SiF_4			$CClF_3$
$(CH_3)_2SiH$			
$SiHCl_3$			
SiH_3Cl			
$(SiH_3)_2O$			
$(SiH_3)_2S$			

Computational Details

As described above the equivalent core calculations approximate the relaxation of the core as an increase in the nuclear charge. The scheme used is as follows. To find the shift in the molecule ZY relative to the reference AB the following scheme was used.

$$[(A+1)B^+ + ZY] - [AB + (Z+1)Y^+]$$

Using this formalism all of the shifts for the test set were calculated.

Optimizations were carried out using hybrid density functional theory with Becke's three-parameter exchange functional and the Lee-Yang-Parr correlation functional (B3LYP).[35-37] The basis set used in our model chemistry is the Pople-style triple-ζ basis set with polarization and diffuse functions on all the hydrogen and heavy atoms.[38] This gives an overall model chemistry of B3LYP/6-31++G(d,p). The method is recommend by the Ortiz group for accurate EPT calculations.[24, 25, 28, 29] All minima were characterized using analytic second derivatives. All EPT calculations used the P3 implementation of the EPT method by Ortiz and coworkers. The sole exception is for Silicon. The P3 poles were either not converged, gave exceptionally poor results (generally the same as Koopmans' Theorem) or had low pole strengths making the results unreliable. The converged second-order poles were therefore used for silicon. Calculations were performed using the Gaussian suite of programs.[39]

Results and Discussion

Overall the EPT is far superior to the equivalent core method. The overall MAD for the equivalent core method is 4.53 eV for the test set while it is only 0.88 eV for the EPT method, table 3.3.2. The largest deviation for the equivalent core method is 23.64 eV (H_2S) while the highest for the EPT method is 2.51 eV (ClF). These large deviations are far too great for either qualitative or quantitative accuracy. For most molecules in the test set the EPT method performs well; the failures are largest for molecules with halides. This is also true for the Z+1 method. If molecules containing halides or oxygen are eliminated from the test set the MAD is 0.40 and the maximum error is 1.55 eV (benzene) for EPT, and 1.08 and the maximum error is 1.85 eV (pyridine) for Z+1.

Table 3.4.2. The results for core-level ionization for a test set of main group elements using equivalent core (a.k.a. Z+1) and EPT methods along with experimental data.

		Shifts from Atomic Reference, eV		
Molecule	Ionized Orbital	Equivalent Core	EPT	Experiment
HF Reference	F1s	0.00	0.00	0.00
CH_3F	F 1s	-0.12	-1.26	-1.52
CHF_3	F 1s	1.68	0.62	0.68
CF_4	F 1s	-0.97	1.41	1.30
CH_4 Reference	C 1s	0.00	0.00	0.00
CBr_4	C 1s	-4.05	6.46	3.95
CCl_4	C 1s	-5.60	7.11	5.48
CF_4	C 1s	-11.22	11.80	11.02
C_2H_4	C 1s	0.17	0.43	0.31
CH_3SiH_3	C 1s	0.53	-0.24	0.02
C_2H_6	C 1s	0.18	-0.08	-0.16
$(CH_3)_2SiH_2$	C 1s	0.79	-0.45	-0.72
$(CH_3SiH_2)_2O$	C 1s	0.75	-0.40	-0.66
$(CH_3SiH_2)_2Se$	C 1s	0.75	-0.22	-0.66
C_6H_6	C 1s	0.70	1.04	-0.52
C_6F_6	C 1s	-3.37	4.70	3.25
Cl_2 Reference	Cl 2s	N/C	0.00	0.00
ClF	Cl 2s	N/C	1.36	0.49
Cl_2 Reference	Cl 2p	N/C	0.00	0.00
CCl_4	Cl 2p	N/C	0.58	-0.80
ClF	Cl 2p	N/C	-1.53	1.38
$CClF_3$	Cl 2p	N/C	0.05	0.02
NH_3 Reference	N 1s	0.00	0.00	0.00
HCN	N 1s	-0.68	1.97	0.79
CH_3NH_2	N 1s	0.46	-0.38	-0.41
C_5H_5N	N 1s	1.16	0.01	-0.69
H_2O Reference	O 1s	0.00	0.00	0.00
CO_2	O 1s	-1.33	2.73	1.44
O_2	O 1s	-3.98	4.84	2.86
N_2O	O 1s	-5.43	7.60	1.44
PCl_3 Reference	P 1s	0.00	0.00	0.00
PF_3	P 1s	-2.26	1.77	5.49
SF_6 Reference	S 1s	0.00	0.00	0.00
H_2S	S 1s	12.04	-12.60	-11.60
SiH_3 Reference	Si 2p	0.00	0.00	0.00
$SiBr_4$	Si 2p	-3.15	2.49	2.39
CH_6Si	Si 2p	0.40	-0.50	-0.41
Si_2H_6	Si 2p	0.57	-0.60	-0.44
$SiCl_4$	Si 2p	-4.05	3.32	2.95
SiF_4	Si 2p	-6.06	5.95	4.45
$(CH_3)_2SiH$	Si 2p	0.73	-0.91	-1.11
$SiHCl_3$	Si 2p	-3.21	3.31	2.15
SiH_3Cl	Si 2p	-1.23	2.67	0.81
$(SiH_3)_2O$	Si 2p	-0.85	0.61	0.52
$(SiH_3)_2S$	Si 2p	-0.31	0.64	0.16

The reasons for the failure of the Z+1 method for halides and oxygen are straightforward. The first failure is if Z is oxygen. The Z+1 core is fluorine, which has very different bonding properties than oxygen. The bonding environment is poorly approximated causing shifts that go beyond just the increased nuclear charge. In general

the failure for the electronegative elements is due to the strongly polarizing effects of the halides and oxygen or the change in the bonding environment due to the shift in the core. As the electronegativity increased the error also increased. It is interesting to note that silicon, which is less polarizable than carbon, showed a smaller error with halides. The most dramatic failures are for hydrogen sulfide and tetrafluoromethane. While the latter is understandable from the earlier discussion, part of the error for H_2S stems the reference molecule SF_6 whose shift is unlikely to be described well with P^+F_6.

Z+1 is most successful for carbon and silicon that do not contain strongly polarizing functional groups. In these cases the Z+1 core provided both a similar bonding environment and the weaker polarizing effects involving the N^+ core in the case of carbon and the P^+ core in the case of silicon. Overall, the success of the method does not seem to be dependent on whether the core-hole is 1s or 2p, large errors were seen for both. We can now make the point that the success of the Z+1 method is dependent on the Z+1 core having similar bonding properties to the Z core. The Z+1 method could only be recommended for cases involving small changexs to the bonding environment and an absence of very polar functional groups.

The EPT method gave much better overall results than the equivalent core method. In our test set Z+1 out performs the EPT method for only one excitation, the Si 2p excitation of $(SiH_3)_2S$. In this case the difference is only 0.03 eV, which is likely fortuitous and not a sign of a more robust method. The large failures of the EPT method are mostly on strongly polarizing functional groups but do not have the same pattern present with the Z+1 method. Errors increase with increased electronegativity for silicon 2p core-holes but decrease with increased electronegativity for carbon 1s core-holes. The

largest error for the EPT method is ClF that is possibly due a failure in cancelation from the Cl_2 reference. Overall, the method is quite robust and close to quantitatively accurate for many molecules in the test set.

From these results we can make several important conclusions. First, the quality of the reference is as equally important as the molecule. This means references should be chosen which are more likely to result in cancelations of error. Second, the errors for core-ionization approximations are greater for halides and oxygen-containing molecules, if the atom of interest is polarizable. For example fluorine is not strongly affected by halide functional groups but silicon and carbon are affected. Finally, the EPT method using high order approximations P3 (P2 for silicon) is much more accurate than the Z+1 method in almost every instance.

References

1. Dreuw, A.; Head-Gordon, M., Single-reference ab initio methods for the calculation of excited states of large molecules. *Chemical Reviews* 2005, *105* (11), 4009-4037.

2. Cheng, C. L.; Wu, Q.; Van Voorhis, T., Rydberg energies using excited state density functional theory. *Journal of Chemical Physics* 2008, *129* (12), -.

3. Wu, Q.; Van Voorhis, T., Constrained density functional theory and its application in long-range electron transfer. *J. Chem. Theory Comput.* 2006, *2* (3), 765-774.

4. Dreuw, A.; Head-Gordon, M., Failure of time-dependent density functional theory for long-range charge-transfer excited states: The zincbacteriochlorin-bacterlochlorin and bacteriochlorophyll-spheroidene complexes. *Journal of the American Chemical Society* 2004, *126* (12), 4007-4016.

5. Dreuw, A.; Weisman, J. L.; Head-Gordon, M., Long-range charge-transfer excited states in time-dependent density functional theory require non-local exchange. *Journal of Chemical Physics* 2003, *119* (6), 2943-2946.

6. Szabo, A.; Ostlund, N. S., *Modern Quantum Chemistry Introduction to Advanced electronic Structure Theory*. First Ed. Revised ed.; Mineola, NY, 1982; p 466.

7. Gilbert, A. T. B.; Besley, N. A.; Gill, P. M. W., Self-Consistent Field Calculations of Excited States Using the Maximum Overlap Method (MOM). *Journal of Physical Chemistry A* 2008, *112* (50), 13164-13171.

8. Rudra, I.; Wu, Q.; Van Voorhis, T., Accurate magnetic exchange couplings in transition-metal complexes from constrained density-functional theory. *Journal of Chemical Physics* 2006, *124* (2), -.

9. Rudra, I.; Wu, Q.; Van Voorhis, T., Predicting exchange coupling constants in frustrated molecular magnets using density functional theory. *Inorg Chem* 2007, *46* (25), 10539-10548.

10. Wu, Q.; Kaduk, B.; Van Voorhis, T., Constrained density functional theory based configuration interaction improves the prediction of reaction barrier heights. *Journal of Chemical Physics* 2009, *130* (3), -.

11. Wu, Q.; Van Voorhis, T., Direct optimization method to study constrained systems within density-functional theory. *Phys. Rev. A* 2005, *72* (2), -.

12. Wu, Q.; Van Voorhis, T., Extracting electron transfer coupling elements from constrained density functional theory. *Journal of Chemical Physics* 2006, *125* (16), -.

13. Wu, Q.; Van Voorhis, T., Direct calculation of electron transfer parameters through constrained density functional theory. *Journal of Physical Chemistry A* 2006, *110* (29), 9212-9218.

14. Eng, J.; Hubner, I. A.; Barriocanal, J.; Opila, R. L.; Doren, D. J., X-ray photoelectron spectroscopy of nitromethane adsorption products on Si(100): A model for N1s core-level shifts in silicon oxynitride films. *J. Appl. Phys.* 2004, *95* (4), 1963-1968.

15. Öhrn, Y.; Born, G., *Advances in Quantum Chemistry*. Academic Press: San Diego, CA, 1981; Vol. 13.

16. Dolgounitcheva, O.; Zakrzewski, V. G.; Sterling, M. R.; Kletsov, A.; Dahnovsky, Y.; Ortiz, J. V., Correlated ab initio electron propagators in the study of molecular wires. *International Journal of Quantum Chemistry* 2006, *106* (15), 3387-3392.

17. Flores-Moreno, R.; Melin, J.; Dolgounitcheva, O.; Zakrzewski, V. G.; Ortiz, J. V., Three Approximations to the Nonlocal and Energy-Dependent Correlation Potential in Electron Propagator Theory. *International Journal of Quantum Chemistry* 2010, *110* (3), 706-715.

18. Flores-Moreno, R.; Ortiz, J. V., Quasiparticle virtual orbitals in electron propagator calculations. *Journal of Chemical Physics* 2008, *128* (16).

19. Flores-Moreno, R.; Zakrzewski, V. G.; Ortiz, J. V., Assessment of transition operator reference states in electron propagator calculations. *Journal of Chemical Physics* 2007, *127*.

20. Guevara-Garcia, A.; Martinez, A.; Ortiz, J. V., Electron binding energies and Dyson orbitals of Al5Om- (m=3,4,5) and Al5O5H2. *Journal of Chemical Physics* 2007, *127* (23).

21. Ortiz, J. V., TOTAL ENERGIES AND ENERGY GRADIENTS IN ELECTRON PROPAGATOR THEORY. *International Journal of Quantum Chemistry* 1992, 1-11.

22. Ortiz, J. V., A COMPARISON OF GROUND-STATE AVERAGES IN ELECTRON PROPAGATOR THEORY. *International Journal of Quantum Chemistry* 1993, 407-418.

23. Ortiz, J. V., IMPROVED ELECTRON PROPAGATOR METHODS - AN INVESTIGATION OF C-4, C-4(-), AND C-4(+). *Journal of Chemical Physics* 1993, *99* (9), 6716-6726.

24. Ortiz, J. V., Partial third-order quasiparticle theory: Comparisons for closed-shell ionization energies and an application to the Borazine photoelectron spectrum. *Journal of Chemical Physics* 1996, *104* (19), 7599-7605.

25. Ortiz, J. V., Partial third-order quasiparticle theory: An application to the photoelectron spectrum of s-tetrazine. *International Journal of Quantum Chemistry* 1997, *63* (2), 291-299.

26. Ortiz, J. V., Approximate Brueckner orbitals in electron propagator calculations. *International Journal of Quantum Chemistry* 1999, *75* (4-5), 615-621.

27. Ortiz, J. V., Brueckner orbitals, Dyson orbitals, and correlation potentials. *International Journal of Quantum Chemistry* 2004, *100* (6), 1131-1135.

28. Ortiz, J. V., An efficient, renormalized self-energy for calculating the electron binding energies of closed-shell molecules and anions. *International Journal of Quantum Chemistry* 2005, *105* (6), 803-808.

29. Ortiz, J. V.; Zakrzewski, V. G., A test of partial third order electron propagator theory: Vertical ionization energies of azabenzenes. *Journal of Chemical Physics* 1996, *105* (7), 2762-2769.

30. Zakrzewski, V. G.; Dolgounitcheva, O.; Ortiz, J. V., Strong Correlation Effects in the Electron Binding Energies of Phthalocyanine. *International Journal of Quantum Chemistry* 2009, *109* (15), 3619-3625.

31. DiLabio, G. A.; Hurley, M. M.; Christiansen, P. A., Simple one-electron quantum capping potentials for use in hybrid QM/MM studies of biological molecules. *Journal of Chemical Physics* 2002, *116* (22), 9578-9584.

32. Pasquarello, A.; Hybertsen, M. S.; Car, R., Theory of Si 2p core-level shifts at the Si(001)-SiO2 interface. *Physical Review B* 1996, *53* (16), 10942-10950.

33. Pasquarello, A.; Hybertsen, M. S.; Car, R., First-principles study of Si 2p core-level shifts at water and hydrogen covered Si(001)2x1 surfaces. *J. Vac. Sci. Technol. B* 1996, *14* (4), 2809-2811.

34. Goldstein, H.; Poole Jr., C. P.; Safko, J., *Classical Mechanics*. Addison-Wesley: 2002.

35. Becke, A. D., Density-Functional Exchange-Energy Approximation with Correct Asymptotic-Behavior. *Phys. Rev. A* 1988, *38* (6), 3098-3100.

36. Becke, A. D., Density-Functional Thermochemistry .3. the Role of Exact Exchange. *Journal of Chemical Physics* 1993, *98* (7), 5648-5652.

37. Lee, C. T.; Yang, W. T.; Parr, R. G., Development of the Colle-Salvetti Correlation-Energy Formula into a Functional of the Electron-Density. *Physical Review B* 1988, *37* (2), 785-789.

38. Hariharan, P. C.; Pople, J. A., Influence of Polarization Functions on Molecular-Orbital Hydrogenation Energies. *Theor. Chim. Acta* 1973, *28* (3), 213-222.

39. M. J. Frisch, G. W. T., H. B. Schlegel, G. E. Scuseria, M. A. Robb, J. R. Cheeseman, J. A. Montgomery, Jr., T. Vreven, K. N. Kudin, J. C. Burant, J. M. Millam, S. S. Iyengar, J. Tomasi, V. Barone, B. Mennucci, M. Cossi, G. Scalmani, N. Rega, G. A. Petersson, H. Nakatsuji, M. Hada, M. Ehara, K. Toyota, R. Fukuda, J. Hasegawa, M. Ishida, T. Nakajima, Y. Honda, O. Kitao, H. Nakai, M. Klene, X. Li, J. E. Knox, H. P. Hratchian, J. B. Cross, V. Bakken, C. Adamo, J. Jaramillo, R. Gomperts, R. E. Stratmann, O. Yazyev, A. J. Austin, R. Cammi, C. Pomelli, J. W. Ochterski,; P. Y. Ayala, K. M., G. A. Voth, P. Salvador, J. J. Dannenberg, V. G. Zakrzewski, S. Dapprich, A. D. Daniels, M. C. Strain, O. Farkas, D. K. Malick, A. D. Rabuck, K. Raghavachari, J. B. Foresman, J. V. Ortiz, Q. Cui, A. G. Baboul, S. Clifford, J. Cioslowski, B. B. Stefanov, G. Liu, A. Liashenko, P. Piskorz, I. Komaromi, R. L. Martin, D. J. Fox, T. Keith, M. A. Al-Laham, C. Y. Peng, A. Nanayakkara, M. Challacombe, P. M. W. Gill, B. Johnson, W. Chen, M. W. Wong, C. Gonzalez, and J. A. Pople *Gaussian Development Version*, Revision E.05; Gaussian, Inc.: Wallingford CT, 2004.

Curriculum Vita and Publications

Indiana University, Dept. of Chemistry
800 East Kirkwood Avenue
Bloomington, IN 47405-7102

Phone: (812) 322-1530
Email: gafergus@indiana.edu

Education

Doctor of Philosophy, Indiana University, Bloomington, IN
December 2009
Area of Specialization: Physical and Materials Chemistry *GPA:* 3.6/4.0
Dissertation: *Reactivity and Spectroscopic Properties of Silicon Surfaces*

Bachelor of Arts, Marist College, Poughkeepsie, NY May 2004
Major: Biology *GPA:* 3.6/4.0
Honors: Magna Cum Laude

Research Experience

2004-Present: Graduate Student (Raghavachari Group, Indiana University)

Research Focus: The surface chemistry of silicon is a rich and exciting area with many unsolved questions. Several problems I addressed include the chemical reactivity of silicon surfaces, understanding surface adsorbate vibrations and modeling x-ray photoelectron spectra. Using computational techniques I have deeply investigated the relationship between the vibrations of finite and infinite systems and developed a technique for determining observed surface vibrations from small cluster models. I also explored the coupling of phonon modes to adsorbate bending modes. I studied the mechanism of molecular line formation across dimer bonds, the reactivity of Lewis Acids with the silicon surface, and the mechanism of atomic hydrogen catalyzed oxygen and nitrogen insertion on the Si(100) surface. Finally, I am finishing the implementation of a method to calculate XPS spectral shifts from first principles.

2001-2003 Research Assistant Computational Chemistry (Galbraith Group, Marist College)

Research Focus: A fundamental problem in molecular structure and bonding is an accurate characterization of delta-bonding. In order to gain a deeper understanding of delta bonding in small molecule transition metal complexes I used valence bond theory to decompose sigma, pi and delta bonds. We were successful in determining delta-bond strength in agreement with other much more expensive calculations.

2001-2003 Research Assistant Microbiology (Kepner Group, Marist College)

Research Focus: To study naturally occurring virus-like-particles (VLP) in the environment, it is necessary to concentrate the particles. Techniques for concentrating VLP's in river water are difficult, time consuming & inefficient. A simpler and more effective method is to use tangential flow filtration. I was successful in developing a method to concentrate VLP's from river water and then quantified the percentage of the total recovered from river water.

Teaching Experience

Associate Instructor 2004-2008

Indiana University, *Bloomington, IN*

Courses: General Chemistry and Graduate Computational Quantum Chemistry

Service Experience

Midwest Theoretical Chemistry Conference, Bloomington, IN 2007

I organized the Midwest Theoretical Chemistry Conference at Indiana University on behalf of Professors Srinivasan Iyengar and Professor Krishnan Raghavachari. I worked on all aspects of the conference including web design, abstract submission and acceptance, accommodations, menu selection, conference book and session organization.

235th American Chemical Society Meeting Computational Spectroscopy Symposia, New Orleans 2008

I assisted with the organization of the computational Spectroscopy Symposia at the 235th Meeting of the American Chemical Society on behalf of Professor Krishnan Raghavachari by targeting scientists for invited talks and suggesting the acceptance of contributed talks.

Work Experience

USS Carl Vinson, August 1995 to August 1999

As an electrician in the U.S. Navy I worked onboard the USS Carl Vinson as a maintenance electrician and work center supervisor. I worked on all electrical equipment outside the nuclear plant. I managed five personnel in support of visual aircraft landing and navigational lighting systems during deployment to a combat zone without any major equipment outages of loss of readiness. I was recognized for superior service with numerous letters of commendation and a Navy Achievement Medal.

Fellowships and Honors

William LeSuer Fellowship sponsored by Lubrizol	2008
Graduate Student Kraft Fellowship	2007
Navy Achievement Medal	1997
Marist College Academic Excellence Scholarship	2001- 2003
American Chemical Society College Recognition Award	2003
Sigma-Zeta Science Honor Society	1999

Computer & Computation Skills

I have maintained a 34 node Linux cluster and numerous Linux and windows workstations. I am proficient with Windows, Mac OS X, Linux & UNIX operating systems. I have made extensive use of Perl scripting for the automation of system administrator tasks, parsing text files and task automation sequential tasks. I am proficient in the FORTRAN 77 programming language and familiar with HTML. I am very proficient with MS Office and the Adobe Creative Suite.

Oral Presentations

Invited Lecture at University of Wisconsin, Madison, WI 2009
Ferguson, G.A., and Raghavachari, K., *Vibrations and Reactivity of Silicon Surfaces.*

235th American Chemical Society Meeting, New Orleans, LA 2008
Ferguson, G.A., and Raghavachari, K., *Surface Vibrations on Si(111): From Cluster to Infinite Lattices.*

Midwest Theoretical Chemistry Conference, Columbus, Ohio 2006
Ferguson, G.A., and Raghavachari, K., *Surface Vibrations of the Functionalized Si(111) Surface.*

Midwest Theoretical Chemistry Conference, Columbia, Missouri 2005

Ferguson, G.A., and Raghavachari, K., *Chemical vs. Thermal control of wet-oxidized Si(100) oxidation*

Peer Reviewed Publications

Ferguson, G.A., and Raghavachari, K. *The emergence of collective vibrations in cluster models: Quantum chemical study of the methyl-terminated Si(111) surface J. Chem. Phys.* **125**, 154708 (2006).

Ferguson, G.A., and Raghavachari, K. *Collective vibrations in cluster models for semiconductor surfaces: Vibrational spectra of acetylenyl and methylacetylenyl functionalized Si(111) J. Chem. Phys.* **127**, 194706 (2007).

Ferguson, G.A., Michalak, D.J., Chabal, Y. and Raghavachari, K. *Near surface phonon and surface adsorbate vibrational interactions of hydrogen-passivated Si(111) J. Phys. Chem. C.* **112**(4); 1034 (2008).

Ferguson, G.A., Das, U. and Raghavachari, K. *The interaction of Lewis acids with the Si(100)-2×1 and Ge(100) 2×1 surfaces J. Phys. Chem. C*. **113**, 10146 (2009).

Ferguson, G.A., Than, C.T.L. and Raghavachari, K. *Line growth on the H/Si(100)-2×1 Surface: A Density functional study of allylic mercaptan reaction mechanism. J. Phys. Chem. C.* **113**, 18817 (2009).

Ferguson, G.A., Rivllion, S., Chabal, Y. and Raghavachari, K *Vibrations of mixed coverage Si(111)-Cl/H surfaces. J. Phys. Chem. C.* 113, 21713 (2009).

Than, C.T-L, **Ferguson, G.A.** and Raghavachari, K. *Quaternary amine induced peptide cyclization*. *J. Phys. Chem. A*. **114**, 481(2010).

Ferguson, G.A., Than, C.T.L. and Raghavachari, K. *Extending molecular lines on the Si(100)-2×1 surface: A theoretical study of the effect of allylic mercaptan adsorbates on radical chain reactions. J. Phys. Chem. Lett.* **1**, 679 (2010).

Articles in preparation:

Ferguson, G.A., and Raghavachari, K. *Surface structure from Vibrational Frequencies: A Detailed Analysis of the Si–H Vibrations of the Hydrogen Terminated Si(100) and Si(111) Surfaces*. (*Submitted to the Journal of Chemical Physics*).

Ferguson, G.A., Chabal, Y. and Raghavachari, K. *Vibrational trends of mixed coverage halide/hydrogen: Si(111) surfaces*.

Ferguson, G.A., Than, C.T-L. and Raghavachari, K. *Reactions of atomic hydrogen with the functionalized Si(100) surface: A DFT problem case*.

Ferguson, G.A., Than, C.T-L., He, Yi, James P. Reilly and Raghavachari, K. *Routes of Methyl-group migration in proteomic studies using mass spectrometry*